William & Mary
CHARTERED 1693

W&M ScholarWorks

Dissertations, Theses, and Masters Projects

Theses, Dissertations, & Master Projects

2022

Diel, Seasonal, And Interannual Changes In Coastal Antarctic Zooplankton Community Composition And Trophic Ecology

John A. Conroy
William & Mary - Virginia Institute of Marine Science, jaconroy12@gmail.com

Follow this and additional works at: https://scholarworks.wm.edu/etd

 Part of the Marine Biology Commons, and the Oceanography Commons

Recommended Citation

Conroy, John A., "Diel, Seasonal, And Interannual Changes In Coastal Antarctic Zooplankton Community Composition And Trophic Ecology" (2022). *Dissertations, Theses, and Masters Projects.* William & Mary. Paper 1673281626.
https://dx.doi.org/10.25773/v5-94dr-je71

This Dissertation is brought to you for free and open access by the Theses, Dissertations, & Master Projects at W&M ScholarWorks. It has been accepted for inclusion in Dissertations, Theses, and Masters Projects by an authorized administrator of W&M ScholarWorks. For more information, please contact scholarworks@wm.edu.

Diel, Seasonal, and Interannual Changes in Coastal Antarctic Zooplankton Community Composition and Trophic Ecology

A Dissertation

Presented to

The Faculty of the School of Marine Science

The College of William & Mary

In Partial Fulfillment

of the Requirements for the Degree of

Doctor of Philosophy

by

John Aidan Conroy

May 2022

APPROVAL PAGE

This dissertation is submitted in partial fulfillment of

the requirements for the degree of

Doctor of Philosophy

John Aidan Conroy

Approved by the Committee, April 2022

Deborah K. Steinberg, Ph.D.
Committee Chair / Advisor

David S. Johnson, Ph.D.

Walker O. Smith, Ph.D.

Michael Vecchione, Ph.D.

Kim S. Bernard, Ph.D.
Oregon State University
Corvallis, Oregon, USA

For my grandparents.

TABLE OF CONTENTS

ACKNOWLEDGEMENTS

I am thankful for the opportunity to work with my advisor, Dr. Debbie Steinberg, who afforded me exceptional opportunities and freedom during my graduate program. Debbie has been endlessly supportive and patient since we first set sail together in 2015. I am fortunate to count her as my teacher, mentor, and friend. I am grateful to my committee members: Drs. Kim Bernard, David Johnson, Walker Smith, and Mike Vecchione. The impacts of their lessons are present throughout this dissertation and in my approach to scientific inquiry.

It was a joy to conduct this dissertation research at VIMS. My colleagues in the Zooplankton Ecology Lab made it fun to go to work every day in Gloucester Point and in Antarctica. Joe Cope is a wonderful friend and lab manager who leads the way. I started graduate school because of my labmates, and I would not be finishing without my fellow Steinberglers: Josh Stone, Brandon Conroy, Tricia Thibodeau, Andrew Corso, Karen Stamieszkin, Kristen Sharpe, Maya Thomas, Tor Mowatt-Larssen, and Claudia Moncada. Special thanks go to the Office of Academic Studies, to Gina Burrell, and to Maxine Butler for helping me navigate the program at VIMS. I cherish the friendships I made through pick-up sports, TGI cookouts, office philosophy hours, trips to the Eastern Shore, and late nights at Hedge House.

Conducting research in Antarctica provided me with an extended academic family. Thank you to the students, staff, and investigators of the Palmer Antarctica Long-Term Ecological Research team who taught me that doing awesome science should be fun. My work was only possible because of the hard-working staff at Palmer Station and the captains, crews, and science teams aboard the R/V *Laurence M. Gould*. Thank you to all of the members of our zooplankton field teams at Palmer Station: Leigh West, Andrew Corso, Kharis Schrage, Rachael Young, and Ashley Hann. I appreciate the laboratory assistance of Maya Thomas, Michael Gibson, Grace Breitenbeck, and Meredith Nolan. I thank my colleagues from the SCAR Krill Action Group, NOAA, and Virginia Sea Grant for their support.

My family's love lifted my spirit throughout my time in graduate school, even when I was far away. My partner Schuyler has impacted my life and work for the better in countless ways over the last five years. I am so happy that we met in Antarctica.

This dissertation was supported by the National Science Foundation Antarctic Organisms and Ecosystems Program (PLR-1440435 and OPP-2026045), the Virginia Institute of Marine Science, and the NOAA Sea Grant Knauss Fellowship Program.

LIST OF TABLES

Chapter 2

Chapter 3

Chapter 4

Appendix A

LIST OF FIGURES

Chapter 2

Chapter 3

ABSTRACT

Throughout the ocean, zooplankton transfer energy from primary producers to higher predators and transport carbon from surface waters to depth. The efficiency of these processes depends in part upon the taxonomic composition and trophic ecology of the zooplankton community. Zooplankton species abundance and distribution shifted over recent decades along the West Antarctic Peninsula during a period of rapid regional warming and sea-ice decline. Although conducted within the context of long-term change, this dissertation research focuses on zooplankton dynamics at finer temporal scales that have received less attention. I analyzed depth-stratified net samples to investigate zooplankton diel vertical migration during Antarctic summer. I further conducted twice-weekly sampling over three field seasons to characterize seasonal and interannual changes in coastal zooplankton composition. I also used field measurements, experimental incubations, and compound-specific stable isotope analysis to study the growth and trophic ecology of a dominant species – the Antarctic krill *Euphausia superba* – during its juvenile stage. Results indicate that several zooplankton taxa conducted diel vertical migration despite nearly continuous daylight during Antarctic summer. Other carnivorous, detritivorous, and seasonally migrating taxa were most abundant in the mesopelagic zone throughout the diel cycle. Vertically migrating zooplankton and mesopelagic residents likely have a substantial impact on vertical carbon flux, which should be better quantified in the Southern Ocean. Repeated shore-based sampling showed that seasonal peaks in coastal zooplankton biomass follow local phytoplankton blooms. A general seasonal succession from larger species that depend more on phytoplankton to smaller, omnivorous species was a consistent phenomenon across multiple taxonomic groups and years. Seasonal abundance patterns for various taxa shifted by a week or more between two consecutive years, consistent with a two-week shift in the timing of sea-ice breakup and the spring phytoplankton bloom. Flexible life history and trophic ecology may limit the risk of reproductive failure despite climate-induced phenology shifts. Exceptionally warm temperatures coincided with a bloom of the gelatinous salp *Salpa thompsoni*, and such conditions may become more common in future decades. Phytoplankton ingestion was insufficient to support rapid growth of juvenile krill during summer in coastal waters, and heterotrophic protists were a critical intermediate trophic link. Phytoplankton consumption was limited due to inefficient feeding on small cells that dominated the available autotrophic prey. Metazoan zooplankton were also important prey for juvenile krill, which are truly secondary consumers. This dissertation research revealed substantial shifts in the trophic ecology and composition of Antarctic zooplankton communities at diel to interannual scales, with implications for regional biogeochemical cycles and food web dynamics. Future work should consider these shorter time scales to detect and understand long-term change in Antarctic marine ecosystems.

Diel, Seasonal, and Interannual Changes in Coastal Antarctic Zooplankton Community Composition and Trophic Ecology

CHAPTER 1
Introduction to the dissertation

Zooplankton in the Southern Ocean food web and biogeochemical cycles

Marine zooplankton comprise a broad diversity of weakly swimming animals that exhibit a wide range of body plans and life-history strategies. This dissertation focuses on metazoan (multicellular) mesozooplankton (0.2-2 mm) and macrozooplankton (>2 mm). Certain members of the larger group, such as euphausiids (krill), are relatively strong swimmers and are elsewhere referred to as micronekton. Most of the study species herein are holoplanktonic and complete their entire life cycles in the plankton, but some attention is paid to the meroplanktonic larvae of fishes and benthic invertebrates. This dissertation addresses various time scales of change in the composition and trophic ecology of Antarctic zooplankton to understand better the role of these animals in the pelagic food web and in regulating biogeochemical cycles. The findings are also discussed in the context of ongoing environmental change.

Meso- and macrozooplankton are globally important to marine ecosystem function as they are energy-rich prey for upper trophic levels and substantial contributors to carbon and nutrient cycling (Le Quéré et al. 2016, Steinberg and Landry 2017, Heneghan et al. 2020). Euphausiids, copepods, salps, and pteropods are important in the Southern Ocean due to their high biomass and/or dominant ecological roles (Johnston et al. in press). Species of these groups provide critical ecosystem services by supporting higher trophic levels that have commercial and conservation interest (McCormack et al. 2021), and by influencing the Southern Ocean's atmospheric carbon sink via particle export (Gleiber et al. 2012), nutrient recycling (Böckmann et al. 2021), and carbonate cycling (Bednaršek et al. 2012). Community-wide, trait-based approaches to studying zooplankton provide an opportunity to simplify the complexity of diverse taxa across shared attributes that describe their ecological roles (Litchman et al. 2013; Kiørboe et

al. 2018). This dissertation presents a combination of species-specific and community-wide approaches to describe the ecology of Southern Ocean zooplankton.

Zooplankton occupy a central role in pelagic food webs by transferring carbon and energy from primary producers to higher trophic levels. Zooplankton can graze a large proportion of phytoplankton standing stock every day, especially in areas of high zooplankton biomass (Bernard et al. 2012). Euphausiids (particularly the Antarctic krill *Euphausia superba*) are key prey for fishes, penguins and other seabirds, cephalopods, and baleen whales and other marine mammals (Trathan and Hill 2016). Antarctic krill are also targeted in the Southern Ocean's largest commercial fishery (Nicol and Foster 2016). Copepods are a major prey item for carnivores, particularly fishes (Hopkins and Torres 1989). Predation within the zooplankton is also an important component of pelagic food webs. Many zooplankton species are carnivorous or omnivorous, including chaetognaths, amphipods, euphausiids, pteropods, and copepods. The high abundance of marine vertebrate predators around Antarctica is believed to be driven by a simple, efficient food web (Valiela 1995), but the importance of intermediate trophic steps is becoming increasingly evident (Sailley et al. 2013; McCormack et al. 2021). Much research has focused on interannual and longer-term change in the abundance of zooplankton in the Southern Ocean (reviewed by Johnston et al. in press), but an improved understanding of shorter-scale variability in the planktonic food web is needed to map carbon and energy flow accurately in the Southern Ocean ecosystem.

Zooplankton play a second major role as gatekeepers of the biological pump – the suite of biological processes by which organisms transport carbon and nutrients from surface waters to depth (Ducklow et al. 2001, Steinberg and Landry 2017). Zooplankton produce fecal pellets that sink and can dominate vertical particle flux from the epipelagic zone to the mesopelagic zone

(Turner 2015). Zooplankton also contribute to the attenuation of this vertical flux as they feed on or fragment sinking particles (Wilson et al. 2008; Cavan et al. 2019). Recent food web modeling suggests that zooplankton fecal pellets may contribute the majority of sinking particulate organic carbon export globally (Bisson et al. 2020). The second major way that zooplankton contribute to the biological pump is by the active transport of carbon and nutrients to depth via vertical migration (Steinberg et al. 2000; Al-Mutairi and Landry 2001). Many zooplankton taxa feed in surface waters at night to reduce the risk posed by visual predators and then descend to deeper, darker waters during daytime (Hays 2003; Bandara et al. 2021). Migrating zooplankton contribute on average 10-20% to global vertical carbon export via the respiration of dissolved inorganic carbon and egestion of particulate organic carbon in the mesopelagic zone (Archibald et al. 2019). Some zooplankton also contribute to this vertical export via seasonal vertical migrations that result in prolonged respiration at depth over winter (Kobari et al. 2008; Jónasdóttir et al. 2015). Understanding the various export pathways is currently a major priority of ocean biogeochemistry (Siegel et al. 2016; Boyd et al. 2019), particularly in the Southern Ocean and on Antarctic continental shelves, which constitute a disproportionately strong sink of atmospheric carbon (Brown et al. 2019; Long et al. 2021) and where zooplankton strongly influence the efficiency with which carbon is exported to depth (Cavan et al. 2015; Henson et al. 2019).

The changing West Antarctic Peninsula ecosystem

The coastal ecosystem along the West Antarctic Peninsula (WAP) is characterized by seasonally high production, significant interannual variability, and abundant vertebrate predator populations (Ducklow et al. 2013). Biological hot spots are located along the coastal WAP's

latitudinal climate gradient: from Anvers Island in the north where, due to rapid regional warming, a maritime (warmer, wetter) climate has developed, to Avian and Charcot Islands in the south where polar (colder, drier) conditions still persist (Schofield et al. 2013). The U.S. research base Palmer Station is located on Anvers Island. These hot spots are located at the heads of submarine canyons, which cut across the shelf and support elevated phytoplankton biomass, zooplankton biomass, and seabird colonies (Schofield et al. 2013, Kavanaugh et al. 2015, Bernard et al. 2017). On the WAP shelf, ~10% of net primary production is exported from the euphotic zone via passively sinking particles during mid-summer peaks in vertical flux (Ducklow et al. 2008, Buesseler et al. 2010). Fecal pellets produced mostly by krill, but also copepods and salps, dominate this passive flux both on the WAP continental shelf and near Anvers Island (Gleiber et al. 2012, Stukel et al. 2015).

Rapid regional warming has impacted the physical state of the coastal WAP ecosystem. The WAP warmed at five times the global rate over the second half of the 20th century, particularly in winter months, when average air temperature increased by >6° C (Vaughan et al. 2003). Over the same period, summer sea surface temperature and salinity increased by 1° C and 0.25, respectively (Meredith and King 2005). Since the late 1970s, the first day of sea-ice retreat has shifted earlier in the spring while the initiation of ice advance has migrated into later autumn, resulting in a three-month decline in the annual sea-ice season (Stammerjohn et al. 2008, 2012). A slight cooling trend observed since the turn of the century is consistent with the WAP's natural variability (Turner et al. 2016; Henley et al. 2019), but climate projections through 2100 predict warming along the WAP at a rate comparable to that seen over the second half of the 20th century (Bracegirdle et al. 2008).

Changing ice, ocean, and atmospheric conditions have impacted the WAP phytoplankton.

Stronger winds and reduced sea ice caused deeper mixing, a decrease in phytoplankton biomass, and a shift from large diatoms to smaller cells north of Anvers Island between 1978 and 2006 (Montes-Hugo et al. 2009). Near Anvers Island and southward, a shift from perennial to seasonal ice cover, resulting in more open water and exposing phytoplankton to increased irradiance, has driven the opposite trend: an increase in phytoplankton biomass and diatom dominance (Montes-Hugo et al. 2009, Schofield et al. 2017). A recent increase in sea ice from 2008 to 2016 resulted in shallower mixing and higher photosynthetic efficiency from Anvers Island southward (Schofield et al. 2018; Brown et al. 2019).

Changes have occurred in WAP zooplankton as well, including an increase in abundance in some species of copepods, pteropods, and euphausiids, and a range expansion for the open water tunicate *Salpa thompsoni* (Gleiber 2014; Steinberg et al. 2015; Thibodeau et al. 2019). In general, pteropods and salps favor warmer, ice-free waters while euphausiids and copepods respond favorably to increased phytoplankton production. The WAP Antarctic krill population is characterized by periodic successful recruitment events, which coincide with peaks in phytoplankton biomass every 4-6 years (Ross et al. 2014, Saba et al. 2014, Steinberg et al. 2015). Weaker winds and delayed sea-ice retreat enhance water column stability in years of elevated phytoplankton biomass leading to strong krill recruitment (Saba et al. 2014). These favorable local conditions are associated with a negative phase in wintertime Southern Annular Mode, which is projected to trend positive in future decades (Thompson et al. 2011, Saba et al. 2014). Complex species responses to increased temperature (Burrows et al. 2019, Edwards et al. 2021) and changes in other environmental variables (Montes-Hugo et al. 2009, McHenry et al. 2019) make it difficult to predict future zooplankton community structure.

Structure of dissertation

This dissertation examines change in the community composition and trophic ecology of zooplankton in the coastal WAP at diel, seasonal, and interannual scales. The research was conducted as part of the Palmer Antarctica Long-Term Ecological Research (PAL LTER) program, an interdisciplinary project that has studied the WAP ecosystem since 1990. The dissertation is comprised of five chapters and an appendix. This first chapter introduces the dissertation. Chapter 2 assesses the diel vertical migration behavior of 14 zooplankton taxa using data from seven years of depth-stratified net samples collected through the epipelagic and mesopelagic zones. This chapter has been published in *Deep-Sea Research Part I*. Chapter 3 presents seasonal and interannual changes in the taxonomic and size composition of zooplankton near Anvers Island for three successive field seasons. Chapter 4 utilized a multi-method approach to constrain the trophic position and dietary composition of juvenile Antarctic krill in the coastal waters near Anvers Island during three consecutive field seasons. Chapter 5 concludes the dissertation and presents perspectives on future work. Appendix A is a time-series analysis of data from the PAL LTER and U.S. Antarctic Marine Living Resources programs. The analysis links larval supply and recruitment of Antarctic krill along the Antarctic Peninsula, including areas north of Anvers Island. This appendix has been published in *Integrative and Comparative Biology*.

References

Al-Mutairi H, Landry MR (2001) Active export of carbon and nitrogen at Station ALOHA by diel migrant zooplankton. Deep Sea Research Part II 48:2083–2103.

Archibald KM, Siegel DA, Doney SC (2019) Modeling the Impact of Zooplankton Diel Vertical Migration on the Carbon Export Flux of the Biological Pump. Global Biogeochemical Cycles 33:181–199.

Bandara K, Varpe Ø, Wijewardene L, Tverberg V, Eiane K (2021) Two hundred years of zooplankton vertical migration research. Biological Reviews 96:1547-1589.

Bednaršek N, Tarling GA, Fielding S, Bakker DCE (2012) Population dynamics and biogeochemical significance of *Limacina helicina antarctica* in the Scotia Sea (Southern Ocean). Deep Sea Research Part II 59–60:105–116.

Bernard KS, Cimino M, Fraser W, Kohut J, Oliver MJ, Patterson-Fraser D, Schofield OME, Statscewich H, Steinberg DK, Winsor P (2017) Factors that affect the nearshore aggregations of Antarctic krill in a biological hotspot. Deep Sea Research Part I 126:139–147.

Bernard KS, Steinberg DK, Schofield OME (2012) Summertime grazing impact of the dominant macrozooplankton off the Western Antarctic Peninsula. Deep Sea Research Part I 62:111–122.

Bisson K, Siegel DA, DeVries T (2020) Diagnosing Mechanisms of Ocean Carbon Export in a Satellite-Based Food Web Model. Frontiers in Marine Science 7:505.

Böckmann S, Koch F, Meyer B, Pausch F, Iversen M, Driscoll R, Laglera LM, Hassler C, Trimborn S (2021) Salp fecal pellets release more bioavailable iron to Southern Ocean phytoplankton than krill fecal pellets. Current Biology 31:2737-2746.e3.

Boyd PW, Claustre H, Levy M, Siegel DA, Weber T (2019) Multi-faceted particle pumps drive carbon sequestration in the ocean. Nature 568:327.

Bracegirdle TJ, Connolley WM, Turner J (2008) Antarctic climate change over the twenty first century. Journal of Geophysical Research: Atmospheres 113.

Brown MS, Munro DR, Feehan CJ, Sweeney C, Ducklow HW, Schofield OM (2019) Enhanced oceanic CO_2 uptake along the rapidly changing West Antarctic Peninsula. Nature Climate Change 9:678–683.

Buesseler KO, McDonnell AMP, Schofield OME, Steinberg DK, Ducklow HW (2010) High particle export over the continental shelf of the west Antarctic Peninsula. Geophysical Research Letters 37 L22606.

Burrows MT, Bates AE, Costello MJ, Edwards M, Edgar GJ, Fox CJ, Halpern BS, Hiddink JG, Pinsky ML, Batt RD, García Molinos J, Payne BL, Schoeman DS, Stuart-Smith RD, Poloczanska ES (2019) Ocean community warming responses explained by thermal affinities and temperature gradients. Nature Climate Change 9:959–963.

Cavan EL, Laurenceau-Cornec EC, Bressac M, Boyd PW (2019) Exploring the ecology of the mesopelagic biological pump. Progress in Oceanography 176:102125.

Cavan EL, Le Moigne FAC, Poulton AJ, Tarling GA, Ward P, Daniels CJ, Fragoso GM, Sanders RJ (2015) Attenuation of particulate organic carbon flux in the Scotia Sea, Southern Ocean, is controlled by zooplankton fecal pellets. Geophysical Research Letters 42:821–830.

Ducklow H, Fraser W, Meredith M, Stammerjohn S, Doney S, Martinson D, Sailley S, Schofield O, Steinberg D, Venables H, Amsler C (2013) West Antarctic Peninsula: An Ice-Dependent Coastal Marine Ecosystem in Transition. Oceanography 26:190–203.

Ducklow HW, Erickson M, Kelly J, Montes-Hugo M, Ribic CA, Smith RC, Stammerjohn SE, Karl DM (2008) Particle export from the upper ocean over the continental shelf of the west Antarctic Peninsula: A long-term record, 1992–2007. Deep Sea Research Part II 55:2118–2131.

Ducklow HW, Steinberg DK, Buesseler KO (2001) Upper ocean carbon export and the biological pump. Oceanography 14:50–58.

Edwards M, Hélaouët P, Goberville E, Lindley A, Tarling GA, Burrows MT, Atkinson A (2021) North Atlantic warming over six decades drives decreases in krill abundance with no associated range shift. Communications Biology 4:1–10.

Gleiber MR (2014) Long-term change in copepod community structure in the Western Antarctic Peninsula: Linkage to climate and implications for carbon cycling. (Master's Thesis). The College of William & Mary.

Gleiber MR, Steinberg DK, Ducklow HW (2012) Time series of vertical flux of zooplankton fecal pellets on the continental shelf of the western Antarctic Peninsula. Marine Ecology Progress Series 471:23–36.

Hays GC (2003) A review of the adaptive significance and ecosystem consequences of zooplankton diel vertical migrations. In: *Migrations and Dispersal of Marine Organisms*. Springer, p 163–170

Heneghan RF, Everett JD, Sykes P, Batten SD, Edwards M, Takahashi K, Suthers IM, Blanchard JL, Richardson AJ (2020) A functional size-spectrum model of the global marine ecosystem that resolves zooplankton composition. Ecological Modelling 435:109265.

Henley SF, Schofield OM, Hendry KR, Schloss IR, Steinberg DK, Moffat C, Peck LS, Costa DP, Bakker DCE, Hughes C, Rozema PD, Ducklow HW, Abele D, Stefels J, Van

Leeuwe MA, Brussaard CPD, Buma AGJ, Kohut J, Sahade R, Friedlaender AS, Stammerjohn SE, Venables HJ, Meredith MP (2019) Variability and change in the west Antarctic Peninsula marine system: Research priorities and opportunities. Progress in Oceanography 173:208–237.

Henson S, Le Moigne F, Giering S (2019) Drivers of Carbon Export Efficiency in the Global Ocean. Global Biogeochemical Cycles 33:891–903.

Hopkins TL, Torres JJ (1989) Midwater food web in the vicinity of a marginal ice zone in the western Weddell Sea. Deep Sea Research Part A 36:543–560.

Johnston NM, Murphy EJ, Atkinson AA, Constable AJ, Cotté CS, Cox M, Daly K, Driscoll R, Flores H, Halfter S, Henschke N, Hill SL, Höfer J, Hunt BP, Kawaguchi S, Lindsay DJ, Loeb V, Manno C, Meyer B, Pakhomov E, Pinkerton MH, Reiss C, Richerson K, Smith W, Steinberg DK, Swadling KM, Tarling GA, Thorpe SE, Veytia D, Ward P, Weldrick CK, Yang G (in press) Status, change and futures of zooplankton in the Southern Ocean. Frontiers in Ecology and Evolution.

Jónasdóttir SH, Visser AW, Richardson K, Heath MR (2015) Seasonal copepod lipid pump promotes carbon sequestration in the deep North Atlantic. Proceedings of the National Academy of Sciences 112:12122–12126.

Kavanaugh MT, Abdala FN, Ducklow H, Glover D, Fraser W, Martinson D, Stammerjohn S, Schofield O, Doney SC (2015) Effect of continental shelf canyons on phytoplankton biomass and community composition along the western Antarctic Peninsula. Marine Ecology Progress Series 524:11–26.

Kiørboe T, Visser A, Andersen KH (2018) A trait-based approach to ocean ecology. ICES Journal of Marine Science 75:1849–1863.

Kobari T, Steinberg DK, Ueda A, Tsuda A, Silver MW, Kitamura M (2008) Impacts of ontogenetically migrating copepods on downward carbon flux in the western subarctic Pacific Ocean. Deep Sea Research Part II 55:1648–1660.

Le Quéré C, Buitenhuis ET, Moriarty R, Alvain S, Aumont O, Bopp L, Chollet S, Enright C, Franklin DJ, Geider RJ, Harrison SP, Hirst AG, Larsen S, Legendre L, Platt T, Prentice IC, Rivkin RB, Sailley S, Sathyendranath S, Stephens N, Vogt M, Vallina SM (2016) Role of zooplankton dynamics for Southern Ocean phytoplankton biomass and global biogeochemical cycles. Biogeosciences 13:4111–4133.

Litchman E, Ohman MD, Kiørboe T (2013) Trait-based approaches to zooplankton communities. Journal of Plankton Research 35:473–484.

Long MC, Stephens BB, McKain K, Sweeney C, Keeling RF, Kort EA, Morgan EJ, Bent JD, Chandra N, Chevallier F, Commane R, Daube BC, Krummel PB, Loh Z, Luijkx IT, Munro D, Patra P, Peters W, Ramonet M, Rödenbeck C, Stavert A, Tans P, Wofsy SC (2021) Strong Southern Ocean carbon uptake evident in airborne observations. Science 374:1275–1280.

McCormack SA, Melbourne-Thomas J, Trebilco R, Blanchard JL, Raymond B, Constable A (2021) Decades of dietary data demonstrate regional food web structures in the Southern Ocean. Ecology and Evolution 11:227–241.

McHenry J, Welch H, Lester SE, Saba V (2019) Projecting marine species range shifts from only temperature can mask climate vulnerability. Global Change Biology 25:4208–4221.

Meredith MP, King JC (2005) Rapid climate change in the ocean west of the Antarctic Peninsula during the second half of the 20th century. Geophysical Research Letters 32:L19604.

Montes-Hugo M, Doney SC, Ducklow HW, Fraser W, Martinson D, Stammerjohn SE, Schofield

O (2009) Recent changes in phytoplankton communities associated with rapid regional climate change along the western Antarctic Peninsula. Science 323:1470–1473.

Nicol S, Foster J (2016) The Fishery for Antarctic Krill: Its Current Status and Management Regime. In: *Biology and Ecology of Antarctic Krill*. Advances in Polar Ecology, Siegel V (ed) Springer International Publishing, Cham, p 387–421

Ross RM, Quetin LB, Newberger T, Shaw CT, Jones JL, Oakes SA, Moore KJ (2014) Trends, cycles, interannual variability for three pelagic species west of the Antarctic Peninsula 1993-2008. Marine Ecology Progress Series 515:11–32.

Saba GK, Fraser WR, Saba VS, Iannuzzi RA, Coleman KE, Doney SC, Ducklow HW, Martinson DG, Miles TN, Patterson-Fraser DL, Stammerjohn SE, Steinberg DK, Schofield OM (2014) Winter and spring controls on the summer food web of the coastal West Antarctic Peninsula. Nature Communications 5:1–8.

Sailley SF, Ducklow HW, Moeller HV, Fraser WR, Schofield OM, Steinberg DK, Garzio LM, Doney SC (2013) Carbon fluxes and pelagic ecosystem dynamics near two western Antarctic Peninsula Adélie penguin colonies: an inverse model approach. Marine Ecology Progress Series 492:253–272.

Schofield O, Brown M, Kohut J, Nardelli S, Saba G, Waite N, Ducklow H (2018) Changes in the upper ocean mixed layer and phytoplankton productivity along the West Antarctic Peninsula. Philosophical Transactions of the Royal Society A 376:20170173.

Schofield O, Ducklow H, Bernard K, Doney S, Patterson-Fraser D, Gorman K, Martinson D, Meredith M, Saba G, Stammerjohn S, Steinberg D, Fraser W (2013) Penguin Biogeography Along the West Antarctic Peninsula: Testing the Canyon Hypothesis with Palmer LTER Observations. Oceanography 26:204–206.

Schofield O, Saba G, Coleman K, Carvalho F, Couto N, Ducklow H, Finkel Z, Irwin A, Kahl A, Miles T, Montes-Hugo M, Stammerjohn S, Waite N (2017) Decadal variability in coastal phytoplankton community composition in a changing West Antarctic Peninsula. Deep Sea Research Part I 124:42–54.

Siegel DA, Buesseler KO, Behrenfeld MJ, Benitez-Nelson CR, Boss E, Brzezinski MA, Burd A, Carlson CA, D'Asaro EA, Doney SC, Perry MJ, Stanley RHR, Steinberg DK (2016) Prediction of the Export and Fate of Global Ocean Net Primary Production: The EXPORTS Science Plan. Frontiers in Marine Science 3:22.

Stammerjohn S, Massom R, Rind D, Martinson D (2012) Regions of rapid sea ice change: An inter-hemispheric seasonal comparison. Geophysical Research Letters 39:L06501.

Stammerjohn SE, Martinson DG, Smith RC, Yuan X, Rind D (2008) Trends in Antarctic annual sea ice retreat and advance and their relation to El Niño–Southern Oscillation and Southern Annular Mode variability. Journal of Geophysical Research: Oceans 113:C03S90.

Steinberg DK, Carlson CA, Bates NR, Goldthwait SA, Madin LP, Michaels AF (2000) Zooplankton vertical migration and the active transport of dissolved organic and inorganic carbon in the Sargasso Sea. Deep Sea Research Part I 47:137–158.

Steinberg DK, Landry MR (2017) Zooplankton and the Ocean Carbon Cycle. Annual Review of Marine Science 9:413–444.

Steinberg DK, Ruck KE, Gleiber MR, Garzio LM, Cope JS, Bernard KS, Stammerjohn SE, Schofield OME, Quetin LB, Ross RM (2015) Long-term (1993–2013) changes in macrozooplankton off the Western Antarctic Peninsula. Deep Sea Research Part I 101:54–70.

Stukel MR, Asher E, Couto N, Schofield O, Strebel S, Tortell P, Ducklow HW (2015) The imbalance of new and export production in the Western Antarctic Peninsula, a potentially "leaky" ecosystem. Global Biogeochemical Cycles 29:1400–1420.

Thibodeau PS, Steinberg DK, Stammerjohn SE, Hauri C (2019) Environmental controls on pteropod biogeography along the Western Antarctic Peninsula. Limnology and Oceanography 64:S240–S256.

Thompson DWJ, Solomon S, Kushner PJ, England MH, Grise KM, Karoly DJ (2011) Signatures of the Antarctic ozone hole in Southern Hemisphere surface climate change. Nature Geoscience 4:741–749.

Trathan PN, Hill SL (2016) The Importance of Krill Predation in the Southern Ocean. In: *Biology and Ecology of Antarctic Krill*. Advances in Polar Ecology, Siegel V (ed) Springer International Publishing, Cham, p 321–350

Turner J, Lu H, White I, King JC, Phillips T, Hosking JS, Bracegirdle TJ, Marshall GJ, Mulvaney R, Deb P (2016) Absence of 21st century warming on Antarctic Peninsula consistent with natural variability. Nature 535:411–415.

Turner JT (2015) Zooplankton fecal pellets, marine snow, phytodetritus and the ocean's biological pump. Progress in Oceanography 130:205–248.

Valiela I (1995) Marine Ecological Processes, 2nd edition. Springer, New York.

Vaughan DG, Marshall GJ, Connolley WM, Parkinson C, Mulvaney R, Hodgson DA, King JC, Pudsey CJ, Turner J (2003) Recent rapid regional climate warming on the Antarctic Peninsula. Climatic Change 60:243–274.

Wilson SE, Steinberg DK, Buesseler KO (2008) Changes in fecal pellet characteristics with depth as indicators of zooplankton repackaging of particles in the mesopelagic zone of

the subtropical and subarctic North Pacific Ocean. Deep Sea Research Part II 55:1636–1647.

CHAPTER 2
Zooplankton diel vertical migration during Antarctic summer

Please cite this chapter as: Conroy JA, Steinberg DK, Thibodeau PS, Schofield O. 2020. Zooplankton diel vertical migration during Antarctic summer. *Deep-Sea Research Part I* 162:103324. https://doi.org/10.1016/j.dsr.2020.103324

Abstract

Zooplankton diel vertical migration (DVM) during summer in the polar oceans is presumed to be dampened due to near continuous daylight. We analyzed zooplankton diel vertical distribution patterns in a wide range of taxa along the Western Antarctic Peninsula (WAP) to assess if DVM occurs, and if so, what environmental controls modulate DVM in the austral summer. Zooplankton were collected during January and February in paired day-night, depth-stratified tows through the mesopelagic zone along the WAP from 2009-2017, as well as in day and night epipelagic net tows from 1993-2017. The copepod *Metridia gerlachei*, salp *Salpa thompsoni*, pteropod *Limacina helicina antarctica*[1], and ostracods consistently conducted DVM between the mesopelagic and epipelagic zones. Migration distance for *M. gerlachei* and ostracods decreased as photoperiod increased from 17 to 22 h daylight. The copepods *Calanoides acutus* and *Rhincalanus gigas*, as well as euphausiids *Thysanoessa macrura* and *Euphausia crystallorophias,* conducted shallow (mostly within the epipelagic zone) DVMs into the upper 50 m at night. *Rhincalanus gigas*, *T. macrura*, and *L. h. antarctica* DVM behavior was modulated by chlorophyll *a* concentration, mixed layer depth, and depth of the subsurface chlorophyll *a* maximum, respectively. Carnivorous and detritivorous taxa – including the calanoid copepod *Paraeuchaeta antarctica*, ostracods, chaetognaths, and *Tomopteris* spp. polychaetes – as well as seasonally migrating copepods, were most abundant in the mesopelagic zone regardless of the diel cycle. *Paraeuchaeta antarctica* underwent reverse DVM within the top 100 m. The impacts of Antarctic zooplankton summer DVM and the resident mesopelagic assemblage on carbon export should be better quantified.

[1] When this chapter was written *Limacina helicina antarctica* Woodward, 1854 was considered the valid name for the species in this study. The species has been described since as *Limacina rangii* (d'Orbigny, 1835). The usage appearing in the publication of this study is retained for Chapter 2, but the currently recognized name is used in Chapter 3.

1. Introduction

Many zooplankton and fishes throughout the world's oceans undergo diel vertical migration (DVM), feeding in productive surface waters at night and seeking refuge from visual predators at mesopelagic depths during the daytime (Hays, 2003). A global estimate suggests ~50% of sound-scattering mesopelagic biomass performs DVM (Klevjer et al., 2016). Diverse zooplankton taxa independently evolved DVM behavior, as it optimizes the adaptive balance between feeding and predator evasion (Zaret and Suffern, 1976; Stich and Lampert, 1981; Gliwicz, 1986; Hays, 2003). While predator avoidance is the accepted evolutionary driver for DVM, shifts in downwelling irradiance at sunrise and sunset are the dominant proximate cues for this behavior (Ringelberg and Van Gool, 2003; Cohen and Forward, 2009). Thus, it was assumed that DVM is restricted in polar regions and may cease altogether in mid- winter and summer during 24-h darkness and light, respectively (Blachowiak-Samolyk et al., 2006).

DVM studies in the polar oceans show seasonal variability in behavior, with DVM magnitude changing in relation to photoperiod. During moored Acoustic Doppler Current Profiler deployments in the Ross, Lazarev, and Weddell Seas, DVM continued through Antarctic winter but ceased during the period of extended daylight from November to February (Cisewski et al., 2010; Cisewski and Strass, 2016; Picco et al., 2017). Persistent winter DVM occurs as far north as 77°N (Hobbs et al., 2018), although zooplankton DVM is restricted to small-scale (6 to 8 m) migrations within the upper 30 m during Arctic winter (Ludvigsen et al., 2018). Therefore, the apparent pause of DVM during Antarctic summer may in fact be due to seasonal changes in DVM amplitude as some species undertake shallower migrations during summer that go undetected by conventional sampling (Flores et al., 2014; Daase et al., 2016). Asynchronous migrations throughout the diel cycle may also explain why acoustic records do not detect summer DVM in the Southern Ocean (Cottier et al., 2006).

In addition to photoperiod, other environmental conditions are likely to influence the amplitude of zooplankton DVM during polar summer. Phytoplankton blooms may halt DVM as zooplankton remain in surface waters to feed (Cisewski et al., 2010; Cisewski and Strass, 2016). The depth of the subsurface chlorophyll *a* maximum can also influence zooplankton DVM, as observed with Arctic copepods (La et al., 2015a). Similarly, vertically migrating Arctic zooplankton concentrate just below the mixed layer (Berge et al., 2014). In the southern California Current, increased light attenuation results in a decreased amplitude of copepod DVM (Ohman and Romagnan, 2016). The interaction between light conditions and phytoplankton distribution is thus likely to be a key driver of Antarctic zooplankton vertical distribution.

Few studies address polar mesopelagic zooplankton composition and taxon-specific variability in DVM behavior. Arctic zooplankton demonstrate asynchronous DVM patterns, which are explained by variation in feeding ecology, predation risk, and seasonal migration behavior (Fortier et al., 2001; Cottier et al., 2006; Falk-Petersen et al., 2008). Prior studies assessing zooplankton vertical distribution along the Western Antarctic Peninsula (WAP) have either focused on specific taxonomic groups (e.g., Nordhausen, 1994a; Lopez and Huntley, 1995) or lacked the comparable day and night sampling necessary to assess DVM behavior (Marrari et al., 2011). Additionally, there have not been any comprehensive studies resolving polar DVM variability over interannual timescales.

We analyzed zooplankton diel vertical distribution patterns along the WAP during mid-summer as part of the Palmer Antarctica Long-Term Ecological Research (PAL LTER) program. Zooplankton were sampled at discrete depth intervals through the epi- and mesopelagic zones in paired day and night net tows using a MOCNESS (2009-2017) to assess taxon-specific zooplankton vertical distribution. Day and night epipelagic net tows (1993-2017) throughout the

PAL LTER sampling region provided additional information on DVM behavior. We examined environmental controls (e.g., photoperiod, mixed layer depth) on DVM amplitude in taxa showing clear DVM. Our results show diverse zooplankton DVM modes, depth distributions, and responses to phytoplankton biomass and vertical distribution, all of which can affect zooplankton-mediated carbon export during Antarctic summer.

2. Materials and Methods

2.1. Study region

The PAL LTER study region ranges from Anvers Island (64.77ºS, 64.05ºW) in the north to Charcot Island (69.45ºS, 75.15ºW) in the south, extending from the WAP coast to the continental slope (Ducklow et al., 2012) (Fig. 1). The PAL LTER research grid is composed of sampling lines running perpendicular to the Peninsula every 100 km, and standard grid stations within each line are separated by 20 km (Waters and Smith, 1992). From 1993-2008, the sampling plan included all stations on grid lines 600 to 200. In more recent years, the study area has expanded to include lines 100, 000, and -100, with sampling resolution reduced to three stations per line. As in previous studies, three latitudinal sub-regions were designated to represent hydrographic, sea ice, and ecological gradients (Martinson et al., 2008; Stammerjohn et al., 2008; Steinberg et al., 2015) (Fig. 1), with regional boundaries along sampling grid lines as follows: 'North' (lines 600 to 400), 'South': (lines 300 and 200), and 'Far South' (lines 100 to -100).

2.2. Zooplankton collection

Zooplankton were sampled during austral summer (02 January to 13 February) on annual PAL LTER research cruises aboard the MV *Polar Duke* (1993-1997) and ARSV *Laurence M.*

Gould (1998-2017). Zooplankton sampling was conducted using two types of gear as described below.

2.2.1. Multiple discrete depth sampling through the epi- and mesopelagic zones

A 1.4-m^2 frame, 500-µm mesh Multiple Opening/Closing Net and Environmental Sensing System (MOCNESS) (Wiebe et al., 1985) was used to collect meso- and macrozooplankton in discrete depth intervals from 2009-2017. Each year, paired day (10:07-15:15 local start time) and night (23:03-01:46) MOCNESS tows were carried out in coastal or shelf waters in the 'North', and in most years also the 'South' and 'Far South' (Fig. 1). Sampling time and location were used to calculate solar elevation at the start of tows (Meeus, 1998); daytime solar elevation was > 35.51° and nighttime solar elevation < 0.56°. The MOCNESS was towed obliquely at a speed of 2-2.5 knots, with a typical tow duration of 2.25-3 h. On average, 790 m^3 (range 161-1900 m^3) of water was filtered within a single depth interval as measured by a flow meter mounted on the system.

Eight discrete depth intervals were sampled during the upcast as follows: 500-400, 400-300, 300-250, 250-200, 200-150, 150-100, 100-50, and 50-0 m. Occasionally, the deeper intervals were not sampled when towing in waters shallower than the deep target depths. On four occasions, two depth intervals were combined due to net sampling errors. In these cases, the taxon density in each interval was assumed to equal the density calculated for the combined interval. Sea ice conditions occasionally prevented MOCNESS sampling in the South and Far South regions, therefore, the sample size $n = 7$ for paired day/night tows in the North, while $n = 6$ for the South, and $n = 4$ for the Far South from 2009-2015. Data from additional paired

MOCNESS tows in 2016 and 2017 are presented for euphausiids and salps only (for these taxa, n = 10 for the North, n = 8 for the South, and remains n = 4 for the Far South).

A pair of day (09:54 local start time) and night (22:03) tows was also carried out over the continental slope in 2017 (Fig. 1). In this case, eight discrete depth intervals were sampled during the upcast as follows: 1000-750, 750-500, 500-400, 400-300, 300-200, 200-100, 100-50, and 50-0 m (100-0 m for day, due to a net sampling error). Salp data from this slope sample are presented independent of the coastal and shelf data.

2.2.2. Epipelagic sampling

Macrozooplankton were also collected from 1993-2017 throughout the PAL LTER study area using a 2 x 2 m square, 700-µm mesh Metro net towed obliquely to 120 m (Ross et al., 2008, Steinberg et al., 2015) (Fig. 1). The net depth and tow profile were monitored with a depth sensor linked to the conducting hydro wire. Average volume filtered was 9023 m^3 (range 1715-71929 m^3), calculated using a General Oceanics flow meter suspended in the net opening. Ship speed was 2–2.5 knots while towing, and typical tow duration was 30–35 minutes.

Epipelagic samples were designated night tows when the sun was below the horizon, accounting for atmospheric refraction (calculated solar elevation ≤ -0.833° at the start of the tow) (Atkinson et al., 2008; Steinberg et al., 2015). Sample size varied by taxon (day n = 966-1071 and night n = 181-198), as not all taxa were identified during shipboard processing throughout the time series.

2.3. Taxonomic composition

2.3.1. Discrete depth samples

All euphausiids and salps collected in MOCNESS tows were identified and quantified at sea. Whole samples were then preserved in sodium borate-buffered 4% formaldehyde and shipped to the Virginia Institute of Marine Science (Gloucester Point, VA, USA) for further taxonomic analysis to quantify all non-euphausiid or salp taxa. Samples were size-fractionated using a 5-mm mesh, with all individuals in this larger size fraction identified and counted. This size-fractionation step removed large, abundant taxa (i.e., salps and euphausiids) from the microscopic analysis. At least 1/64 of the < 5-mm size fraction was counted under a stereo dissecting microscope after dividing the sample with a plankton splitter. A minimum of 100 individuals of the most abundant species was enumerated in this smaller size fraction.

Discrete depth analyses focused on abundant taxonomic groups. Five common calanoid copepod species were included: *Metridia gerlachei*, *Calanoides acutus*, *Calanus propinquus*, *Rhincalanus gigas*, and *Paraeuchaeta antarctica*. Identification included adults and conspicuous copepodites. Discrete depth-stratified data were only analyzed for the smaller, but abundant, euphausiids *Thysanoessa macrura* and *Euphausia crystallorophias*, because the larger Antarctic krill *Euphausia superba* was underrepresented due to avoidance of the 1.4-m^2 MOCNESS (Nordhausen, 1994b). The pelagic tunicate *Salpa thompsoni* was included. The thecosome (shelled) pteropod *Limacina helicina antarctica* was analyzed individually while the gymnosome (shell-less) pteropods *Clione antarctica* and *Spongiobranchea australis* were grouped together (as in Thibodeau et al., 2019). *Tomopteris* spp. polychaetes were combined into a single group including *T. carpenteri*. Other groups were analyzed by major taxa, such as ostracods, amphipods (including the hyperiids *Themisto gaudichaudii*, *Cyllopus lucasii*, *Hyperiella*

macronyx, *Hyperoche medusarum*, *Primno macropa*, *Vibilia stebbingi*, *Scina* spp., and the gammarid *Eusirus* spp.), and chaetognaths (inclusive of large, conspicuous *Pseudosagitta gazellae* and *P. maxima*).

2.3.2. Epipelagic samples

Grid-wide epipelagic tows were sorted at sea as reported in Steinberg et al. (2015). All above taxa were included in the analysis of epipelagic samples except for the calanoid copepods and ostracods. The Antarctic krill *Euphausia superba* was included in analysis of epipelagic samples.

2.4. Vertical structure

Night to day ratios (N:D) were calculated to identify diel changes in surface abundance of each taxon. For paired day and night MOCNESS samples, abundance was integrated to 150 m and to 50 m (individuals m^{-2}) when a taxon was present in both the day and night tows (Steinberg et al., 2008). These values are referred to as MOCNESS 150 m N:D and MOCNESS 50 m N:D, respectively. MOCNESS N:D data typically ranged across multiple orders of magnitude and were positively skewed. A relatively few large values were influential on the mean MOCNESS N:D values, typically resulting in large mean values compared to the median (Supplemental Tables 1 and 2). Therefore, the median was used to describe the central tendency of MOCNESS N:D data. Additionally, mean day abundance and mean night abundance were calculated from epipelagic (0-120 m) samples to calculate grid-wide N:D ratios for 1993-2017. These values are referred to as grid-wide 120 m N:D.

The vertical distribution of taxa in the MOCNESS discrete depth samples was quantified using weighted mean depth (WMD). WMD (m) is calculated as follows:

$$WMD = \sum(n_i \times z_i \times d_i) / \sum(n_i \times z_i)$$

where for depth interval *i*, d_i is the midpoint (m), z_i is the interval thickness (m), and n_i is abundance (no. m^{-3}) (Andersen et al., 2001). WMD was only calculated for tows reaching 500 m. Night WMD was subtracted from day WMD to determine the amplitude of diel migration (ΔWMD, m). Data used in the analyses are available at: https://pal.lternet.edu/data.

2.5. Environmental controls

The environmental water column data used in this analysis was collected at sampling stations where paired day-night MOCNESS tows were conducted. Discrete chlorophyll *a* (chl-*a*) measurements were made fluorometrically (Parsons et al., 1984). Primary productivity rates were measured with 24-h incubations of ^{14}C uptake at various light levels (Steemann Nielsen, 1952; Schofield et al., 2018). Both chl-*a* and primary production were depth-integrated to 100 m. The depth of the subsurface chl-*a* maximum (Z_{SCM}) and euphotic zone defined by the 1% isolume ($Z_{1\%}$) were determined with a fluorometer and a photosynthetically active radiation (PAR) sensor, respectively, mounted on the CTD rosette. Mixed layer depth (MLD) was calculated as the depth of maximum buoyancy frequency from the same CTD casts (Carvalho et al., 2017). Photoperiod (hours) was calculated for all day-night MOCNESS tow pairs using latitude and day of year (Kirk, 2011).

2.6. Statistical analyses

Single-factor ANOVA was used to test for differences in ΔWMD and log-adjusted MOCNESS N:D ratios among the North, South, and Far South sub-regions. The significance level (α) was set at 0.05. There was no significant difference among latitudinal sub-regions for any taxa for MOCNESS 150 m N:D or MOCNESS 50 m N:D (ANOVA; $p > 0.06$). All statistical tests were conducted with R version 3.3.2 (R Core Team, 2016).

Differences between day and night surface abundance (0-150 m and 0-50 m) from MOCNESS pairs were tested using the Wilcoxon signed-rank test. This non-parametric test does not require transformation of non-normal data and gave comparable results to the paired *t*-test using log-transformed data (Supplemental Tables 1 and 2). Differences between unpaired day and night grid-wide epipelagic abundance (0-120 m) were tested using the Wilcoxon rank-sum test.

Multiple linear regression was used to identify environmental controls on ΔWMD for taxa that made DVMs from the mesopelagic zone into the epipelagic zone. Only *M. gerlachei* and ostracods were included in this analysis; ΔWMD was not a sensitive metric for *L. h. antarctica*, because it was concentrated in the epipelagic zone, and *Salpa thompsoni* was excluded due to an insufficient sample size. ΔWMD did not differ among latitudinal sub-regions for *M. gerlachei* or ostracods (ANOVA; $p > 0.96$). Therefore, data for the analysis were combined across the entire sampling region.

MOCNESS 50 m N:D was a sensitive metric for taxa that were concentrated in the epipelagic zone or conducted DVM within the epipelagic zone. These taxa included *L. h. antarctica*, *C. acutus*, *R. gigas*, *T. macrura*, and *E. crystallorophias*. Generalized linear models with a gamma distribution and log link function were used to identify environmental controls on

MOCNESS 50 m N:D. The gamma distribution is appropriate for ratios, because it is constrained to positive, continuous values. The log link function also ensures positive fitted values. Significant model fits were not achieved for the shallow migrators *C. acutus* and *E. crystallorophias*.

A suite of nine models was fitted for each individual taxon included in ΔWMD analysis (multiple linear regression) and in MOCNESS 50 m N:D analysis (generalized linear model with gamma distribution and log link function). The water column properties investigated in this study were correlated with one another and therefore were not included in the same models to avoid problematic collinearity. For example, as MLD deepened so did Z_{SCM} (Pearson's $r = 0.69$; $p = 0.0004$). $Z_{1\%}$ deepened as depth-integrated chl-*a* decreased (Pearson's $r = -0.60$; $p = 0.004$) and as Z_{SCM} deepened (Pearson's $r = 0.44$; $p = 0.044$). None of the water column properties were correlated with photoperiod. Therefore, the nine models included each explanatory variable individually (i.e., photoperiod, chl-*a*, Z_{SCM}, $Z_{1\%}$, and MLD) as well as photoperiod paired with each of the water column properties. Model selection statistics are presented in Supplemental Tables 3-7. Final models were selected according to the lowest Akaike Information Criterion value corrected for small sample size (AICc) (Hurvich and Tsai, 1989) using the model.sel function in the MuMIn package (Bartoń, 2016). Presented models satisfied assumptions as verified by plotting residuals versus fitted values and explanatory variables.

3. Results

3.1. Environmental conditions

Mean photoperiod during MOCNESS sampling was 20 h 11 min (range: 17 h 41 min to 21 h 47 min), and mean $Z_{1\%}$, was 47 m (range: 16-81 m). Mean depth-integrated chl-*a* was 126

mg m^{-2} (range: 13-517 mg m^{-2}), and mean depth-integrated primary production was 2489 mg C m^{-2} d^{-1} (range: 605-5354 mg C m^{-2} d^{-1}). Mean MLD was 28 m (range: 5-79 m), and mean Z_{SCM} was 20 m (range: 4-60 m).

3.2. Diel vertical depth distributions by taxon

3.2.1. Calanoid copepods

The calanoid copepod *Metridia gerlachei* was the most abundant taxon in MOCNESS tows and a strong diel vertical migrator (Fig. 2), with a median MOCNESS 150 m N:D of 8.0 (Wilcoxon signed-rank test $p = 0.002$) (Table 1). Much of the *M. gerlachei* population did not migrate and resided between 300-500 m, particularly in the North (Fig. 2a). The *M. gerlachei* depth distribution was more even in the South and Far South (Fig. 2b-c). *Calanoides acutus* was the second-most abundant calanoid and although its abundance from 0-150 m did not differ significantly between day and night (Wilcoxon signed-rank test $p = 0.64$) (Table 1), it was more abundant during night tows from 0-50 m with a median MOCNESS 50 m N:D of 2.3 (Fig. 3d; Table 2) (Wilcoxon signed-rank test $p = 0.001$). Like *M. gerlachei*, *C. acutus* vertical distribution also varied with latitudinal sub-region. *Calanoides acutus* was distributed relatively evenly with depth in the North and South (Fig. 3a-b) but was concentrated between 250-400 m in the Far South (Fig. 3c), where it was also an order of magnitude more abundant at this depth zone compared to the other sub-regions.

In contrast to *M. gerlachei* and *C. acutus, Calanus propinquus*, *Rhincalanus gigas*, and *Paraeuchaeta antarctica* were an order of magnitude less abundant and did not vary appreciably with latitudinal sub-region. *Calanus propinquus* was most abundant in the surface 50 m (Fig. 4a) unlike other calanoid copepods, which had peak abundances in the mesopelagic zone (day and

night). Epipelagic *C. propinquus* abundance did not differ between day and night (Tables 1 and 2). *Rhincalanus gigas* was most abundant from 250-300 m during the day and from 200-250 m at night (Fig. 4b), and abundance in the surface 50 m was significantly greater at night than during the day (Wilcoxon signed-rank test $p = 0.004$). Median *R. gigas* MOCNESS 50 m N:D was 36.6 (Table 2). *Paraeuchaeta antarctica* was most abundant from 300-500 m and mostly remained resident in the mesopelagic zone during day and night (Fig 4c). Although scarce in the epipelagic zone, *P. antarctica* was significantly more abundant from 0-50 m during the day (Wilcoxon signed-rank test $p = 0.012$) (Table 2), which suggests this species conducted reverse DVM.

3.2.2. Euphausiids

The abundant krill species *Thysanoessa macrura* was concentrated in the epipelagic zone during day and night, but ascended at night, especially into the upper 50 m (Fig. 5a). Some degree of DVM by *T. macrura* was supported by all metrics tested. This species was significantly more abundant in 0-50 m depths at night compared to day (Wilcoxon signed-rank test $p = 0.006$) (Table 2), and *T. macrura* median MOCNESS 50 m N:D was 11.7. *Thysanoessa macrura* was also more abundant at night vs. day in the upper 0-150 m (MOCNESS tows; Wilcoxon signed-rank test $p = 0.003$; median MOCNESS 150 m N:D = 1.4) (Table 1) and from 0-120 m during nighttime grid-wide epipelagic tows (Wilcoxon rank-sum test $p = 0.0003$; grid-wide 120 m N:D = 1.6) (Table 3). *Euphausia crystallorophias* was less abundant than *T. macrura*, but similarly was concentrated in the upper 100 m (Fig. 5b) and migrated into the top 50 m at night, as indicated by higher abundance from 0-50 m at night than day (Wilcoxon signed-rank test $p = 0.047$) and a median MOCNESS 50 m N:D of 8.8 (Table 2). *Euphausia*

superba remained in the epipelagic zone through the diel cycle with a grid-wide 120 m N:D of 0.93 (Table 3).

3.2.3. Other crustaceans

Ostracods migrated nightly into the upper 200 m (Fig. 6a), with significantly higher abundance from 0-150 m at night vs. day (Wilcoxon signed-rank test $p = 0.0003$) and a median MOCNESS 150 m N:D of 2.9 (Table 1). Mean ostracod abundance peaked in the 200-250 m layer, where they were about 50% more abundant during day than night (Fig. 6a). Most of the ostracod community did not migrate and resided between 200-500 m throughout the diel cycle. Amphipods were an order of magnitude less abundant than ostracods, with two distinct abundance peaks in the mesopelagic zone during day, and highest abundance from 100-200 m at night (Fig. 6b). Amphipods were significantly more abundant in nighttime epipelagic tows and had a grid-wide 120 m N:D of 2.1 (Wilcoxon rank-sum test $p = 2.6 \times 10^{-12}$) (Table 3).

3.2.4. Salps

Salpa thompsoni was a strong diel vertical migrator. Mean abundance over the continental shelf was highest from 200-400 m during the day, and from 0-200 m at night (Fig. 7a). *Salpa thompsoni* median MOCNESS 150 m N:D was 9.0, although salps were only present in three day-night MOCNESS tow pairs along the continental shelf (Table 1). Salps were also significantly more abundant at night in epipelagic tows, with a grid-wide 120 m N:D of 2.6 (Wilcoxon rank-sum test $p = 7.7 \times 10^{-17}$) (Table 3). Over the continental slope, *S. thompsoni* migrated mostly from daytime residence depths in the 200-300 m layer into the surface 100 m at night (Fig. 7b), with MOCNESS 100 m N:D = 94.6 and MOCNESS 200 m N:D = 6.3. Salps

were relatively scarce below 300 m, although a small, deep peak occurred from 750-1000 m on the slope.

3.2.5. Pteropods

The thecosome (shelled) pteropod *Limacina helicina antarctica* was concentrated in surface waters but also migrated from 150-250 m during the day into the upper epipelagic zone at night (Fig. 8a). This result is supported by their higher abundance in the upper 150 m at night from MOCNESS tows (Wilcoxon signed-rank test $p = 0.021$) (Table 1) and from 0-120 m at night in epipelagic tows (Wilcoxon rank-sum test $p = 0.004$) (Table 3). Median *L. h. antarctica* MOCNESS 150 m N:D was 1.7 (Table 1), and grid-wide 120 m N:D was 1.4 (Table 3). Gymnosome (shell-less) pteropods were less abundant than *L. h. antarctica* in the epipelagic zone and were distributed relatively evenly with depth, with highest mean gymnosome abundance from 0-50 m during the day (Fig. 8b). However, DVM by gymnosomes is indicated grid-wide, with significantly higher abundance at night in the epipelagic zone and a grid-wide 120 m N:D of 1.4 (Wilcoxon rank-sum test $p = 0.0002$) (Table 3).

3.2.6. Gelatinous carnivores

Chaetognaths and *Tomopteris* spp. polychaetes were mostly resident in the mesopelagic zone and relatively scarce from 0-100 m (Fig. 9). Mean abundance of both taxa was highest from 200-250 m during the day and from 150-200 m at night (*Tomopteris* spp. also had a second night peak at 300-400 m) (Fig. 9). Median chaetognath MOCNESS 150 m N:D was 1.0 (Table 1) and although grid-wide 120 m N:D was 0.6, epipelagic abundance did not differ between day and night (Tables 1-3), suggesting chaetognaths did not undergo DVM. However, *Tomopteris* spp.

polychaetes did appear to undergo DVM as they were significantly more abundant during night epipelagic tows and had a grid-wide 120 m N:D of 1.9 (Wilcoxon rank-sum test $p = 0.0002$) (Table 3).

3.3. Environmental controls on DVM

For strong migrators traveling between the mesopelagic and epipelagic zones, migration distance (i.e., ΔWMD) was sensitive to photoperiod and vertical water column structure. For the copepod *M. gerlachei*, photoperiod and Z_{SCM} best explained ΔWMD (Table 4), with *M. gerlachei* making shorter vertical migrations as photoperiod grew longer and when Z_{SCM} was shallower (Fig. 10a). Similarly, photoperiod and MLD best explained ostracod ΔWMD (Table 4). Ostracods made shorter DVMs as photoperiod grew longer and when MLD was deeper (Fig. 10b; note– an outlier that was excluded prior to model selection for ostracods is included for visualization in this figure).

For taxa making shorter-distance DVMs mostly within the epipelagic zone, the magnitude of DVM into the surface layer (i.e., MOCNESS 50 m N:D) was best explained by phytoplankton abundance and distribution. The final models each included a different, single explanatory variable for the copepod *R. gigas*, euphausiid *T. macrura*, and pteropod *L. h. antarctica*. *Rhincalanus gigas* DVM into the surface 50 m decreased as depth-integrated chl-*a* increased (Fig. 11a; Table 5). *Thysanoessa macrura* DVM decreased when MLD was deeper (Fig. 11b), and similarly *L. h. antarctica* DVM decreased when Z_{SCM} was deeper (Fig. 11c – a finding robust to the inclusion of an outlier value – see inset) (Table 5).

4. Discussion

4.1. Zooplankton DVM modes

4.1.1. DVM between epipelagic and mesopelagic zones

Four taxa performed consistent DVM between the mesopelagic zone during day and epipelagic zone at night. The copepod *Metridia gerlachei* migrated into the upper 100 m at night, consistent with results from prior studies in the northern WAP (Hopkins, 1985; Lopez and Huntley, 1995; King and LaCasella, 2003). Similarly, a portion of the ostracod community made relatively extensive (~100 m) DVMs resulting in a 21% decrease in abundance from 200-300 m and a 3.5-fold increase in abundance from 0-200 m at night. Ostracod DVM is well-documented in the Atlantic and Pacific Oceans (Angel, 1979; Steinberg et al., 2008). Population-wide DVM by *Salpa thompsoni* from 300 m into surface waters supports previous observations throughout the Southern Ocean during summer (Piatkowski, 1985; Casareto and Nemoto, 1986; Perissinotto and Pakhomov, 1998; Pakhomov et al., 2011). Although rarely encountered deeper than 300 m during summer, the pteropod *Limacina helicina antarctica* underwent DVM between the epipelagic and upper mesopelagic zones. In the Lazarev Sea, *L. h. antarctica* also conducted DVM from November to February (Hunt et al., 2008). Collectively, *M. gerlachei*, ostracods, *S. thompsoni*, and *L. h. antarctica* constitute an assemblage of strong vertical migrators along the WAP during summer.

Evidence for amphipod, gymnosome pteropod, and *Tomopteris* spp. polychaete DVM was less consistent than for the above species, but these taxa were each more abundant at night compared to day in grid-wide epipelagic tows. All amphipod species were grouped together, but DVM is likely species-specific. For example, the hyperiid amphipod *Cyllopus lucasii* was more abundant through the upper 200 m at night during summer, autumn, and winter in the Lazarev

Sea where there was no evidence for DVM by the hyperiids *Hyperiella dilatata* and *Primno macropa* (Flores et al., 2014). *Themisto gaudichaudii* (synonym *Parathemisto gaudichaudii*) is abundant along the WAP (Steinberg et al., 2015), and this amphipod made DVMs from ~200 m to the surface 50 m in the Atlantic Ocean (Williams and Robins, 1981). Prior evidence for *Clione antarctica* and *Spongiobranchia australis* DVM is inconsistent (Hunt et al., 2008), but our epipelagic day-night abundance data suggest these gymnosome pteropods conduct DVM, likely to feed on their primary prey *L. h. antarctica* (Lalli and Gilmer, 1989; Van der Spoel and Dadon, 1999) in the epipelagic zone at night. At night, *Tomopteris* spp. polychaete abundance decreased 37% from 200-300 m and increased 3-fold in the surface 0-200 m. We suggest a portion of the amphipod, gymnosome, and *Tomopteris* spp. assemblage conducted DVM to feed in the upper 200 m while other individuals remained at depth.

4.1.2. DVM within epipelagic zone

The copepods *Calanoides acutus* and *Rhincalanus gigas* made shallow DVMs from the 50-100 m layer into the upper 50 m at night. Shallow DVMs within the upper 70 m for *C. acutus* and upper 90 m for *R. gigas* were also reported in January near South Georgia (Atkinson et al., 1992a, 1992b). A study in the Drake Passage and northern Antarctic Peninsula found no *C. acutus* DVM during December to March (Huntley and Escritor, 1991), but was limited to vertical resolution of 0-100 and 100-200 m, making it unlikely to detect shallow DVM.

The krill species *Thysanoessa macrura* and *Euphausia crystallorophias* performed shallow DVM. DVM within the epipelagic zone was reported during spring and autumn further north of our study site for *T. macrura* (Loeb and Shulenberger, 1987; Nordhausen, 1994a) and *E. crystallorophias* (using acoustics; Everson, 1987). Summer surveys in the northern WAP

(Nordhausen, 1992) and Amundsen Sea (La et al., 2015b) did not detect DVM by *T. macrura* and *E. crystallorophias*, respectively, possibly due to limitations of sampling methods in detecting shallow DVM. Net avoidance by the larger, faster *E. crystallorophias* was not apparent in the northern WAP during winter (Nordhausen et al. 1994b) but was during autumn (Everson, 1987), which could exaggerate the shallow DVM signal and contribute to higher nighttime abundance depicted in Figure 5b.

4.1.3. DVM within mesopelagic zone

Chaetognaths and the copepod *R. gigas* both undertook a modest DVM within the mesopelagic zone between 150 and 300 m, possibly indicating predator-prey coupling. The chaetognaths *Eukronia hamata* and *Sagitta gazellae* predominately fed on the copepods *C. acutus*, *C. propinquus*, and *M. gerlachei* in the upper 200 m of the Weddell Sea in autumn (Hopkins and Torres, 1989). Chaetognaths along the WAP mainly remained in deeper layers during summer to feed on abundant copepod prey. Although less numerous, *R. gigas* is a larger (Gleiber, 2014), and perhaps preferable, copepod prey item compared to *M. gerlachei* or *C. acutus*.

4.1.4. Reverse DVM

The copepod *Paraeuchaeta antarctica* made relatively short reverse DVMs, from 0-50 m during the day to 50-100 m at night. The primarily carnivorous *P. antarctica* is the largest copepod in this study (mean adult prosome length 7 mm; Gleiber, 2014), making it particularly vulnerable to visual predators in surface waters (Aksnes and Giske, 1993; Ohman and Romagnan, 2016). Reverse DVM is adaptive for species susceptible to predators that undertake

normal DVM (Ohman et al., 1983). The reverse DVM of *P. antarctica* is likely used to avoid vertically migrating visual predators.

4.2. Non-migrating zooplankton

4.2.1. Epipelagic non-migrators

The copepod *Calanus propinquus* was concentrated in the upper 50 m and did not consistently undertake DVM. *Calanus propinquus* feeds omnivorously (Atkinson, 1998; Pasternak and Schnack-Schiel, 2001) and was concentrated in the upper 100 m year-round in the Scotia Sea (Atkinson and Sinclair, 2000). Therefore, it appears *C. propinquus* typically remains resident in surface waters on both seasonal and diel time scales.

The negligible difference between night and day *E. superba* abundance in our 120 m tows was expected since this depth was selected to collect Antarctic krill across its main summer depth range (Ross et al., 1996). Acoustic studies have documented sporadic DVM within the upper 100 m during summer while DVM is more pronounced during spring and autumn (Everson, 1983; Godlewska and Klusek, 1987; Demer and Hewitt, 1995; Ross et al., 1996). The daytime formation of larger schools and nighttime dispersal into smaller schools may be a more consistent predator avoidance behavior for *E. superba* in the summer (Everson, 1983; Zhou and Dorland, 2004; Tarling et al., 2018).

4.2.2. Mesopelagic carnivores and detritivores

The copepod *P. antarctica*, ostracods, chaetognaths, and *Tomopteris* spp. polychaetes were concentrated in the mesopelagic zone regardless of the diel cycle, and together compose a deep carnivorous and detritivorous assemblage. The carnivorous *P. antarctica* (synonym

Euchaeta antarctica) preyed mainly on other copepods in the Weddell Sea (Hopkins and Torres, 1989) and near South Georgia where feeding continued through winter (Øresland and Ward, 1993). Thus, *P. antarctica* likely remains resident in the mesopelagic zone where metazoan prey is sufficiently abundant throughout the year. While vertically migrating ostracods feed in productive surface waters, the more numerous mesopelagic residents feed as carnivores or detritivores (Angel, 1972; Lampitt et al., 1993; Vannier et al., 1998). Elevated ostracod abundance from 200-500 m was also observed in the northern WAP during summer (Blachowiak-Samolyk and Żmijewska, 1997) and in Marguerite Bay during autumn (Marrari et al., 2011). Chaetognaths along the WAP likely remained in deeper layers during summer to feed on abundant copepod prey as previously discussed. Chaetognaths were the numerically dominant macrozooplankton in the mesopelagic zone throughout the year in the Lazarev Sea (Flores et al., 2014) and are similarly important in the WAP mesopelagic zone. Small *Tomopteris* spp. polychaetes in the epipelagic zone fed on phytoplankton in the northern WAP during summer (Phleger et al., 1998) and during autumn in the Weddell Sea (Hopkins and Torres, 1989). However, *Tomopteris spp*. polychaetes in the mesopelagic zone are carnivores or detritivores (Steinberg et al., 1994; Jumars et al., 2015). In particular, individuals larger than 20 mm are primarily carnivorous (Jumars et al. 2015), and large *Tomopteris* spp. individuals in our study exceeded 60 mm, further supporting their role as carnivores in the mesopelagic zone.

Amphipods and gymnosome pteropods were distributed throughout the water column, with a substantial portion of the population residing in the mesopelagic zone during day and night. A diet study in the Weddell Sea during March found multiple amphipod species were feeding mainly on copepods, larval euphausiids, and gelatinous zooplankton (Hopkins and Torres, 1989). Therefore, carnivory explains increased amphipod density below 100 m where

metazoan prey is abundant. Although the highest gymnosome abundance was in surface waters, their consistent mesopelagic presence suggests gymnosomes consume other prey in addition to the shelled pteropod *L. h. antarctica.* A genetic diet analysis of the Arctic *Clione limacina* found this species fed on amphipods and calanoid copepods in addition to shelled pteropods (Kallevik, 2013). Similar to other mesopelagic zooplankton, amphipods and gymnosome pteropods likely have multiple feeding modes.

4.2.3. Seasonal vertical migrators

The copepods *M. gerlachei*, *R. gigas*, and *C. acutus* all make seasonal vertical migrations, although *M. gerlachei* and *R. gigas* feed through winter while *C. acutus* enters diapause at depth once it has acquired sufficient lipid reserves (Atkinson, 1998; Pasternak and Schnack-Schiel, 2001; Schnack-Schiel, 2001). Elevated mesopelagic concentrations for these species in our study are more similar to autumn or winter depth distributions farther north in the Scotia Sea (Atkinson and Sinclair, 2000; Ward et al., 2012). High *M. gerlachei* and *R. gigas* concentrations from 200-500 m are likely indicative of carnivorous and detritivorous feeding, which may be more important along the WAP where the productive season is shorter vs. lower latitudes. High mesopelagic abundance indicates *C. acutus* adults were likely in diapause and had not yet fully begun their ascent (Atkinson and Shreeve, 1995) in the Far South where we sampled pre-bloom conditions and mean depth-integrated chl-*a* was only 38 mg m^{-2}. Reduced seasonal sea ice coverage coincident with increasing phytoplankton biomass in the PAL LTER study area (Stammerjohn et al., 2008; Montes-Hugo et al., 2009) may result in earlier ascents for seasonally migrating copepods.

Indications that the pteropod *L. h. antarctica* conducts a seasonal vertical migration to feed in WAP surface waters during summer and overwinter at depth include that this species was concentrated from 0-100 m during our sampling but was most abundant from 100-200 m during autumn in Marguerite Bay (Marrari et al., 2011). Furthermore, *L. h. antarctica* is typically absent from a moored sediment trap sampling at 170 m on the WAP shelf during summer but commonly collected from June to October (Thibodeau et al., 2020). A seasonal vertical migration for the closely related *Limacina helicina helicina* is also suggested in the Arctic Ocean (Kobayashi, 1974).

4.3. Environmental controls on DVM

4.3.1. DVM between epipelagic and mesopelagic zones

The copepod *M. gerlachei* and ostracods made shorter DVMs as photoperiod increased from 17 to 22 h, consistent with previous work demonstrating the sensitivity of polar zooplankton to seasonal irradiance cycles. Acoustic studies throughout the Southern Ocean (64°S to 74°S) suggest that DVM ceases during summer (Cisewski et al., 2010; Cisewski and Strass, 2016; Picco et al., 2017). In these studies, sound scattering layers remained in surface waters around-the-clock rather than descending during the day. However, our results show some taxa continue to migrate between the epipelagic and mesopelagic zones, responding to relatively small changes in photoperiod during Antarctic summer from 64°S to 70°S.

Metridia gerlachei made DVMs over a greater depth range when Z_{SCM} was deeper, likely due to changing phytoplankton availability and predation risk. Deeper Z_{SCM} was associated with reduced light attenuation. With a deep Z_{SCM}, *M. gerlachei* encountered maximum phytoplankton concentrations farther from the surface at night, but DVM distance increased as *M. gerlachei*

migrated deeper to avoid visual predators during day. This finding is consistent with previous work in the southern California Current, where reduced light attenuation was associated with longer DVM distances – particularly deeper daytime depths – for migrating copepods (Ohman and Romagnan, 2016). *Metridia gerlachei* (mean prosome length 3 mm; Gleiber, 2014) is within the size range of the strongest vertical migrators in that study, and therefore may be similarly susceptible to visual predators. Z_{SCM} thus influences *M. gerlachei* DVM distance directly by concentrating prey distribution and indirectly by modulating predation threat (i.e., via light attenuation).

Ostracods made shorter DVMs when MLD was deeper, likely because migrating ostracods ascended from the mesopelagic zone at night until reaching elevated phytoplankton concentrations in the mixed layer. A shallow mixed layer results in a longer nighttime feeding ascent and a longer return to mesopelagic daytime residence depth. In an acoustic study during Arctic autumn, migrating zooplankton sound scattering layers were coincident with, or just below, the MLD at midnight (Berge et al., 2014). Deeper MLD is associated with reduced sea ice coverage along the WAP (Schofield et al., 2018), which may result in shorter ostracod DVMs under future regional climate conditions.

4.3.2. DVM within epipelagic zone

Depth-integrated chlorophyll *a* concentration influenced DVM by the copepod *R. gigas* within the epipelagic zone. *Rhincalanus gigas* remained in the surface 0-50 m during day and night to feed on elevated phytoplankton biomass, as indicated by decreasing N:D with increasing chl-*a*. Gut content analysis showed *R. gigas* feeds primarily on phytoplankton during summer (Pasternak and Schnack-Schiel, 2001). Elevated chl-*a* was also associated with increased light

attenuation, reducing the susceptibility of *R. gigas* to visual predators in surface waters and limiting any benefit gained by daytime migration out of the upper 50 m. Future long-term declines in regional sea ice coverage, upper ocean stability, and chl-*a* concentration in the PAL LTER study region (Montes-Hugo et al., 2009; Brown et al., 2019) may increase the amplitude of *R. gigas* DVM.

The 0-50 m N:D ratio for the euphausiid *T. macrura* and for the pteropod *L. h. antarctica* increased with shallower MLD and Z_{SCM}, respectively, as these taxa appeared to cue on vertical phytoplankton distribution. MLD and Z_{SCM} were positively correlated in our study. We suggest increased 0-50 m N:D indicates a larger portion of the population migrated into the upper 50 m at night when phytoplankton was concentrated near the surface. When MLD and Z_{SCM} were deeper, *T. macrura* and *L. h. antarctica* DVM into the upper 50 m likely decreased because phytoplankton availability and predator avoidance were both maximized below the 50 m threshold of our sampling resolution. During autumn, Arctic zooplankton sound scattering layers migrated to the MLD at midnight (Berge et al., 2014). Migrating pteropods and copepods ascended to the Z_{SCM} at night during Arctic summer (Daase et al., 2016). Deeper MLD under reduced sea ice conditions along the WAP (Schofield et al., 2018) may result in deeper nighttime distributions for *T. macrura* euphausiids and *L. h. antarctica* pteropods.

4.4. Zooplankton-mediated carbon export

Zooplankton vertical structure and behavior play key roles in mediating carbon export (Steinberg and Landry, 2017; Cavan et al., 2019), and regional, taxon-specific data are needed to accurately model the contribution of zooplankton DVM to the global biological carbon pump (e.g., Aumont et al., 2018; Archibald et al., 2019). DVM between the epipelagic and mesopelagic

zones by WAP zooplankton through Antarctic summer likely results in substantial active carbon transport out of the euphotic zone, which may help resolve surprisingly low regional particle export to primary production ratios (Stukel et al., 2015; Ducklow et al., 2018). Zooplankton DVM is an important control on POC export in the Scotia Sea (Cavan et al., 2015; Liszka et al., 2019), and likely plays a similar role along the WAP where zooplankton fecal pellets constitute 67% of summer POC flux at 170 m (Gleiber et al., 2012). Future work also should estimate active transport of dissolved carbon (i.e., respiration of CO_2 and excretion of DOC at depth). Additionally, seasonal vertical migrators (e.g., *C. acutus* copepods and *L. h. antarctica* pteropods) transfer carbon to the ocean interior as they respire and die in the mesopelagic zone, but this "lipid pump" (for copepods) is yet to be quantified in the Southern Ocean (Kobari et al., 2008; Jónasdóttir et al., 2015). Abundant mesopelagic zooplankton also consume sinking detritus and produce fecal pellets, which regulates POC availability to mesopelagic and benthic food webs (Wilson et al., 2008; Belcher et al., 2017). Our findings show it will be essential to consider species feeding ecology and variable DVM amplitudes when assessing zooplankton roles in Southern Ocean carbon cycling. Finally, documented long-term changes in WAP zooplankton composition (e.g., Steinberg et al., 2015; Thibodeau et al., 2019) as well as phytoplankton biomass and vertical distribution (e.g., Brown et al., 2019) will alter zooplankton-mediated export pathways.

Acknowledgements

Thank you to the Captain, officers, and crew of the ARSV *Laurence M. Gould*, as well as Antarctic Support Contract personnel for their scientific and logistical support. We are grateful to many student volunteers and PAL LTER scientists for support at sea. We thank Joe Cope for

data collection and management efforts on this project, Domi Paxton for laboratory assistance, Miram Gleiber for copepod identification advice, and Nicole Waite for providing CTD and optical data. Comments from Kim Bernard, David Johnson, Walker Smith, Mike Vecchione, and two anonymous reviewers improved this manuscript. This research was supported by the National Science Foundation Antarctic Organisms and Ecosystems Program (PLR-1440435). A.G. "Casey" Duplantier Jr. and the 1st Advantage Credit Union of Newport News, VA, USA provided additional funding to support J.A.C. and P.S.T.'s participation on PAL LTER cruises. This paper is Contribution No. 3907 of the Virginia Institute of Marine Science, William & Mary.

References

Aksnes, D.L., Giske, J., 1993. A theoretical model of aquatic visual feeding. Ecol. Model. 67, 233–250. https://doi.org/10.1016/0304-3800(93)90007-F

Andersen, V., Gubanova, A., Nival, P., Ruellet, T., 2001. Zooplankton Community During the Transition from Spring Bloom to Oligotrophy in the Open NW Mediterranean and Effects of Wind Events. 2. Vertical Distributions and Migrations. J. Plankton Res. 23, 243–261. https://doi.org/10.1093/plankt/23.3.243

Angel, M.V., 1979. Studies on Atlantic halocyprid ostracods: their vertical distributions and community structure in the central gyre region along latitude 30°N from off Africa to Bermuda. Prog. Oceanogr. 8, 3–124. https://doi.org/10.1016/0079-6611(79)90009-0

Angel, M.V., 1972. Planktonic Oceanic Ostracods—Historical, Present and Future. Proc. R. Soc. Edinb. Sect. B Biol. Sci. 73, 213–228. https://doi.org/10.1017/S0080455X00002277

Archibald, K.M., Siegel, D.A., Doney, S.C., 2019. Modeling the Impact of Zooplankton Diel Vertical Migration on the Carbon Export Flux of the Biological Pump. Glob. Biogeochem. Cycles 33, 181–199. https://doi.org/10.1029/2018GB005983

Atkinson, A., 1998. Life cycle strategies of epipelagic copepods in the Southern Ocean. J. Mar. Syst. 15, 289–311. https://doi.org/10.1016/S0924-7963(97)00081-X

Atkinson, A., Shreeve, R.S., 1995. Response of the copepod community to a spring bloom in the Bellingshausen Sea. Deep Sea Res. Part II Top. Stud. Oceanogr. 42, 1291–1311. https://doi.org/10.1016/0967-0645(95)00057-W

Atkinson, A., Siegel, V., Pakhomov, E.A., Rothery, P., Loeb, V., Ross, R.M., Quetin, L.B., Schmidt, K., Fretwell, P., Murphy, E.J., Tarling, G.A., Fleming, A.H., 2008. Oceanic

circumpolar habitats of Antarctic krill. Mar. Ecol. Prog. Ser. 362, 1–23. https://doi.org/10.3354/meps07498

Atkinson, A., Sinclair, J.D., 2000. Zonal distribution and seasonal vertical migration of copepod assemblages in the Scotia Sea. Polar Biol. 23, 46–58. https://doi.org/10.1007/s003000050007

Atkinson, A., Ward, P., Williams, R., Poulet, S.A., 1992a. Diel vertical migration and feeding of copepods at an oceanic site near South Georgia. Mar. Biol. 113, 583–593. https://doi.org/10.1007/BF00349702

Atkinson, A., Ward, P., Williams, R., Poulet, S.A., 1992b. Feeding rates and diel vertical migration of copepods near South Georgia: comparison of shelf and oceanic sites. Mar. Biol. 114, 49–56. https://doi.org/10.1007/BF00350855

Aumont, O., Maury, O., Lefort, S., Bopp, L., 2018. Evaluating the Potential Impacts of the Diurnal Vertical Migration by Marine Organisms on Marine Biogeochemistry. Glob. Biogeochem. Cycles 32, 1622–1643. https://doi.org/10.1029/2018GB005886

Bartoń, K, 2016. MuMIn: Multi-Model Inference. R package version 1.15.6. https://CRAN.R-project.org/package=MuMIn

Belcher, A., Manno, C., Ward, P., Henson, S.A., Sanders, R., Tarling, G.A., 2017. Copepod faecal pellet transfer through the meso- and bathypelagic layers in the Southern Ocean in spring. Biogeosciences 14 (6), 1511–1525. https://doi.org/10.5194/bg-14-1511-2017

Berge, J., Cottier, F., Varpe, Ø., Renaud, P.E., Falk-Petersen, S., Kwasniewski, S., Griffiths, C., Søreide, J.E., Johnsen, G., Aubert, A., Bjærke, O., Hovinen, J., Jung-Madsen, S., Tveit, M., Majaneva, S., 2014. Arctic complexity: a case study on diel vertical migration of zooplankton. J. Plankton Res. 36, 1279–1297. https://doi.org/10.1093/plankt/fbu059

Blachowiak-Samolyk, K., Kwasniewski, S., Richardson, K., Dmoch, K., Hansen, E., Hop, H., Falk-Petersen, S., Mouritsen, L.T., 2006. Arctic zooplankton do not perform diel vertical migration (DVM) during periods of midnight sun. Mar. Ecol. Prog. Ser. 308, 101–116. https://doi.org/10.3354/meps308101

Blachowiak-Samolyk, K., Żmijewska, M.I., 1997. Planktonic Ostracoda in Croker Passage (Antarctic Peninsula) during two austral seasons: summer 1985/1986 and winter 1989. Pol. Polar Res. 18, 79–87.

Brown, M.S., Munro, D.R., Feehan, C.J., Sweeney, C., Ducklow, H.W., Schofield, O.M., 2019. Enhanced oceanic CO_2 uptake along the rapidly changing West Antarctic Peninsula. Nat. Clim. Chang. 9, 678-683. https://doi.org/10.1038/s41558-019-0552-3

Carvalho, F., Kohut, J., Oliver, M.J., Schofield, O., 2017. Defining the ecologically relevant mixed-layer depth for Antarctica's coastal seas. Geophys. Res. Lett. 44, 338–345. https://doi.org/10.1002/2016GL071205

Casareto B.E., Nemoto T., 1986. Salps of the Southern Ocean (Australian Sector) during the 1983-84 summer, with special reference to the species *Salpa thompsoni*, Foxton 1961. Mem. Natl. Inst. Polar Res. 40, 221–239.

Cavan, E.L., Laurenceau-Cornec, E.C., Bressac, M., Boyd, P.W., 2019. Exploring the ecology of the mesopelagic biological pump. Prog. Oceanogr. 176, 102125. https://doi.org/10.1016/j.pocean.2019.102125

Cavan, E.L., Le Moigne, F.A.C., Poulton, A.J., Tarling, G.A., Ward, P., Daniels, C.J., Fragoso, G.M., Sanders, R.J., 2015. Attenuation of particulate organic carbon flux in the Scotia Sea, Southern Ocean, is controlled by zooplankton fecal pellets. Geophys. Res. Lett. 42, 821–830. https://doi.org/10.1002/2014GL062744

Cisewski, B., Strass, V.H., 2016. Acoustic insights into the zooplankton dynamics of the eastern Weddell Sea. Prog. Oceanogr. 144, 62–92. https://doi.org/10.1016/j.pocean.2016.03.005

Cisewski, B., Strass, V.H., Rhein, M., Krägefsky, S., 2010. Seasonal variation of diel vertical migration of zooplankton from ADCP backscatter time series data in the Lazarev Sea, Antarctica. Deep Sea Res. Part I Oceanogr. Res. Pap. 57, 78–94. https://doi.org/10.1016/j.dsr.2009.10.005

Cohen, J.H., Forward Jr., R.B., 2009. Zooplankton Diel Vertical Migration – A Review Of Proximate Control. Oceanogr. Mar. Biol. Annu. Rev. 47, 77–109. https://doi.org/10.1201/9781420094220.ch2

Cottier, F.R., Tarling, G.A., Wold, A., Falk-Petersen, S., 2006. Unsynchronised and synchronised vertical migration of zooplankton in a high Arctic fjord. Limnol. Oceanogr. 51, 2586–2599. https://doi.org/10.4319/lo.2006.51.6.2586

Daase, M., Hop, H., Falk-Petersen, S., 2016. Small-scale diel vertical migration of zooplankton in the High Arctic. Polar Biol. 39, 1213–1223. https://doi.org/10.1007/s00300-015-1840-7

Demer, D.A., Hewitt, R.P., 1995. Bias in acoustic biomass estimates of *Euphausia superba* due to diel vertical migration. Deep Sea Res. Part I Oceanogr. Res. Pap. 42, 455–475. https://doi.org/10.1016/0967-0637(94)E0005-C

Ducklow, H., Clarke, A., Dickhut, R., Doney, S.C., Geisz, H., Huang, K., Martinson, D.G., Meredith, M.P., Moeller, H.V., Montes-Hugo, M., Schofield, O., Stammerjohn, S.E., Steinberg, D., Fraser, W., 2012. The Marine System of the Western Antarctic Peninsula, in: Rogers, A.D., Johnston, N.M., Murphy, E.J., Clarke, A. (Eds.), Antarctic Ecosystems. John Wiley & Sons, Ltd, pp. 121–159. https://doi.org/10.1002/9781444347241.ch5

Ducklow, H.W., Stukel, M.R., Eveleth, R., Doney, S.C., Jickells, T., Schofield, O., Baker, A.R., Brindle, J., Chance, R., Cassar, N., 2018. Spring–summer net community production, new production, particle export and related water column biogeochemical processes in the marginal sea ice zone of the Western Antarctic Peninsula 2012–2014. Philos. Trans. R. Soc. A 376, 20170177. https://doi.org/10.1098/rsta.2017.0177

Everson, I., 1987. Some aspects of the small scale distribution of *Euphausia crystallorophias*. Polar Biol. 8, 9–15. https://doi.org/10.1007/BF00297158

Everson I., 1983. Variations in vertical distribution and density of krill swarms in the vicinity of South Georgia. Mem. Natl. Inst. Polar Res. 27, 84–92.

Falk-Petersen, S., Leu, E., Berge, J., Kwasniewski, S., Nygård, H., Røstad, A., Keskinen, E., Thormar, J., von Quillfeldt, C., Wold, A., Gulliksen, B., 2008. Vertical migration in high Arctic waters during autumn 2004. Deep Sea Res. Part II Top. Stud. Oceanogr. 55, 2275–2284. https://doi.org/10.1016/j.dsr2.2008.05.010

Flores, H., Hunt, B.P.V., Kruse, S., Pakhomov, E.A., Siegel, V., van Franeker, J.A., Strass, V., Van de Putte, A.P., Meesters, E.H.W.G., Bathmann, U., 2014. Seasonal changes in the vertical distribution and community structure of Antarctic macrozooplankton and micronekton. Deep Sea Res. Part I Oceanogr. Res. Pap. 84, 127–141. https://doi.org/10.1016/j.dsr.2013.11.001

Fortier, M., Fortier, L., Hattori, H., Saito, H., Legendre, L., 2001. Visual predators and the diel vertical migration of copepods under Arctic sea ice during the midnight sun. J. Plankton Res. 23, 1263–1278. https://doi.org/10.1093/plankt/23.11.1263

Gleiber, M.R., 2014. Long-term Change in Copepod Community Structure in the Western

Antarctic Peninsula: Linkage to Climate and Implications for Carbon Cycling (Master's Thesis). The College of William & Mary.

Gleiber, M.R., Steinberg, D.K., Ducklow, H.W., 2012. Time series of vertical flux of zooplankton fecal pellets on the continental shelf of the western Antarctic Peninsula. Mar. Ecol. Prog. Ser. 471, 23-36. https://doi.org/10.3354/meps10021

Gliwicz, M.Z., 1986. Predation and the evolution of vertical migration in zooplankton. Nature 320, 746–748. https://doi.org/10.1038/320746a0

Godlewska, M., Klusek, Z., 1987. Vertical distribution and diurnal migrations of krill — *Euphausia superba* Dana — from hydroacoustical observations, SIBEX, December 1983/January 1984. Polar Biol. 8, 17–22. https://doi.org/10.1007/BF00297159

Hays, G.C., 2003. A review of the adaptive significance and ecosystem consequences of zooplankton diel vertical migrations, in: Migrations and Dispersal of Marine Organisms. Springer, pp. 163–170. https://doi.org/10.1007/978-94-017-2276-6_18

Hobbs, L., Cottier, F.R., Last, K.S., Berge, J., 2018. Pan-Arctic diel vertical migration during the polar night. Mar. Ecol. Prog. Ser. 605, 61–72. https://doi.org/10.3354/meps12753

Hopkins, T.L., 1985. The Zooplankton community of Croker Passage, Antarctic Peninsula. Polar Biol. 4, 161–170. https://doi.org/10.1007/BF00263879

Hopkins, T.L., Torres, J.J., 1989. Midwater food web in the vicinity of a marginal ice zone in the western Weddell Sea. Deep Sea Res. Part I Oceanogr. Res. Pap. 36, 543–560. https://doi.org/10.1016/0198-0149(89)90005-8

Hunt, B.P.V., Pakhomov, E.A., Hosie, G.W., Siegel, V., Ward, P., Bernard, K., 2008. Pteropods in Southern Ocean ecosystems. Prog. Oceanogr. 78, 193–221. https://doi.org/10.1016/j.pocean.2008.06.001

Huntley, M., Escritor, F., 1991. Dynamics of *Calanoides acutus* (Copepoda: Calanoida) in Antarctic coastal waters. Deep Sea Res. Part I Oceanogr. Res. Pap. 38, 1145–1167. https://doi.org/10.1016/0198-0149(91)90100-T

Hurvich, C.M., Tsai, C.-L., 1989. Regression and time series model selection in small samples. Biometrika 76, 297–307. https://doi.org/10.1093/biomet/76.2.297

Jónasdóttir, S.H., Visser, A.W., Richardson, K., Heath, M.R., 2015. Seasonal copepod lipid pump promotes carbon sequestration in the deep North Atlantic. Proc. Natl. Acad. Sci. 112, 12122–12126. https://doi.org/10.1073/pnas.1512110112

Jumars, P.A., Dorgan, K.M., Lindsay, S.M., 2015. Diet of Worms Emended: An Update of Polychaete Feeding Guilds. Annu. Rev. Mar. Sci. 7, 497-520. https://doi.org/10.1146/annurev-marine-010814-020007

Kallevik, I.H.F., 2013. Alternative prey choice in the pteropod *Clione limacina* (Gastropoda) studied by DNA-based methods (Master's Thesis). UiT Norges arktiske universitet.

King, A., LaCasella, E.L., 2003. Seasonal variations in abundance, diel vertical migration, and population structure of *Metridia gerlachei* at Port Foster, Deception Island, Antarctica. Deep Sea Res. Part II Top. Stud. Oceanogr. 50, 1753–1763. https://doi.org/10.1016/S0967-0645(03)00091-2

Kirk, J.T.O., 2011. Light and Photosynthesis in Aquatic Ecosystems, 3rd ed. Cambridge University Press, Cambridge.

Klevjer, T.A., Irigoien, X., Røstad, A., Fraile-Nuez, E., Benítez-Barrios, V.M., Kaartvedt, S., 2016. Large scale patterns in vertical distribution and behaviour of mesopelagic scattering layers. Sci. Rep. 6, srep19873. https://doi.org/10.1038/srep19873

Kobari, T., Steinberg, D.K., Ueda, A., Tsuda, A., Silver, M.W., Kitamura, M., 2008. Impacts of

ontogenetically migrating copepods on downward carbon flux in the western subarctic Pacific Ocean. Deep Sea Res. Part II Top. Stud. Oceanogr. 55, 1648–1660. https://doi.org/10.1016/j.dsr2.2008.04.016

Kobayashi, H.A., 1974. Growth cycle and related vertical distribution of the thecosomatous pteropod *Spiratella* ("*Limacina*") *helicina* in the central Arctic Ocean. Mar. Biol. 26, 295–301. https://doi.org/10.1007/BF00391513

La, H.S., Kang, M., Dahms, H.-U., Ha, H.K., Yang, E.J., Lee, H., Kim, Y.N., Chung, K.H., Kang, S.-H., 2015a. Characteristics of mesozooplankton sound-scattering layer in the Pacific Summer Water, Arctic Ocean. Deep Sea Res. Part II Top. Stud. Oceanogr. 120, 114–123. https://doi.org/10.1016/j.dsr2.2015.01.005

La, H.S., Lee, H., Fielding, S., Kang, D., Ha, H.K., Atkinson, A., Park, J., Siegel, V., Lee, S., Shin, H.C., 2015b. High density of ice krill (*Euphausia crystallorophias*) in the Amundsen sea coastal polynya, Antarctica. Deep Sea Res. Part I Oceanogr. Res. Pap. 95, 75–84. https://doi.org/10.1016/j.dsr.2014.09.002

Lalli, C.M., Gilmer, R.W., 1989. Pelagic snails: the biology of holoplanktonic gastropod mollusks. Stanford University Press.

Lampitt, R.S., Wishner, K.F., Turley, C.M., Angel, M.V., 1993. Marine snow studies in the Northeast Atlantic Ocean: distribution, composition and role as a food source for migrating plankton. Mar. Biol. 116, 689–702. https://doi.org/10.1007/BF00355486

Liszka, C.M., Manno, C., Stowasser, G., Robinson, C., Tarling, G.A., 2019. Mesozooplankton Community Composition Controls Fecal Pellet Flux and Remineralization Depth in the Southern Ocean. Front. Mar. Sci. 6. https://doi.org/10.3389/fmars.2019.00230

Loeb, V.J., Shulenberger, E., 1987. Vertical distributions and relations of euphausiid populations

off Elephant Island, March 1984. Polar Biol. 7, 363–373. https://doi.org/10.1007/BF00293226

Lopez, M.D.G., Huntley, M.E., 1995. Feeding and diel vertical migration cycles of *Metridia gerlachei* (Giesbrecht) in coastal waters of the Antarctic Peninsula. Polar Biol. 15, 21–30.

Ludvigsen, M., Berge, J., Geoffroy, M., Cohen, J.H., De La Torre, P.R., Nornes, S.M., Singh, H., Sørensen, A.J., Daase, M., Johnsen, G., 2018. Use of an Autonomous Surface Vehicle reveals small-scale diel vertical migrations of zooplankton and susceptibility to light pollution under low solar irradiance. Sci. Adv. 4, eaap9887. https://doi.org/10.1126/sciadv.aap9887

Marrari, M., Daly, K.L., Timonin, A., Semenova, T., 2011. The zooplankton of Marguerite Bay, western Antarctic Peninsula—Part II: Vertical distributions and habitat partitioning. Deep Sea Res. Part II Top. Stud. Oceanogr. 58, 1614–1629. https://doi.org/10.1016/j.dsr2.2010.12.006

Martinson, D.G., Stammerjohn, S.E., Iannuzzi, R.A., Smith, R.C., Vernet, M., 2008. Western Antarctic Peninsula physical oceanography and spatio–temporal variability. Deep Sea Res. Part II Top. Stud. Oceanogr. 55, 1964–1987. https://doi.org/10.1016/j.dsr2.2008.04.038

Meeus, J.H., 1998. Astronomical algorithms, 2nd ed. Willmann-Bell, Incorporated, Richmond, VA.

Montes-Hugo, M., Doney, S.C., Ducklow, H.W., Fraser, W., Martinson, D., Stammerjohn, S.E., Schofield, O., 2009. Recent changes in phytoplankton communities associated with rapid regional climate change along the western Antarctic Peninsula. Science 323, 1470-1473. https://doi.org/10.1126/science.1164533

Nordhausen, W., 1994a. Distribution and diel vertical migration of the euphausiid *Thysanoessa macrura* in Gerlache Strait, Antarctica. Polar Biol. 14, 219–229. https://doi.org/10.1007/BF00239170

Nordhausen, W., 1994b. Winter abundance and distribution of *Euphausia superba*, *E. crystallorophias*, and *Thysanoessa macrura* in Gerlache Strait and Crystal Sound, Antarctica. Mar. Ecol. Prog. Ser. 109, 131-142.

Nordhausen, W., 1992. Distribution and growth of larval and adult *Thysanoessa macrura* (Euphausiacea) in the Bransfield Strait Region, Antarctica. Mar. Ecol. Prog. Ser. 83, 185–196.

Ohman, M.D., Frost, B.W., Cohen, E.B., 1983. Reverse diel vertical migration: an escape from invertebrate predators. Science 220, 1404–1407. https://doi.org/10.1126/science.220.4604.1404

Ohman, M.D., Romagnan, J.-B., 2016. Nonlinear effects of body size and optical attenuation on Diel Vertical Migration by zooplankton. Limnol. Oceanogr. 61, 765–770. https://doi.org/10.1002/lno.10251

Øresland, V., Ward, P., 1993. Summer and winter diet of four carnivorous copepod species around South Georgia. Mar. Ecol. Prog. Ser. 98, 73–78.

Pakhomov, E.A., Hall, J., Williams, M.J.M., Hunt, B.P.V., Stevens, C.J., 2011. Biology of *Salpa thompsoni* in waters adjacent to the Ross Sea, Southern Ocean, during austral summer 2008. Polar Biol. 34, 257–271. https://doi.org/10.1007/s00300-010-0878-9

Parsons, R.T., Maita, Y., Lalli, C.M., 1984. *A Manual of Chemical and Biological Methods for Seawater Analysis*. Pergammon.

Pasternak, A.F., Schnack-Schiel, S.B., 2001. Feeding patterns of dominant Antarctic copepods:

an interplay of diapause, selectivity, and availability of food. Hydrobiologia 453, 25–36. https://doi.org/10.1023/A:1013147413136

Perissinotto, R., Pakhomov, E.A., 1998. The trophic role of the tunicate *Salpa thompsoni* in the Antarctic marine ecosystem. J. Mar. Syst. 17, 361–374. https://doi.org/10.1016/S0924-7963(98)00049-9

Phleger, C.F., Nichols, P.D., Virtue, P., 1998. Lipids and trophodynamics of Antarctic zooplankton. Comp. Biochem. Physiol. B Biochem. Mol. Biol. 120, 311–323. https://doi.org/10.1016/S0305-0491(98)10020-2

Piatkowski, U., 1985. Distribution, abundance and diurnal migration of macrozooplankton in Antarctic surface waters. Meeresforsch.-Rep. Mar. Res. 30, 264–279.

Picco, P., Schiano, M.E., Pensieri, S., Bozzano, R., 2017. Time-frequency analysis of migrating zooplankton in the Terra Nova Bay polynya (Ross Sea, Antarctica). J. Mar. Syst. 166, 172–183. https://doi.org/10.1016/j.jmarsys.2016.07.010

R Core Team, 2016. R: A language and environment for statistical computing. R Foundation for Statistical Computing, Vienna, Austria. https://www.R-project.org

Ringelberg, J., Van Gool, E., 2003. On the combined analysis of proximate and ultimate aspects in diel vertical migration (DVM) research. Hydrobiologia 491, 85–90. https://doi.org/10.1023/A:1024407021957

Ross, R.M., Quetin, L.B., Lascara, C.M., 1996. Distribution of Antarctic krill and dominant zooplankton west of the Antarctic Peninsula. Antarct. Res. Ser. 70, 199–217.

Ross, R.M., Quetin, L.B., Martinson, D.G., Iannuzzi, R.A., Stammerjohn, S.E., Smith, R.C., 2008. Palmer LTER: Patterns of distribution of five dominant zooplankton species in the

epipelagic zone west of the Antarctic Peninsula, 1993-2004. Deep Sea Res. Part II Top. Stud. Oceanogr. 55, 2086-2105. https://doi.org/10.1016/j.dsr2.2008.04.037

Schnack-Schiel, S.B., 2001. Aspects of the study of the life cycles of Antarctic copepods, in: Copepoda: Developments in Ecology, Biology and Systematics. Springer, pp. 9–24. https://doi.org/10.1007/0-306-47537-5_2

Schofield, O., Brown, M., Kohut, J., Nardelli, S., Saba, G., Waite, N., Ducklow, H., 2018. Changes in the upper ocean mixed layer and phytoplankton productivity along the West Antarctic Peninsula. Philos. Trans. R. Soc. A 376, 20170173. https://doi.org/10.1098/rsta.2017.0173

Stammerjohn, S.E., Martinson, D.G., Smith, R.C., Iannuzzi, R.A., 2008. Sea ice in the western Antarctic Peninsula region: Spatio-temporal variability from ecological and climate change perspectives. Deep Sea Res. Part II Top. Stud. Oceanogr. 55, 2041–2058. https://doi.org/10.1016/j.dsr2.2008.04.026

Steemann Nielsen, E., 1952. The Use of Radio-active Carbon (C^{14}) for Measuring Organic Production in the Sea. Journal du Conseil 18, 117-140.

Steinberg, D.K., Cope, J.S., Wilson, S.E., Kobari, T., 2008. A comparison of mesopelagic mesozooplankton community structure in the subtropical and subarctic North Pacific Ocean. Deep Sea Res. Part II Top. Stud. Oceanogr. 55, 1615–1635. https://doi.org/10.1016/j.dsr2.2008.04.025

Steinberg, D.K., Landry, M.R., 2017. Zooplankton and the Ocean Carbon Cycle. Annu. Rev. Mar. Sci. 9, 413-444. https://doi.org/10.1146/annurev-marine-010814-015924

Steinberg, D.K., Ruck, K.E., Gleiber, M.R., Garzio, L.M., Cope, J.S., Bernard, K.S., Stammerjohn, S.E., Schofield, O.M.E., Quetin, L.B., Ross, R.M., 2015. Long-term

(1993–2013) changes in macrozooplankton off the Western Antarctic Peninsula. Deep Sea Res. Part I Oceanogr. Res. Pap. 101, 54–70. https://doi.org/10.1016/j.dsr.2015.02.009

Steinberg, D.K., Silver, M.W., Pilskaln, C.H., Coale, S.L., Paduan, J.B., 1994. Midwater zooplankton communities on pelagic detritus (giant larvacean houses) in Monterey Bay, California. Limnol. Oceanogr. 39, 1606–1620. https://doi.org/10.4319/lo.1994.39.7.1606

Stich, H.-B., Lampert, W., 1981. Predator evasion as an explanation of diurnal vertical migration by zooplankton. Nature 293, 396–398. https://doi.org/10.1038/293396a0

Stukel, M.R., Asher, E., Couto, N., Schofield, O., Strebel, S., Tortell, P., Ducklow, H.W., 2015. The imbalance of new and export production in the Western Antarctic Peninsula, a potentially "leaky" ecosystem. Glob. Biogeochem. Cycles 29, 1400–1420. https://doi.org/10.1002/2015GB005211

Tarling, G.A., Thorpe, S.E., Fielding, S., Klevjer, T., Ryabov, A., Somerfield, P.J., 2018. Varying depth and swarm dimensions of open-ocean Antarctic krill *Euphausia superba* Dana, 1850 (Euphausiacea) over diel cycles. J. Crustac. Biol. 38, 716–727. https://doi.org/10.1093/jcbiol/ruy040

Thibodeau, P.S., Steinberg, D.K., Stammerjohn, S.E., Hauri, C., 2019. Environmental controls on pteropod biogeography along the Western Antarctic Peninsula. Limnol. Oceanogr. 64, S240–S256. https://doi.org/10.1002/lno.11041

Thibodeau, P.S., Steinberg, D.K., McBride, C.E., Conroy, J.A., Keul, N., Ducklow, H.W., 2020. Long-term observations of pteropod phenology along the Western Antarctic Peninsula. Deep Sea Res. Part I Oceanogr. Res. Pap. 166, 103363. https://doi.org/10.1016/j.dsr.2020.103363

Van der Spoel, S., Dadon, J.R., 1999. Pteropoda, in: South Atlantic Zooplankton. Backhuys, pp. 868–1706.

Vannier, J., Abe, K., Ikuta, K., 1998. Feeding in myodocopid ostracods: functional morphology and laboratory observations from videos. Mar. Biol. 132, 391–408. https://doi.org/10.1007/s002270050406

Ward, P., Atkinson, A., Tarling, G., 2012. Mesozooplankton community structure and variability in the Scotia Sea: A seasonal comparison. Deep Sea Res. Part II Top. Stud. Oceanogr. 59–60, 78–92. https://doi.org/10.1016/j.dsr2.2011.07.004

Waters, K.J., Smith, R.C., 1992. Palmer LTER: A sampling grid for the Palmer LTER program. Antarct. J. U. S. 27, 236–239.

Wiebe, P.H., Morton, A.W., Bradley, A.M., Backus, R.H., Craddock, J.E., Barber, V., Cowles, T.J., Flierl, G.R., 1985. New development in the MOCNESS, an apparatus for sampling zooplankton and micronekton. Mar. Biol. 87, 313–323. https://doi.org/10.1007/BF00397811

Williams, R., Robins, D.B., 1981. Seasonal Variability in Abundance and Vertical Distribution of *Parathemisto gaudichaudi* (Amphipoda: Hyperiidea) in the North East Atlantic Ocean. Mar. Ecol. Prog. Ser. 4, 289–298.

Wilson, S.E., Steinberg, D.K., Buesseler, K.O., 2008. Changes in fecal pellet characteristics with depth as indicators of zooplankton repackaging of particles in the mesopelagic zone of the subtropical and subarctic North Pacific Ocean. Deep Sea Res. Part II Top. Stud. Oceanogr. 55, 1636–1647. https://doi.org/10.1016/j.dsr2.2008.04.019

Zaret, T.M., Suffern, J.S., 1976. Vertical migration in zooplankton as a predator avoidance mechanism. Limnol. Oceanogr. 21, 804–813. https://doi.org/10.4319/lo.1976.21.6.0804

Zhou, M., Dorland, R.D., 2004. Aggregation and vertical migration behavior of *Euphausia superba*. Deep Sea Res. Part II Top. Stud. Oceanogr. 51, 2119–2137. https://doi.org/10.1016/j.dsr2.2004.07.009

Table 1. Diel, depth-integrated zooplankton abundance (0-150 m) from MOCNESS tows along the WAP continental shelf. For euphausiids and *Salpa thompsoni*, Day and Night $n = 22$ (samples from 2009-2017). For all other taxa, Day and Night $n = 17$ (samples from 2009-2015). Night:Day n varies because taxa were not always present in both day and night paired tows. p-values are for the Wilcoxon signed-rank test comparing paired day-night abundance values when a taxon was present in both tows.

	Day (individuals m^{-2})		Night (individuals m^{-2})		Night:Day			
Taxon	**Median**	**Range**	**Median**	**Range**	**Median**	**25% - 75% Quantiles**	***p***	***n***
Calanoid copepods								
Metridia gerlachei	32.7	0.1 - 1975.0	249.5	3.1 - 2860.8	8.0	6.2 - 32.0	0.002	17
Calanoides acutus	37.1	4.2 - 230.6	51.6	7.3 - 269.1	1.0	0.8 - 1.5	0.64	17
Calanus propinquus	4.8	0.0 - 165.4	7.3	1.0 - 75.7	1.7	0.4 - 4.4	0.67	16
Rhincalanus gigas	4.2	0.3 - 20.3	3.9	0.0 - 14.8	1.2	0.5 - 2.3	0.82	16
Paraeuchaeta antarctica	0.9	0.0 - 4.5	1.4	0.0 - 7.1	1.1	0.6 - 2.3	0.68	12
Euphausiids								
Thysanoessa macrura	5.0	0.2 - 60.4	9.9	0.1 - 74.9	1.4	1.1 - 2.5	0.003	22
Euphausia crystallorophias	0.2	0.0 - 18.3	0.1	0.0 - 61.6	0.7	0.5 - 5.6	0.58	11
Other crustaceans								
Ostracoda	3.8	0.0 - 38.2	20.1	1.2 - 219.1	2.9	1.7 – 7.4	0.0003	16
Amphipoda	1.9	0.0 - 8.5	1.3	0.0 - 16.4	0.9	0.6 – 2.1	0.56	15
Gelatinous zooplankton								
Salpa thompsoni †	0.0	0.0 - 19.4	0.0	0.0 - 174.4	9.0	4.5 - 9.0	0.75	3
Limacina helicina antarctica	1.2	0.0 - 53.2	3.4	0.0 - 56.1	1.7	1.2 - 3.6	0.021	13
Gymnosomata	0.5	0.0 - 25.3	0.6	0.0 - 3.3	0.8	0.5 - 1.3	0.34	12
Chaetognatha	24.0	0.7 - 118.6	21.8	1.7 - 84.1	1.0	0.6 - 1.6	0.75	17
***Tomopteris* spp.**	0.04	0.0 - 1.1	0.4	0.0 - 1.6	1.2	1.1 - 6.7	0.30	9

† See Figure 7b for *Salpa thompsoni* data from the continental slope.

Table 2. Diel, depth-integrated zooplankton abundance (0-50 m) from MOCNESS tows along the WAP continental shelf. For euphausiids and *Salpa thompsoni*, Day and Night $n = 22$ (samples from 2009-2017). For all other taxa, Day and Night $n = 17$ (samples from 2009-2015). Night:Day n varies because taxa were not always present in both day and night paired tows. p-values are for the Wilcoxon signed-rank test comparing paired day-night abundance values when a taxon was present in both tows.

	Day (individuals m^{-2})		Night (individuals m^{-2})		Night:Day			
Taxon	**Median**	**Range**	**Median**	**Range**	**Median**	**25% - 75% Quantiles**	***p***	***n***
Calanoid copepods								
Metridia gerlachei	4.0	0.0 - 153.8	7.6	0.0 - 948.6	1.8	1.4 - 7.0	0.013	13
Calanoides acutus	9.0	0.0 - 76.0	13.8	0.0 - 155.5	2.3	1.6 - 2.9	0.001	12
Calanus propinquus	0.2	0.0 - 159.5	4.0	0.0 - 62.0	2.1	0.9 - 4.2	0.38	8
Rhincalanus gigas	0.3	0.0 - 4.9	13.8	0.0 - 155.5	36.6	18.2 – 112.4	0.004	9
Paraeuchaeta antarctica	4.0	0.0 - 62.0	0.1	0.0 - 1.6	0.2	0.1 - 0.4	0.012	9
Euphausiids								
Thysanoessa macrura	0.2	0.0 - 54.8	3.1	0.1 - 47.1	11.7	3.6 - 19.4	0.006	16
Euphausia crystallorophias	0.0	0.0 - 4.7	0.1	0.0 - 56.3	8.8	4.3 - 13.1	0.047	7
Other crustaceans								
Ostracoda	1.0	0.0 - 23.3	0.9	0.0 - 24.0	1.3	1.0 - 2.1	0.24	11
Amphipoda	0.3	0.0 - 8.0	0.3	0.0 - 3.2	0.7	0.5 - 2.4	0.85	10
Gelatinous zooplankton								
Salpa thompsoni	0.0	0.0 - 5.4	0.0	0.0 - 63.0	1.2	0.6 - 6.5	0.75	3
Limacina helicina antarctica	0.6	0.0 - 28.4	0.9	0.0 - 31.7	2.8	1.7 – 3.6	0.13	9
Gymnosomata	0.0	0.0 - 25.0	0.1	0.0 - 2.5	1.2	0.4 - 1.3	1.00	6
Chaetognatha	1.9	0.0 - 14.2	1.6	0.0 - 10.4	0.9	0.7 - 1.5	0.68	13
***Tomopteris* spp.**	0.0	0.0 - 1.1	0.0	0.0 - 0.8	0.5	NA	NA	1

Table 3. Diel, depth-integrated zooplankton abundance (0-120 m) from grid-wide epipelagic tows across the PAL LTER sampling region from 1993-2017. *n* varies because not all taxa were identified consistently throughout the time series. *p*-values are for the Wilcoxon rank-sum test.

	Day (individuals m^{-2})			Night (individuals m^{-2})				
Taxon	**Mean**	**SE**	***n***	**Mean**	**SE**	***n***	**Night:Day**	***p***
Euphausiids								
Thysanoessa macrura	22.9	2.0	1063	36.9	6.8	197	1.6	0.0003
Euphausia crystallorophias	2.9	0.38	1067	6.2	2.3	196	2.1	0.77
Euphausia superba	13.7	2.0	1071	12.7	6.1	198	0.9	0.001
Other crustaceans								
Amphipoda	0.36	0.025	1026	0.75	0.13	185	2.1	2.6×10^{-12}
Gelatinous zooplankton								
Salpa thompsoni	4.9	1.4	1069	12.5	3.0	197	2.6	7.7×10^{-17}
Limacina helicina antarctica	7.3	0.62	1056	9.9	1.1	195	1.4	0.004
Gymnosomata	0.22	0.014	1050	0.31	0.039	193	1.4	0.0002
Chaetognatha	1.5	0.16	994	0.88	0.20	183	0.6	0.088
***Tomopteris* spp.**	0.051	0.0049	966	0.095	0.014	181	1.9	0.0002

Table 4. Statistics from multiple linear regression models assessing the impact of environmental variables on zooplankton ΔWMD from MOCNESS tows (0-500 m) along the WAP continental shelf from 2009-2015.

Variable	*n*	Coefficient	SE	*t*	*p*	Partial R^2
***Metridia gerlachei* ΔWMD (adjusted R^2 = 0.76; *p* = 0.001)**	11					
Photoperiod		-19.8	4.6	-4.3	0.003	0.70
Depth of chl-*a* maximum		2.27	0.47	4.8	0.001	0.75
Intercept		400.0	92.5	4.3	0.003	
Ostracoda ΔWMD (adjusted R^2 = 0.79; *p* = 0.002)	10					
Photoperiod		-12.1	3.0	-4.1	0.005	0.70
Mixed layer depth		-0.666	0.23	-2.9	0.022	0.55
Intercept		283.8	59.7	4.8	0.002	

Table 5. Statistics from generalized linear models (with a gamma distribution and log link function) assessing the impact of environmental variables on zooplankton 50m N:D from MOCNESS tows along the WAP continental shelf from 2009-2015 (for *Rhincalanus gigas* and *Limacina helicina antarctica*) and 2009-2017 (for *Thysanoessa macrura*).

Variable	*n*	Coefficient	SE	*t*	*p*
***Rhincalanus gigas* 50m N:D (deviance explained = 35%)**	8				
Chl-*a* concentration		-0.0088	0.0031	-2.8	0.031
Intercept		5.15	0.41	12.6	1.5×10^{-5}
***Thysanoessa macrura* 50m N:D (deviance explained = 27%)**	15				
Mixed layer depth		-0.035	0.011	-3.1	0.008
Intercept		3.67	0.42	8.7	8.8×10^{-7}
***Limacina helicina antarctica* 50m N:D (deviance explained = 40%)**	8				
Depth of chl-*a* maximum		-0.055	0.020	-2.7	0.035
Intercept		2.06	0.61	3.4	0.015

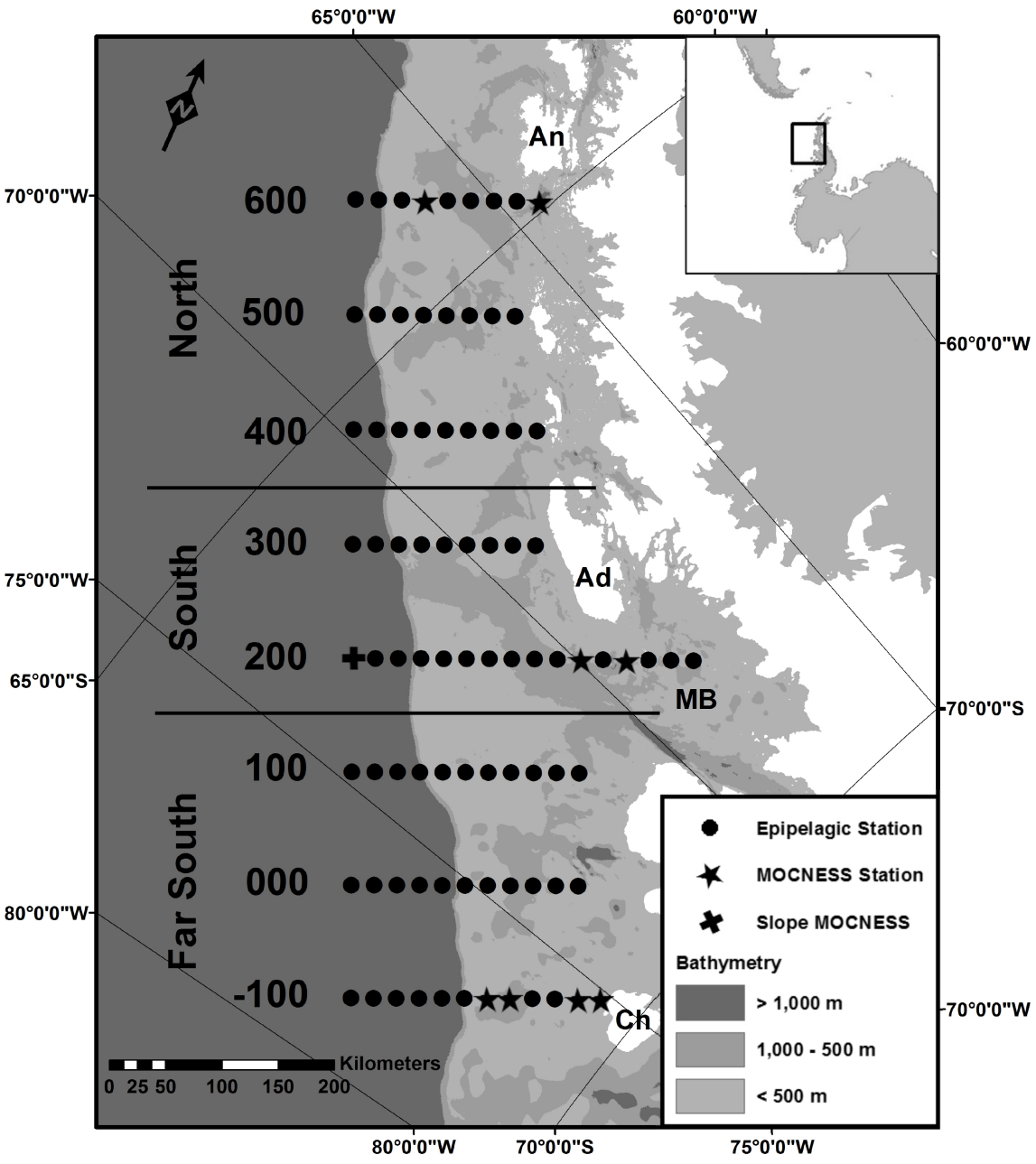

Figure 1. PAL LTER study area along the Western Antarctic Peninsula. 'North,' 'South,' and 'Far South' regions are indicated. Circles indicate epipelagic sampling stations (1993-2017). Stars indicate paired day-night MOCNESS sampling locations on the shelf (2009-2017). Cross indicates paired day-night MOCNESS sampling station on the slope (2017). Shading indicates bathymetry. An: Anvers Island; Ad: Adelaide Island; MB: Marguerite Bay; Ch: Charcot Island.

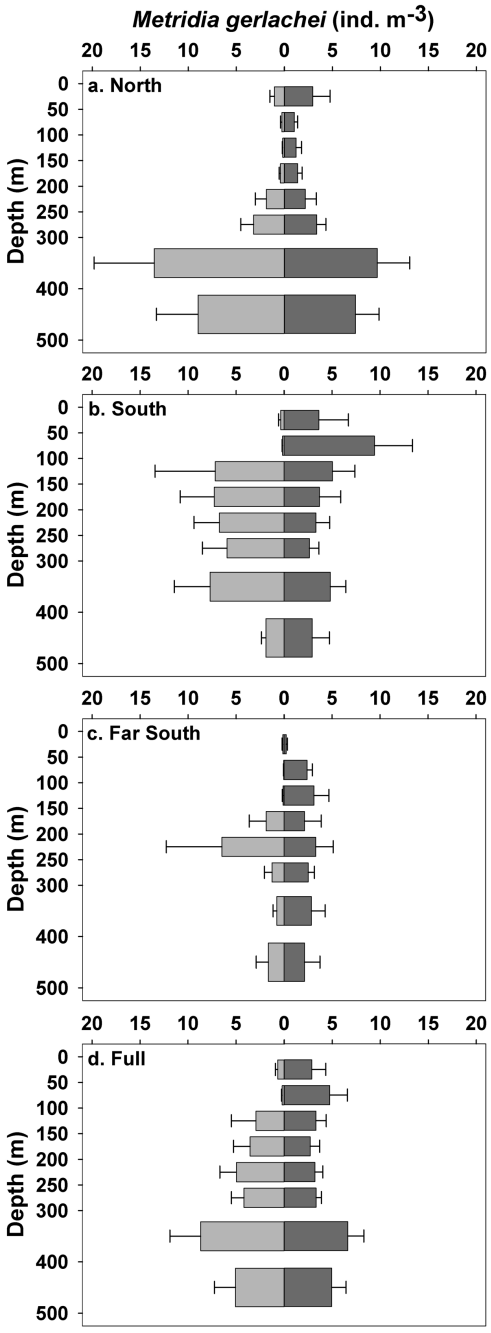

Figure 2. Mean day (light gray, left) and night (dark gray, right) abundance of the calanoid copepod *Metridia gerlachei* in the North (a), South (b), Far South (c) sub-regions, and full shelf sampling region (d) at discrete depth intervals from 0-500 m. Error bars indicate one standard error. North n = 5-7; South n = 5-6; Far South n = 2-4; Full n = 12-17.

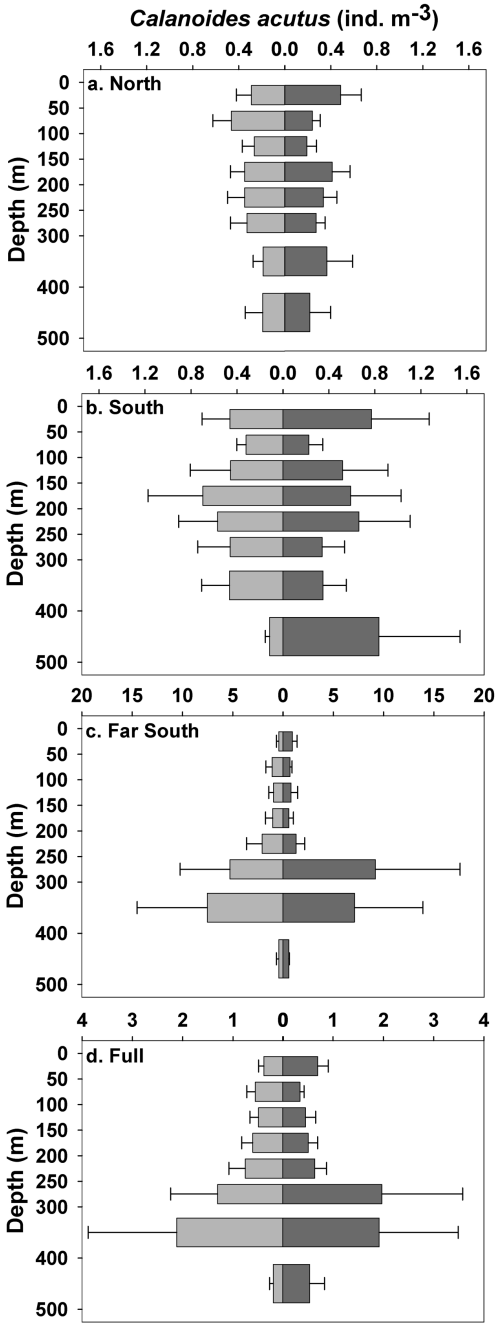

Figure 3. Mean day (light gray, left) and night (dark gray, right) abundance of the calanoid copepod *Calanoides acutus* in the North (a), South (b), Far South (c) sub-regions, and full shelf sampling region (d) at discrete depth intervals from 0-500 m. Error bars indicate one standard error. North n = 5-7; South n = 5-6; Far South n = 2-4; Full n = 12-17. Note different scaling on x-axes.

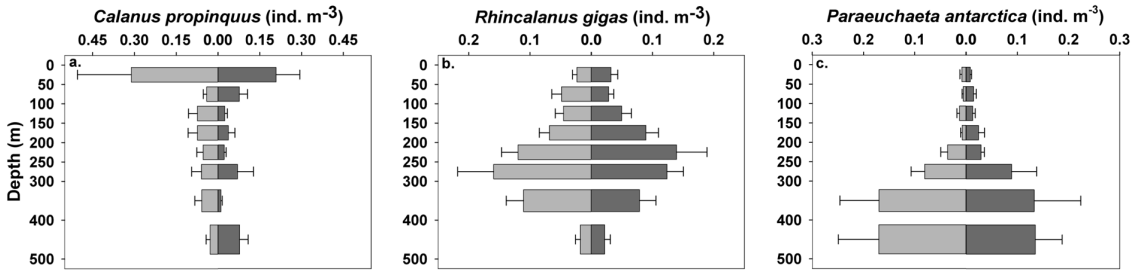

Figure 4. Mean day (light gray, left) and night (dark gray, right) abundance of the calanoid copepods *Calanus propinquus* (a), *Rhincalanus gigas* (b), and *Paraeuchaeta antarctica* (c) sampled at discrete depth intervals from 0-500 m for the full shelf sampling region. Error bars indicate one standard error. Full n = 12-17. Note different scaling on x-axes.

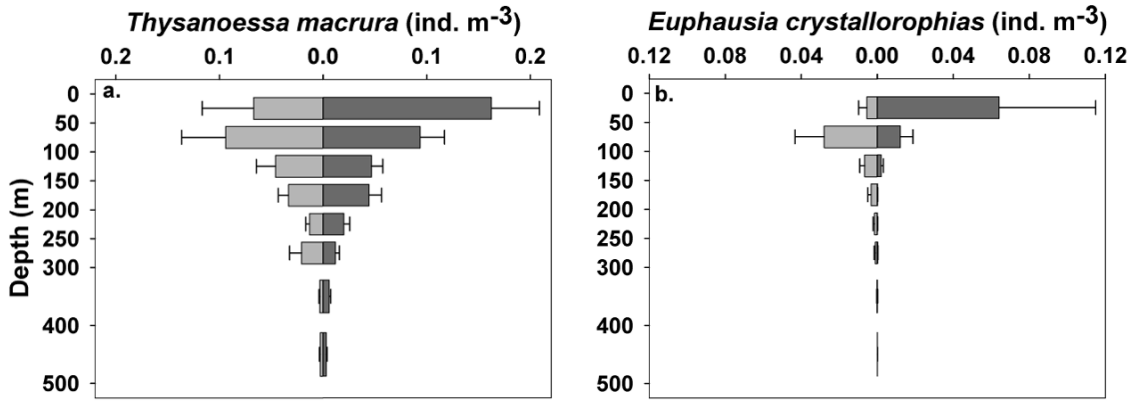

Figure 5. Mean day (light gray, left) and night (dark gray, right) abundance of the euphausiids *Thysanoessa macrura* (a) and *Euphausia crystallorophias* (b) sampled at discrete depth intervals from 0-500 m for the full shelf sampling region. Error bars indicate one standard error. Full n = 17-22. Note different scaling on x-axes.

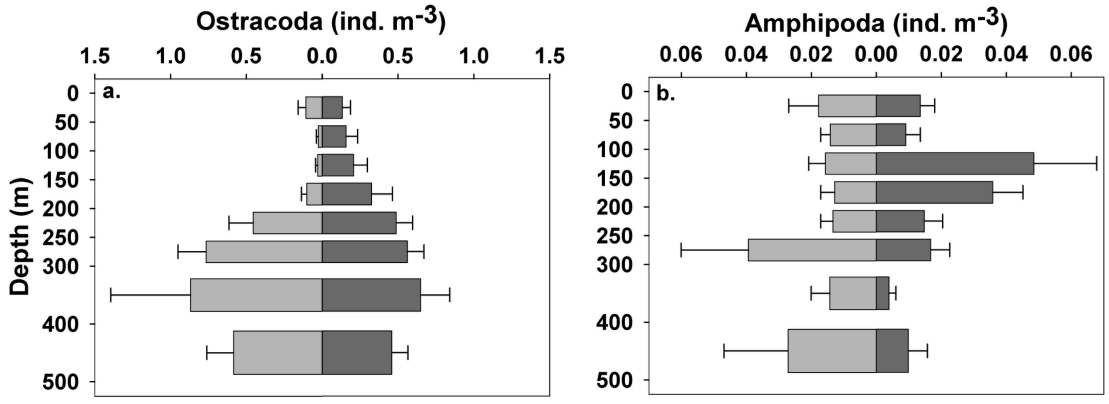

Figure 6. Mean day (light gray, left) and night (dark gray, right) abundance of ostracods (a) and amphipods (b) sampled at discrete depth intervals from 0-500 m for the full shelf sampling region. Error bars indicate one standard error. Full n = 12-17. Note different scaling on x-axes.

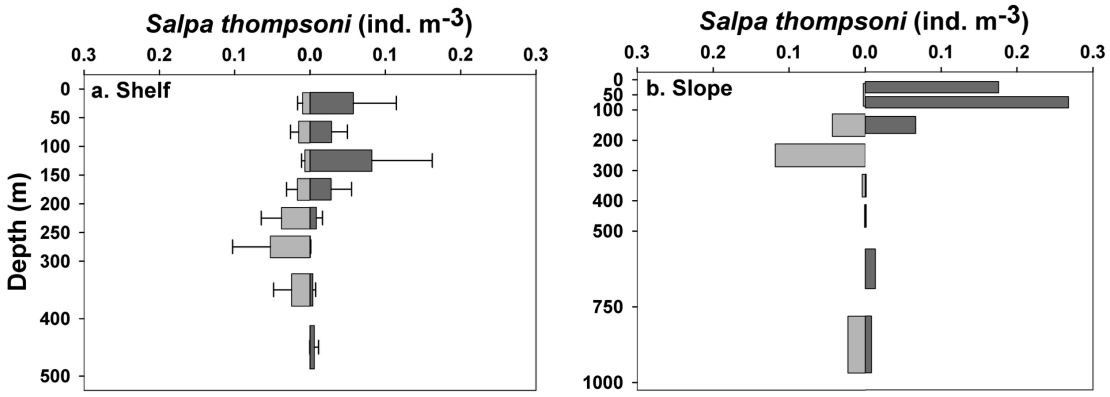

Figure 7. Mean day (light gray, left) and night (dark gray, right) abundance of *Salpa thompsoni* from the full continental shelf sampling region (a) and a single pair of tows on the continental slope (b) sampled at discrete depth intervals from 0-500 m and 0-1000 m, respectively. Error bars indicate one standard error. Full Shelf n = 17-22; Slope n = 1. Note different scaling on y-axes.

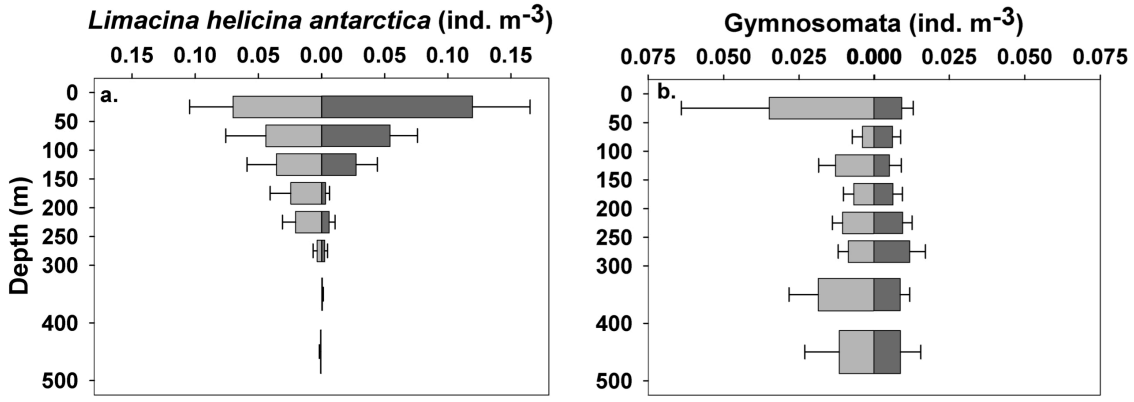

Figure 8. Mean day (light gray, left) and night (dark gray, right) abundance of the pteropod *Limacina helicina antarctica* (a) and gymnosome pteropods (b) sampled at discrete depth intervals from 0-500 m for the full shelf sampling region. Error bars indicate one standard error. Full n = 12-17. Note different scaling on x-axes.

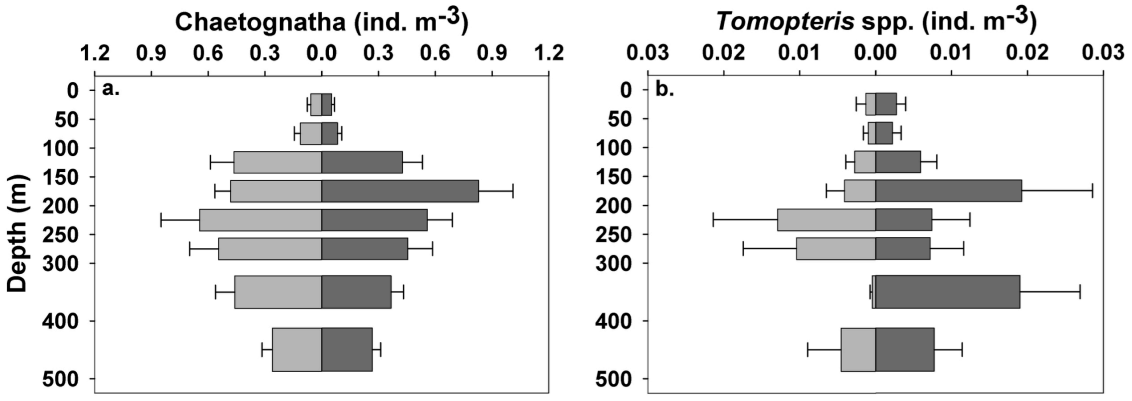

Figure 9. Mean day (light gray, left) and night (dark gray, right) abundance of chaetognaths (a) and *Tomopteris* spp. polychaetes (b) sampled at discrete depth intervals from 0-500 m for the full shelf sampling region. Error bars indicate one standard error. Full n = 12-17. Note different scaling on x-axes.

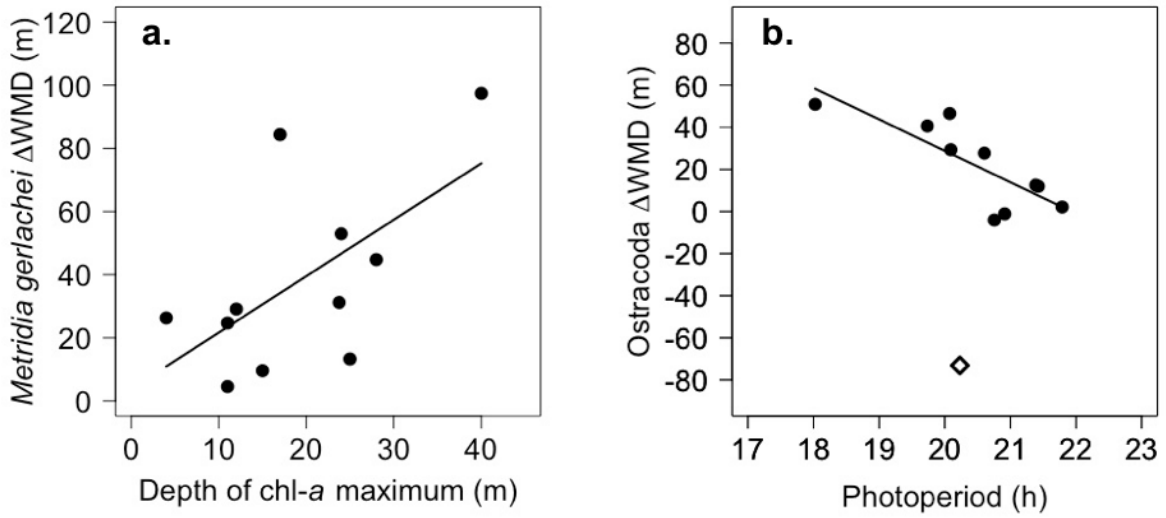

Figure 10. Environmental controls on ΔWMD. (a) Depth of chlorophyll *a* maximum versus *Metridia gerlachei* ΔWMD. (b) Photoperiod versus Ostracod ΔWMD. Solid lines indicate the linear regression with all *M. gerlachei* data points and without the ostracod outlier value, indicated by an open diamond. *M. gerlachei*: $n = 11$, $p = 0.048$, $R^2 = 0.30$; Ostracod (without outlier): $n = 10$, $p = 0.005$, $R^2 = 0.60$.

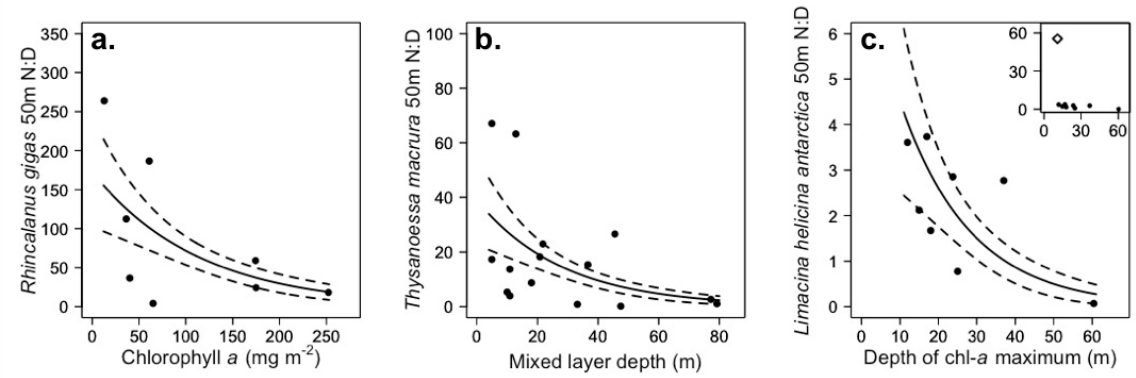

Figure 11. Environmental controls on 50 m N:D. (a) Depth-integrated chlorophyll *a* concentration versus *Rhincalanus gigas* 50 m N:D. (b) Mixed layer depth versus *Thysanoessa macrura* 50 m N:D. (c) Depth of chlorophyll *a* maximum versus *Limacina helicina antarctica* 50 m N:D. Inset includes an outlier *L. h. antarctica* 50 m N:D value indicated by an open diamond. Solid line indicates generalized linear model fit. Dashed lines indicate one standard error. *R. gigas*: $n = 8$, $p = 0.031$, deviance explained = 35%; *T. macrura*: $n = 15$, $p = 0.008$, deviance explained = 27%; *L. h. antarctica* (without outlier): $n = 8$, $p = 0.035$, deviance explained = 40%.

Supplemental Table 1. Diel, depth-integrated zooplankton abundance (0-150 m) from MOCNESS tows along the WAP continental shelf. For euphausiids and *Salpa thompsoni*, Day and Night $n = 22$ (samples from 2009-2017). For all other taxa, Day and Night $n = 17$ (samples from 2009-2015). Night:Day n varies because taxa were not always present in both day and night paired tows. p-values are for the paired t-test comparing log-transformed day-night abundance values when a taxon was present in both tows.

	Day (individuals m^{-2})		Night (individuals m^{-2})		Night:Day			
Taxon	**Mean**	**SE**	**Mean**	**SE**	**Mean**	**SE**	***p t*-test**	***n***
Calanoid copepods								
Metridia gerlachei	168.7	114.0	494.0	169.3	80.2	45.1	0.00004	17
Calanoides acutus	71.8	17.1	74.5	17.5	1.5	0.5	0.64	17
Calanus propinquus	21.2	9.9	15.5	5.0	3.0	0.9	0.47	16
Rhincalanus gigas	5.9	1.4	5.5	1.1	2.9	1.2	0.68	16
Paraeuchaeta antarctica	1.3	0.3	1.8	0.4	4.0	2.1	0.39	12
Euphausiids								
Thysanoessa macrura	10.3	3.3	15.1	3.5	5.0	2.2	0.024	22
Euphausia crystallorophias	2.0	1.0	3.9	2.8	3.5	1.4	0.56	11
Other crustaceans								
Ostracoda	9.3	2.9	38.4	13.0	7.5	2.7	0.0002	16
Amphipoda	2.4	0.5	3.6	1.1	2.5	1.2	0.78	15
Gelatinous zooplankton								
Salpa thompsoni	1.6	1.1	8.4	7.9	6.0	3.0	0.76	3
Limacina helicina antarctica	7.5	3.6	10.1	3.5	3.5	1.1	0.008	13
Gymnosomata	2.6	1.5	1.0	0.3	1.4	0.5	0.40	12
Chaetognatha	31.7	7.5	28.1	5.4	1.6	0.4	0.90	17
***Tomopteris* spp.**	0.25	0.1	0.5	0.1	5.1	2.7	0.14	9

Supplemental Table 2. Diel, depth-integrated zooplankton abundance (0-50 m) from MOCNESS tows along the WAP continental shelf. For euphausiids and *Salpa thompsoni*, Day and Night $n = 22$ (samples from 2009-2017). For all other taxa, Day and Night $n = 17$ (samples from 2009-2015). Night:Day n varies because taxa were not always present in both day and night paired tows. p-values are for the paired t-test comparing log-transformed day-night abundance values when a taxon was present in both tows.

	Day (individuals m^{-2})		Night (individuals m^{-2})		Night:Day			
Taxon	**Mean**	**SE**	**Mean**	**SE**	**Mean**	**SE**	***p t*-test**	***n***
Calanoid copepods								
Metridia gerlachei	29.2	10.9	127.4	64.4	889.5	884.0	0.044	13
Calanoides acutus	19.2	5.4	34.7	10.6	2.4	0.3	0.000	12
Calanus propinquus	15.6	9.6	10.4	4.2	14.7	12.6	0.25	8
Rhincalanus gigas	1.2	0.4	1.6	0.6	79.4	30.3	0.000	9
Paraeuchaeta antarctica	10.4	4.2	0.4	0.1	0.3	0.1	0.004	9
Euphausiids								
Thysanoessa macrura	3.4	2.5	8.1	2.3	17.3	5.1	0.000	16
Euphausia crystallorophias	0.3	0.2	3.2	2.5	9.9	3.2	0.034	7
Other crustaceans								
Ostracoda	4.1	1.7	5.0	1.8	2.3	0.9	0.53	11
Amphipoda	0.9	0.5	0.7	0.2	1.5	0.4	0.66	10
Gelatinous zooplankton								
Salpa thompsoni	0.5	0.3	2.9	2.9	4.3	3.7	0.80	3
Limacina helicina antarctica	3.5	1.7	6.0	2.3	8.1	5.9	0.21	9
Gymnosomata	1.7	1.5	0.5	0.2	0.9	0.3	0.35	6
Chaetognatha	2.9	0.9	2.6	0.8	1.8	0.6	0.44	13
***Tomopteris* spp.**	0.06	0.1	0.1	0.1	0.5	NA	NA	1

Supplemental Table 3. Summary of model selection statistics from multiple linear regression models assessing the impact of environmental variables on *Metridia gerlachei* ΔWMD from MOCNESS tows (0-500 m) along the WAP continental shelf from 2009-2015. Statistics – AICc: corrected Akaike Information Criterion; ΔAICc: difference from lowest AICc; AICc weight – relative model support or probability. Explanatory variables – Photoperiod: day length; Z_{SCM}: depth of subsurface chlorophyll *a* maximum; MLD: mixed layer depth; Chl: chlorophyll *a* concentration depth-integrated to 100 m; $Z_{1\%}$: depth of 1% surface irradiance.

Explanatory variables	AICc	ΔAICc	AICc weight
Photoperiod + Z_{SCM}	101.3	0.00	0.967
Z_{SCM}	109.3	7.95	0.018
Photoperiod	111.2	9.83	0.007
MLD	113.9	12.60	0.002
Chl	114.1	12.72	0.002
Photoperiod + MLD	114.2	12.85	0.002
$Z_{1\%}$	114.3	12.99	0.001
Photoperiod + $Z_{1\%}$	116.4	15.05	0.001
Photoperiod + Chl	116.4	15.07	0.001

Supplemental Table 4. Summary of model selection statistics from multiple linear regression models assessing the impact of environmental variables on Ostracoda ΔWMD from MOCNESS tows (0-500 m) along the WAP continental shelf from 2009-2015. Statistics and explanatory variables as defined for Supplementary Table 3.

Explanatory variables	AICc	ΔAICc	AICc weight
Photoperiod + MLD	85.2	0.00	0.666
Photoperiod	87.1	1.96	0.250
MLD	91.3	6.13	0.031
Photoperiod + Chl	92.1	6.91	0.021
Photoperiod + Z_{SCM}	92.8	7.69	0.014
Photoperiod + $Z_{1\%}$	93.0	7.84	0.013
$Z_{1\%}$	97.2	12.09	0.002
Z_{SCM}	97.3	12.18	0.002
Chl	97.4	12.22	0.001

Supplemental Table 5. Summary of model selection statistics from generalized linear models (with a gamma error distribution and log link function) assessing the impact of environmental variables on *Rhincalanus gigas* MOCNESS 50 m N:D along the WAP continental shelf from 2009-2015. Statistics and explanatory variables as defined for Supplementary Table 3.

Explanatory variables	AICc	ΔAICc	AICc weight
Chl	95.7	0.00	0.386
Z_{SCM}	96.6	0.88	0.248
$Z_{1\%}$	97.3	1.56	0.177
MLD	97.9	2.22	0.127
Photoperiod	99.7	3.99	0.052
Photoperiod + Chl	105.0	9.29	0.004
Photoperiod + Z_{SCM}	105.8	10.10	0.002
Photoperiod + $Z_{1\%}$	106.0	10.32	0.002
Photoperiod + MLD	106.7	11.00	0.002

Supplemental Table 6. Summary of model selection statistics from generalized linear models (with a gamma error distribution and log link function) assessing the impact of environmental variables on *Thysanoessa macrura* MOCNESS 50 m N:D along the WAP continental shelf from 2009-2017. Statistics and explanatory variables as defined for Supplementary Table 3.

Explanatory variables	AICc	ΔAICc	AICc weight
MLD	117.8	0.00	0.449
Photoperiod + MLD	119.2	1.44	0.218
$Z_{1\%}$	120.7	2.95	0.103
Chl	121.7	3.96	0.062
Photoperiod	122.0	4.19	0.055
Z_{SCM}	122.4	4.64	0.044
Photoperiod + Chl	123.0	5.19	0.033
Photoperiod + Z_{SCM}	124.0	6.24	0.020
Photoperiod + $Z_{1\%}$	124.0	6.59	0.017

Supplemental Table 7. Summary of model selection statistics from generalized linear models (with a gamma error distribution and log link function) assessing the impact of environmental variables on *Limacina helicina antarctica* MOCNESS 50 m N:D along the WAP continental shelf from 2009-2015. Statistics and explanatory variables as defined for Supplementary Table 3.

Explanatory variables	AICc	ΔAICc	AICc weight
Z_{SCM}	35.8	0.00	0.627
Photoperiod	39.4	3.55	0.106
Chl	39.7	3.87	0.091
MLD	39.8	3.96	0.087
$Z_{1\%}$	40.0	4.19	0.077
Photoperiod + Z_{SCM}	44.2	8.41	0.009
Photoperiod + MLD	48.4	12.57	0.001
Photoperiod + Chl	48.5	12.70	0.001
Photoperiod + $Z_{1\%}$	48.7	12.86	0.001

CHAPTER 3
Seasonal and interannual changes in a coastal Antarctic zooplankton community

This chapter is in preparation for submission as: Conroy JA, Steinberg DK, Thomas MI, West LT. Seasonal and interannual changes in a coastal Antarctic zooplankton community.

Abstract

Seasonal fluctuations are key features of high-latitude marine ecosystems, where zooplankton exhibit a wide array of adaptations within their life cycles. Repeated, sub-seasonal sampling of Antarctic zooplankton is rare, even along the West Antarctic Peninsula (WAP) where multidecadal changes in sea ice and phytoplankton are well documented. We quantified zooplankton biomass, size structure, and composition at two coastal time-series stations in the northern WAP over three field seasons (November-March) with different sea-ice, temperature, and phytoplankton conditions. Biomass of mesozooplankton was consistent and low, while high biomass of macrozooplankton occasionally resulted in a 'top-heavy' size distribution. Zooplankton taxonomic composition and size changed between years and throughout each field season as the water column warmed seasonally. Seasonal succession was apparent in decreasing zooplankton size and a shift from herbivores to omnivores. Seasonal abundance patterns for many (but not all) zooplankton taxa shifted by a week or more between two consecutive years, consistent with a two-week shift in the timing of sea-ice breakup and the spring phytoplankton bloom. Climate-induced phenology shifts may result in seasonal trophic mismatches, but flexible life history and feeding ecology can limit the risk of reproductive failure for zooplankton. Record-high temperatures in early 2020 coincided with a bloom of the gelatinous salp *Salpa thompsoni*, which likely had a substantial grazing impact and possibly increased competition for phytoplankton prey. Such conditions are predicted to become more common along the WAP as climate warming progresses, and unraveling the ecological and biogeochemical consequences will require sustained observation.

1. Introduction

The seasonal timing of zooplankton migration, reproduction, and growth is coupled with annual cycles of prey availability and temperature throughout the global ocean (Ji et al. 2010). As a consequence, seasonal patterns of zooplankton biomass and abundance change from year to year (Mackas et al. 2012). These cycles are particularly pronounced in high-latitude ecosystems where zooplankton employ a range of life-history strategies that vary with body size, trophic level, and life span (Visser et al. 2020). The West Antarctic Peninsula (WAP) is one such seasonally-productive ecosystem that has also undergone considerable physical and ecological change over recent decades (Henley et al. 2019). While coastal time-series programs document the intra-seasonal drivers and variability of physical conditions, chemical stocks, and phytoplankton along the WAP since the 1990's (Kim et al. 2016, 2018), such data are scarce for zooplankton.

Limited prior results from sampling on the scale of weeks to months demonstrate the impact of temperature, sea-ice coverage, and phytoplankton biomass on zooplankton growth, reproduction, and distribution in the Southern Ocean. Past work focused on individual macrozooplankton species, such as the Antarctic krill *Euphausia superba* (Bernard et al. 2017, Nardelli et al. 2021), the salp *Salpa thompsoni* (Loeb & Santora 2012, Groeneveld et al. 2020), and the pteropod *Limacina rangii*, the currently recognized name (Janssen et al. 2019) for the species previously called *Limacina helicina antarctica* (Thibodeau et al. 2020). While seasonal shifts in abundance, vertical distribution, and species composition have been described for copepod assemblages in the Southern Ocean (Atkinson 1998, Schnack-Schiel 2001), community-wide (multi-taxa) zooplankton studies with sub-seasonal resolution are particularly rare (Froneman et al. 1997, Hunt & Hosie 2006). Climate-induced phenology shifts may increase the likelihood of seasonal trophic mismatches between zooplankton and phytoplankton

(Richardson 2008, Thackeray et al. 2016), but data limitation hinders the assessment of zooplankton phenology and seasonal succession in the Southern Ocean.

In addition to taxonomy, zooplankton composition and seasonal succession can be related to organismal traits (Litchman et al. 2013, Kiørboe et al. 2018). Size is a key trait that governs an individual's metabolic rate and also has consequences for ecosystem-level processes such as particle export (Brown et al. 2004, Stamieszkin et al. 2015). Different feeding modes are favored during different periods of the annual cycle, resulting in seasonal shifts in both zooplankton and prey (Kenitz et al. 2017). Survival (e.g., seasonal and diel vertical migration) and reproductive traits (e.g., spawn timing) are particularly important in high-latitude environments where zooplankton adapt a range of strategies to endure winter (Visser et al. 2020). These traits provide a useful perspective for interpreting seasonal patterns across the broad range of taxonomic groups that comprise zooplankton assemblages.

To address the above knowledge gaps, we analyzed zooplankton biomass and the abundance of major taxa at two coastal time-series stations as part of the Palmer Antarctica Long-Term Ecological Research (PAL LTER) program. Net sampling was conducted twice per week across three consecutive field seasons to examine changes in spring-summer zooplankton composition. We assessed the impact of environmental conditions (e.g., phytoplankton biomass and temperature) on zooplankton at seasonal to interannual scales. Our findings document the spring-summer seasonal succession of Antarctic zooplankton and provide novel insights on how their phenology may be expected to change under a warming climate.

2. Materials and Methods

2.1. Zooplankton collection

Daytime sampling trips from Palmer Station (64° 46’ S, 64° 03’ W) were conducted aboard a rigid-hulled inflatable boat during three consecutive field seasons spanning austral spring to late summer: 17 November 2017 to 12 March 2018, 6 November 2018 to 11 March 2019, and 6 January 2020 to 2 March 2020. Macro- and mesozooplankton were collected twice weekly as weather permitted southwest of Anvers Island at PAL LTER Stations B and E, respectively located ~1 and 5 km from Palmer Station (Fig. 1). The bottom depth is ~70 m at Station B and ~160 m at Station E, which is northeast of the Palmer Deep canyon. Zooplankton were collected using two net types: a 1 x 1 m square, 700-µm mesh Metro net and a 1-m diameter, 200-µm mesh ring net, which were both towed obliquely to a target depth of 50 m. Duplicate tows were typically conducted with each net at both sampling stations. A General Oceanics flow meter was used to determine the volume of water filtered (mean = 407 ± 106 m^3 std. dev. for 700-µm net; mean = 197 ± 84 m^3 for 200-µm net). Due to a flowmeter malfunction, volume filtered was calculated from a polynomial regression fit with the length of wire out for twelve 200-µm net tows in January 2020. Maximum net depth was estimated during each tow based on the length and angle of wire out and recorded using a Star-Oddi DST centi-TD (mean = 50 ± 4 m std. dev. for 700-µm net; mean = 50 ± 7 m for 200-µm net).

2.2. Zooplankton analysis

The Metro and ring nets were used to quantify different taxa. Both replicate tows with the 700-µm net were assessed for taxonomic composition, and data are presented for the following taxa: euphausiids (krill) *Euphausia superba* and *Thysanoessa macrura*, the thecosome (shelled)

pteropod *Limacina rangii*, gymnosome (un-shelled) pteropods (including *Clione limacina* and *Spongiobranchaea australis*), the salp *Salpa thompsoni* (individuals of the blastozooid life stage > 3 mm and oozooid life stage > 10 mm), amphipods, and larval fishes. These animals were sorted live and counted in the aquarium room at Palmer Station. On rare occasions when subsampling was necessary, a random subsample containing at least 100 individuals of the abundant taxon was taken by stirring the sample to homogenize it and subsampling with an aquarium net.

One of the 200-µm net samples from each station was used for taxonomic analysis, and data are presented for the following taxa: the copepods *Oithona* spp., *Calanoides acutus* (>1 mm only), *Calanus propinquus* (>1 mm only), *Rhincalanus gigas* (>1 mm only), and small calanoids (0.2-1 mm); chaetognaths; asteroid larvae (bipinnaria and brachiolaria stages); and nemertean pilidium larvae. The >1 mm limit for calanoid copepod species ensured consistent classification across analysts. Globigerinid foraminifera data were limited and thus were only analyzed to test an observed association with sea ice. Large taxa (typically > 2 mm) from the 200-µm ring net tows were sorted live and counted at Palmer Station. The complete samples were preserved in 3.7% formaldehyde buffered with sodium borate. Then they were returned to the Virginia Institute of Marine Science (Gloucester Point, VA, USA) for further microscopic enumeration. Preserved samples were size-fractionated with nested sieves into the following five size classes: 0.2-0.5, 0.5-1, 1-2, 2-5, and > 5 mm. All individuals in the three largest size fractions were typically identified and counted. Typically, at least 1/64 of the two smallest size fractions was counted under a stereo dissecting microscope after dividing the sample with a Folsom plankton splitter. Size fractions were split such that at least 100 individuals of the most abundant taxon were present.

The second 200-μm net sample from each station was split in half with a Folsom plankton splitter immediately upon collection. One-half of the catch was processed and flash frozen on board for future analysis. Upon return to Palmer Station, the second half of the catch was size-fractionated with nested sieves (into the same size classes as above), concentrated on pre-weighed 200 μm mesh filters, and frozen at -20° C. Samples were thawed, weighed to determine wet biomass, dried at 60° C for at least 24 hours, and weighed again to determine dry biomass. Zooplankton dry weight density (g dry wt m^{-3}) was then depth-integrated to 50 m (g dry wt m^{-2}).

2.3. Environmental data

Due to the localized nature of sea-ice dynamics, the date of the first Conductivity-Temperature-Depth (CTD) cast at Palmer Station was used to demarcate local sea-ice breakup. In all three years, small-boat operations were delayed until sea-ice concentration declined to ~50%. Satellite-based data provided a broader spatial and multi-decadal context for the date of sea-ice retreat. The satellite-based date of sea-ice retreat was calculated from daily sea-ice concentration for the 50 x 50 km area south and west of Anvers Island using the Bootstrap passive microwave algorithm (version 3.1) (Stammerjohn et al. 2008, Schofield et al. 2017). The date of retreat was defined as the final day for which sea-ice concentration remained above 15% for 5 consecutive days. Local ice coverage was also recorded at the start of each net tow using a scale of 10% increments.

PAL LTER Stations B and E were usually sampled for water column properties on the same mornings of zooplankton collections (Schofield et al. 2017). CTD (SeaBird Electronics Seacat SBE 19plus sensor) casts sampled to depths of 60 and 75 m at Stations B and E,

respectively. Data from downcast profiles were averaged in 1-m bins. The average temperature (T) and maximum temperature (T_{max}) in the upper 50 m were calculated for each cast. Discrete water samples for fluorometric chlorophyll-*a* (chl-*a*) analysis were collected in Niskin bottles at seven depths on the upcast, filtered through Whatman GF/F filters, and frozen at -80° C. Samples were extracted in 90% acetone at -20° C for 24 h and analyzed with a Turner 10AU fluorometer. Chl-*a* profiles were depth-integrated to 50 m. Sampling coverage was greater for these environmental variables than for zooplankton collection across all three field seasons and spanned the following date ranges: 14 November 2017 to 26 March 2018, 2 November 2018 to 28 March 2019, and 2 December 2019 to 19 March 2020.

The coast near Palmer Station experiences a mixed tide, fluctuating between several days of semidiurnal tide (i.e., two high and two low tides each day) and several days of diurnal tide (i.e., one high and one low tide each day) (Amos 1993). The tidal regime influences surface current direction as well as the nearshore biomass and swarm characteristics of *E. superba* (Bernard & Steinberg 2013, Bernard et al. 2017). Tide height data at 1-minute intervals were obtained from the Palmer Station tide gauge via the Antarctic Meteorological Research Center (https://amrc.ssec.wisc.edu/usap/palmer/). The tidal regime for each sampling day was manually classified as diurnal or semidiurnal tide based on the number of maxima and minima in tide level.

2.4. Data analysis

Chl-*a*, zooplankton dry weight, and taxa abundance data were $\log_{10}$-transformed for statistical analysis. Zeroes in the taxa abundance data were replaced with one-half of the lowest non-zero value for a given data set (O'Brien 2013). Average T and T_{max} were not transformed.

Paired *t*-tests tested whether values differed between Stations B and E across the three field seasons. Average T, T_{max}, chl-*a* (n = 106 sample pairs each), and zooplankton dry weight (n = 50 sample pairs) did not differ between stations ($|t| \leq 1.7$; $p \geq 0.10$). The abundance of some taxa did differ between sampling stations, and these results are presented below. One-way ANOVA and Tukey's Honestly Significant Differences (HSD) were used to test whether the mean values of average T, T_{max}, chl *a*, zooplankton dry weight, and taxa abundance differed between years. Pearson's correlation was used to test relationships between known zooplankton predator-prey pairs and an observed connection between foraminifera and sea ice.

Variation in zooplankton size structure was analyzed by plotting normalized biomass size spectra. Normalized biomass was calculated as the dry weight density divided by the size interval of a given size fraction (i.e., 0.3, 0.5, 1, 3, or 5 mm) (Rykaczewski & Checkley 2008). Visual inspection revealed that the larger size fractions (> 2 mm) often contributed relatively high biomass, making it inappropriate to calculate spectral slope from a linear best-fit line. Thus, samples were divided into low (< 0.03 g DW m^{-2}; n = 34 samples), medium (0.03-0.1 g DW m^{-2}; n = 46), and high (> 0.1 g DW m^{-2}; n = 36) zooplankton biomass conditions to allow comparison of the size spectra as a function of total biomass.

A multivariate analysis of the abundance data for 15 taxa was conducted to assess change in taxonomic composition. Foraminifera and oozooids of *S. thompsoni* were excluded from this analysis; blastozooids of *S. thompsoni* were included. This analysis was conducted using the 'vegan' package (version 2.5-7) (Oksanen et al. 2020) in R (R Core Team 2021). When duplicate tows were conducted, the mean of multiple density values was used. Analysis of similarities (ANOSIM) using the Bray-Curtis dissimilarity and 10,000 permutations tested whether community structure differed significantly between years and between Stations B and E.

Non-metric multidimensional scaling (NMDS) was used to visualize the similarity of sampling dates for an individual station within a given year. NMDS is an ordination technique that reduces a multidimensional dataset into a smaller number of dimensions so that similar samples are located closer to one another. NMDS using the Bray-Curtis dissimilarity matrix is able to accommodate zeroes and skewed data. NMDS was executed with the function 'metaMDS' using a square-root transformation and Wisconsin double standardization.

Linear regression analysis on the NMDS ordinations was used to identify the directional gradients of environmental variables hypothesized to impact zooplankton composition (e.g., Dietrich et al. 2021). Days since local sea-ice breakup (based on first day of boat-based sampling) was used to examine the seasonal progression of each year. Average *T* and chl-*a* are commonly related to zooplankton life-history processes (chl-*a* was $\log_{10}$-transformed). Tidal regime was hypothesized to impact zooplankton composition, because it influences local surface currents (Bernard et al. 2017). The resulting vectors indicate the direction of maximal change for a given environmental variable, and the r^2-statistic indicates the correlation strength along a vector's axis. This regression analysis was conducted with the 'envfit' function of 'vegan' using 10,000 permutations.

The central date of zooplankton density was calculated using a "center of gravity" metric for individual biomass size classes and taxa (Edwards & Richardson 2004, Mackas et al. 2012). For this calculation, dates were numbered sequentially beginning with 1 November. The central date for a given size-fraction or taxon was calculated as the sum of the products of daily densities (N_D) and sampled day numbers (D), divided by the sum of daily densities: $\frac{\sum N_D \times D}{\sum N_D}$. Only data collected from 5 December to 12 March were included, as this period was consistently sampled during the 2017-2018 and 2018-2019 field seasons. The 2019-2020 field season was excluded

due to limited sampling coverage. Central dates were calculated individually for Stations B and E. In cases of bimodal distributions, the central date calculated using this method falls between two peaks.

3. Results

3.1. Sea ice and temperature

The date of local sea-ice breakup varied by four weeks across the three field seasons: 16 November 2017, 2 November 2018, and 29 November 2019 (Fig. 2). This interannual pattern in local sea-ice breakup (mid-, early-, and later-season, respectively) corresponds with satellite observations indicating sea-ice retreat dates of 26 November 2017, 23 November 2018, and 7 December 2019 for the area 50 km south and west of Anvers Island.

Water temperature in the upper 50 m (range: -1.7° C to 2.5° C) warmed throughout each field season and differed substantially among years. Winter Water ($T \leq$ -1.2° C) persisted until ~10 December regardless of the timing of local sea-ice breakup (Fig. 2). From mid-December onwards, the water column generally warmed from the surface through depth. During the summer period of 26 December to 21 March, average T and T_{max} differed significantly across years (ANOVA: avg T, $F = 8.4$; T_{max}, $F = 50$; $p < 0.0004$). Average T was colder in 2018-2019 than in the other two years (Tukey's HSD: $p < 0.005$), while T_{max} was significantly different across all years, being warmest in 2019-2020 and coldest in 2018-2019 (Tukey's HSD: $p < 0.00002$) (Table 1).

3.2. Phytoplankton biomass

The timing and magnitude of phytoplankton accumulation changed across field seasons and was related to the timing of local sea-ice breakup. Chl-*a* concentration was low upon sea-ice breakup then increased over the following 2-3 weeks to a peak typically exceeding 200 mg m^{-2} (Fig. 3). Regardless of initial bloom timing, chl-*a* remained relatively high until dropping below 50 mg m^{-2} in January, then increasing above 60 mg m^{-2} in late January and early February each year. A final chl-*a* peak (> 100 mg m^{-2}) occurred in March of each year. Despite similar seasonal patterns, mean chl-*a* differed significantly between years (ANOVA: $F = 3.9$; $p = 0.02$) and was higher in 2018-2019 than in 2017-2018 (Tukey's HSD: $p = 0.039$) or 2019-2020 (Tukey's HSD: $p = 0.061$) (Table 1).

3.3. Zooplankton biomass and size composition

Similar to chl-*a*, zooplankton dry weight (range: 0.007 to 3.0 g m^{-2}) and seasonal patterns differed among years. Zooplankton biomass maxima in December 2017 and January 2018 occurred 2-3 weeks after chl-*a* peaks (Fig. 3a-b). Zooplankton and phytoplankton biomass then both remained low in February and March 2018 (Fig. 3a-b). The following year was characterized by zooplankton biomass peaks in December and February also following phytoplankton peaks (Fig. 3c-d). Mean zooplankton biomass was higher in 2020 than in the other two field seasons (ANOVA: $F = 31$; $p < 10^{-10}$; Tukey's HSD: $p < 10^{-7}$) (Table 1) and was highest during the second half of January, following a phytoplankton peak in late December (Fig. 3e-f).

The size structure of the zooplankton assemblage changed on weekly, seasonal, and annual time scales. The largest (> 5 mm) size class periodically dominated in 2017-2018 (Fig. 4a-b) and 2018-2019 (Fig. 4c-d) but was consistently dominant in 2020 (Fig. 4e-f) when total

biomass was high (Table 1). The 2-5 mm size class was relatively important from January onwards in 2018 and 2019, particularly at Station E (Fig. 4b, d). The smallest (0.2-0.5 mm) size class dominated when animals > 2 mm were scarce, while the intermediate sizes (1-2 mm and 0.5-1 mm) typically constituted less than 20% of total zooplankton biomass (Fig. 4). Comparing the size spectra for low, medium, and high biomass conditions revealed that mesozooplankton (0.2-2 mm) formed a relatively consistent background biomass (Fig. 5). Increased total biomass was due to higher abundance of macrozooplankton (> 2 mm), with the largest size class (> 5 mm) in particular driving the highest biomass conditions (Fig. 5).

3.4. Zooplankton taxonomic composition and seasonal patterns

Multivariate analysis of 15 taxa revealed interannual and seasonal changes in zooplankton composition. Taxonomic composition differed significantly among years (ANOSIM $R = 0.16$ $p = 0.0001$) and between sampling stations (ANOSIM $R = 0.11$; $p = 0.0001$). NMDS scores illustrated seasonal succession (Fig. 6) and were significantly correlated with average *T* and the number of days since sea-ice breakup (Table 2) in all cases except for Station B in 2019-2020 (Fig. 6e). Chl-*a* was significantly correlated with the ordination scores for Station E in 2017-2018 (Fig. 6b; Table 2), and tidal regime was not significantly related with NMDS scores in any case. Central abundance dates averaged over both Stations B and E illustrate overall seasonal succession in zooplankton taxonomic and size class composition (Fig. 7). The earliest mean central abundance dates were for *Euphausia superba* and pteropods, while *Thysanoessa macrura* and the copepods *Calanus propinquus* and *Oithona* spp. were the latest taxa (Fig. 7a). In 2017-2018 and 2018-2019 *E. superba* dominated the > 5 mm size class, which had the earliest mean central biomass date (Fig. 7b). Similarly, *Oithona* spp. and *T. macrura*

respectively dominated the 0.2-0.5 and 2-5 mm size classes, which were the latest size classes (Fig. 7b). Other taxa and size classes had intermediate central abundance and biomass dates.

A seasonal succession in euphausiid species was apparent in all three years (Fig. 8). Although *T. macrura* was more abundant at Station E (Table 3), daily mean density for both euphausiid species was calculated using Stations B and E combined due to frequent absence on a given sampling event. Mean density of *E. superba* was highest in November and December with seasonal declines beginning in January (Fig. 8). *Thysanoessa macrura* was always less abundant than *E. superba* during November and December but was often more abundant in February and always more abundant in March. The central abundance date for *E. superba* was 65 and 57 days earlier than that of *T. macrura* in 2017-2018 and 2018-2019, respectively (Fig. 8a-b). An earlier transition in euphausiid species composition and earlier central abundance dates for *E. superba* and *T. macrura* (7 and 15 days earlier, respectively) coincided with local sea-ice breakup occurring two weeks earlier in 2018-2019 compared to 2017-2018.

Seasonality in gelatinous macrozooplankton was apparent in years when they were abundant. Pteropods were most abundant in 2017-2018 at Station E (Tables 3, 4) where the thecosome (shelled) pteropod *Limacina rangii* and its shell-less gymnosome pteropod predators were positively correlated (Pearson's $r = 0.75$; $p < 0.0001$). Both pteropods declined from early December until March, and their central abundance dates differed by only two days (Fig. 9a). The salp *Salpa thompsoni* bloomed in 2020 (Table 4) and constituted 70% of the zooplankton dry weight on average during that year. Abundance of salp blastozooids peaked in the second half of January, followed by a smaller peak in late February at Station E (where data coverage was extended); conversely, salp oozooids were an order of magnitude more abundant in February vs. January (Fig. 9b).

Copepod seasonal patterns are presented for Station B (Fig. 10), where all groups were more abundant (Table 3). Abundance typically increased rapidly for all groups following sea-ice breakup (Fig. 10), with the exception of *C. propinquus* (Fig. 10c). *Oithona* spp. decreased after this initial peak and then increased from late January until March (Fig. 10a), and *C. propinquus*, *Rhincalanus gigas,* and small calanoids occasionally followed the same pattern (Fig. 10c-e). As the season progressed, abundance of *Calanoides acutus* declined (Fig. 10b), as did *R. gigas* and small calanoids in 2018-2019 (Fig. 10d-e); conversely, *C. propinquus* increased in abundance throughout the 2017-2018 season (Fig. 10c). The copepods *Oithona* spp., *R. gigas*, and small calanoids were less abundant in 2019-2020 compared to preceding years (Table 4). The central abundance dates for *C. acutus*, *C. propinquus*, and *R. gigas* were relatively stable at Station B and changed by ≤ 6 days between 2017-2018 and 2018-2019 (Fig. 10b-d). In contrast, the central abundance dates for *Oithona* spp. and small calanoids respectively were 10 and 19 days earlier in 2018-2019 (Fig. 10a, e) when local sea-ice breakup was 14 days earlier.

Carnivorous zooplankton were also more abundant at Station B (Table 3) and were positively correlated to their prey. At Station B, chaetognaths exhibited dual early- and late-season peaks in 2017-2018 and 2018-2019 and a mid-January peak in 2020 (Fig. 11a), which were also common patterns for copepods (Fig. 10). Across all years and stations, chaetognath abundance was most strongly correlated with that of *Oithona* spp., *R. gigas*, and small calanoid copepods (Pearson's $r = 0.40\text{-}0.51$; $p < 10^{-5}$). Similar to *Oithona* spp. and small calanoids at Station B, chaetognath and amphipod central abundance dates were respectively 19 and 16 days earlier in 2018-2019 compared to 2017-2018 (Fig. 11). Amphipod abundance was relatively steady at Station B in 2017-2018 and 2018-2019 but was higher following sea-ice retreat (Fig. 11b). Chaetognaths were more abundant in 2018-2019 than in other years (Fig. 11a;

Table 4), and the highest amphipod densities occurred in 2020 during the salp bloom (Fig. 11b, 9b; Table 4).

Seasonal changes in planktonic larval abundance were also apparent at Station B. Larval fishes were more abundant at Station B (Table 3), peaked each year shortly after sea-ice breakup, and then continued at moderate levels for ~one month before falling to persistent low concentrations (Fig. 12a). The timing of these seasonal peaks was 1-month later in spring 2017 compared to spring 2018, consistent with interannual changes in the timing of local sea-ice breakup (Fig. 2) and peaks in likely copepod prey (Fig. 10a, e). Central abundance date did not capture this phenological shift for larval fishes, because it was restricted to data from 5 December onward (Fig. 12a). Larval asteroids and nemerteans (Fig. 12b, c, respectively) were most abundant in January in all years, although nemerteans were rare in 2017-2018. Compared to 2017-2018, asteroid central abundance date was 19 days later in 2018-2019 when there was a large summer phytoplankton bloom. In contrast, phenology of nemerteans was similar between years, with their central abundance date varying by only 6 days.

Foraminifera were positively correlated with the local sea-ice coverage at Station E in 2018-2019 (Pearson's $r = 0.62$; $p = 0.0002$) (Fig. 13). Foraminifera abundance was highest upon local sea-ice break-up in November, and subsequent diminishing peaks coincided with periodic ice coverage in December and January, until both foraminifera and sea ice became mostly absent in February and March (Fig. 13).

4. Discussion

4.1. Environmental context

Distinctions between satellite-based and sampling-based estimation for timing of sea-ice retreat emphasize the localized nature of sea-ice processes. Satellite-based sea-ice concentration suggests the timing of sea-ice retreat across the three years of this study was consistent with the 1979-2020 average, with the dates of sea-ice retreat for the 50 x 50 km area near Palmer Station being within nine days of the long-term mean (28 November ± 30 days std. dev.). While sea-ice duration along the WAP is characterized by high variability and multi-decadal decline, this is primarily due to the changing date of advance, rather than the relatively stable date of retreat (Stammerjohn et al. 2008). Though the timing of retreat is more consistent than sea-ice advance, the date of sea-ice breakup varied by 27 days across three years according to the first day of boat-based sampling. We posit increased light availability and the local onset of increased phytoplankton productivity more closely coincide with this boat-based metric rather than the spatially-coarser satellite view.

The surface-intensified warming pattern we observed suggests that atmospheric forcing drove water-temperature patterns in each of the three years of this study. Although warm Upper Circumpolar Deep Water can reach this coastal area, it does not regularly intrude into the surface mixed layer during summer (Carvalho et al. 2016, Hudson et al. 2019). Colder water temperatures in the 2018-2019 field season were coincident with below-average surface temperatures across the Antarctic Peninsula during January and February 2019 (Clem et al. 2020). Despite early breakup, sea ice persisted longer than in the prior, warmer year (S. Nardelli unpubl. data). The warmest water temperatures coincided with record-setting surface air

temperatures along the Antarctic Peninsula in February 2020 (Xu et al. 2021). Therefore, nearshore ocean temperature in this study appears to reflect broader-scale atmospheric processes.

The seasonal progression of phytoplankton biomass accumulation followed known patterns, and chl-*a* concentration was low to moderate for the study site. Shallow mixed layers relieve light limitation and allow rapid phytoplankton growth in nutrient-replete waters following sea-ice retreat (Mitchell & Holm-Hansen 1991, Nelson & Smith Jr. 1991). Wind and meltwater influence mixing and stratification to drive subsequent phytoplankton biomass peaks in late January and early March near Palmer Station (Carvalho et al. 2016, Nardelli et al. 2021). Mean December-February chl-*a* concentration during each of the three study years (65-83 mg m^{-2}) was below the long-term mean for 1991-2012 (108 mg m^{-2}) (Saba et al. 2014). Therefore, while chl-*a* was highest in our study during the summer of 2018-2019, phytoplankton biomass was only moderate in the context of the longer-term record.

4.2. Zooplankton biomass and size structure

Resource availability and predator-prey interactions drive the pattern of zooplankton biomass lagging behind phytoplankton biomass seasonally (Sommer et al. 2012). Recruitment of overwintering larvae (Atkinson 1991, Ward et al. 2012), ascension of seasonal vertical migrators (Atkinson & Shreeve 1995, La et al. 2019), and dampened diel vertical migration (Cisewski et al. 2010, Conroy et al. 2020) likely caused increased daytime zooplankton biomass following peaks in phytoplankton biomass accumulation. While meso- and macrozooplankton responded to phytoplankton growth, it is unlikely that during 2017-2018 and 2018-2019 their grazing caused seasonal declines in phytoplankton biomass. Combined daily grazing by copepods, euphausiids, pteropods, and salps along the WAP is estimated at 0.5% of phytoplankton standing stock and

1.2% of daily primary productivity during summer (Bernard et al. 2012, Gleiber et al. 2016). An exception is during salp blooms such as occurred in 2019-2020, which can lead to a daily grazing impact of up to 30% of phytoplankton standing stock (and 169% of primary productivity) (Bernard et al. 2012), likely contributing to the low chl-*a* conditions during that year.

High concentration of biomass in the macrozooplankton size class (> 2 mm) illustrates key characteristics of Antarctic zooplankton more broadly. The size of individual zooplankton is relatively large in polar regions due to low temperature, high oxygen concentration, and large phytoplankton (Brun et al. 2016, Brandão et al. 2021). And while subpolar regions have a much higher proportion of larger size classes of zooplankton compared to subtropical regions (e.g., Steinberg et al. 2008), the extreme 'top-heavy' zooplankton biomass conditions documented in this study are likely a distinct feature of polar regions. For example, in the California Current ecosystem the zooplankton spectral slope increases (but still remains negative) during upwelling events as relatively short-lived species respond to increased productivity (Rykaczewski & Checkley 2008). The inverted biomass distribution demonstrated here is likely possible due to high predator-to-prey size ratios and broad prey preferences (Woodson et al. 2018) characteristic of *Euphausia superba* and *Salpa thompsoni* (predator:prey ratios exceeding 10,000:1) (Schmidt & Atkinson 2016, Pauli et al. 2021, Stukel et al. 2021). Model simulations demonstrate the exceptional grazing and particle export impacts of large, long-lived macrozooplankton throughout the Southern Ocean (Le Quére et al. 2016, Karakuş et al. 2021).

By repeatedly sampling at a high frequency over three years, we demonstrate the patchiness of krill aggregations and ephemeral nature of salp blooms in contrast to the relatively homogenous distribution of mesozooplankton (dominated by copepods). As noted above, large taxa can have outsized roles in ecosystem-level processes, but these ecological impacts are

limited in space and time while those of mesozooplankton are more consistent. For example, *Oithona* spp. copepods (dominant in 0.2-0.5 mm size class) may be the most productive zooplankton in the Southern Ocean due to their numerical abundance (Fransz & Gonzalez 1995), and calanoid copepods (dominant in 0.5-2 mm) are likely more productive than *E. superba* (Voronina 1998). Distinguishing multiple size classes of zooplankton is an effective way to model global ocean ecosystems (Le Quéré et al. 2016, Heneghan et al. 2020), and we suggest that regional studies attempt to resolve the distribution of zooplankton size classes at finer resolution. Such (sub)mesoscale considerations have proven valuable for understanding phytoplankton ecology (McGillicuddy 2016, Lévy et al. 2018), and modeling krill distribution at the scale of ≤10 km has revealed important biophysical and predator-prey interactions in the California Current ecosystem (Cimino et al. 2020, Fiechter et al. 2020).

4.3. Interannual changes in taxonomic composition

Multivariate analysis revealed strong interannual differences that obscured seasonal changes until each year was considered individually. Regional time-series programs have previously reported substantial interannual changes in zooplankton composition along the Antarctic Peninsula (Steinberg et al. 2015, Dietrich et al. 2021). Our findings suggest that the PAL LTER regional cruises during a brief summer window effectively capture interannual changes in community structure despite the embedded seasonality shown in the present study. The abundance of individual taxa may be dependent on seasonal timing, but interannual changes were clearly distinguished for most taxa in this study. Furthermore, deeper sampling (to 120 m for macrozooplankton, and to 300 m for mesozooplankton) and coverage throughout the diel

cycle during regional PAL LTER cruises reduce effects due to changes in zooplankton vertical distribution, which likely impacted the seasonal patterns we found.

The impact of earlier sea-ice breakup and higher summer phytoplankton biomass rippled through the planktonic food web in 2018-2019. Copepod abundance and mesozooplankton biomass were high in November 2018 as the spring phytoplankton bloom developed. Increased copepod abundance along the WAP from 1993-2013 was explained by the combination of earlier sea-ice retreat and higher phytoplankton biomass driving earlier recruitment and greater total copepod abundance (Gleiber 2014). The bottom-up forcing we detected further appeared to translate to carnivorous chaetognaths, which were most abundant during 2018-2019. Compared to 2017-2018 (when local sea-ice breakup was 14 days later) central abundance dates for small calanoids, *Oithona* spp. copepods, chaetognaths, and amphipods were 10-19 days earlier at Station B. This finding suggests that sea ice, phytoplankton, copepods, and carnivorous zooplankton are phenologically coupled. Long-term changes in sea-ice retreat and phytoplankton biomass (Montes-Hugo et al. 2009, Schofield et al. 2017) are thus likely to impact zooplankton phenology as well.

The salp bloom during 2019-2020 resulted in a variety of ecological interactions. Salp blooms near the Antarctic Peninsula are associated with relatively warm water and low chl-*a* (Loeb et al. 1997, Groeneveld et al. 2020), and the warm conditions in early 2020 promoted the salp bloom we observed. Grazing by salps likely contributed to low chl-*a* conditions (discussed above) which may have resulted in competition with other herbivorous taxa (Loeb et al. 1997, Stukel et al. 2021), causing decreased copepod abundance. Increased abundance of amphipods (particularly hyperiids), which form parasitic and commensal relationships with salps (Madin

and Harbison 1977, Phleger et al. 2000), during 2019-2020 was also likely linked to the salp bloom.

4.4. Seasonal succession

Within each field season, days since sea-ice breakup and warming water temperatures were associated with changing zooplankton taxonomic composition. Chl-*a* and tidal regime generally were not related to taxonomic structure. This suggests that (at our sampling resolution) advection and short-term phytoplankton changes were less important than a gradual restructuring of species composition as temperature increased after sea-ice breakup and throughout austral summer.

One component of seasonal succession was a transition to more omnivorous species. For example, the krill *E. superba* was more abundant in spring and occupies a lower trophic position than the krill species *Thysanoessa macrura* (Yang et al. 2021), which increased in abundance from spring into autumn. A similar transition occurred for copepods. The herbivorous *Calanoides acutus* peaked before the omnivorous and detritivorous *Calanus propinquus* and *Oithona* spp. copepods (Atkinson 1998). The copepod *Rhincalanus gigas* exhibited a bimodal seasonal distribution and is a generalist omnivore (Atkinson 1998), suggesting it takes advantage of different prey sources throughout the season. The pteropod *Limacina rangii* largely relies on herbivory (Thibodeau et al. 2022) and decreased from spring into autumn.

Carnivorous chaetognaths and gymnosome pteropods were correlated with their respective prey, copepods and the thecosome pteropod *L. rangii*. Chaetognaths were positively correlated with *Oithona* spp. and small calanoid copepods, which together constituted the vast majority of copepods in this study. A significant positive relationship between chaetognaths and

the relatively scarce copepod *R. gigas* suggests this copepod may be preferred prey, likely due to its large size, as was previously suggested due to the similar diel vertical distribution of these two taxa (Conroy et al. 2020). A positive correlation between the annual abundance of gymnosome pteropods and their prey *L. rangii* was previously demonstrated along the WAP (Thibodeau et al. 2019). Our results show this pteropod predator-prey pair is tightly coupled at the seasonal scale as well.

In addition to differences in feeding ecology, reproductive timing and overwintering strategies help explain why some taxa were more abundant early in the seasonal cycle. Early spawning, recruitment, and seasonal vertical migration are characteristic for *C. acutus*, *R. gigas*, and *L. rangii* (Atkinson & Shreeve 1995, Thibodeau et al. 2020). A large portion of the small calanoids also followed this springtime recruitment or ascension pattern. Larval *E. superba* remain in surface waters during winter and recruit as juveniles in spring when they feed on phytoplankton throughout the day before initiating diel vertical migration in late summer (Nicol 2006, Nardelli et al. 2021). The seasonal decline in *E. superba* in our study may also be due to high predation mortality. The rapid rise in the density of larval fishes we observed following local sea-ice breakup allows for completion of larval development during the productive summer period when fishes feed on calanoid copepods (Kellermann 1989, Loeb et al. 1993). Foraminifera live within sea ice (Lipps & Krebs 1974, Spindler & Dieckmann 1986), and we found them to be abundant in the water column when sea ice was present. Few studies have focused on Antarctic foraminifera in recent decades (Bergami et al. 2009, Pinkerton et al. 2020), but the effects of a circumpolar release of foraminifera upon annual sea-ice retreat on both food web structure and biogeochemistry should be investigated.

A broad range of life-history strategies also result in patterns other than a spring maximum and seasonal decline. The seasonal increase in *C. propinquus* and *Oithona* spp. is likely tied to recruitment rather than a seasonal ascent. These copepods have a prolonged reproductive period and feed year-round rather than undergoing winter diapause (Metz 1995, Atkinson 1998, Pasternak & Schnack-Schiel 2001). Delayed recruitment likely explains the occasional late-season increases in *R. gigas* and small calanoids. A horizontal migration may drive the seasonal increase of the krill *T. macrura*, a species which generally shifts southward and towards coastal waters at the end of summer (Nordhausen 1994, Loeb & Santora 2015). Persistent sampling of a *S. thompsoni* bloom through January and February allowed us to follow the stages of this species' complex life history. *Salpa thompsoni* blooms develop from asexual reproduction by a relatively small number of oozooids ('solitary' stage) that each release chains containing hundreds of blastozooids ('aggregate' stage; Loeb & Santora 2012), which were abundant in January. The blastozooids then reproduce sexually, resulting in increased oozooid abundance as the bloom progressed in February 2020. The oozooids then overwinter at depth (Loeb & Santora 2012) and begin the life cycle again the following summer.

Small seasonal fluctuations in the abundance of larval asteroids and nemerteans reflect life-history traits of the dominant local species. The sea star *Odontaster validus* and ribbon worm *Parborlasia corrugatus* are abundant, well-studied species that spawn planktotrophic larvae, which may spend 5-6 months in the plankton (Pearse & Bosch 1986, Peck 1993). Both of these species spawn throughout the year, although reproductive output is concentrated in winter (Pearse et al. 1991, Stanwell-Smith et al. 1999). The minor fluctuations (rather than distinct seasonal trends) that we observed in larval abundance are likely due to multiple spawning pulses or advection. These larvae may feed on dissolved organic matter, bacteria, and detritus in

addition to phytoplankton (Rivkin et al. 1986, Peck 1993), thus the lack of synchronization with phytoplankton biomass accumulation in our study supports previous work suggesting that larvae rely more upon increased phytoplankton productivity for growth and survival after settlement rather than when in the plankton (Bowden et al. 2009).

4.5. Phenological and long-term change

Our findings suggest many zooplankton taxa exhibit phenological plasticity to deal with extreme seasonality in the WAP. Phenological shifts (typically, earlier when warmer) are a fundamental response of marine plankton to climate variability and change (Mackas et al. 2012, Beaugrand & Kirby 2018). We documented ≥1-week phenological shifts in the krill *E. superba* and *T. macrura*, *Oithona* spp. and small calanoid copepods, amphipods, chaetognaths, and larval fishes that coincided with a 2-week earlier sea-ice breakup and onset of phytoplankton productivity. Temperature is the dominant driver of zooplankton phenology at lower latitudes (Ji et al. 2010, Mackas et al. 2012), but earlier accumulation occurred in the coldest year of our study. While the timing of sea-ice breakup and increased phytoplankton productivity may drive interannual phenology shifts at the WAP, seasonal warming likely influences taxonomic composition within each year.

While some zooplankton taxa showed phenological responses to phytoplankton shifts, seasonal trophic mismatches remain possible. Phytoplankton phenology is commonly observed to shift faster than that of zooplankton in response to warming temperatures (Richardson 2008, Thackeray et al. 2016). The large copepods *C. acutus*, *R. gigas*, and *C. propinquus* exhibited limited phenological plasticity at Station B (<1 week change in central abundance date between years), suggesting the spawning stages of these species may be more susceptible to trophic

mismatches. However, direct evidence of decreased fitness due to seasonal mismatches is rare (Kharouba & Wolkovich 2020). Species inhabit areas along the WAP over which sea-ice duration varies by as much as three months (Stammerjohn et al. 2008) and cope with changing environmental conditions via various physiological and behavioral responses such as diapause, vertical migration, and omnivory (Atkinson 1998, Conroy et al. 2020) that may preempt phenological responses (Beaugrand & Kirby 2018). Thus, flexible life history and feeding ecology can limit the risk of reproductive failure for zooplankton despite warming-induced trophic mismatches (Atkinson et al. 2015).

Our third field season captured conditions that are predicted to become more common as climate change progresses along the WAP. Warmer surface temperatures (Bracegirdle et al. 2008), reduced phytoplankton (particularly diatom) biomass (Brown et al. 2019), and more frequent salp blooms (Moline et al. 2004) are all hypothesized regional consequences of climate change. Copepod and krill abundances are positively related to phytoplankton productivity (Gleiber 2014, Steinberg et al. 2015), while warmer conditions favor pteropods (Thibodeau et al. 2019) and salps (Groeneveld et al. 2020). The substantial grazing impact of pteropods and salps (Bernard et al. 2012) may intensify competition among zooplankton species for their phytoplankton prey (Loeb et al. 1997), but the degree of competition depends upon feeding selectivity across species (Pauli et al. 2021, Stukel et al. 2021).

The ecological consequences of shifting zooplankton composition or phenology will be complex. For example, prey availability to vertebrate predators is complicated by seasonal distribution changes at the scale of local foraging (Beltran et al. 2021, Nardelli et al. 2021), and carbon supply to mesopelagic food webs depends upon the remineralization depth of various zooplankton fecal pellet types (Iversen et al. 2017, Liszka et al. 2019). Detecting long-term

change in zooplankton seasonal dynamics and unravelling these ecological and biogeochemical consequences will only be possible with sustained, coordinated observation of the WAP ecosystem.

Acknowledgements

This work was supported by the National Science Foundation Antarctic Organisms and Ecosystems Program (PLR-1440435 and OPP-2026045). M.I. Thomas was supported by the VIMS Research Experience for Undergraduates program (NSF OCE-1659656). Tide data were made available by the University of Wisconsin-Madison and Madison College AMRDC (NSF 1924730 and 1951603). Thank you to the Antarctic Support Contract personnel at Palmer Station for their scientific and logistical support. We thank Kharis Schrage, Andrew Corso, Ashley Hann, and Rachael Young for their field contributions to this project. Michael Gibson assisted with laboratory work. Sharon Stammerjohn, Oscar Schofield, Schuyler Nardelli, and Nicole Waite provided environmental data. Comments from Kim Bernard, David Johnson, Walker Smith, and Mike Vecchione improved this manuscript.

References

Amos AF (1993) RACER: The tides at Palmer Station. Antarctic Journal of the United States 28:162.

Atkinson A (1998) Life cycle strategies of epipelagic copepods in the Southern Ocean. Journal of Marine Systems 15:289–311.

Atkinson A (1991) Life cycles of *Calanoides acutus*, *Calanus simillimus* and *Rhincalanus gigas* (Copepoda: Calanoida) within the Scotia Sea. Mar Biol 109:79–91.

Atkinson A, Harmer RA, Widdicombe CE, McEvoy AJ, Smyth TJ, Cummings DG, Somerfield PJ, Maud JL, McConville K (2015) Questioning the role of phenology shifts and trophic mismatching in a planktonic food web. Progress in Oceanography 137:498–512.

Atkinson A, Shreeve RS (1995) Response of the copepod community to a spring bloom in the Bellingshausen Sea. Deep Sea Research Part II: Topical Studies in Oceanography 42:1291–1311.

Beaugrand G, Kirby RR (2018) How Do Marine Pelagic Species Respond to Climate Change? Theories and Observations. Annual Review of Marine Science 10:169–197.

Beltran RS, Kilpatrick AM, Breed GA, Adachi T, Takahashi A, Naito Y, Robinson PW, Smith WO, Kirkham AL, Burns JM (2021) Seasonal resource pulses and the foraging depth of a Southern Ocean top predator. Proceedings of the Royal Society B: Biological Sciences 288:20202817.

Bergami C, Capotondi L, Langone L, Giglio F, Ravaioli M (2009) Distribution of living planktonic foraminifera in the Ross Sea and the Pacific sector of the Southern Ocean (Antarctica). Marine Micropaleontology 73:37–48.

Bernard KS, Cimino M, Fraser W, Kohut J, Oliver MJ, Patterson-Fraser D, Schofield OME,

Statscewich H, Steinberg DK, Winsor P (2017) Factors that affect the nearshore aggregations of Antarctic krill in a biological hotspot. Deep Sea Research Part I: Oceanographic Research Papers 126:139–147.

Bernard KS, Steinberg DK (2013) Krill biomass and aggregation structure in relation to tidal cycle in a penguin foraging region off the Western Antarctic Peninsula. ICES Journal of Marine Science 70:834–849.

Bernard KS, Steinberg DK, Schofield OME (2012) Summertime grazing impact of the dominant macrozooplankton off the Western Antarctic Peninsula. Deep Sea Research Part I: Oceanographic Research Papers 62:111–122.

Bowden DA, Clarke A, Peck LS (2009) Seasonal variation in the diversity and abundance of pelagic larvae of Antarctic marine invertebrates. Marine Biology 156:2033–2047.

Bracegirdle TJ, Connolley WM, Turner J (2008) Antarctic climate change over the twenty first century. Journal of Geophysical Research: Atmospheres 113.

Brandão MC, Benedetti F, Martini S, Soviadan YD, Irisson J-O, Romagnan J-B, Elineau A, Desnos C, Jalabert L, Freire AS, Picheral M, Guidi L, Gorsky G, Bowler C, Karp-Boss L, Henry N, de Vargas C, Sullivan MB, Stemmann L, Lombard F (2021) Macroscale patterns of oceanic zooplankton composition and size structure. Sci Rep 11:15714.

Brown JH, Gillooly JF, Allen AP, Savage VM, West GB (2004) Toward a metabolic theory of ecology. Ecology 85:1771–1789.

Brown MS, Munro DR, Feehan CJ, Sweeney C, Ducklow HW, Schofield OM (2019) Enhanced oceanic CO_2 uptake along the rapidly changing West Antarctic Peninsula. Nat Clim Chang 9:678–683.

Brun P, Payne MR, Kiørboe T (2016) Trait biogeography of marine copepods – an analysis across scales. Ecology Letters 19:1403–1413.

Carvalho F, Kohut J, Oliver MJ, Sherrell RM, Schofield O (2016) Mixing and phytoplankton dynamics in a submarine canyon in the West Antarctic Peninsula. Journal of Geophysical Research: Oceans 121:5069–5083.

Cimino MA, Santora JA, Schroeder I, Sydeman W, Jacox MG, Hazen EL, Bograd SJ (2020) Essential krill species habitat resolved by seasonal upwelling and ocean circulation models within the large marine ecosystem of the California Current System. Ecography 43:1536–1549.

Cisewski B, Strass VH, Rhein M, Krägefsky S (2010) Seasonal variation of diel vertical migration of zooplankton from ADCP backscatter time series data in the Lazarev Sea, Antarctica. Deep Sea Research Part I: Oceanographic Research Papers 57:78–94.

Clem KR, Barreira S, Fogt RL, Colwell S, Keller LM, Lazzara MA, Mikolajczyk D (2020) Atmospheric circulation and surface observations. in State of the Climate in 2019. Bull Amer Meteor Soc 101:S293–S296.

Conroy JA, Steinberg DK, Thibodeau PS, Schofield O (2020) Zooplankton diel vertical migration during Antarctic summer. Deep Sea Research Part I: Oceanographic Research Papers 162:103324.

Dietrich K, Santora J, Reiss C (2021) Winter and summer biogeography of macrozooplankton community structure in the northern Antarctic Peninsula ecosystem. Progress in Oceanography 196:102610.

Edwards M, Richardson AJ (2004) Impact of climate change on marine pelagic phenology and trophic mismatch. Nature 430:881–884.

Fiechter J, Santora JA, Chavez F, Northcott D, Messié M (2020) Krill hotspot formation and phenology in the California Current Ecosystem. Geophysical Research Letters 47:e2020GL088039

Fransz HG, Gonzalez SR (1995) The production of *Oithona similis* (Copepoda: Cyclopoida) in the Southern Ocean. ICES Journal of Marine Science 52:549–555.

Froneman P, Pakhomov E, Perissinotto R, Laubscher R, McQuaid C (1997) Dynamics of the plankton communities of the Lazarev Sea (Southern Ocean) during seasonal ice melt. Marine Ecology Progress Series 149:201–214.

Gleiber MR (2014) Long-term change in copepod community structure in the Western Antarctic Peninsula: Linkage to climate and implications for carbon cycling. MS thesis, College of William & Mary, Williamsburg, VA

Gleiber MR, Steinberg DK, Ducklow HW (2012) Time series of vertical flux of zooplankton fecal pellets on the continental shelf of the western Antarctic Peninsula. Marine Ecology Progress Series 471:23–36.

Gleiber MR, Steinberg DK, Schofield OM (2016) Copepod summer grazing and fecal pellet production along the Western Antarctic Peninsula. Journal of Plankton Research 38:732–750.

Groeneveld J, Berger U, Henschke N, Pakhomov EA, Reiss CS, Meyer B (2020) Blooms of a key grazer in the Southern Ocean – an individual-based model of *Salpa thompsoni*. Progress in Oceanography:102339.

Heneghan RF, Everett JD, Sykes P, Batten SD, Edwards M, Takahashi K, Suthers IM, Blanchard JL, Richardson AJ (2020) A functional size-spectrum model of the global marine ecosystem that resolves zooplankton composition. Ecological Modelling 435:109265.

Henley SF, Schofield OM, Hendry KR, Schloss IR, Steinberg DK, Moffat C, Peck LS, Costa DP, Bakker DCE, Hughes C, Rozema PD, Ducklow HW, Abele D, Stefels J, Van Leeuwe MA, Brussaard CPD, Buma AGJ, Kohut J, Sahade R, Friedlaender AS, Stammerjohn SE, Venables HJ, Meredith MP (2019) Variability and change in the west Antarctic Peninsula marine system: Research priorities and opportunities. Progress in Oceanography 173:208–237.

Hudson K, Oliver MJ, Bernard K, Cimino MA, Fraser W, Kohut J, Statscewich H, Winsor P (2019) Reevaluating the Canyon Hypothesis in a Biological Hotspot in the Western Antarctic Peninsula. Journal of Geophysical Research: Oceans 124:6345–6359.

Hunt BPV, Hosie GW (2006) The seasonal succession of zooplankton in the Southern Ocean south of Australia, part I: The seasonal ice zone. Deep Sea Research Part I: Oceanographic Research Papers 53:1182–1202.

Iversen MH, Pakhomov EA, Hunt BPV, van der Jagt H, Wolf-Gladrow D, Klaas C (2017) Sinkers or floaters? Contribution from salp pellets to the export flux during a large bloom event in the Southern Ocean. Deep Sea Research Part II: Topical Studies in Oceanography 138:116–125.

Janssen AW, Bush SL, Bednaršek N (2019) The shelled pteropods of the northeast Pacific Ocean (Mollusca: Heterobranchia, Pteropoda). Zoosymposia 13:305-356.

Ji R, Edwards M, Mackas DL, Runge JA, Thomas AC (2010) Marine plankton phenology and life history in a changing climate: current research and future directions. J Plankton Res 32:1355–1368.

Karakuş O, Völker C, Iversen M, Hagen W, Gladrow DW, Fach B, Hauck J (2021) Modeling the Impact of Macrozooplankton on Carbon Export Production in the Southern Ocean. Journal of Geophysical Research: Oceans 126:e2021JC017315.

Kellermann A (1989) The larval fish community in the zone of seasonal ice cover and its seasonal and interannual variability. Arch. FischereiWeiss. 39:89-109.

Kenitz KM, Visser AW, Mariani P, Andersen KH (2017) Seasonal succession in zooplankton feeding traits reveals trophic trait coupling. Limnology and Oceanography 62:1184–1197.

Kharouba HM, Wolkovich EM (2020) Disconnects between ecological theory and data in phenological mismatch research. Nat Clim Chang 10:406–415.

Kim H, Doney SC, Iannuzzi RA, Meredith MP, Martinson DG, Ducklow HW (2016) Climate forcing for dynamics of dissolved inorganic nutrients at Palmer Station, Antarctica: An interdecadal (1993-2013) analysis. Journal of Geophysical Research: Biogeosciences 121:2369–2389.

Kim H, Ducklow HW, Abele D, Ruiz Barlett EM, Buma AG, Meredith MP, Rozema PD, Schofield OM, Venables HJ, Schloss IR (2018) Inter-decadal variability of phytoplankton biomass along the coastal West Antarctic Peninsula. Philosophical Transactions of the Royal Society A: Mathematical, Physical and Engineering Sciences 376:20170174.

Kiørboe T, Visser A, Andersen KH (2018) A trait-based approach to ocean ecology. ICES Journal of Marine Science 75:1849–1863.

La HS, Park K, Wåhlin A, Arrigo KR, Kim DS, Yang EJ, Atkinson A, Fielding S, Im J, Kim T-W, Shin HC, Lee S, Ha HK (2019) Zooplankton and micronekton respond to climate fluctuations in the Amundsen Sea polynya, Antarctica. Scientific Reports 9:1–7.

Le Quéré C, Buitenhuis ET, Moriarty R, Alvain S, Aumont O, Bopp L, Chollet S, Enright C, Franklin DJ, Geider RJ, Harrison SP, Hirst AG, Larsen S, Legendre L, Platt T, Prentice IC, Rivkin RB, Sailley S, Sathyendranath S, Stephens N, Vogt M, Vallina SM (2016) Role of zooplankton dynamics for Southern Ocean phytoplankton biomass and global biogeochemical cycles. Biogeosciences 13:4111–4133.

Lévy M, Franks PJS, Shafer Smith K (2018) The role of submesoscale currents in structuring marine ecosystems. Nature Communications 9:4758.

Lipps JH, Krebs WN (1974) Planktonic foraminifera associated with Antarctic sea ice. The Journal of Foraminiferal Research 4:80–85.

Liszka CM, Manno C, Stowasser G, Robinson C, Tarling GA (2019) Mesozooplankton Community Composition Controls Fecal Pellet Flux and Remineralization Depth in the Southern Ocean. Front Mar Sci 6:230.

Litchman E, Ohman MD, Kiørboe T (2013) Trait-based approaches to zooplankton communities. J Plankton Res 35:473–484.

Loeb V, Siegel V, Holm-Hansen O, Hewitt R, Fraser W, Trivelpiece W, Trivelpiece S (1997) Effects of sea-ice extent and krill or salp dominance on the Antarctic food web. Nature 387:897–900.

Loeb VJ, Kellermann AK, Koubbi P, North AW, White MG (1993) Antarctic larval fish assemblages: a review. Bulletin of Marine Science 53:416–449.

Loeb VJ, Santora JA (2015) Climate variability and spatiotemporal dynamics of five Southern Ocean krill species. Progress in Oceanography 134:93–122.

Loeb VJ, Santora JA (2012) Population dynamics of *Salpa thompsoni* near the Antarctic

Peninsula: Growth rates and interannual variations in reproductive activity (1993–2009). Progress in Oceanography 96:93–107.

Mackas DL, Greve W, Edwards M, Chiba S, Tadokoro K, Eloire D, Mazzocchi MG, Batten S, Richardson AJ, Johnson C, Head E, Conversi A, Peluso T (2012) Changing zooplankton seasonality in a changing ocean: Comparing time series of zooplankton phenology. Progress in Oceanography 97–100:31–62.

Madin LP, Harbison GR (1977) The associations of Amphipoda Hyperiidea with gelatinous zooplankton—I. Associations with Salpidae. Deep Sea Research 24:449–463.

McGillicuddy Jr. DJ (2016) Mechanisms of Physical-Biological-Biogeochemical Interaction at the Oceanic Mesoscale. Annual Review of Marine Science 8:125-159.

Metz C (1995) Seasonal variation in the distribution and abundance of *Oithona* and *Oncaea* species (Copepoda, Crustacea) in the southeastern Weddell Sea, Antarctica. Polar Biol 15:187–194.

Mitchell BG, Holm-Hansen O (1991) Observations of modeling of the Antarctic phytoplankton crop in relation to mixing depth. Deep Sea Research Part A Oceanographic Research Papers 38:981–1007.

Moline MA, Claustre H, Frazer TK, Schofield O, Vernet M (2004) Alteration of the food web along the Antarctic Peninsula in response to a regional warming trend. Global Change Biology 10:1973–1980.

Montes-Hugo M, Doney SC, Ducklow HW, Fraser W, Martinson D, Stammerjohn SE, Schofield O (2009) Recent changes in phytoplankton communities associated with rapid regional climate change along the western Antarctic Peninsula. Science 323:1470–1473.

Nardelli SC, Cimino MA, Conroy JA, Fraser WR, Steinberg DK, Schofield O (2021) Krill

availability in adjacent Adélie and gentoo penguin foraging regions near Palmer Station, Antarctica. Limnology and Oceanography 66:2234–2250.

Nelson DM, Smith Jr WO (1991) Sverdrup revisited: Critical depths, maximum chlorophyll levels, and the control of Southern Ocean productivity by the irradiance-mixing regime. Limnology and Oceanography 36:1650–1661.

Nicol S (2006) Krill, Currents, and Sea Ice: *Euphausia superba* and Its Changing Environment. BioScience 56:111–120.

Nordhausen W (1994) Winter abundance and distribution of *Euphausia superba*, *E. crystallorophias*, and *Thysanoessa macrura* in Gerlache Strait and Crystal Sound, Antarctica. Marine Ecology-Progress Series 109:131–142.

O'Brien TD (2013) Time-series data analysis and visualization. In: O'Brien TD, Wiebe PH, Falkenhaug T (eds) ICES Zooplankton Status Report 2010/2011. International Council for the Exploration of the Sea, Copenhagen, p 6-19.

Oksanen J, Blanchet FG, Friendly M, Kindt R, Legendre P, McGlinn D, Minchin PR, O'Hara RB, Simpson GL, Solymos P, Stevens MHH, Szoecs E, Wagner H (2020) vegan: Community Ecology Package. R package version 2.5-7. https://CRAN.R-project.org/package=vegan

Pasternak AF, Schnack-Schiel SB (2001) Feeding patterns of dominant Antarctic copepods: an interplay of diapause, selectivity, and availability of food. Hydrobiologia 453:25–36.

Pauli N-C, Metfies K, Pakhomov EA, Neuhaus S, Graeve M, Wenta P, Flintrop CM, Badewien TH, Iversen MH, Meyer B (2021) Selective feeding in Southern Ocean key grazers—diet composition of krill and salps. Commun Biol 4:1–12.

Pearse JS, Bosch I (1986) Are the feeding larvae of the commonest Antarctic asteroid really

demersal? Bulletin of Marine Science 39:477–484.

Pearse JS, McClintock JB, Bosch I (1991) Reproduction of Antarctic Benthic Marine Invertebrates: Tempos, Modes, and Timing. American Zoologist 31:65–80.

Peck LS (1993) Larval development in the Antarctic nemertean *Parborlasia corrugatus* (Heteronemertea: Lineidae). Marine Biology 116:301–310.

Phleger CF, Nelson MM, Mooney B, Nichols PD (2000) Lipids of Antarctic salps and their commensal hyperiid amphipods. Polar Biol 23:329–337.

Pinkerton MH, Décima M, Kitchener JA, Takahashi KT, Robinson KV, Stewart R, Hosie GW (2020) Zooplankton in the Southern Ocean from the continuous plankton recorder: Distributions and long-term change. Deep Sea Research Part I: Oceanographic Research Papers 162:103303.

R Core Team (2021) R: A language and environment for statistical computing. R Foundation for Statistical Computing, Vienna, Austria. https://www.R-project.org/

Richardson AJ (2008) In hot water: zooplankton and climate change. ICES Journal of Marine Science 65:279-295.

Rivkin RB, Bosch I, Pearse JS, Lessard EJ (1986) Bacterivory: a novel feeding mode for asteroid larvae. Science 233:1311–1314.

Rykaczewski RR, Checkley DM (2008) Influence of ocean winds on the pelagic ecosystem in upwelling regions. PNAS 105:1965–1970.

Saba GK, Fraser WR, Saba VS, Iannuzzi RA, Coleman KE, Doney SC, Ducklow HW, Martinson DG, Miles TN, Patterson-Fraser DL, Stammerjohn SE, Steinberg DK, Schofield OM (2014) Winter and spring controls on the summer food web of the coastal West Antarctic Peninsula. Nat Commun 5:1–8.

Schmidt K, Atkinson A (2016) Feeding and Food Processing in Antarctic Krill (*Euphausia superba* Dana). In: Biology and Ecology of Antarctic Krill. Advances in Polar Ecology, Siegel V (ed) Springer International Publishing, Cham, p 175–224

Schnack-Schiel SB (2001) Aspects of the study of the life cycles of Antarctic copepods. In: Copepoda: Developments in Ecology, Biology and Systematics. Springer, p 9–24

Schofield O, Saba G, Coleman K, Carvalho F, Couto N, Ducklow H, Finkel Z, Irwin A, Kahl A, Miles T, Montes-Hugo M, Stammerjohn S, Waite N (2017) Decadal variability in coastal phytoplankton community composition in a changing West Antarctic Peninsula. Deep Sea Research Part I: Oceanographic Research Papers 124:42–54.

Sommer U, Adrian R, De Senerpont Domis L, Elser JJ, Gaedke U, Ibelings B, Jeppesen E, Lürling M, Molinero JC, Mooij WM, van Donk E, Winder M (2012) Beyond the Plankton Ecology Group (PEG) Model: Mechanisms Driving Plankton Succession. Annu Rev Ecol Evol Syst 43:429–448.

Spindler M, Dieckmann GS (1986) Distribution and abundance of the planktic foraminifer *Neogloboquadrina pachyderma* in sea ice of the Weddell Sea (Antarctica). Polar Biol 5:185–191.

Stamieszkin K, Pershing AJ, Record NR, Pilskaln CH, Dam HG, Feinberg LR (2015) Size as the master trait in modeled copepod fecal pellet carbon flux. Limnology and Oceanography 60:2090–2107.

Stammerjohn SE, Martinson DG, Smith RC, Iannuzzi RA (2008) Sea ice in the western Antarctic Peninsula region: Spatio-temporal variability from ecological and climate change perspectives. Deep Sea Research Part II: Topical Studies in Oceanography 55:2041–2058.

Stanwell-Smith D, Peck LS, Clarke A, Murray AWA, Todd CD (1999) The distribution, abundance and seasonality of pelagic marine invertebrate larvae in the maritime Antarctic. Philosophical Transactions of the Royal Society of London B: Biological Sciences 354:471–484.

Steinberg DK, Cope JS, Wilson SE, Kobari T (2008) A comparison of mesopelagic mesozooplankton community structure in the subtropical and subarctic North Pacific Ocean. Deep Sea Research Part II: Topical Studies in Oceanography 55:1615–1635.

Steinberg DK, Ruck KE, Gleiber MR, Garzio LM, Cope JS, Bernard KS, Stammerjohn SE, Schofield OME, Quetin LB, Ross RM (2015) Long-term (1993–2013) changes in macrozooplankton off the Western Antarctic Peninsula. Deep Sea Research Part I: Oceanographic Research Papers 101:54–70.

Stukel MR, Décima M, Selph KE, Gutiérrez-Rodríguez A (2021) Size-specific grazing and competitive interactions between large salps and protistan grazers. Limnology and Oceanography 66:2521–2534.

Thackeray SJ, Henrys PA, Hemming D, Bell JR, Botham MS, Burthe S, Helaouet P, Johns DG, Jones ID, Leech DI, Mackay EB, Massimino D, Atkinson S, Bacon PJ, Brereton TM, Carvalho L, Clutton-Brock TH, Duck C, Edwards M, Elliott JM, Hall SJG, Harrington R, Pearce-Higgins JW, Høye TT, Kruuk LEB, Pemberton JM, Sparks TH, Thompson PM, White I, Winfield IJ, Wanless S (2016) Phenological sensitivity to climate across taxa and trophic levels. Nature 535:241–245.

Thibodeau PS, Song B, Moreno CM, Steinberg DK (2022) Feeding ecology and microbiome of the pteropod *Limacina helicina antarctica*. Aquatic Microbial Ecology 88:19-24.

Thibodeau PS, Steinberg DK, McBride CE, Conroy JA, Keul N, Ducklow HW (2020) Long-

term observations of pteropod phenology along the Western Antarctic Peninsula. Deep Sea Research Part I: Oceanographic Research Papers 166:103363.

Thibodeau PS, Steinberg DK, Stammerjohn SE, Hauri C (2019) Environmental controls on pteropod biogeography along the Western Antarctic Peninsula. Limnology and Oceanography 64:S240–S256.

Visser AW, Brun P, Chakraborty S, Dencker TS, van Denderen PD, van Gemert R, van Someren Gréve H, Heilmann I, Holm MW, Jónasdóttir SH, Kenitz KM, Kiørboe T, Lindegren M, Mariani P, Nielsen LT, Pancic M, Payne M, Pécuchet L, Schnedler-Meyer NA, Thygesen UH, Törnroos A, Andersen KH (2020) Seasonal strategies in the world's oceans. Progress in Oceanography 189:102466.

Voronina NM (1998) Comparative abundance and distribution of major filter-feeders in the Antarctic pelagic zone. Journal of Marine Systems 17:375–390.

Ward P, Atkinson A, Tarling G (2012) Mesozooplankton community structure and variability in the Scotia Sea: A seasonal comparison. Deep-Sea Research II 59-60:78–92.

Woodson CB, Schramski JR, Joye SB (2018) A unifying theory for top-heavy ecosystem structure in the ocean. Nat Commun 9:23.

Xu M, Yu L, Liang K, Vihma T, Bozkurt D, Hu X, Yang Q (2021) Dominant role of vertical air flows in the unprecedented warming on the Antarctic Peninsula in February 2020. Commun Earth Environ 2:1–9.

Yang G, Atkinson A, Hill SL, Guglielmo L, Granata A, Li C (2021) Changing circumpolar distributions and isoscapes of Antarctic krill: Indo-Pacific habitat refuges counter long-term degradation of the Atlantic sector. Limnology and Oceanography 66:272–287.

Table 1. Summary statistics of water temperature and plankton biomass variables for each field season at Palmer Station. Temperature observations (0-50 m) only include sampling between 26 December and 21 March. Chlorophyll *a* and zooplankton dry weight (integrated from 0-50 m) include all sampling dates. Data from Stations B and E are included.

Field season	**Average temperature (° C)**		**T_{max} (° C)**		**Zooplankton dry weight (g m^{-2})**		**Chlorophyll *a* (mg m^{-2})**	
	mean ± SD	***n***	**mean ± SD**	***n***	**mean ± SD**	***n***	**mean ± SD**	***n***
2017-2018	1.2 ± 0.46	49	1.6 ± 0.34	49	0.15 ± 0.30	40	67 ± 38	76
2018-2019	0.95 ± 0.32	50	1.3 ± 0.34	50	0.093 ± 0.16	60	96 ± 77	84
2019-2020	1.3 ± 0.47	50	1.9 ± 0.32	50	0.92 ± 0.79	16	69 ± 54	58

Table 2. Results of regression analysis for non-metric multidimensional scaling (NMDS) ordinations from Stations B and E across each year of sampling.

	NMDS 1	NMDS 2	r^2	p
2017-2018				
Station B (n = 24)				
Days from ice breakup	0.73	0.68	0.67	< 0.0001
Temperature	0.51	0.86	0.72	< 0.0001
Chlorophyll *a*	-0.13	-0.99	0.07	0.47
Station E (n = 23)				
Days from ice breakup	0.91	0.42	0.75	< 0.0001
Temperature	0.66	0.75	0.57	0.0009
Chlorophyll *a*	-0.28	-0.96	0.40	0.007
2018-2019				
Station B (n = 33)				
Days from ice breakup	0.33	0.95	0.54	< 0.0001
Temperature	0.60	0.80	0.55	< 0.0001
Chlorophyll *a*	-0.72	0.69	0.01	0.86
Station E (n = 32)				
Days from ice breakup	0.99	0.12	0.70	< 0.0001
Temperature	0.97	0.24	0.51	0.0002
Chlorophyll *a*	-0.87	-0.50	0.003	0.96
2019-2020				
Station B (n = 10)				
Days from ice breakup	1.00	0.001	0.50	0.08
Temperature	0.30	0.95	0.06	0.81
Chlorophyll *a*	-0.38	-0.92	0.34	0.22
Station E (n = 8)				
Days from ice breakup	0.98	0.21	0.90	0.004
Temperature	0.69	0.72	0.77	0.02
Chlorophyll *a*	-0.30	0.95	0.25	0.48

Table 3. Zooplankton taxonomic abundance comparisons between Stations B and E. For taxa quantified from 700-µm net tows, n = 145 tows at Station B and n = 137-145 tows at Station E. For taxa quantified from 200-µm net tows, n = 69 tows at Station B and n = 65 tows at Station E. Paired t-tests were conducted using data collected on the same day at both stations. Daily means were calculated when replicate tows were available. Only data from the 2019-2020 field season were used in the paired t-test for *Salpa thompsoni* as it was predominantly absent in other years.

Taxon	**Station B**	**Station E**	**Paired *t*-test**		
	mean ± SD (ind. m^{-3})	**mean ± SD (ind. m^{-3})**	***t***	***p***	***n***
Euphausiids					
E. superba	0.11 ± 0.63	0.043 ± 0.15	0.31	0.75	68
T. macrura	0.015 ± 0.090	0.13 ± 0.29	-2.2	0.031	68
Gelatinous macrozooplankton					
L. rangii	0.0075 ± 0.022	0.028 ± 0.054	-5.9	< 0.0001	68
Gymnosomes	0.0016 ± 0.0025	0.0024 ± 0.0047	-0.65	0.52	68
S. thompsoni blastozooids	0.052 ± 0.28	0.11 ± 0.45	-1.6	0.15	9
Copepods					
Oithona spp.	36.3 ± 32.4	21.8 ± 21.9	3.4	0.001	63
C. acutus	0.069 ± 0.061	0.043 ± 0.057	5.0	< 0.0001	63
C. propinquus	0.067 ± 0.072	0.041 ± 0.058	3.8	0.0003	63
R. gigas	0.047 ± 0.034	0.032 ± 0.047	4.6	< 0.0001	63
Small calanoids	6.9 ± 7.7	1.7 ± 4.1	11.2	< 0.0001	63
Carnivorous zooplankton					
Chaetognaths	0.030 ± 0.031	0.0094 ± 0.014	6.0	< 0.0001	63
Amphipods	0.0051 ± 0.0081	0.0040 ± 0.012	4.8	< 0.0001	68
Larvae					
Asteroids	0.18 ± 0.24	0.17 ± 0.30	0.97	0.34	63
Nemerteans	0.40 ± 0.70	0.51 ± 1.0	-1.0	0.31	63
Fishes	0.012 ± 0.025	0.0032 ± 0.0040	2.6	0.012	68

Table 4. Summary of interannual abundance comparisons for various zooplankton taxa using one-way analysis of variance (ANOVA) and Tukey's Honestly Significant Differences (HSD) with significance level set to 0.05.

Taxon	Tukey's HSD	ANOVA	
		F	***p***
Euphausiids			
E. superba	No differences	2.8	0.06
T. macrura	2018-2019 & 2019-2020 > 2017-2018	13.9	< 0.0001
Gelatinous macrozooplankton			
L. rangii	2017-2018 & 2019-2020 > 2018-2019	108.9	< 0.0001
Gymnosomes	2017-2018 > 2018-2019	21.3	< 0.0001
S. thompsoni blastozooids	2019-2020 > 2017-2018 & 2018-2019	850.7	< 0.0001
Copepods			
Oithona spp.	2017-2018 & 2018-2019 > 2019-2020	10.2	< 0.0001
C. acutus	No differences	0.97	0.38
C. propinquus	2017-2018 > 2019-2020 > 2018-2019	53.8	< 0.0001
R. gigas	2017-2018 & 2018-2019 > 2019-2020	20.4	< 0.0001
Small calanoids	2017-2018 & 2018-2019 > 2019-2020	8.5	0.0003
Carnivorous zooplankton			
Chaetognaths	2018-2019 > 2017-2018 & 2019-2020	9.3	0.0002
Amphipods	2019-2020 > 2017-2018 & 2018-2019	32.3	< 0.0001
Larvae			
Asteroids	No differences	1.5	0.22
Nemerteans	2019-2020 > 2018-2019 > 2017-2018	67.7	< 0.0001
Fishes	2017-2018 > 2018-2019 > 2019-2020	12.8	< 0.0001

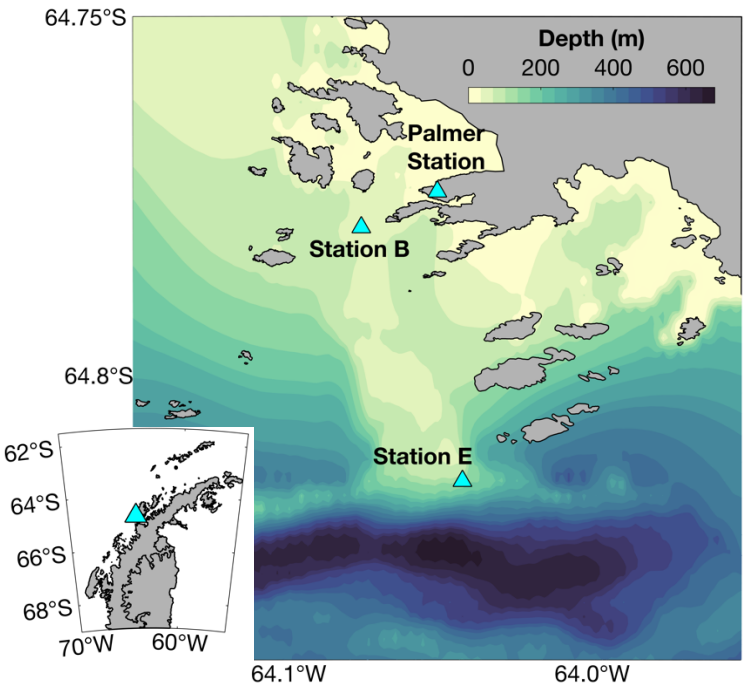

Figure 1. Map of the study area indicating time-series Stations B (~70 m depth) and E (~160 m depth) near Palmer Station on Anvers Island. Shading represents bathymetry. Palmer Station is marked by the triangle along the West Antarctic Peninsula in the inset map.

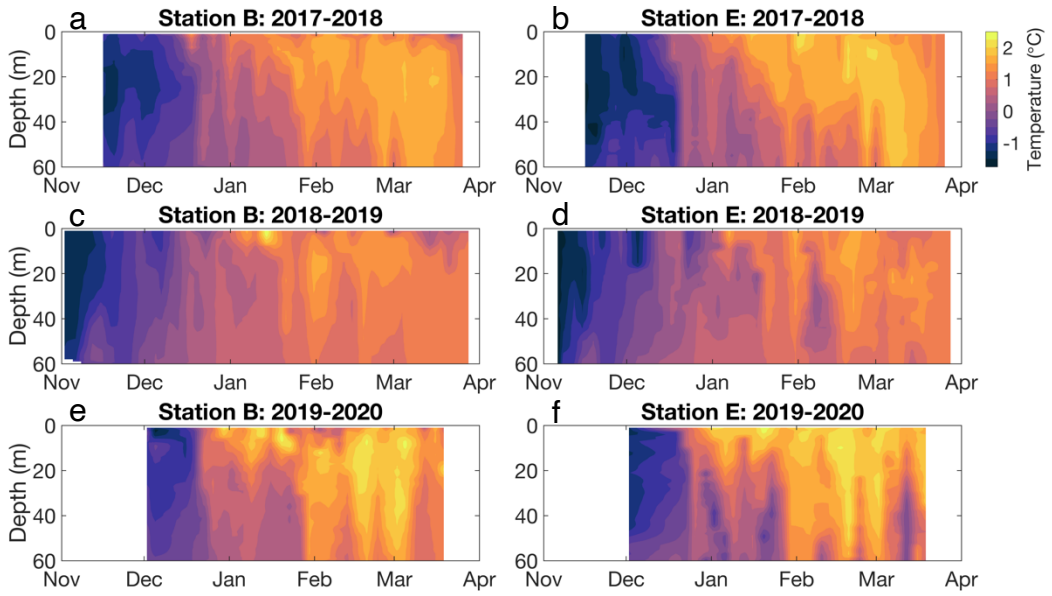

Figure 2. Temperature time series from Stations B (a, c, e) and E (b, d, f) during the 2017-2018 (a-b), 2018-2019 (c-d), and 2019-2020 (e-f) field seasons. Vertical temperature profiles (collected twice per week) were interpolated to produce section plots. Time series begin at the first date local sea-ice breakup allowed boat-based water sampling from Palmer Station.

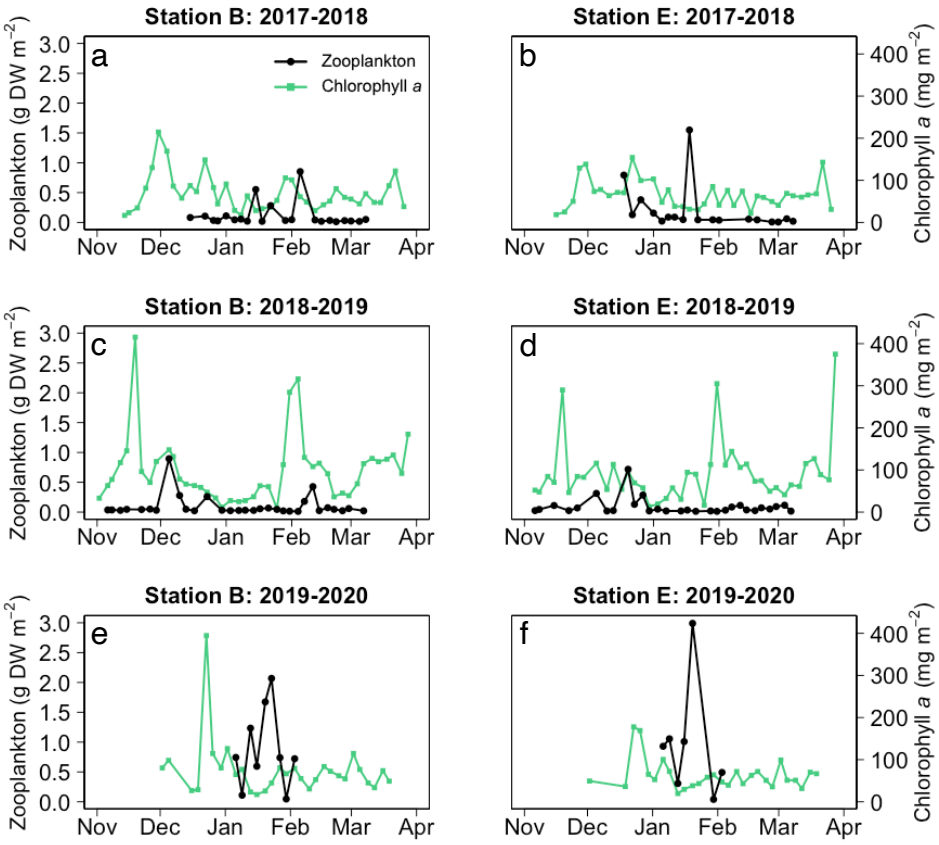

Figure 3. Chlorophyll *a* and zooplankton dry weight time series from Stations B (a, c, e) and E (b, d, f) during the 2017-2018 (a-b), 2018-2019 (c-d), and 2019-2020 (e-f) field seasons. Both variables were integrated from 0 to 50 m.

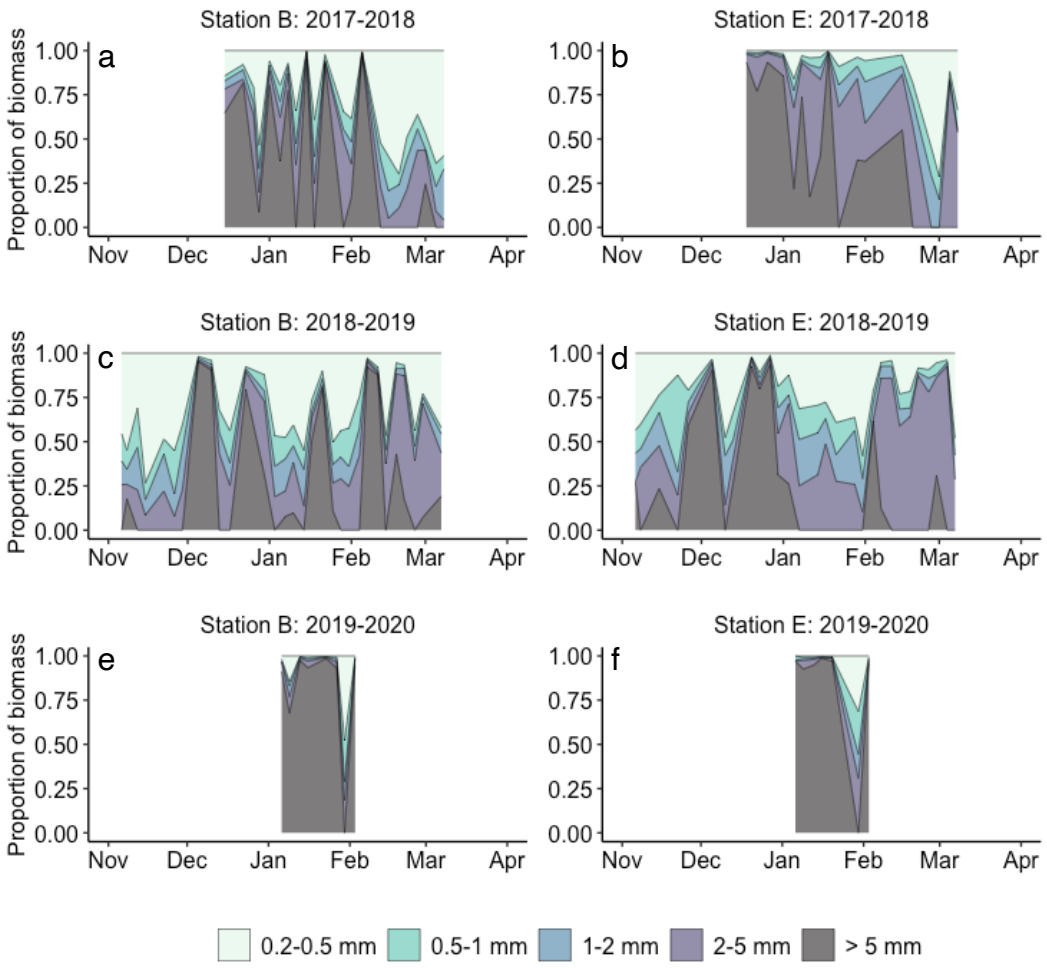

Figure 4. Time series of zooplankton biomass size composition from Stations B (a, c, e) and E (b, d, f) during the 2017-2018 (a-b), 2018-2019 (c-d), and 2019-2020 (e-f) field seasons. Stacked area charts indicate the proportional contribution of five zooplankton size classes to the total dry weight on each sampling day.

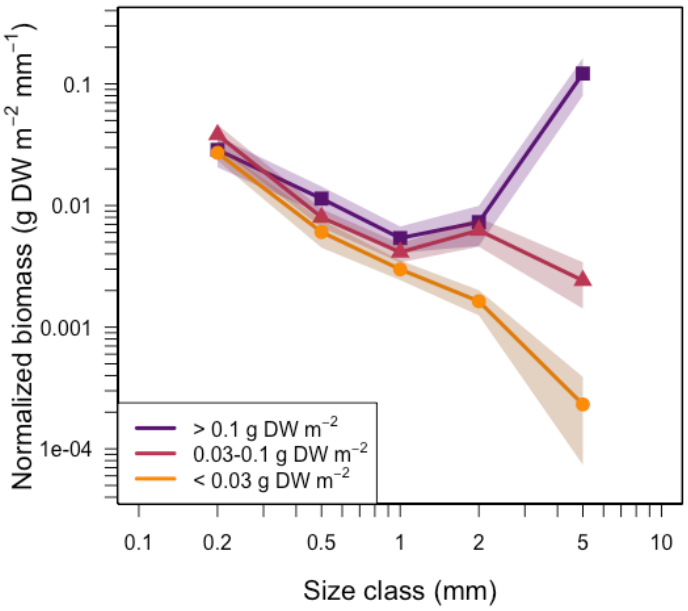

Figure 5. Mean normalized zooplankton biomass size spectra as a function of total dry weight density. Data were divided into three categories with similar sample size based on the total dry weight density integrated from 0 to 50 m (n = 34-46 samples per point). Shading indicates two standard errors of the mean.

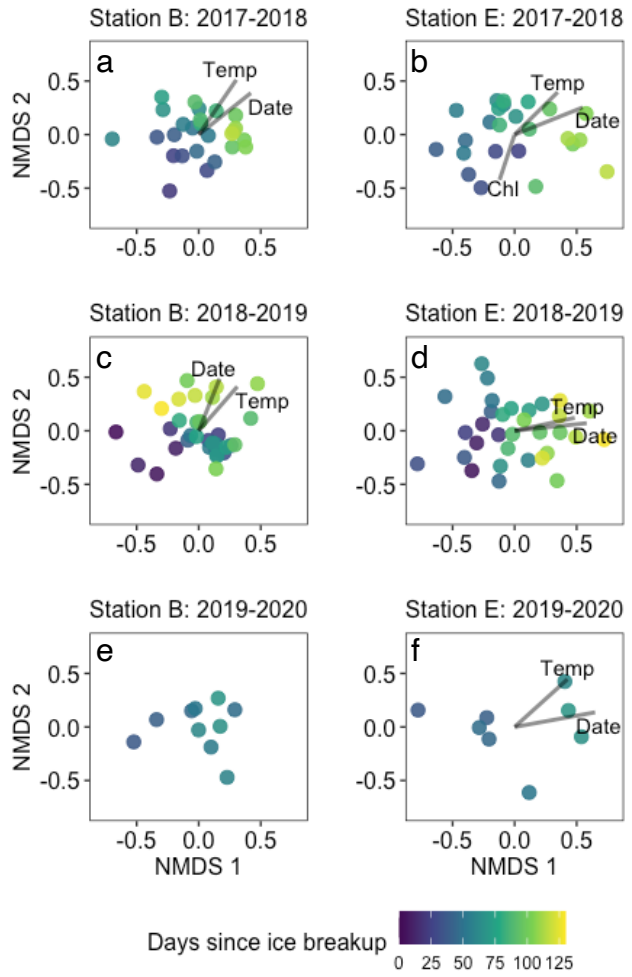

Figure 6. Non-metric multidimensional scaling ordinations for zooplankton taxonomic composition at Stations B (a, c, e) and E (b, d, f) during the 2017-2018 (a-b), 2018-2019 (c-d), and 2019-2020 (e-f) field seasons. Each point marks a sampling date. Vector direction represents the axis of maximal change for the environmental variable, and vector length indicates correlation strength with the environmental variable. Color of point indicates days since local sea-ice breakup. NMDS stress = 0.04-0.22.

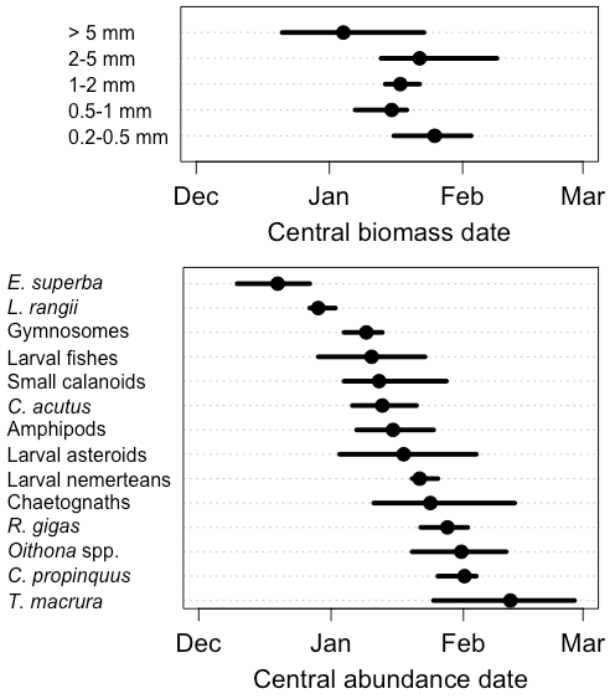

Figure 7. Central date of zooplankton a) taxonomic abundance and b) size-fractionated biomass. Central dates were calculated individually for Stations B and E for the 2017-2018 and 2018-2019 field seasons. Therefore, the sample size $n = 4$ central dates for all taxa and size classes except *L. h. antarctica*, for which $n = 3$ due to absence. Points indicate the mean central date and error bars indicate the range across two years and two stations.

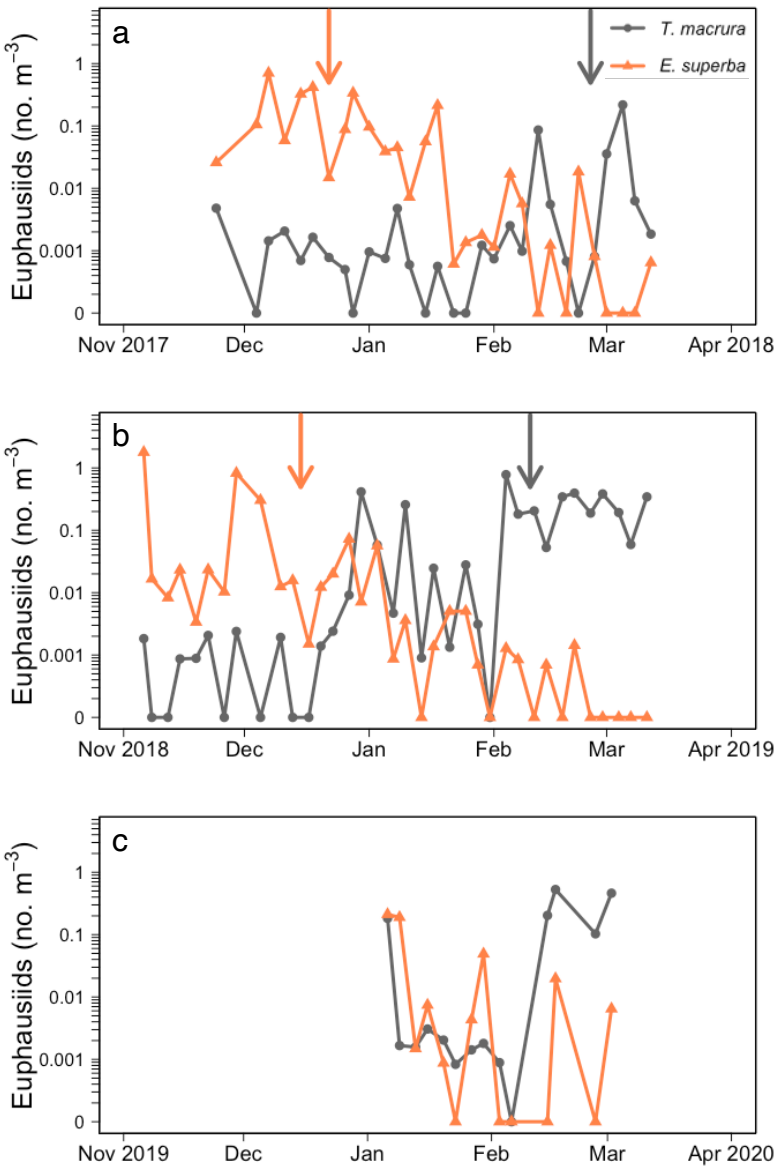

Figure 8. Time series of mean *Euphausia superba* and *Thysanoessa macrura* abundance in a) 2017-2018, b) 2018-2019, and c) 2019-2020 field seasons. Mean daily abundance was calculated from 700-µm net tows at Stations B and E combined (n = 1, or typically daily mean of 2-4). Vertical arrows indicate the corresponding central abundance date for each species for the 2017-2018 and 2018-2019 field seasons**.**

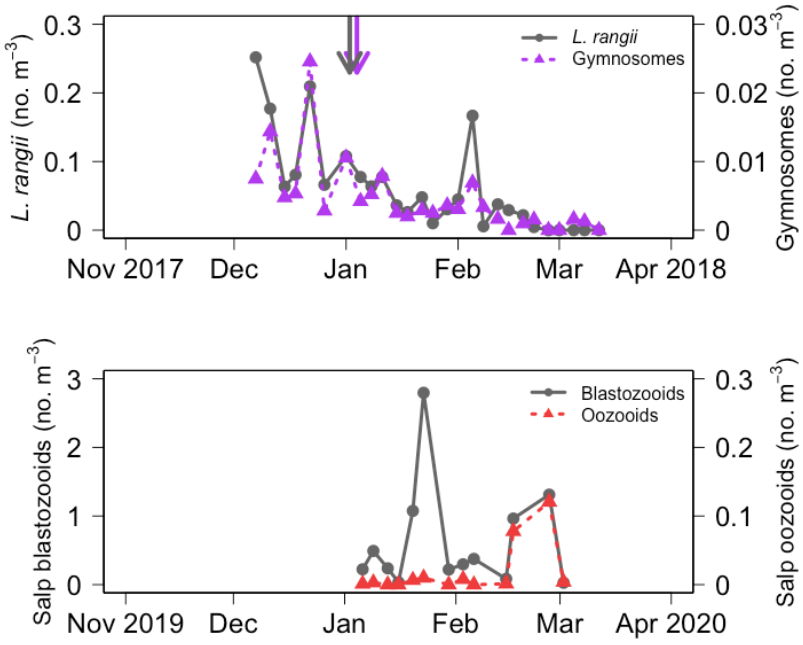

Figure 9. Time series of gelatinous macrozooplankton at Station E. a) Thecosome (*Limacina rangii*) and gymnosome pteropods, and b) the two life-history stages of the salp *Salpa thompsoni* (blastozooid 'aggregate' stage, and oozooid 'solitary' stage). Data are from the 2017-2018 field season for pteropods and from the 2019-2020 field season for salps. Mean daily abundance was calculated from 700-µm net tows (n = 1, or typically daily mean of n = 2). Vertical arrows indicate the corresponding central abundance date for each pteropod group in panel a. Note different y-axis scales within and between plots.

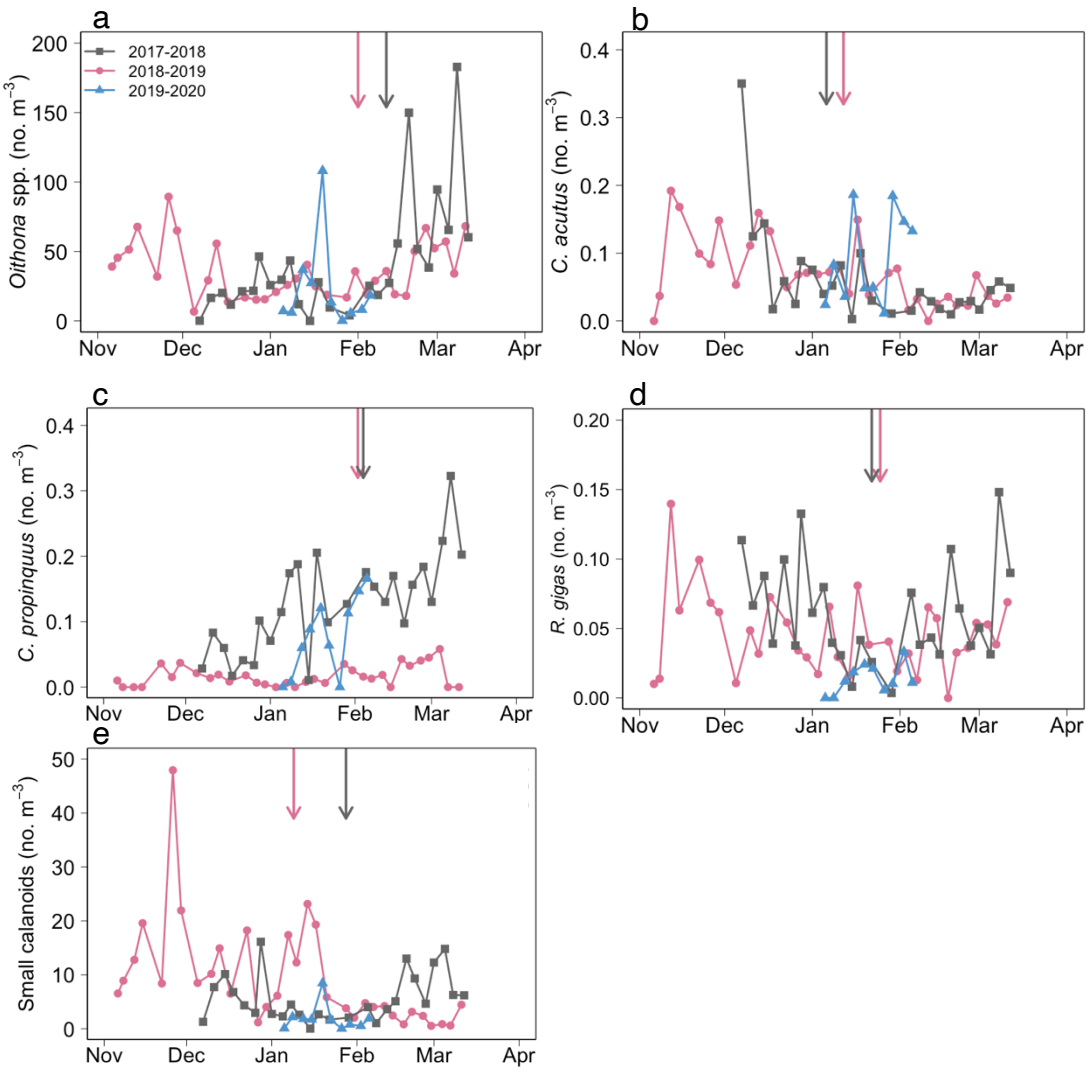

Figure 10. Time series of copepods at Station B. a) *Oithona* spp., b) *Calanoides acutus*, c) *Calanus propinquus*, d) *Rhincalanus gigas*, and e) small calanoids. Different colors and symbols indicate different field seasons. Abundance quantified from 200-µm net tows (n = 1 sample per day**)**. Vertical arrows indicate the corresponding central abundance date for the 2017-2018 and 2018-2019 field seasons. Note different y-axis scales.

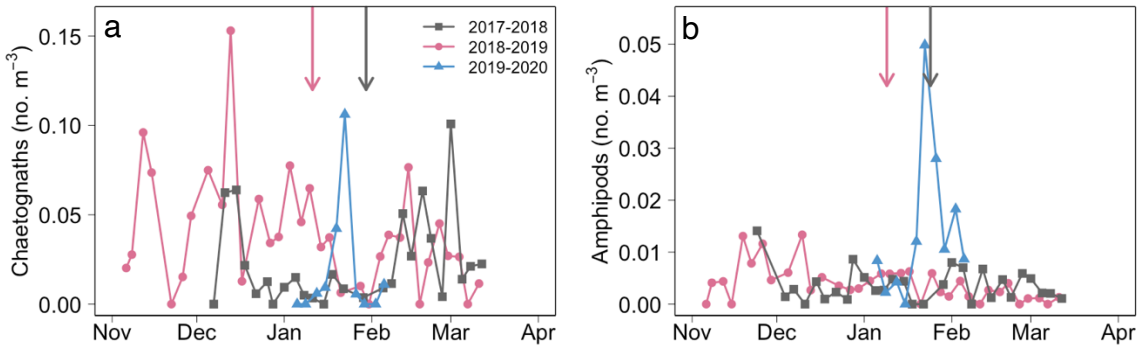

Figure 11. Time series of carnivorous zooplankton at Station B. a) chaetognaths, and b) amphipods. Different colors and symbols indicate different field seasons. Abundance quantified from 200-µm net tows for chaetognaths (n = 1 sample per day**)** and from 700-µm net tows for amphipods (n = 1, or typically daily mean of n = 2). Vertical arrows indicate the corresponding central abundance date for the 2017-2018 and 2018-2019 field seasons. Note different y-axis scales.

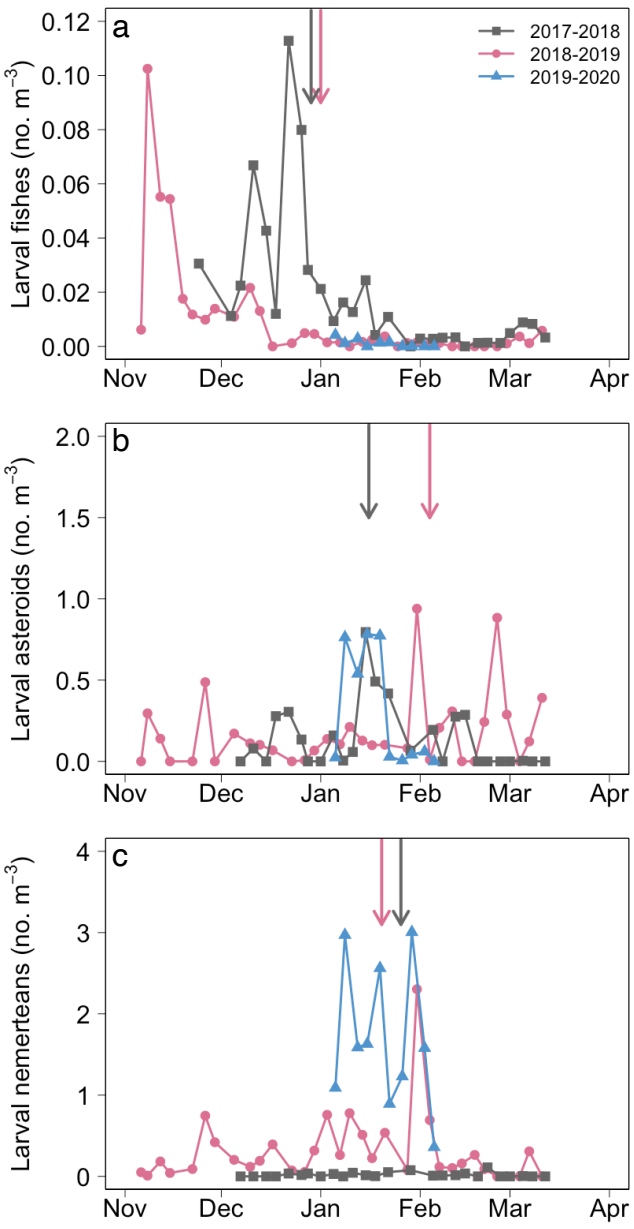

Figure 12. Time series of planktonic larvae at Station B. a) larval fishes, b) asteroids, and c) nemerteans. Different colors and symbols indicate different field seasons. Abundance quantified from 700-µm net tows for fishes (n = 1, or typically daily mean of n = 2) and from 200-µm net tows for asteroids and nemerteans (n = 1 sample per day). Vertical arrows indicate the corresponding central abundance date for the 2017-2018 and 2018-2019 field seasons. Note different y-axis scales.

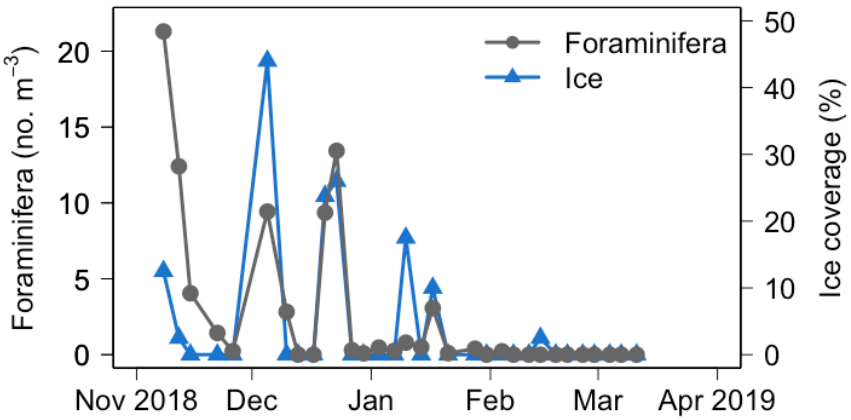

Figure 13. Time series of foraminifera abundance and daily mean ice coverage at Station E during the 2018-2019 field season. Foraminifera abundance quantified from 200-µm net tows (n = 1 sample per day). Ice coverage is from visual observations during net tows.

CHAPTER 4
Omnivory is critical for juvenile Antarctic krill during summer in coastal waters

This chapter is in preparation for submission as: Conroy JA, Steinberg DK, Nardelli SC, Schofield O. Omnivory is critical for juvenile Antarctic krill during summer in coastal waters.

Abstract

The Antarctic krill *Euphausia superba* is typically considered a primary consumer but is notable for its trophic flexibility, which includes feeding on protistan and metazoan zooplankton. Constraining krill trophic position is important for understanding carbon and energy flow from phytoplankton to vertebrate predators and to the deep ocean. We used repeated field sampling and experiments to study feeding by juvenile krill during three austral summers near Palmer Station, Antarctica. Our multi-method approach included a seasonal metabolic budget, gut fluorescence measurements, imaging flow cytometry, and compound-specific isotope analysis of amino acids in krill. Field measurements coupled to experimentally-derived functional response curves suggest that phytoplankton ingestion alone was insufficient to support the growth and basal metabolism of juvenile krill. The minimum feasible trophic position of juvenile krill was 2.65, and phytoplankton consumption was limited due to inefficient feeding on nanoplankton (2-20 μm), which constituted the majority of autotrophic prey. Comparing trophic position estimates using $\delta^{15}N$ of alanine and glutamic acid indicated a substantial and consistent food-web contribution from heterotrophic protists. The mean trophic position of juvenile krill changed interannually by 0.2-0.5 due to the variable contribution of metazoan prey. The dietary fractions of major prey groups were constrained for each study year using concurrent field data. Phytoplankton constituted on average 24% (range: 14-35%) of summer prey ingestion. Metazoans were the dominant prey group in two years, with an overall mean contribution to ingestion of 49% (27-75%). Heterotrophic protists, by subtraction, comprised the remainder of the diet, contributing on average 27% (0-59%). Because juvenile krill are truly omnivorous even during summer, the population- and ecosystem-level impacts of climate-driven environmental change may be more complex than anticipated based on the presumption of herbivory.

1. Introduction

The Antarctic krill *Euphausia superba* (hereafter "krill") is a dominant species in the Southern Ocean and may be the most abundant wild animal species on Earth by biomass (Atkinson et al. 2009; Bar-On et al. 2018). Krill are key contributors to particle export (Gleiber et al. 2012; Belcher et al. 2019), support large populations of vertebrate predators (Trathan and Hill 2016), and are targeted by the Southern Ocean's largest commercial fishery (Nicol and Foster 2016). Krill are omnivores, and while phytoplankton typically are considered their staple prey, the dietary contributions of heterotrophic protists and copepods are difficult to assess (Hewes et al. 1985; Price et al. 1988; Schmidt and Atkinson 2016). The trophic position of krill impacts the proportion of phytoplankton production that is vertically exported or made available to higher trophic levels, because organic matter is lost via respiration with each trophic transfer.

Krill generally feed in surface waters during summer on prey that cover a broad size range and employ various trophic modes. The exceptionally fine (2-3 μm) mesh of their feeding basket suggests that krill may efficiently capture nanoplankton (2-20 μm) (McClatchie and Boyd 1983; Suh and Nemoto 1987), but laboratory studies instead show higher retention efficiency and clearance rate on microplankton (20-200 μm) (Meyer and El-Sayed 1983; Boyd et al. 1984; Quetin and Ross 1985). Common nano- and microplankton prey include autotrophic diatoms, heterotrophic ciliates, and flagellates (Schmidt et al. 2006), the latter group likely including autotrophs, heterotrophs, and mixotrophs (Gast et al. 2018). Krill also may ingest small mesozooplankton such as abundant *Oithona* spp. copepods (< 500 μm) while filter feeding, as suggested for other euphausiid species (Gibbons et al. 1991; Schmidt 2010). Krill raptorial attacks also likely allow capture of larger calanoid copepods (Abrahamsen et al. 2010; Schmidt and Atkinson 2016). This feeding flexibility results in a wide range of possible dietary compositions and trophic positions for krill during summer.

Ontogenetic, seasonal, and regional changes in krill trophic ecology are evident. Over a lifetime of ~6 years, mass-specific feeding declines as metabolic rates slow (Schmidt and Atkinson 2016) and trophic position generally increases (Polito et al. 2013; Schmidt et al. 2014). Juvenile (age-class 1) krill are particularly flexible, with variable dependence on ice algae and heterotrophs during winter (Bernard et al. 2019) and phytoplankton, copepods, and protistan grazers during summer (Schmidt et al. 2006). These previous observations indicate that juvenile krill ingest heterotrophic prey along with (not in place of) phytoplankton. Higher-productivity continental shelf regions such as the West Antarctic Peninsula (WAP) are associated with faster krill growth, presumably due to diatom-dominated diets (Atkinson et al. 2006; Schmidt et al. 2014). However, phytoplankton ingestion rates are insufficient to satisfy even minimum respiratory requirements, let alone growth, of both juvenile and adult krill during summer along the WAP (Bernard et al. 2012). Juvenile krill thus likely supplement their diets by feeding on animals to an uncertain extent.

We conducted a multi-method study of juvenile krill in the coastal WAP near Palmer Station to examine this dietary flexibility. We repeatedly collected juvenile krill to calculate a seasonal growth curve and to measure phytoplankton ingestion from gut fluorescence. Phytoplankton ingestion was also calculated using functional response curves derived from 24-h feeding incubations, and imaging flow cytometry revealed size-selective feeding. Trophic position estimates using compound-specific isotope analysis of amino acids (CSIA-AA) accounted for trophic steps through protistan and metazoan prey. We used these data to create a metabolic carbon budget for juvenile krill and to constrain the seasonal contribution of major prey groups. Our results show that juvenile krill heavily rely upon heterotrophic prey even in a season and location favorable for herbivory.

2. Materials and Methods

2.1. Krill collection, seasonal growth, and carbon requirement

We collected krill southwest of Anvers Island as part of the Palmer Antarctica Long-Term Ecological Research (PAL LTER) program. Our sampling within 15 km of Palmer Station (64° 46' S, 64° 03' W) spanned November to March over three field seasons: 2017-2018, 2018-2019, and 2019-2020 (Conroy et al. in prep.). We collected krill aboard a rigid-hulled inflatable boat using two net types: a 1 x 1 m square, 700-μm mesh Metro net and a 1-m diameter, 200-μm mesh ring net. We sampled from 0-50 m at PAL LTER Stations B and E roughly twice per week (Conroy et al. in prep.) and less consistently at other fixed sampling locations or by targeting krill swarms that were identified using an echosounder. We measured krill to the nearest 0.01 mm using Standard Length 1 (Mauchline 1980) upon return to Palmer Station. This measurement spans from the anterior tip of the rostrum to the posterior end of the uropod. A random subsample of at least 100 individuals was measured when krill were abundant. Otherwise, all krill were measured for a given tow.

The daily length mode for juvenile krill was used to calculate a seasonal growth curve. Krill collected in multiple tows on the same date were pooled for modal analysis, and only dates with >20 measured krill were included (median: 106 krill measured per date; range: 21-431). Lengths were binned into 1-mm intervals, and a kernel density estimate was fit to each daily length-frequency distribution using the function 'density' in R (R Core Team 2021). We slightly modified the approach for identifying juvenile length modes in different field seasons. Juveniles dominated the samples in 2017-2018, and the juvenile mode corresponded with the kernel density maximum. For 2018-2019 and 2019-2020, all local maxima were identified, negligible peaks were excluded, and then the local maximum at the smallest length was identified as the

juvenile mode. Three dates were excluded from 2018-2019 when the juvenile mode was anomalously small. Length data spanned 6 November to 2 March and included 23 dates from 2017-2018, 22 dates from 2018-2019, and 10 dates from 2019-2020. All data were used to calculate a single seasonal growth curve, as no differences were apparent among years. The length-at-date data were fit to a Von Bertalanffy growth model using the function 'nls' in R. The resulting model fit exhibited homoscedasticity, and the residuals were normally distributed.

The Von Bertalanffy model fit was then used to calculate a daily carbon budget for juvenile krill. Length (mm) was converted to dry weight (mg) according to Ryabov et al. (2017). Carbon was assumed to constitute 46.3% of dry weight, which was the mean of values for juvenile krill collected in December (Ikeda and Bruce 1986) and February (Färber-Lorda et al. 2009). A two-day moving window was then used to calculate daily growth rate in mg C d^{-1}. The minimum daily respiratory requirement (mg C d^{-1}) was calculated from dry weight according to Holm-Hansen and Huntley (1984). Minimum carbon ingestion was calculated as the sum of daily growth and respiration, divided by an assimilation efficiency of 85%. Previous work reported mean assimilation efficiencies of 84-88% for krill (Meyer et al. 2003; Fuentes et al. 2016).

2.2. Phytoplankton chl-a *ingestion: gut fluorescence*

Ingestion rates for chl-*a* were calculated for field-collected samples using the gut fluorescence technique (Bernard et al. 2012). Individual krill were removed immediately from the catch, measured for length in the enclosed cabin, and frozen in liquid N_2 at sea. We typically froze up to five individuals of each size class per tow when krill were present. Samples were stored at -80° C until analysis at Palmer Station. Gut pigments were extracted from whole animals in 90% acetone for at least 48 h at -20° C, and then samples were centrifuged and

returned to room temperature for determination of pigment concentration before and after acidification using a Turner 10AU fluorometer. Only individuals from the identified juvenile size class were considered in the present analysis, and only samples with at least three replicate individuals were included.

Ingestion rate (μg chl-*a* equivalent ind.$^{-1}$ h^{-1}) was calculated as the product of gut pigment content (sum of phaeopigments and chl-*a*, in μg) and gut evacuation rate (h^{-1}). We used a value of 1.48 h^{-1} for the gut evacuation rate, which is the mean of three experimentally-derived rates for juvenile krill during summer along the WAP (Bernard et al. 2012). Hourly ingestion rate was multiplied by 24 h to calculate daily ingestion rate (μg chl-*a* equiv. ind.$^{-1}$ d^{-1}). Ingestion rate and mass-specific ingestion rate (μg chl-*a* equiv. mg DW^{-1} d^{-1}) were log-transformed for linear regression to test for relationships with standard length and log-transformed chl-*a* concentration. Chl-*a* concentrations at the sampling stations were measured via fluorometric analysis of bottle samples and integrated from 0-50 m (Schofield et al. 2017; Conroy et al., in prep.).

*2.3. Phytoplankton chl-*a *ingestion: functional response*

We conducted experimental feeding incubations with juvenile krill to measure clearance and ingestion rates on natural plankton communities. Krill were collected from the upper 50 m in tows lasting <15 minutes at ship speeds of ~2 knots, typically with a non-filtering cod end. Upon return to Palmer Station, animals were transferred to 20-L buckets of whole seawater from the Palmer Station seawater intake and acclimated to experimental conditions for 24 h. Typically ~12 animals were in each acclimation bucket. Buckets were staged in an outdoor flow-through incubator (0.5 m depth) covered with window screening to maintain ambient temperature and light conditions (~33% light transmittance). We collected whole seawater the following day from

the chl-*a* maximum and filled 20-L experimental buckets to 19 L. One liter was removed from each bucket to process initial samples for chl-*a* and imaging flow cytometry. Four to ten actively swimming krill were transferred from acclimation buckets to each of 4-6 experimental replicates. An additional 4-6 replicates were maintained as experimental controls without krill. In one case, experimental seawater was diluted with 0.2-µm filtered seawater so that treatments of 100%, 30%, and 10% whole seawater were incubated on a single date but treated as separate experimental units, because measuring clearance rate at low prey concentrations is critical for distinguishing functional response types (Kiørboe et al. 2018). Three krill replicates were maintained along with a single control for each concentration. All experimental buckets were gently stirred on average every 2 h to re-suspend cells. Experiments ran for 24 h, after which krill were removed, measured for length, and frozen at -80° C. Final samples for chl-*a* and imaging flow cytometry were collected from each replicate. Replicates were excluded if krill were dead or inactive at the end of the experiment.

Chl-*a* samples were filtered through Whatman GF/F filters and frozen at -80° C until analysis at Palmer Station. Instantaneous growth rate (d^{-1}), instantaneous grazing rate (d^{-1}), and clearance rate (L $ind.^{-1}$ d^{-1}) were calculated according to Frost (1972). Negative grazing rates may indicate trophic cascades within experiments (Nejstgaard et al. 2001) and were excluded for fitting functional response curves. Ingestion rate was calculated as the product of clearance rate and initial concentration (Marin et al. 1986). Type II (Holling 1965) and type III (Kiørboe et al. 1982) functional response curves were fit using the 'nls' function in R. The fitted chl-*a* functional response curve was used to calculate field grazing rates according to the maximum chl-*a* concentration (chl_{max}) measured at PAL LTER Station B. *In situ* chl-*a* was measured

typically twice per week on downcasts with a Wet Labs ECO fluorometer. Fluorescence data were binned into 1-m depth intervals prior to identifying the chl_{max}.

2.4. Phytoplankton carbon ingestion

Chl-*a* was converted to phytoplankton carbon (C_{phyto}) using two different regression fits to historical data. Paired bottle samples of chl-*a* and particulate organic carbon (POC) near Palmer Station were aggregated from 17 summer field seasons between 1992 to 2012 (PAL LTER 2017, https://doi.org/10.6073/pasta/db8a3048806917b7c2b30e1ee7a9dd88; PAL LTER 2022, https://doi.org/10.6073/pasta/d275e5736e201ce52946c675bebe46f6). Data were not available for the 2007-2008 and 2008-2009 field seasons. 2010-2011 was excluded due to anomalously low POC values. Data were restricted to the months of November-February, depths of 0-50 m, POC values > 5 μg L^{-1}, and chl-*a* values from 0.05-20 μg L^{-1}. This screening resulted in a data set with 3,768 paired POC and chl-*a* values. The minimum observed POC at a given chl-*a* concentration likely represents C_{phyto}, because heterotrophs and detritus can increase POC without increasing chl-*a* (Sathyendranath et al. 2009). Quantile regression on log-transformed data is a method for estimating C_{phyto} as a function of chl-*a*. We implemented this approach with the 'rq' function in the package 'quantreg' and used the 0.02 quantile, because the outlier removal approach of Sathyendranath et al. (2009) was not appropriate for our data. We also fit an ordinary least squares regression to the log-transformed data as an alternative method that predicts higher C_{phyto} values. Both of these approaches were used to transform chl-*a* values from feeding experiments, and the predicted C_{phyto} was used to fit new functional responses. We converted chl_{max} time series in the same manner to calculate high and low C_{phyto} ingestion time series for each field season.

2.5. Size-selective grazing and particle size distribution

Initial and final experimental particle size distributions were derived from 5-mL samples analyzed with an Imaging FlowCytobot (IFCB; McLane Labs, Falmouth, MA, USA). The IFCB captures images and measures chl-*a* fluorescence and scattered light for particles from ~10-150 μm (Olson and Sosik 2007). Images included both photosynthetic and non-photosynthetic particles, because the instrument was set to trigger with a side scatter or fluorescence threshold. For three experiments, IFCB samples were preserved in 50% glutaraldehyde, frozen in liquid N_2, and stored at -80° C until analysis at Rutgers University. Preservation may lead to underestimation of total biovolume and cell abundance, but relative changes (as considered here within experiments) were consistent in a comparison of live and preserved samples (Nardelli et al. in prep.). The proportional contribution of different taxonomic groups was also similar in live and preserved comparisons. Particle images were extracted and processed according to Sosik and Olson (2007). All particles with a diameter of 4-40 μm were categorized into 13 discrete bins based on equivalent spherical diameter, and all bin widths were equal on a logarithmic scale. The biovolume concentration ($\mu m^3\ L^{-1}$) was summed within each bin for every sample. Instantaneous growth and grazing rates for each size class were calculated according to Frost (1972), negative grazing rates were excluded, and clearance rates were reported as the mean of individual experiment means.

2.6. Compound-specific isotope analysis of amino acids

Krill regularly were frozen at -80° C after measurement at Palmer Station to produce a catalog of frozen samples from which a subset could be processed for CSIA-AA. After each field season, 4-10 sampling dates were selected to achieve the widest temporal coverage and to allow

grouping of samples with similarly sized krill within different periods of each season. Krill were prepared for analysis at the Virginia Institute of Marine Science. Each sample consisted of 6-78 individuals collected on the same day. We measured individual krill for length, dissected the third and fourth abdominal segments, and removed the exoskeleton while the sample was on ice (Schmidt et al. 2004). All dissected abdominal segments from a given day were pooled into a single sample and freeze-dried for 24 h. Dry samples were homogenized, and sample weights ranged from 5.7-34.5 mg. Samples were processed at the Stable Isotope Facility at the University of California, Davis for CSIA-AA of ^{15}N.

Amino acids were liberated from krill samples by acid hydrolysis with 6 M HCl. Amino acids were made suitable for gas chromatography by derivatization as N-acetyl methyl esters (Corr et al. 2007; Walsh et al. 2014). Amino acid derivatives were separated on an Agilent DB-35 column. GC-C-IRMS was performed on a Thermo Trace GC 1310 gas chromatograph coupled to a Thermo Scientific Delta V Advantage isotope-ratio mass spectrometer via a GC IsoLink II combustion interface (Yarnes and Herszage 2017). The combustion reactor was a NiO tube containing CuO and NiO wires maintained at 1000° C. Water was removed through a Nafion dryer before the analyte gases were transferred to the IRMS, and CO_2 was removed from the post-combustion carrier stream through the use of a liquid N_2 trap. All krill samples were analyzed in duplicate injections. The standard deviation of $\delta^{15}N$ for amino acids used in subsequent analyses averaged 0.3‰ and ranged from 0.01 to 1‰. Initial $\delta^{15}N$ values were adjusted based on the known isotopic composition of norleucine, which was used as an internal reference. Then $\delta^{15}N$ values were adjusted based on an external reference mixture of 10 amino acids and scale-normalized to air using a second external reference mixture of 10 amino acids

(Yarnes and Herszage 2017). Replicates of the external reference materials were measured every five samples.

2.7. Trophic position and dietary composition

CSIA-AA provides an internal index for trophic position, thereby resolving a serious issue of bulk isotope analysis, which cannot account for asynchronous changes in the isotopic signature of primary producers and consumers (Schmidt et al. 2004). Each amino acid has a unique trophic discrimination factor (TDF), defined as the increase in $\delta^{15}N$ from one trophic level to the next (Chikaraishi et al. 2009). "Trophic" amino acids show relatively large increases in $\delta^{15}N$ with each trophic step while N fractionation is limited in "source" amino acids (McClelland and Montoya 2002). Therefore, the difference in $\delta^{15}N$ values between "trophic" and "source" amino acids is used to determine a consumer's trophic position (*TP*):

$$TP = \frac{\left(\delta^{15}N_{trophic} - \delta^{15}N_{source} - \beta\right)}{TEF} + 1$$

where β is the mean difference between $\delta^{15}N$ values of the trophic and source amino acids within primary producers, and *TEF* is the trophic enrichment factor, which is the difference between trophic and source TDFs (Chikaraishi et al. 2009). Alanine and glutamic acid are trophic amino acids that both enrich through metazoans. Alanine also is enriched in ^{15}N due to trophic steps through protistan grazers, but glutamic acid is not (Gutiérrez-Rodríguez et al. 2014; Décima et al. 2017). We therefore calculated trophic position twice, using glutamic acid (TP_{Glu}) and using alanine (TP_{Ala}). Phenylalanine was the source amino acid in both cases. We used values of β_{Glu} = 3.4‰; β_{Ala} = 3.2‰; TEF_{Glu} = 6.1‰; and TEF_{Ala} = 4.5‰ according to Décima and Landry (2020).

Our multi-method approach made it possible to constrain a range of feasible dietary contributions from major prey groups. We integrated the high and low C_{phyto} ingestion rates each year from 1 December to 28 February and divided by minimum carbon ingestion to constrain the dietary fraction of phytoplankton. We constrained the dietary fraction of metazoans (DF_{meta}) using TP_{Glu}:

$$DF_{meta} = \frac{TP_{Glu} - 2}{\overline{TP_{Glu_{meta}}} - 1}$$

where $\overline{TP_{Glu_{meta}}}$ is the mean trophic position of metazoan prey if estimated with glutamic acid and phenylalanine. We solved this equation with the mean value of TP_{Glu} for each year and used values of 2 and 2.5 for $\overline{TP_{Glu_{meta}}}$. The dietary fraction of heterotrophic protists was a closure term (i.e, total diet composition must sum to 100%) and was not independently assessed.

3. Results

3.1. Seasonal growth and carbon requirement

November to March was a period of rapid growth and increasing metabolic demand for juvenile krill. The length mode increased from 13-16 mm in early November to 26-30 mm in late February (Fig. 1a). Length-based growth rate was derived from the Von Bertalanffy model fit and declined from 0.21 mm d^{-1} on 6 November to 0.082 mm d^{-1} on 3 March. The mean length-based growth rate over that period was 0.13 mm d^{-1}. Converting units from the Von Bertalanffy model fit revealed the opposite seasonal trend for carbon-based growth rate (Fig. 1b). Mean carbon-based growth rate was 0.14 mg C d^{-1} and increased from 0.07 mg C d^{-1} on 6 November to a maximum of 0.17 mg C d^{-1} on 23 February. More carbon was required for growth than for respiration until 22 December, but after 20 February daily growth equaled <50% of the

respiratory demand (Fig. 1b). Minimum carbon ingestion increased seasonally from 0.12 mg C d^{-1} (8.1% of body C) to 0.65 mg C d^{-1} (3.6% of body C) (Fig. 1c).

*3.2. Phytoplankton chl-*a *ingestion*

As measured by the gut fluorescence method, mean chl-*a* ingestion rate was 0.73 μg chl-*a* ind^{-1} d^{-1} (range: 0.08-2.6 μg ind^{-1} d^{-1}; $n = 48$ tows). Seasonal patterns in grazing rate changed among years (Fig. 2a), but the mean grazing rate was not significantly different between years (ANOVA: $F = 1.4$; $p = 0.26$). Mean grazing rate increased with depth-integrated chl-*a* concentration (linear regression: $t = 2.5$; $p = 0.016$; $r^2 = 0.12$) but was not significantly correlated with the mean length of krill (linear regression: $t = 1.1$; $p = 0.26$). Mass-specific grazing rate was more strongly related with chl-*a* concentration (Fig. 2b) and declined by an order of magnitude as krill grew from 11 to 29 mm (Fig. 2c) (multiple linear regression: $|t| \geq 3.0$; $p \leq 0.005$; $r^2 = 0.47$). Dry mass increased 20-fold over this size range.

Chl-*a* ingestion in experimental feeding incubations was comparable to gut fluorescence measurements and fit a Type III functional response. Mean initial chl-*a* ranged from 0.10 to 3.1 μg L^{-1} across 13 experiments, and mean ingestion rates ranged from 0.11 to 4.0 μg ind^{-1} d^{-1} (Fig. 3a). The experimental data fit a Type III functional response better than a Type II response due to declining clearance rates at low chl-*a* concentrations (Fig. 3b). The model fit indicated that clearance rate reached a maximum of 1.8 L ind^{-1} d^{-1} when chl-*a* was 0.98 μg L^{-1} and then gradually declined as chl-*a* increased. According to this functional response curve, chl-*a* ingestion rate was 2.6 μg ind^{-1} d^{-1} (i.e., equal to the maximum rate from gut fluorescence) when chl-*a* concentration was 1.6 μg L^{-1}. At the high end of our experimental range, chl-*a* concentration of 3.0 μg L^{-1} coincided with a modeled ingestion rate of 3.6 μg ind^{-1} d^{-1}.

The chl-*a* ingestion time series calculated from the experimental functional response and *in situ* chl_{max} measurements yielded higher values than the gut fluorescence method. Across three field seasons, chl_{max} at PAL LTER Station B ranged from 0.2 to 19.1 μg L^{-1} over 104 sampling dates and was below our maximum experimental concentration of 3.1 μg L^{-1} for 76% of observations (Fig. 4). Chl_{max} was significantly higher in 2018-2019 (median: 2.8 μg L^{-1}) than in 2017-2018 (1.3 μg L^{-1}) or 2019-2020 (1.5 μg L^{-1}) (ANOVA: $F = 13.9$; $p < 0.00001$; Tukey's HSD: $p < 0.005$). The mean chl-*a* grazing rate from the functional response model was 2.8 μg ind^{-1} d^{-1} (Fig. 5), which exceeded the highest daily grazing rate from the gut fluorescence method (i.e., 2.6 μg ind^{-1} d^{-1}). Mean chl-*a* ingestion was 3.4 μg ind^{-1} d^{-1} in 2018-2019 and significantly higher compared to 2.2 and 2.6 μg ind^{-1} d^{-1} respectively in 2017-2018 and 2019-2020 (ANOVA: $F = 14.5$; $p < 0.00001$; Tukey's HSD: $p < 0.004$).

3.3. Phytoplankton carbon ingestion

Calculating C_{phyto} from chl-*a* using two different methods produced C_{phyto} values that differed by a factor of 2-4. Our quantile regression fit was similar to that of Sathyendranath et al. (2009) but predicted lower C_{phyto} when chl-*a* was above 0.4 μg L^{-1} (Fig. 6). The quantile and ordinary least squares regression fits converged as chl-*a* increased. The ordinary least squares fit predicted C_{phyto} to be 4.4 times higher compared to the quantile regression when chl-*a* was 0.05 μg L^{-1}, and this decreased to a 2.0-fold difference at 20 μg L^{-1} (Fig. 6). When applied to the chl_{max} time series, the ordinary least squares estimates of C_{phyto} at Station B (median = 233 μg L^{-1}) were on average 2.7 times higher than those from the quantile regression (median = 85 μg L^{-1}) (Fig. 7). Mean experimental C_{phyto} ingestion was on average 2.4 (range: 2.0-3.0) times higher

when using the ordinary least squares regression, and the functional response curves for C_{phyto} predicted lower maximum clearance rates than those for chl-*a* (Fig. 8).

Despite a two-fold difference in seasonal C_{phyto} ingestion, both methods indicate that autotrophic prey were inadequate to satisfy juvenile krill dietary needs during summer near Palmer Station. The minimum carbon ingestion to support growth and respiration from 1 December to 28 February was 39.3 mg C ind^{-1} (Fig. 1c). In comparison, the high and low C_{phyto} ingestion rates for that same period ranged from 5.5-13.8 mg C ind^{-1} across the three field seasons (Fig. 9). Accordingly, phytoplankton accounted for only 14-35% of the minimum carbon ingestion required by juvenile krill during our three summer field seasons (Table 1). This deficit was the result of consistent phytoplankton ingestion while krill grew larger and respiratory requirements increased (Fig. 9). Heterotrophic prey likely comprised the remaining 65-86% of necessary carbon ingestion, suggesting the minimum *TP* of juvenile krill was 2.65.

3.4. Size-selective grazing and particle size distribution

Imaging flow cytometry from 11 feeding experiments revealed a mismatch between the size-selectivity of juvenile krill and the size distribution of their potential prey, with phytoplankton biomass concentrated within small cells that krill consumed inefficiently. Mean clearance rate increased from ~1 L ind^{-1} d^{-1} on particles sized 4-12 μm to 4.5 L ind^{-1} d^{-1} on particles 34-40 μm, the largest size bin in our analysis (Fig. 10a). In contrast, 5-12 μm particles accounted for 62% of mean initial prey biovolume in our feeding experiments (Fig. 10b). The variability in total phytoplankton biomass across experiments was likely due to changes in 5-12 μm cells, the biovolume of which was more variable than that of larger size classes.

3.5. Trophic position and dietary composition

Trophic position estimates using the $\delta^{15}N$ values of amino acids support the importance of heterotrophic prey for juvenile krill during summer. The source amino acid phenylalanine $\delta^{15}N$ values ranged from 0.7-2.7‰ while the $\delta^{15}N$ values of the trophic amino acids glutamic acid and alanine ranged from 12.0-16.3‰ and 12.6-18.2‰, respectively (Fig. 11). TP_{Glu} (mean = 2.6) was significantly lower than TP_{Ala} (mean = 3.3) (paired *t*-test: $t = 16.1$; $p = 1.2 \times 10^{-13}$) (Fig. 12). This difference presumably was due to trophic steps through heterotrophic protists, which TP_{Glu} does not detect. The mean difference in TP estimates between the two methods was 0.8 and did not change significantly between years (ANOVA: $F = 1.2$; $p = 0.32$) (Fig. 12c), indicating that heterotrophic protists were a substantial, consistent trophic link between phytoplankton and juvenile krill. In contrast, mean TP_{Glu} and TP_{Ala} were both 0.2-0.5 trophic steps lower in 2017-2018 compared to 2018-2019 and 2019-2020 (ANOVA: $F > 5.2$; $p < 0.02$; Tukey's HSD: $p < 0.05$) (Fig. 12a-b), suggesting that the trophic contribution of metazoan prey increased in the latter two years.

Our multi-method approach on average attributes approximately one-half of krill dietary composition to metazoans and ca. 25% each to phytoplankton and heterotrophic protists. Seasonal phytoplankton contributions to minimum krill carbon ingestion were consistent across years, with a multi-year mean of 24% (Table 1; Fig. 9). The relative contribution of metazoans was more variable among years according to TP_{Glu}, and annual means ranged from 33% in 2017-2018 to 63% in 2019-2020 (Table 1; Fig. 12a). The assumed TP_{Glu} of metazoan prey themselves impacted their annual contribution by 13-25%, but metazoans composed the largest dietary fraction in 2018-2019 and 2019-2020 regardless of method. The relative proportion of heterotrophic protists was most sensitive to method selection (≥ 30% range within years) but was

simply a closure term to complete the diet (Table 1). Interannual differences were also substantial for heterotrophic protists, which comprised the largest mean dietary fraction in 2017-2018 (44%) but the smallest in the following two years. Overall, this analysis indicates phytoplankton consistently comprised less than one-third of the juvenile krill diet during summer and that the relative contributions of metazoan and protistan heterotrophs changed annually.

4. Discussion

4.1. Seasonal growth and carbon requirement

Summer is a period of rapid growth for juvenile krill, and our measured growth rates appear robust when compared with other methods. Our mean daily growth rate during January and February was 0.11 mm d^{-1}. Similarly, a length-frequency approach utilizing net surveys from 1992 to 2008 in the northern Antarctic Peninsula reported mean growth rates of ~0.1 mm d^{-1} between January and February for 20-30 mm krill (Shelton et al. 2013). Growth rates of 0.07-0.08 mm d^{-1} derived from instantaneous growth incubations during four field seasons at Palmer Station in the early 1990s (Ross et al. 2000) were half of our mean growth rate (0.15 mm d^{-1}) for the period of 15 November to 14 January. However, instantaneous growth rates decline quickly during experimental incubations and should be corrected to avoid substantial underestimation (Kawaguchi et al. 2006; Tarling et al. 2006). After accounting for this correction, a meta-analysis of instantaneous growth data found a seasonal decline in daily growth rate from ~0.2 mm d^{-1} in early summer to <0.1 mm d^{-1} by early autumn (Kawaguchi et al. 2006), similar to the pattern from our Von Bertalanffy model fit. Given the agreement between these independent methods and studies, our length-based seasonal growth curve is a reasonable basis from which to constrain minimum metabolic demand.

Minimum daily carbon ingestion rates of 4-8% krill body carbon are well below the highest calculated daily rations of ~20% body carbon (Clarke et al. 1988; Atkinson et al. 2006). Consequently, phytoplankton may account for an even smaller dietary fraction than the 14-35% reported here. We assumed investment in reproduction was negligible, because krill typically do not reach maturity until at least 32 mm (age-class 2) (Siegel and Loeb 1994; Reiss 2016). Excretion, however, was not calculated and may be substantial. Experimentally-measured dissolved organic carbon (DOC) release by krill during January and February was 202 μmol g^{-1} h^{-1} (Ruiz-Halpern et al. 2011). While excretion of assimilated material may be the dominant form of DOC release (Saba et al. 2011), sloppy feeding and leaching fecal pellets release unassimilated DOC (Møller et al. 2003; Møller 2007). These distinct DOC release mechanisms are unassessed for krill, and therefore excretion rates remain unknown. The respiratory cost of swimming also is not trivial (Swadling et al. 2005) but is excluded from our carbon budget due to uncertainty. Our calculated minimum daily carbon ingestion was thus conservative, because it accounted only for respiration and somatic growth.

4.2. Phytoplankton ingestion

Repeated gut fluorescence measurements provided valuable insight into the regional variability, functional response, and allometry of krill grazing. Chl-*a* ingestion rates were intermediate compared to those from two previous studies of juvenile krill using gut fluorescence. Our values (0.1-2.6 μg ind^{-1} d^{-1}) were lower than measured during January along the WAP where chl-*a* ingestion ranged from 1.4-6.6 μg ind^{-1} d^{-1} (Bernard et al. 2012). Grazing rates in that study may have been higher due to the inclusion of larger animals (age-class 2) within the juvenile category and were particularly elevated in the Southern WAP compared to

the northern WAP near Palmer Station (Bernard et al. 2012). In contrast, our mean of 0.7 μg ind^{-1} d^{-1} was similar to measurements for juvenile krill in the eastern Atlantic sector at 56-60° S during December and January, which ranged from 0.5-0.6 μg ind^{-1} d^{-1} (Pakhomov and Froneman 2004). No significant change in grazing rate (and the order-of-magnitude decline in mass-specific grazing) over the size range considered in our study supported the use of a single functional response for krill from age-class 1. The positive relationship between grazing rate and chl-*a* concentration using gut fluorescence supported the use of a functional feeding response that was investigated more thoroughly by our independent experiments.

Unlike in some prior studies, we found a type III functional response in our krill feeding experiments that indicates saturating ingestion as chl-*a* concentration increases. This finding likely reflects the use of natural plankton communities at natural densities in our incubations, which mimic *in situ* prey conditions. Prior studies show increasing ingestion at chl-*a* concentrations as high as ~20 μg L^{-1}, which may be due to the artificial concentration of large prey (Price et al. 1988; Atkinson and Snÿder 1997; Meyer et al. 2010) (see Section 4.4). At least one previous study also reported a type III functional response for krill (Boyd et al. 1984), and saturating functional responses are observed or assumed for other euphausiids, copepods, and forage fishes (Rose et al. 2015; Agersted and Nielsen 2016; Kiørboe et al. 2018). Type III responses in particular are expected for active feeders (Kiørboe et al. 2018) such as krill, which seek out prey and reduce feeding effort in the absence of prey (Hamner et al. 1983). Although our experimental volume (18 L) was relatively large for a feeding study, clearance rates may be depressed within experimental containers (Price et al. 1988). The small size of the animals in our study likely reduced this effect compared to prior work with larger adult krill. Chl-*a* ingestion calculated using the functional response curve was higher than when using the gut fluorescence

technique, perhaps because 24-h experiments captured diel periodicity that cannot be detected otherwise.

Phytoplankton ingestion (<1-9% krill body carbon d^{-1}) was insufficient to meet juvenile krill metabolic demand. Similarly, during January in the eastern Atlantic sector of the Southern Ocean, daily phytoplankton ingestion was <2% of krill body carbon except at a single ice-edge station where a bloom was underway (Perissinotto et al. 1997). Stomach content analysis in the same study found that protistan and metazoan zooplankton represented >50% of identifiable prey items at 3 of 6 stations. Further analysis and addition of samples from South Georgia and the Lazarev Sea showed that heterotrophic material constituted on average 79% of stomach content mass for krill collected during January-March (Perissinotto et al. 2000). Additionally, daily phytoplankton ingestion was on average 0.5% of body carbon for juvenile krill during January along the WAP (Bernard et al. 2012). At the high end, experimental incubations using sea-ice derived algae found that daily phytoplankton ingestion was 10% of body carbon when C_{phyto} concentration was 600 μg L^{-1} but dropped below 4% of body carbon at a C_{phyto} level of ~300 μg L^{-1} (Meyer et al. 2010). Thus, our finding of inadequate phytoplankton consumption to support krill metabolic C demand is supported by previous studies and other methodologies.

4.3. Size-selective grazing and particle size distribution

There is a clear mismatch between the size-selectivity of krill and the natural size distribution of available prey near Palmer Station. Imaging flow cytometry showed that >60% of natural biovolume was concentrated in nano-sized particles upon which krill fed 50-75% less efficiently compared to larger particles. Small cells persistently dominated across two field seasons at Palmer Station, and mean cell size decreased from late spring to early autumn

(Nardelli et al. in prep.), further supporting a seasonal decrease in the contribution of phytoplankton to krill diet. Our size-specific clearance rates (1-4.5 L ind^{-1} d^{-1}) also agree well with a previous experimental study of similarly sized krill (18-23 mm) and natural plankton prey that reports mean clearance rates of 1 L ind^{-1} d^{-1} on prey <20 μm and 2-3 L ind^{-1} d^{-1} on prey >20 μm (Meyer and El-Sayed 1983).

Climate-driven changes in the WAP ecosystem are expected to exacerbate the mismatch between krill size-selectivity and phytoplankton size distribution near Palmer Station. Warming and ice loss are associated with a shift to smaller-celled phytoplankton, specifically from diatoms to cryptophytes (Moline et al. 2004). Satellite observations from 1978-2006 show that phytoplankton size likely decreased north of Palmer Station while increasing farther south (Montes-Hugo et al. 2009), and this pattern progressed poleward from the 1990s-2010s (Brown et al. 2019; Rogers et al. 2020). Krill abundance and recruitment declined north of Palmer Station while abundance remained steady south of Palmer Station as the southern WAP became an important spawning area after the 1990s (Atkinson et al. 2019; 2022). We hypothesize that phytoplankton size may be a key driver of changing krill biogeography. Indeed, years dominated by diatoms are associated with faster krill growth and lead to successful recruitment (Ross et al. 2000; Saba et al. 2014). The lipid content of krill is also higher in the southern WAP (Ruck et al. 2014) where sea-ice duration is longer and diatoms dominate (Lin et al. 2021). Distinguishing the food-web effects of diatoms on krill condition is difficult (Pond et al. 2005), and the limited direct dietary contribution of phytoplankton likely allows krill to persist despite changes in phytoplankton composition.

4.4. Trophic position and dietary composition

The mean TP_{Ala} of juvenile krill was 3.3 and reveals the importance of heterotrophic protists in the coastal Antarctic food web. TP_{Ala} exceeded 2.65 (i.e., minimum *TP* from metabolic budget analysis) for 96% of samples while TP_{Glu} (mean = 2.6) was below 2.65 for 65% of samples. TP_{Ala} therefore appeared to be more accurate but was more variable due to alanine's relative volatility (Fig. 12) (Décima et al. 2017). Only alanine isotopically detects trophic steps through heterotrophic protists (Gutiérrez-Rodríguez et al. 2014; Décima et al. 2017), which are the dominant grazers in the WAP ecosystem (Garzio et al. 2013; Sailley et al. 2013; Morison and Menden-Deuer 2018). TP_{Ala} thus accounted for important trophic links and revealed that juvenile krill were secondary consumers during summer near Palmer Station. The use of multiple trophic amino acids can decrease variability in *TP* (Nielsen et al. 2015), but when we followed the multi-amino acid approach of Hannides et al. (2020) the resulting *TP* estimates were always less than the minimum feasible estimate, further emphasizing the value of alanine to detect important contributions of heterotrophic protists.

Our multi-method approach for assessing the dietary composition of krill sheds light on the trophic flexibility of this species across the southwest Atlantic region. Krill collected in the Scotia Sea and near South Georgia during January-February 2003 had TP_{Ala} (mean = 3.9) and TP_{Glu} (mean = 3.0) values that were ~0.5 higher than those in our study (Schmidt et al. 2006, calculated from their Table 7). This suggests increased consumption of heterotrophic prey relative to our study, which is expected in this northern region where krill are larger due to the absence of local recruitment (Atkinson et al. 2019, 2022). Much of the stomach contents of krill is unidentifiable visually, but heterotrophic protists can dominate the identified portion (Schmidt

et al. 2006). Our multi-method approach also suggested that heterotrophic protists comprised the largest dietary fraction in 2017-2018, but metazoans were the main prey in 2018-2019 and 2019-2020. High experimental clearance rates on copepods (Price et al. 1988; Atkinson and Snÿder 1997) support the latter finding, but copepods are often relatively rare in identified stomach contents compared to phytoplankton and heterotrophic protists (Schmidt et al. 2014). Fatty acid trophic markers confirm that copepods are consistent prey for krill across regions and seasons (Schmidt et al. 2014), but dietary fractions remain uncertain and there is continued need to reconcile dietary information across various methods (Schmidt and Atkinson 2016).

Current hypotheses underlying krill population dynamics should be re-evaluated within a framework that emphasizes omnivory. A simulation model including only autotrophic prey suggests that competition-driven starvation of larval and juvenile krill during autumn is the key driver of regional population cycles along the WAP (Ryabov et al. 2017). Our results also demonstrate that phytoplankton is insufficient to support juvenile krill from summer into autumn, but autumn starvation may be reduced if juvenile krill feed substantially on heterotrophic prey. Thus, future models should include heterotrophic prey. Empirical relationships show that larval abundance, recruitment success, and post-larval abundance are all positively related to phytoplankton productivity (Loeb et al. 2009; Saba et al. 2014; Steinberg et al. 2015). One interpretation is that higher reproductive output and overwinter survival are due to increased phytoplankton consumption. We do not rule this out but note that elevated phytoplankton biomass also coincides with elevated abundance of heterotrophic prey, including copepods and heterotrophic protists (Loeb et al. 2009; Garzio and Steinberg 2013; Gleiber 2014). Given that larger krill occupy higher trophic positions (Polito et al. 2013; Schmidt et al. 2014), we expect that omnivory is even more important for spawners. Additional trophic steps between

phytoplankton and krill reduce food-web efficiency and require increased primary productivity to support an equivalent level of krill production.

4.5. Seasonal shift in trophic role

Comparison with a previous CSIA-AA study supports the increasing consumption of copepod prey from early summer into autumn. Mean TP_{Ala} and TP_{Glu} were 2.9 and 2.8, respectively, for krill collected near the South Shetland Islands in March (Schmidt et al. 2004, calculated from their Table 2b). In comparison, we estimated mean TP_{Ala} of 3.3 and mean TP_{Glu} of 2.6. These differences suggest increased importance of metazoans but decreased importance of heterotrophic protists during autumn compared to our summer study. That pattern is consistent with a seasonal increase in copepod abundance (Conroy et al. in prep) and a presumed seasonal decline in heterotrophic protist abundance due to close coupling of both with phytoplankton (Garzio and Steinberg 2013; Morison and Menden-Deuer 2018). The onset of diel vertical migration by krill beginning in March (Nardelli et al. 2021) also decouples juvenile krill from phytoplankton but allows them to prey on zooplankton at depth during daytime.

Genetic analyses of krill stomach contents similarly indicate a seasonal shift from phytoplankton to copepod prey between spring and autumn. Diatoms (dominated by chain-forming *Chaetoceros* spp.) made up 75% of prey sequence reads in the stomachs of adult krill (>32 mm) during December in the coastal WAP (Cleary et al. 2018). Large diatoms are most abundant early in the growing season (Moline et al. 2004; Nardelli et al. in prep.). Metazoans constituted on average 9.4% of prey sequence reads during December, and the copepods *Metridia* spp. and *Oithona* spp. were most common (Cleary et al. 2018). *Oithona* spp. copepods dominated numerically and increased from November-March during our study years

(Conroy et al. in prep.). Genetic diet analysis in the northern Antarctic Peninsula from March-May indicated that copepods (mainly *Oithona, Metridia*, and *Calanus* spp.) were the most common prey class in krill stomachs (27% of sequence reads) (Pauli et al. 2021). Krill also positively selected for copepods and assimilated them more efficiently than other prey types in that study. Copepods are thus an important resource for juvenile krill, which must rely on prey other than phytoplankton to satisfy their growing metabolic demand from spring into autumn.

4.6. Conclusion

Heterotrophic prey dominated the diets of juvenile krill across three summer field seasons near Palmer Station. We calculated a minimum feasible *TP* of 2.65 for juvenile krill and suggest this is a low-end estimate for post-larval krill due to the setting of our study. Coastal waters are the most productive along the WAP (Vernet et al. 2008; Brown et al. 2019), phytoplankton productivity is highest during summer, and juvenile krill are expected to rely less on omnivory compared to larger individuals (Polito et al. 2013; Schmidt et al. 2014). The mean TP_{Ala} of 3.3 further supports classification of krill as true secondary consumers. Although krill may have lower *TP*s during ice-edge phytoplankton blooms or anomalously productive summers, our observations agree with a regional food-web model showing the dominant flow of carbon is from small phytoplankton through heterotrophic protists near Palmer Station (Sailley et al. 2013). Additionally, our work strengthens the body of evidence demonstrating that krill consistently feed on copepods across regions and seasons (Schmidt et al. 2014). The trophic flexibility of krill may be incorporated into food-web models to test how different degrees of omnivory impact the transfer of carbon from phytoplankton to vertebrate predators (Hill et al. 2012; Ballerini et al.

2014), to the fishing fleet (Dahood et al. 2020), and to the ocean interior (Le Quéré et al. 2016; Karakuş et al. 2021).

The physiological impacts of changing krill diet composition (from months to decades) are likely complex and require further study so that they might be linked to population-level consequences. CSIA-AA time series could be a valuable tool for understanding past change in the trophic role of krill and may be recovered from preserved sample collections (Hetherington et al. 2019; Swalethorp et al. 2020). Such data would be particularly valuable when paired with population demographics, physiological measurements, and prey data (Schmidt and Atkinson 2016; Steinke et al. 2021). Faster growth rates are associated with diets rich in diatoms or heterotrophs but not cryptophytes or prymnesiophytes (Ross et al. 2000; Pond et al. 2005; Schmidt et al. 2006). Increased diatom consumption likely promotes immediate growth and reproduction while a copepod-rich diet could favor longer-term storage for overwintering (Hagen et al. 2007; Schmidt et al. 2014). Clarifying these connections from diet to physiology to population dynamics will improve predictions of changing krill abundance and distribution in the WAP ecosystem.

Acknowledgements

Thank you to the Antarctic Support Contract personnel at Palmer Station for their scientific and logistical support. We thank Leigh West, Kharis Schrage, Andrew Corso, Ashley Hann, Rachael Young, and PAL LTER colleagues for their contributions to this field project. We thank Kim Bernard, Sasha Kramer, Kyle Hinson, Chris Yarnes, and Brian Popp for technical advice. This work was supported by the National Science Foundation Antarctic Organisms and Ecosystems

Program (PLR-1440435 and OPP-2026045) and student research grants from the Virginia Institute of Marine Science.

References

Abrahamsen MB, Browman HI, Fields DM, Skiftesvik AB (2010) The three-dimensional prey field of the northern krill, *Meganyctiphanes norvegica*, and the escape responses of their copepod prey. Marine Biology 157:1251–1258.

Agersted MD, Nielsen TG (2016) Functional biology of sympatric krill species. Journal of Plankton Research 38:575–588.

Atkinson A, Hill SL, Pakhomov EA, Siegel V, Reiss CS, Loeb VJ, Steinberg DK, Schmidt K, Tarling GA, Gerrish L, Sailley SF (2019) Krill (*Euphausia superba*) distribution contracts southward during rapid regional warming. Nature Climate Change 9:142–147.

Atkinson A, Hill SL, Reiss CS, Pakhomov EA, Beaugrand G, Tarling GA, Yang G, Steinberg DK, Schmidt K, Edwards M, Rombolá E, Perry FA (2022) Stepping stones towards Antarctica: Switch to southern spawning grounds explains an abrupt range shift in krill. Global Change Biology 28:1359–1375.

Atkinson A, Shreeve RS, Hirst AG, Rothery P, Tarling GA, Pond DW, Korb RE, Murphy EJ, Watkins JL (2006) Natural growth rates in Antarctic krill (*Euphausia superba*): II. Predictive models based on food, temperature, body length, sex, and maturity stage. Limnology and Oceanography 51:973–987.

Atkinson A, Siegel V, Pakhomov EA, Jessopp MJ, Loeb V (2009) A re-appraisal of the total biomass and annual production of Antarctic krill. Deep Sea Research Part I 56:727–740.

Atkinson A, Snÿder R (1997) Krill-copepod interactions at South Georgia, Antarctica, I. Omnivory by *Euphausia superba*. Marine Ecology Progress Series 160:63–76.

Ballerini T, Hofmann EE, Ainley DG, Daly K, Marrari M, Ribic CA, Smith WO, Steele JH

(2014) Productivity and linkages of the food web of the southern region of the western Antarctic Peninsula continental shelf. Progress in Oceanography 122:10–29.

Bar-On YM, Phillips R, Milo R (2018) The biomass distribution on Earth. Proceedings of the National Academy of Sciences 115:6506–6511.

Belcher A, Henson SA, Manno C, Hill SL, Atkinson A, Thorpe SE, Fretwell P, Ireland L, Tarling GA (2019) Krill faecal pellets drive hidden pulses of particulate organic carbon in the marginal ice zone. Nature Communications 10:889.

Bernard KS, Cimino M, Fraser W, Kohut J, Oliver MJ, Patterson-Fraser D, Schofield OME, Statscewich H, Steinberg DK, Winsor P (2017) Factors that affect the nearshore aggregations of Antarctic krill in a biological hotspot. Deep Sea Research Part I 126:139–147.

Bernard KS, Gunther LA, Mahaffey SH, Qualls KM, Sugla M, Saenz BT, Cossio AM, Walsh J, Reiss CS (2019) The contribution of ice algae to the winter energy budget of juvenile Antarctic krill in years with contrasting sea ice conditions. ICES Journal of Marine Science 76:206–216.

Bernard KS, Steinberg DK, Schofield OME (2012) Summertime grazing impact of the dominant macrozooplankton off the Western Antarctic Peninsula. Deep Sea Research Part I 62:111–122.

Boyd CM, Heyraud M, Boyd CN (1984) Feeding of the Antarctic krill *Euphausia superba*. Journal of Crustacean Biology 4:123–141.

Brown MS, Munro DR, Feehan CJ, Sweeney C, Ducklow HW, Schofield OM (2019) Enhanced oceanic CO_2 uptake along the rapidly changing West Antarctic Peninsula. Nature Climate Change 9:678–683.

Chikaraishi Y, Ogawa NO, Kashiyama Y, Takano Y, Suga H, Tomitani A, Miyashita H, Kitazato H, Ohkouchi N (2009) Determination of aquatic food-web structure based on compound-specific nitrogen isotopic composition of amino acids. Limnology and Oceanography: Methods 7:740–750.

Clarke A, Quetin LB, Ross RM (1988) Laboratory and field estimates of the rate of faecal pellet production by Antarctic krill, *Euphausia superba*. Marine Biology 98:557–563.

Cleary AC, Durbin EG, Casas MC (2018) Feeding by Antarctic krill *Euphausia superba* in the West Antarctic Peninsula: differences between fjords and open waters. Marine Ecology Progress Series 595:39–54.

Conroy JA, Steinberg DK, Thomas MI, West LT (in prep.) Seasonal and interannual changes in a coastal Antarctic zooplankton community.

Corr LT, Berstan R, Evershed RP (2007) Optimisation of derivatisation procedures for the determination of δ13C values of amino acids by gas chromatography/combustion/isotope ratio mass spectrometry. Rapid Communications in Mass Spectrometry 21:3759–3771.

Dahood A, de Mutsert K, Watters GM (2020) Evaluating Antarctic marine protected area scenarios using a dynamic food web model. Biological Conservation 251:108766.

Décima M, Landry MR (2020) Resilience of plankton trophic structure to an eddy-stimulated diatom bloom in the North Pacific Subtropical Gyre. Marine Ecology Progress Series 643:33–48.

Décima M, Landry MR, Bradley CJ, Fogel ML (2017) Alanine δ15N trophic fractionation in heterotrophic protists. Limnology and Oceanography 62:2308–2322.

Färber-Lorda J, Gaudy R, Mayzaud P (2009) Elemental composition, biochemical composition

and caloric value of Antarctic krill: Implications in Energetics and carbon balances. Journal of Marine Systems 78:518–524.

Frost BW (1972) Effects of size and concentration of food particles on the feeding behavior of the marine planktonic copepod *Calanus pacificus*. Limnology and Oceanography 17:805–815.

Fuentes V, Alurralde G, Meyer B, Aguirre GE, Canepa A, Wölfl A-C, Hass HC, Williams GN, Schloss IR (2016) Glacial melting: an overlooked threat to Antarctic krill. Scientific Reports 6:27234.

Garzio LM, Steinberg DK (2013) Microzooplankton community composition along the Western Antarctic Peninsula. Deep Sea Research Part I 77:36–49.

Garzio LM, Steinberg DK, Erickson M, Ducklow HW (2013) Microzooplankton grazing along the Western Antarctic Peninsula. Aquatic Microbial Ecology 70:215–232.

Gast RJ, Fay SA, Sanders RW (2018) Mixotrophic Activity and Diversity of Antarctic Marine Protists in Austral Summer. Frontiers in Marine Science 5:13.

Gibbons MJ, Pillar SC, Stuart V (1991) Selective carnivory by *Euphausia lucens*. Continental Shelf Research 11:625–640.

Gleiber MR (2014) Long-term change in copepod community structure in the Western Antarctic Peninsula: Linkage to climate and implications for carbon cycling. (Master's Thesis). The College of William & Mary.

Gleiber MR, Steinberg DK, Ducklow HW (2012) Time series of vertical flux of zooplankton fecal pellets on the continental shelf of the western Antarctic Peninsula. Marine Ecology Progress Series 471:23–36.

Gutiérrez-Rodríguez A, Décima M, Popp BN, Landry MR (2014) Isotopic invisibility of

protozoan trophic steps in marine food webs. Limnology and Oceanography 59:1590–1598.

Hagen W, Yoshida T, Virtue P, Kawaguchi S, Swadling KM, Nicol S, Nichols PD (2007) Effect of a carnivorous diet on the lipids, fatty acids and condition of Antarctic krill, *Euphausia superba*. Antarctic Science 19:183–188.

Hamner WM, Hamner PP, Strand SW, Gilmer RW (1983) Behavior of Antarctic krill, *Euphausia superba*: chemoreception, feeding, schooling, and molting. Science 220:433–435.

Hannides CCS, Popp BN, Close HG, Benitez-Nelson CR, Ka'apu-Lyons CA, Gloeckler K, Wallsgrove N, Umhau B, Palmer E, Drazen JC (2020) Seasonal dynamics of midwater zooplankton and relation to particle cycling in the North Pacific Subtropical Gyre. Progress in Oceanography 182:102266.

Hetherington ED, Kurle CM, Ohman MD, Popp BN (2019) Effects of chemical preservation on bulk and amino acid isotope ratios of zooplankton, fish, and squid tissues. Rapid Communications in Mass Spectrometry 33:935–945.

Hewes CD, Holm-Hansen O, Sakshaug E (1985) Alternate Carbon Pathways at Lower Trophic Levels in the Antarctic Food Web. In: *Antarctic Nutrient Cycles and Food Webs*. Siegfried WR, Condy PR, Laws RM (eds) Springer, Berlin, Heidelberg, p 277–283

Hill SL, Keeble K, Atkinson A, Murphy EJ (2012) A foodweb model to explore uncertainties in the South Georgia shelf pelagic ecosystem. Deep Sea Research Part II 59–60:237–252.

Holling CS (1965) The Functional Response of Predators to Prey Density and its Role in Mimicry and Population Regulation. The Memoirs of the Entomological Society of Canada 97:5–60.

Holm-Hansen O, Huntley M (1984) Feeding requirements of krill in relation to food sources. Journal of Crustacean Biology 4:156–173.

Ikeda T, Bruce B (1986) Metabolic activity and elemental composition of krill and other zooplankton from Prydz Bay, Antarctica, during early summer (November–December). Marine Biology 92:545–555.

Karakuş O, Völker C, Iversen M, Hagen W, Gladrow DW, Fach B, Hauck J (2021) Modeling the Impact of Macrozooplankton on Carbon Export Production in the Southern Ocean. Journal of Geophysical Research: Oceans 126:e2021JC017315.

Kawaguchi S, Candy SG, King R, Naganobu M, Nicol S (2006) Modelling growth of Antarctic krill. I. Growth trends with sex, length, season, and region. Marine Ecology Progress Series 306:1–15.

Kiørboe T, Møhlenberg F, Nicolajsen H (1982) Ingestion rate and gut clearance in the planktonic copepod *Centropages hamatus* (Lilljeborg) in relation to food concentration and temperature. Ophelia 21:181–194.

Kiørboe T, Saiz E, Tiselius P, Andersen KH (2018) Adaptive feeding behavior and functional responses in zooplankton. Limnology and Oceanography 63:308–321.

Le Quéré C, Buitenhuis ET, Moriarty R, Alvain S, Aumont O, Bopp L, Chollet S, Enright C, Franklin DJ, Geider RJ, Harrison SP, Hirst AG, Larsen S, Legendre L, Platt T, Prentice IC, Rivkin RB, Sailley S, Sathyendranath S, Stephens N, Vogt M, Vallina SM (2016) Role of zooplankton dynamics for Southern Ocean phytoplankton biomass and global biogeochemical cycles. Biogeosciences 13:4111–4133.

Lin Y, Moreno C, Marchetti A, Ducklow H, Schofield O, Delage E, Meredith M, Li Z, Eveillard

D, Chaffron S, Cassar N (2021) Decline in plankton diversity and carbon flux with reduced sea ice extent along the Western Antarctic Peninsula. Nature Communications 12:4948.

Loeb VJ, Hofmann EE, Klinck JM, Holm-Hansen O, White WB (2009) ENSO and variability of the Antarctic Peninsula pelagic marine ecosystem. Antarctic Science 21:135–148.

Marin V, Huntley ME, Frost B (1986) Measuring feeding rates of pelagic herbivores: analysis of experimental design and methods. Marine Biology 93:49–58.

Mauchline J (1981) Measurement of body length of *Euphausia superba* Dana. Éditeur inconnu.

McClatchie S, Boyd CM (1983) Morphological Study of Sieve Efficiencies and Mandibular Surfaces in the Antarctic Krill, *Euphausia superba*. Canadian Journal of Fisheries and Aquatic Sciences 40:955–967.

McClelland JW, Montoya JP (2002) Trophic Relationships and the Nitrogen Isotopic Composition of Amino Acids in Plankton. Ecology 83:2173–2180.

Meyer B, Atkinson A, Blume B, Bathmann UV (2003) Feeding and energy budgets of larval Antarctic krill *Euphausia superba* in summer. Marine Ecology Progress Series 257:167–178.

Meyer B, Auerswald L, Siegel V, Spahić S, Pape C, Fach BA, Teschke M, Lopata AL, Fuentes V (2010) Seasonal variation in body composition, metabolic activity, feeding, and growth of adult krill *Euphausia superba* in the Lazarev Sea. Marine Ecology Progress Series 398:1–18.

Meyer MA, El-Sayed SZ (1983) Grazing of *Euphausia superba* Dana on natural phytoplankton populations. Polar Biology 1:193–197.

Moline MA, Claustre H, Frazer TK, Schofield O, Vernet M (2004) Alteration of the food web

along the Antarctic Peninsula in response to a regional warming trend. Global Change Biology 10:1973–1980.

Møller EF (2007) Production of dissolved organic carbon by sloppy feeding in the copepods *Acartia tonsa*, *Centropages typicus*, and *Temora longicornis*. Limnology and Oceanography 52:79–84.

Møller EF, Thor P, Nielsen TG (2003) Production of DOC by *Calanus finmarchicus*, *C. glacialis* and *C. hyperboreus* through sloppy feeding and leakage from fecal pellets. Marine Ecology Progress Series 262:185–191.

Montes-Hugo M, Doney SC, Ducklow HW, Fraser W, Martinson D, Stammerjohn SE, Schofield O (2009) Recent changes in phytoplankton communities associated with rapid regional climate change along the western Antarctic Peninsula. Science 323:1470–1473.

Morison F, Menden-Deuer S (2018) Seasonal similarity in rates of protistan herbivory in fjords along the Western Antarctic Peninsula. Limnology and Oceanography 63:2858–2876.

Nardelli SC, Cimino MA, Conroy JA, Fraser WR, Steinberg DK, Schofield O (2021) Krill availability in adjacent Adélie and gentoo penguin foraging regions near Palmer Station, Antarctica. Limnology and Oceanography 66:2234–2250.

Nardelli SC, Stammerjohn SE, Gray PC, Schofield O (in prep.) Coastal phytoplankton seasonal succession and diversity on the West Antarctic Peninsula.

Nejstgaard JC, Naustvoll L-J, Sazhin A (2001) Correcting for underestimation of microzooplankton grazing in bottle incubation experiments with mesozooplankton. Marine Ecology Progress Series 221:59–75.

Nicol S, Foster J (2016) The Fishery for Antarctic Krill: Its Current Status and Management

Regime. In: *Biology and Ecology of Antarctic Krill*. Advances in Polar Ecology, Siegel V (ed) Springer International Publishing, Cham, p 387–421

Nielsen JM, Popp BN, Winder M (2015) Meta-analysis of amino acid stable nitrogen isotope ratios for estimating trophic position in marine organisms. Oecologia 178:631–642.

Olson RJ, Sosik HM (2007) A submersible imaging-in-flow instrument to analyze nano- and microplankton: Imaging FlowCytobot. Limnology and Oceanography: Methods 5:195–203.

Pakhomov EA, Froneman PW (2004) Zooplankton dynamics in the eastern Atlantic sector of the Southern Ocean during the austral summer 1997/1998—Part 2: Grazing impact. Deep Sea Research Part II 51:2617–2631.

Pauli N-C, Metfies K, Pakhomov EA, Neuhaus S, Graeve M, Wenta P, Flintrop CM, Badewien TH, Iversen MH, Meyer B (2021) Selective feeding in Southern Ocean key grazers—diet composition of krill and salps. Communications Biology 4:1–12.

Perissinotto R, Gurney L, Pakhomov EA (2000) Contribution of heterotrophic material to diet and energy budget of Antarctic krill, *Euphausia superba*. Marine Biology 136:129–135.

Perissinotto R, Pakhomov EA, McQuaid CD, Froneman PW (1997) In situ grazing rates and daily ration of Antarctic krill *Euphausia superba* feeding on phytoplankton at the Antarctic Polar Front and the Marginal Ice Zone. Marine Ecology Progress Series 160:77–91.

Polito MJ, Reiss CS, Trivelpiece WZ, Patterson WP, Emslie SD (2013) Stable isotopes identify an ontogenetic niche expansion in Antarctic krill (*Euphausia superba*) from the South Shetland Islands, Antarctica. Marine Biology 160:1311–1323.

Pond DW, Atkinson A, Shreeve RS, Tarling G, Ward P (2005) Diatom fatty acid biomarkers

indicate recent growth rates in Antarctic krill. Limnology and Oceanography 50:732–736.

Price HJ, Boyd KR, Boyd CM (1988) Omnivorous feeding behavior of the Antarctic krill *Euphausia superba*. Marine Biology 97:67–77.

Quetin LB, Ross RM (1985) Feeding by Antarctic Krill, *Euphausia superba*: Does Size Matter? In: *Antarctic Nutrient Cycles and Food Webs*. Siegfried WR, Condy PR, Laws RM (eds) Springer, Berlin, Heidelberg, p 372–377

R Core Team (2021) R: A language and environment for statistical computing. R Foundation for Statistical Computing. Vienna, Austria. https://www.R-project.org/

Reiss CS (2016) Age, Growth, Mortality, and Recruitment of Antarctic Krill, *Euphausia superba*. In: *Biology and Ecology of Antarctic Krill*. Advances in Polar Ecology, Siegel V (ed) Springer International Publishing, Cham, p 101–144

Rogers AD, Frinault BAV, Barnes DKA, Bindoff NL, Downie R, Ducklow HW, Friedlaender AS, Hart T, Hill SL, Hofmann EE, Linse K, McMahon CR, Murphy EJ, Pakhomov EA, Reygondeau G, Staniland IJ, Wolf-Gladrow DA, Wright RM (2020) Antarctic Futures: An Assessment of Climate-Driven Changes in Ecosystem Structure, Function, and Service Provisioning in the Southern Ocean. Annual Review of Marine Science 12:87–120.

Rose KA, Fiechter J, Curchitser EN, Hedstrom K, Bernal M, Creekmore S, Haynie A, Ito S, Lluch-Cota S, Megrey BA, Edwards CA, Checkley D, Koslow T, McClatchie S, Werner F, MacCall A, Agostini V (2015) Demonstration of a fully-coupled end-to-end model for small pelagic fish using sardine and anchovy in the California Current. Progress in Oceanography 138:348–380.

Ross RM, Quetin LB, Baker KS, Vernet M, Smith RC (2000) Growth limitation in young

Euphausia superba under field conditions. Limnology and Oceanography 45:31–43.

Ruck KE, Steinberg DK, Canuel EA (2014) Regional differences in quality of krill and fish as prey along the Western Antarctic Peninsula. Marine Ecology Progress Series 509:39–55.

Ruiz-Halpern S, Duarte CM, Tovar-Sanchez A, Pastor M, Horstkotte B, Lasternas S, Agustí S (2011) Antarctic krill as a source of dissolved organic carbon to the Antarctic ecosystem. Limnology and Oceanography 56:521–528.

Ryabov AB, de Roos AM, Meyer B, Kawaguchi S, Blasius B (2017) Competition-induced starvation drives large-scale population cycles in Antarctic krill. Nature Ecology & Evolution 1:0177.

Saba GK, Fraser WR, Saba VS, Iannuzzi RA, Coleman KE, Doney SC, Ducklow HW, Martinson DG, Miles TN, Patterson-Fraser DL, Stammerjohn SE, Steinberg DK, Schofield OM (2014) Winter and spring controls on the summer food web of the coastal West Antarctic Peninsula. Nature Communications 5:1–8.

Saba GK, Steinberg DK, Bronk DA (2011) The relative importance of sloppy feeding, excretion, and fecal pellet leaching in the release of dissolved carbon and nitrogen by *Acartia tonsa* copepods. Journal of Experimental Marine Biology and Ecology 404:47–56.

Sailley SF, Ducklow HW, Moeller HV, Fraser WR, Schofield OM, Steinberg DK, Garzio LM, Doney SC (2013) Carbon fluxes and pelagic ecosystem dynamics near two western Antarctic Peninsula Adélie penguin colonies: an inverse model approach. Marine Ecology Progress Series 492:253–272.

Sathyendranath S, Platt T, Kovač Ž, Dingle J, Jackson T, Brewin RJW, Franks P, Marañón E, Kulk G, Bouman HA (2020) Reconciling models of primary production and photoacclimation. Applied Optics 59:C100–C114.

Sathyendranath S, Stuart V, Nair A, Oka K, Nakane T, Bouman H, Forget M-H, Maass H, Platt T (2009) Carbon-to-chlorophyll ratio and growth rate of phytoplankton in the sea. Marine Ecology Progress Series 383:73–84.

Schmidt K (2010) Food and Feeding in Northern Krill (*Meganyctiphanes norvegica* Sars). In: *Advances in Marine Biology*. Tarling GA (ed) Academic Press, p 127–171

Schmidt K, Atkinson A (2016) Feeding and Food Processing in Antarctic Krill (*Euphausia superba* Dana). In: *Biology and Ecology of Antarctic Krill*. Advances in Polar Ecology, Siegel V (ed) Springer International Publishing, Cham, p 175–224

Schmidt K, Atkinson A, Petzke K-J, Voss M, Pond DW (2006) Protozoans as a food source for Antarctic krill, *Euphausia superba*: Complementary insights from stomach content, fatty acids, and stable isotopes. Limnology and Oceanography 51:2409–2427.

Schmidt K, Atkinson A, Pond DW, Ireland LC (2014) Feeding and overwintering of Antarctic krill across its major habitats: The role of sea ice cover, water depth, and phytoplankton abundance. Limnology and Oceanography 59:17–36.

Schmidt K, McClelland JW, Mente E, Montoya JP, Atkinson A, Voss M (2004) Trophic-level interpretation based on δ15N values: implications of tissue-specific fractionation and amino acid composition. Marine Ecology Progress Series 266:43–58.

Schofield O, Saba G, Coleman K, Carvalho F, Couto N, Ducklow H, Finkel Z, Irwin A, Kahl A, Miles T, Montes-Hugo M, Stammerjohn S, Waite N (2017) Decadal variability in coastal phytoplankton community composition in a changing West Antarctic Peninsula. Deep Sea Research Part I 124:42–54.

Shelton AO, Kinzey D, Reiss C, Munch S, Watters G, Mangel M (2013) Among-year variation

in growth of Antarctic krill *Euphausia superba* based on length-frequency data. Marine Ecology Progress Series 481:53–67.

Siegel V, Loeb V (1994) Length and age at maturity of Antarctic krill. Antarctic Science 6:479–482.

Siegel V, Reiss CS, Dietrich KS, Haraldsson M, Rohardt G (2013) Distribution and abundance of Antarctic krill (*Euphausia superba*) along the Antarctic Peninsula. Deep Sea Research Part I 77:63–74.

Sosik HM, Olson RJ (2007) Automated taxonomic classification of phytoplankton sampled with imaging-in-flow cytometry. Limnology and Oceanography: Methods 5:205–216.

Steinberg DK, Ruck KE, Gleiber MR, Garzio LM, Cope JS, Bernard KS, Stammerjohn SE, Schofield OME, Quetin LB, Ross RM (2015) Long-term (1993–2013) changes in macrozooplankton off the Western Antarctic Peninsula. Deep Sea Research Part I 101:54–70.

Steinke KB, Bernard KS, Ross RM, Quetin LB (2021) Environmental drivers of the physiological condition of mature female Antarctic krill during the spawning season: implications for krill recruitment. Marine Ecology Progress Series 669:65–82.

Suh H-L, Nemoto T (1987) Comparative morphology of filtering structure of five species of *Euphausia* (Euphausiacea, Crustacea) from the Antarctic Ocean. Proceedings of the NIPR Symposium on Polar Biology 1:72-83.

Swadling KM, Ritz DA, Nicol S, Osborn JE, Gurney LJ (2005) Respiration rate and cost of swimming for Antarctic krill, *Euphausia superba*, in large groups in the laboratory. Marine Biology 146:1169–1175.

Swalethorp R, Aluwihare L, Thompson AR, Ohman MD, Landry MR (2020) Errors associated

with compound-specific δ15N analysis of amino acids in preserved fish samples purified by high-pressure liquid chromatography. Limnology and Oceanography: Methods 18:259–270.

Tarling GA, Shreeve RS, Hirst AG, Atkinson A, Pond DW, Murphy EJ, Watkins JL (2006) Natural growth rates in Antarctic krill (*Euphausia superba*): I. Improving methodology and predicting intermolt period. Limnology and Oceanography 51:959–972.

Trathan PN, Hill SL (2016) The Importance of Krill Predation in the Southern Ocean. In: *Biology and Ecology of Antarctic Krill*. Advances in Polar Ecology, Siegel V (ed) Springer International Publishing, Cham, p 321–350

Vernet M, Martinson D, Iannuzzi R, Stammerjohn S, Kozlowski W, Sines K, Smith R, Garibotti I (2008) Primary production within the sea-ice zone west of the Antarctic Peninsula: I—Sea ice, summer mixed layer, and irradiance. Deep Sea Research Part II 55:2068–2085.

Walsh RG, He S, Yarnes CT (2014) Compound-specific δ13C and δ15N analysis of amino acids: a rapid, chloroformate-based method for ecological studies. Rapid Communications in Mass Spectrometry 28:96–108.

Yarnes CT, Herszage J (2017) The relative influence of derivatization and normalization procedures on the compound-specific stable isotope analysis of nitrogen in amino acids. Rapid Communications in Mass Spectrometry 31:693–704.

Table 1. Mean percent dietary fraction of main prey groups for juvenile krill during three consecutive field seasons. Phytoplankton fraction was estimated as the integrated phytoplankton carbon ingestion for December-February divided by the minimum total carbon ingestion. High and low estimates (indicated in parentheses) were calculated for each year using two different methods to predict phytoplankton carbon. Metazoan fraction was estimated from the trophic position calculated using glutamic acid as the trophic amino acid. High and low estimates were calculated for each year using two different values for the mean trophic position of metazoan prey. Heterotrophic protists were assumed to constitute the remainder of the diet.

Year	% Phytoplankton	% Metazoans	% Heterotrophic protists
2017-2018	23 (14-31)	33 (27-40)	44 (29-59)
2018-2019	26 (17-35)	52 (42-63)	22 (2-41)
2019-2020	22 (14-30)	63 (50-75)	15 (0-36)
Mean	24	49	27

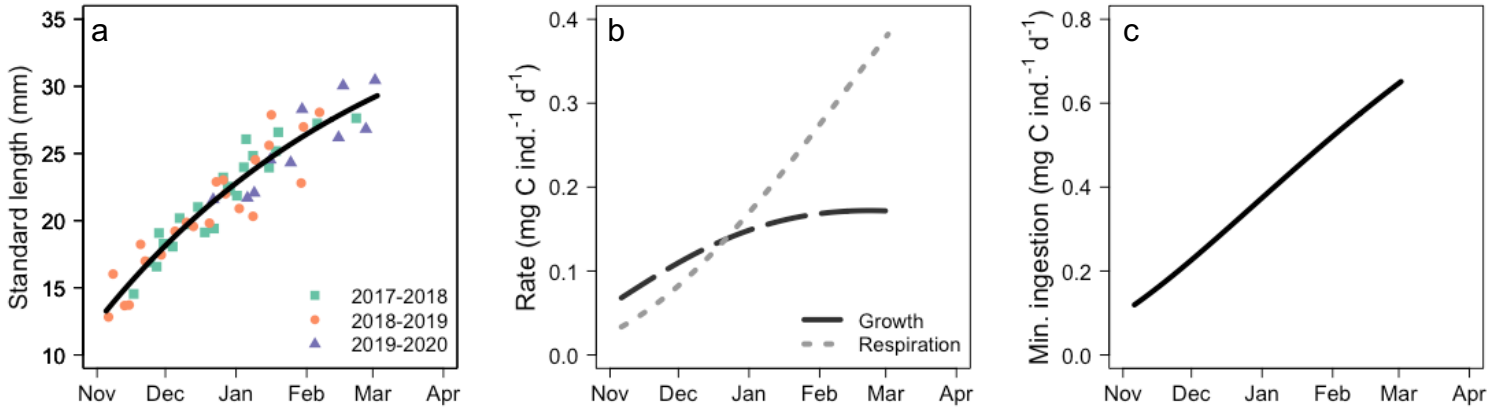

Figure 1. Seasonal time series of juvenile krill growth and metabolic demand. (a) Daily length modes and the Von Bertalanffy model fit, (b) modeled daily growth and respiration rates, and (c) modeled minimum daily carbon ingestion are plotted from November to March for juvenile krill near Palmer Station using data from three successive years.

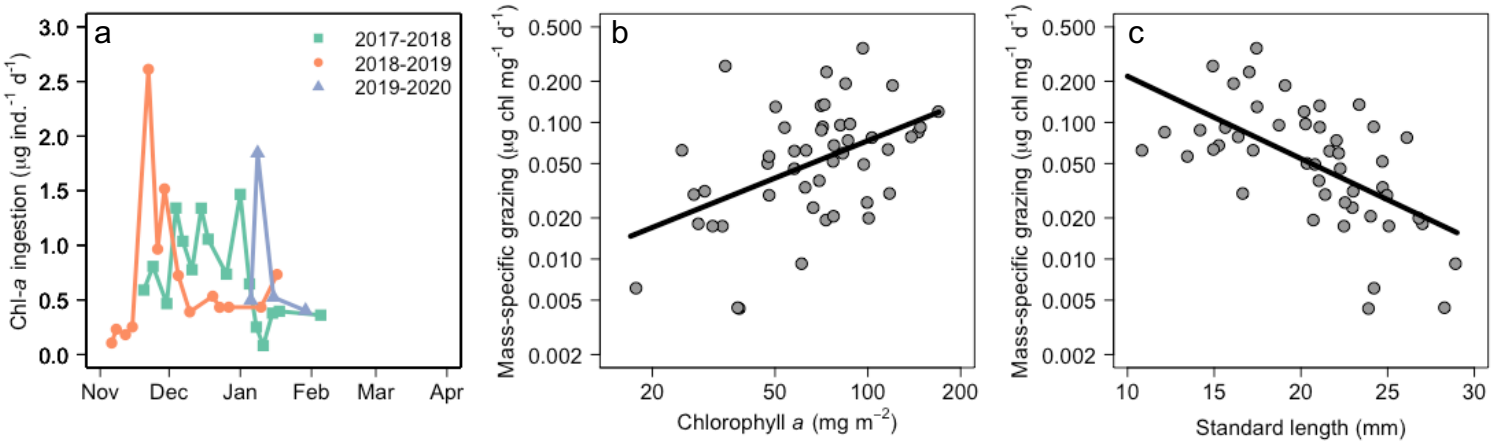

Figure 2. Gut fluorescence-based estimates of phytoplankton chlorophyll-*a* ingestion by juvenile krill. (a) Time series of daily mean chlorophyll-*a* ingestion is plotted for three field seasons. (b) Depth-integrated chlorophyll-*a* concentration and (c) length of krill are plotted against mass-specific grazing. Log-log and log-linear regression fits are plotted in panels b and c, respectively

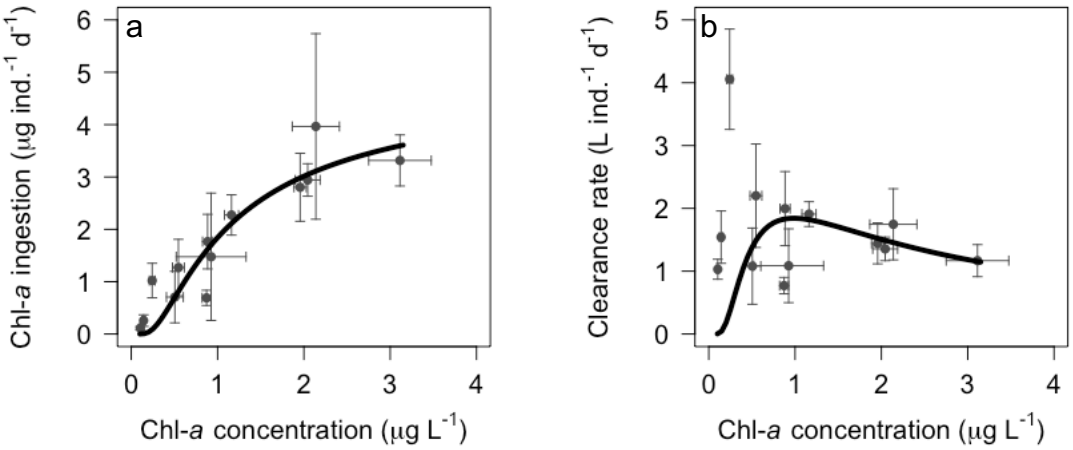

Figure 3. Functional response of juvenile krill feeding on phytoplankton (chlorophyll *a*). Mean (a) ingestion and (b) clearance rates are plotted against mean initial chlorophyll-*a* concentration for 13 experiments. Error bars indicate one standard error, n = 3-6 replicates per experiment. Model fit: chl-*a* ingestion = 0.98 * 1.84 * $e^{1 - 0.98 / \text{chl-}a \text{ concentration}}$

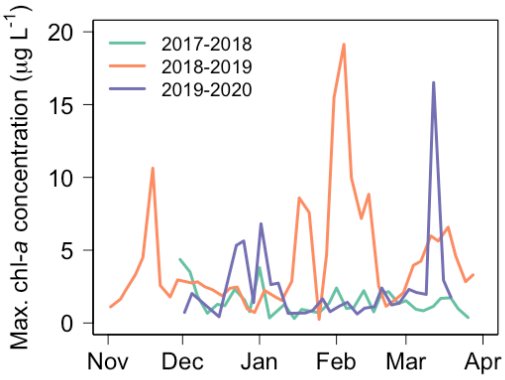

Figure 4. Time series of the maximum chlorophyll-*a* concentration at Palmer Long-Term Ecological Research Station B for three field seasons. Values are the maximum measured concentration at any depth from *in situ* fluorometer casts, typically conducted twice per week from the surface to 60 m.

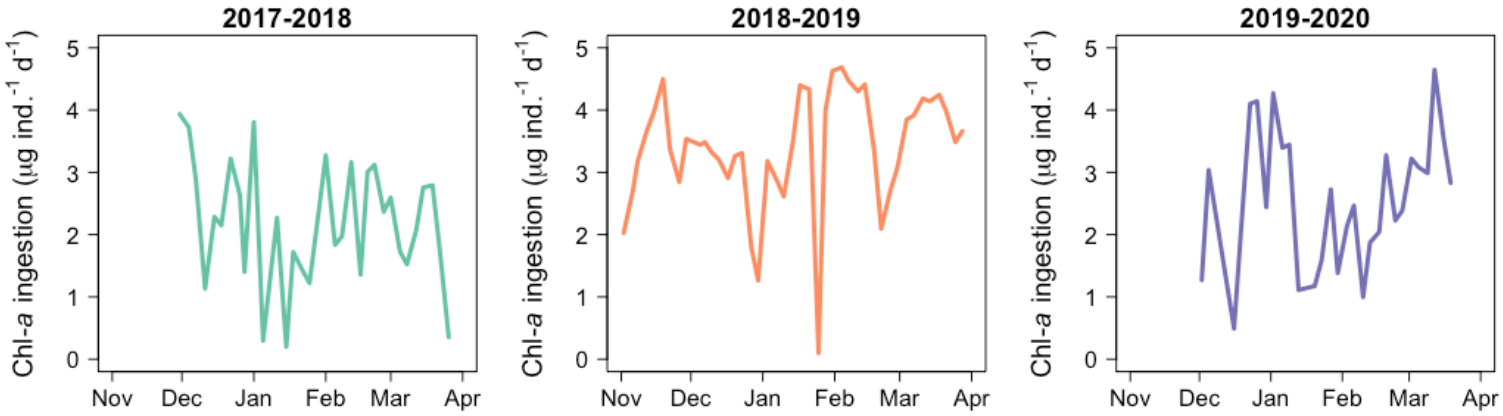

Figure 5. Juvenile krill chlorophyll-*a* ingestion time series calculated using the functional response model and *in situ* chlorophyll-*a* maxima during the 2017-2018, 2018-2019, and 2019-2020 field seasons.

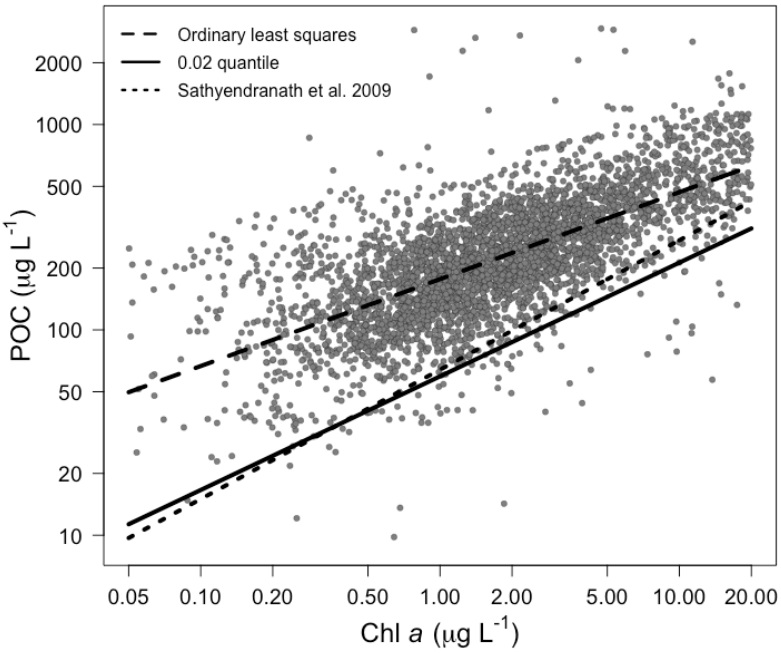

Figure 6. Chlorophyll *a* vs. particulate organic carbon near Palmer Station. Values are from 17 years (1992-2012) of sampling the upper 50 m of water column (n = 3,768). The log-log regression fits using the quantile and ordinary least squares methods from this study are plotted along with the quantile regression fit from Sathyendranath et al. (2009). These relationships are used to convert chlorophyll *a* to phytoplankton carbon concentration.

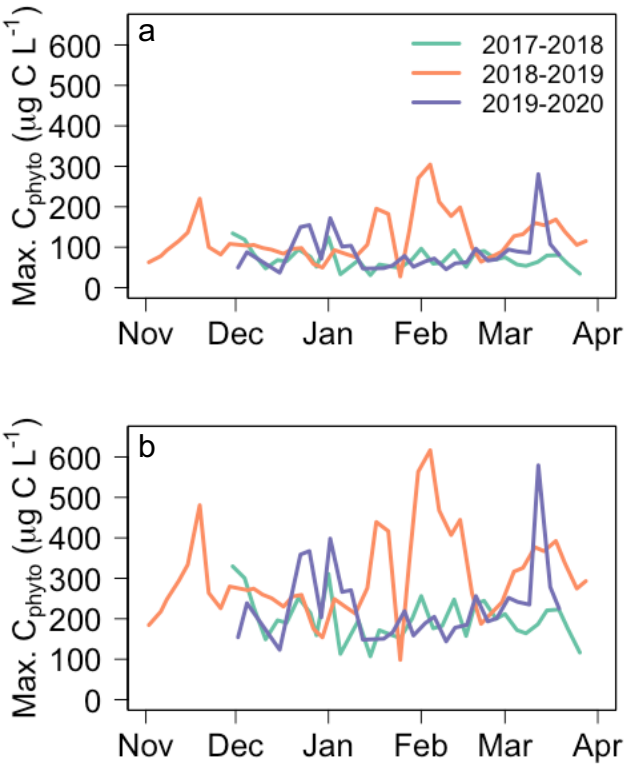

Figure 7. Time series of maximum phytoplankton carbon at Palmer Long-Term Ecological Research Station B for three field seasons. (a) Low and (b) high phytoplankton carbon concentrations were predicted using quantile regression and ordinary least squares regression fits, respectively. Values were converted from the maximum measured chlorophyll-*a* concentration at any depth from *in situ* fluorometer casts, typically conducted twice per week from the surface to 60 m.

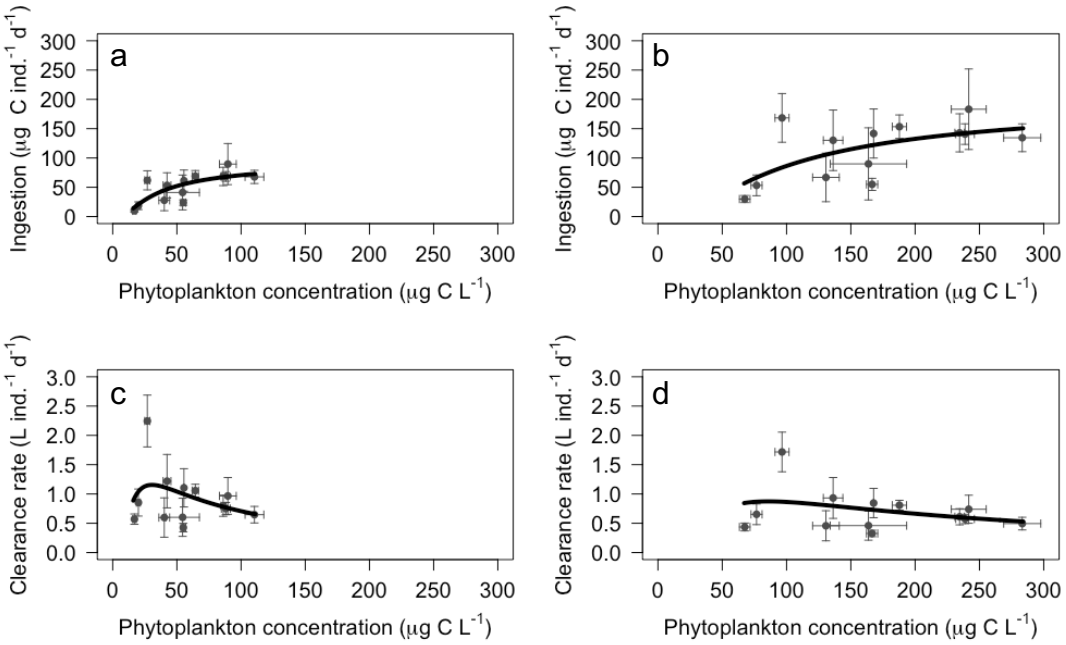

Figure 8. Functional response of juvenile krill feeding on phytoplankton (carbon). Mean (a, b) ingestion and (c, d) clearance rates are plotted against mean initial phytoplankton carbon concentration for 13 experiments. (a, c) Low and (b, d) high estimates of phytoplankton carbon were predicted from chlorophyll-*a* concentration using quantile regression and ordinary least squares regression fits, respectively. Error bars indicate one standard error, n = 3-6 replicates per experiment.

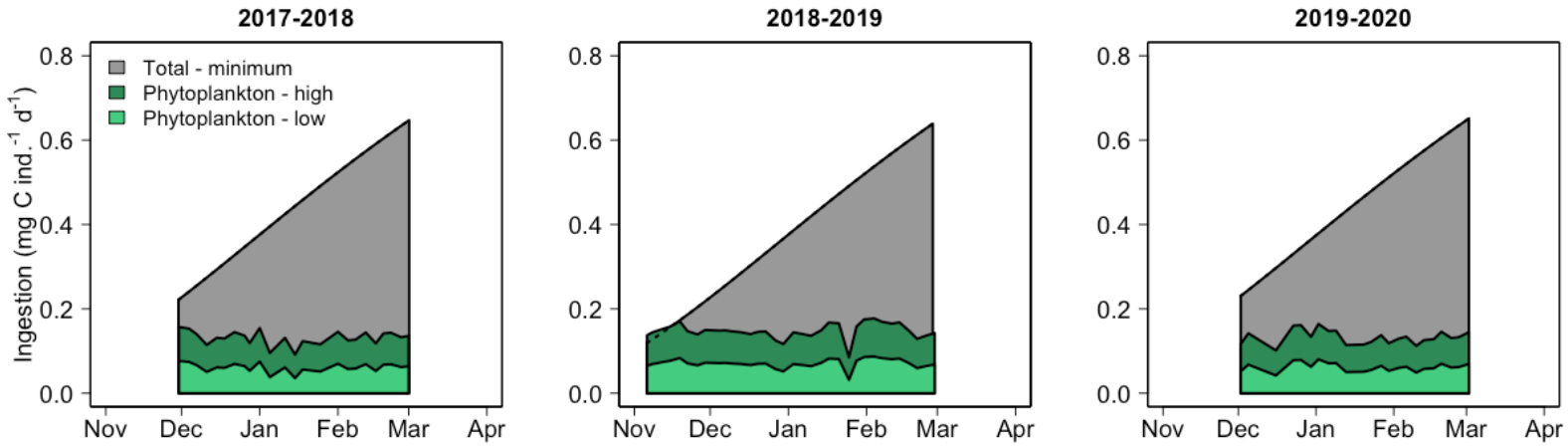

Figure 9. Seasonal time series of juvenile krill daily carbon ingestion for three successive years. The modeled minimum daily carbon ingestion is constant across years and derived from the length time series. Functional response models were paired with phytoplankton carbon maxima estimates to calculate a high and low phytoplankton ingestion time series for each year.

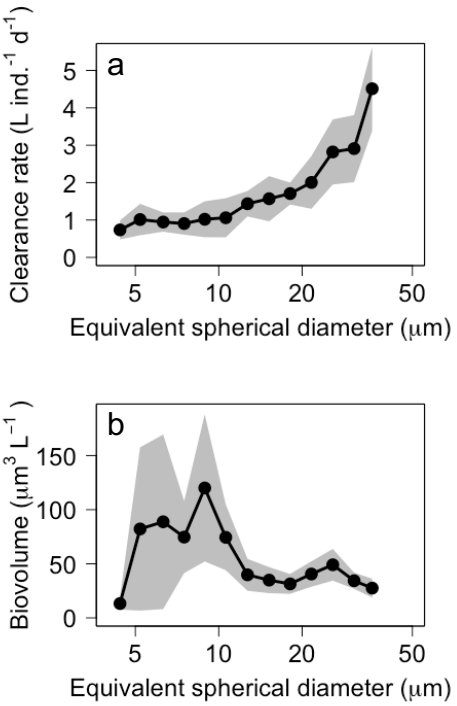

Figure 10. Size-selective grazing by juvenile krill. Equivalent spherical diameter vs. (a) mean clearance rate and (b) initial biovolume. Based on equivalent spherical diameter, potential prey particles were binned into 13 bins of equal width on a logarithmic scale. Shading indicates two standard errors, n = 9-11 experimental means.

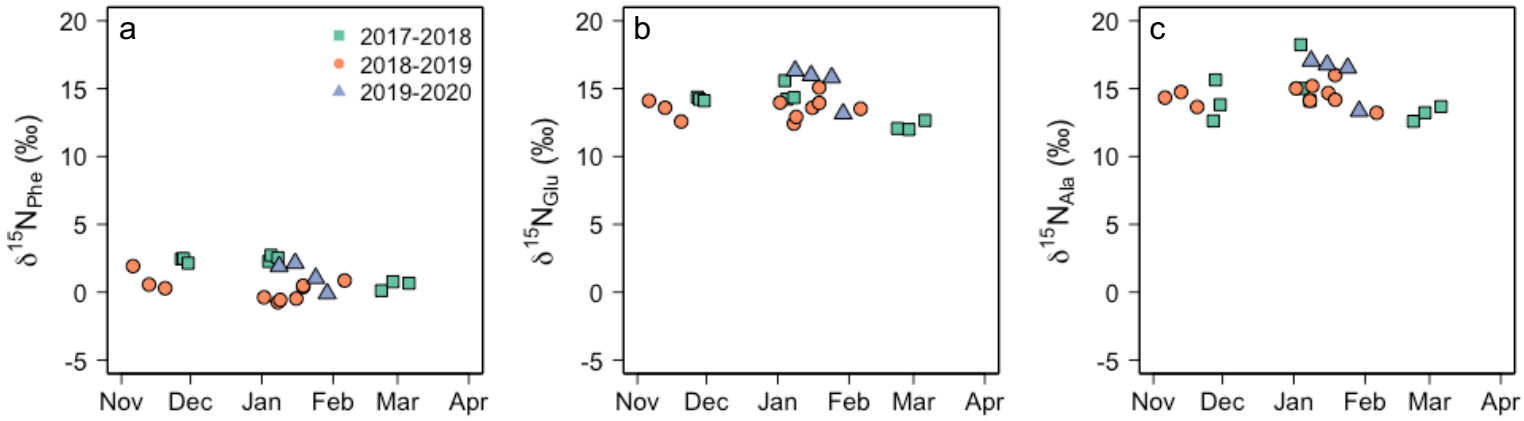

Figure 11. Amino acid $\delta^{15}N$ values in the abdominal muscle of juvenile krill during three consecutive field seasons. Amino acids are (a) phenylalanine, (b) glutamic acid, and (c) alanine. Points indicate the mean of duplicate analytical injections. The average standard deviations for phenylalanine, glutamic acid, and alanine duplicates were 0.4‰, 0.2‰, and 0.2‰, respectively.

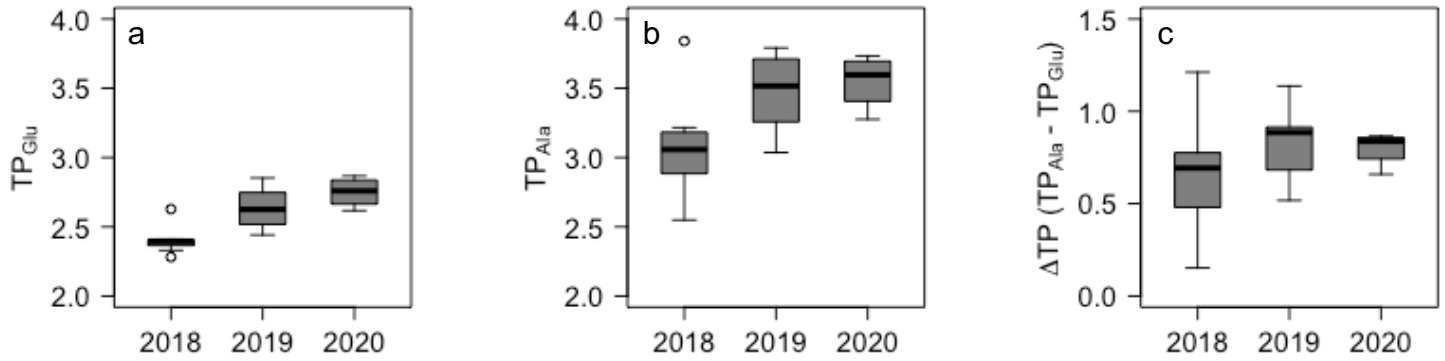

Figure 12. Interannual comparison of juvenile krill trophic position. Trophic position was calculated using (a) glutamic acid and (b) alanine as the trophic amino acid. (c) The difference between the two methods is presented. Black line indicates the median, gray box indicates the interquartile range, and whiskers indicate the range excluding outlier values indicated as points. n = 4-10 samples per year.

CHAPTER 5
Summary and concluding remarks

This dissertation advances understanding of the dynamic nature of zooplankton distribution, abundance, composition, and trophic ecology in coastal Antarctica. Chapter 2 demonstrated that diverse taxa conduct diel vertical migration despite near-continuous daylight during summer. Vertical distribution patterns vary across taxa based on life-history strategies, and environmental conditions influence vertical distribution. Chapter 3 showed that the size and taxonomic composition of Antarctic zooplankton changes substantially among years and within a given summer. These findings suggest Antarctic zooplankton populations may be resilient to climate-driven phenology shifts. Chapter 4 determined that krill are omnivores even during the juvenile life stage in productive coastal waters during summer. A selective grazing preference for microplankton prey limited phytoplankton consumption by krill, because smaller nanoplankton dominated phytoplankton biomass. Each of these chapters provides directions for future research.

The next steps related to Antarctic zooplankton DVM are to quantify impacts on the biological carbon pump and to better understand the environmental controls on vertical distribution. Size-based and taxonomic-specific algorithms for calculating zooplankton metabolic rates should be used to quantify the active transport of carbon from the epipelagic zone to mesopelagic zone by diel vertically migrating zooplankton (Maas et al. 2021). Quantifying the contribution of zooplankton active transport to carbon export may help resolve surprisingly low particle export measurements along the WAP (Stukel et al. 2015; Ducklow et al. 2018). Despite its relatively coarse vertical resolution, net sampling revealed an array of taxon-specific vertical distribution patterns along the WAP. Outfitting autonomous, adaptive sampling platforms with optical and acoustic sensors is a promising approach for better understanding ecological interactions between zooplankton and phytoplankton (Benoit-Bird et

al., 2018; Fossum et al., 2019; Ohman et al., 2019). Finer-scale information on the extent and controls of vertical migration will be important for determining the longevity of zooplankton-mediated carbon sequestration and for improving the implementation of such processes in biogeochemical models (Archibald et al. 2019; Cavan et al. 2019). While additional field studies and model development may require substantial future investments, initial estimates of active transport can be performed with the data made available from this dissertation.

Seasonal succession was apparent in the coastal Antarctic zooplankton community near Palmer Station, as shown in Chapter 3. The diversity of life-history strategies across zooplankton species complicates our understanding of the mechanistic processes underpinning seasonal changes in community structure. The development of seasonal simulation models will be valuable for identifying the relevant population processes that drive community structure changes within a given year. New dynamic, regional food-web models for the WAP (Kim et al. 2021; Schultz et al. 2021) will be valuable tools moving forward and further complexity may be implemented to test specific hypotheses regarding the causes and consequences of zooplankton seasonal succession following existing examples (Mariani et al. 2013; Kenitz et al. 2017). Such models will be a valuable approach for testing the impacts of changing sea-ice and phytoplankton phenology on zooplankton population dynamics and the WAP ecosystem.

These first two main chapters emphasize the dynamic nature of zooplankton distribution and abundance at relatively short time scales. To detect change in the vertical distribution and phenological patterns revealed in this dissertation will require sustained, coordinated observations of zooplankton. Such data have been identified among research priorities in the Southern Ocean and globally (Constable et al. 2016; Lombard et al. 2019). Ship-based surveys effectively capture interannual changes in zooplankton composition and should be continued.

Autonomous sampling platforms can open new, complementary scientific questions by providing subseasonal sampling coverage. Sediment traps (Gleiber et al. 2012; Manno et al. 2020; Thibodeau et al. 2020), underwater gliders (Ohman et al. 2019; Reiss et al. 2021), and moorings (Brierley et al. 2006; La et al. 2019) are flexible tools for higher-resolution zooplankton observation. Advances in acoustic and optical sensors (and data processing) may improve spatiotemporal, size, and taxonomic resolution available from these platforms. Regardless of the sampling approach, it must be consistent and long term to unravel the impacts of a changing environment on the vertical distribution and phenology of Antarctic zooplankton.

The importance of omnivory for krill represents a fundamental shift in conceptualization of the Antarctic marine food web that has been developing over recent decades. The application of multiple new approaches including imaging flow cytometry and compound-specific isotope analysis validated ideas about this complexity that were proposed in the 1980s (Hewes et al. 1985; Price et al. 1988). My findings build on recent literature that emphasizes complexity in krill population dynamics and trophic ecology (Walsh et al. 2020; Atkinson et al. 2022). A simple food chain from phytoplankton to krill to predator is clearly a gross simplification, with the importance of alternate trophic pathways being emphasized within the microbial plankton (Sailley et al. 2013) and animal (McCormack et al. 2021) components of Antarctic food webs. Projections about the habitat suitability for krill often depend on empirical relationships with chlorophyll *a* (Hill et al. 2013; Veytia et al. 2020), but given the trophic flexibility demonstrated in Chapter 4, such changes may be difficult to predict from contemporary relationships with environmental conditions. Future work should prioritize collection of data that informs physiological condition of krill along with their prey availability (Schmidt and Atkinson 2016; Meyer et al. 2020). As noted above, these observations must be sustained to detect change and to

relate dietary switches to population responses.

Antarctic zooplankton composition and trophic ecology will change in coming decades, although uncertainty remains high for some environmental drivers and zooplankton responses (Johnston et al. in press). Changing physical (Morley et al. 2020), chemical (Henley et al. 2021), bottom-up (Pinkerton et al. 2021), and top-down (Bestley et al. 2020; Savoca et al. 2021) forces will drive complex responses for zooplankton species and the entire ecosystem (Beaugrand and Kirby 2018; Gruber et al. 2021). Such changes in the Southern Ocean will have global consequences and modify ecosystem services upon which humans rely, including fisheries production, carbon sequestration, and tourism (Rogers et al. 2020; Cavanagh et al. 2021; Murphy et al. 2021). An inclusive approach to designing, implementing, and managing a marine protected area along the WAP can bolster resilience of the ecosystem (Sylvester and Brooks 2020; Grorud-Calvert et al. 2021). Management of the krill fishery in particular is a key component of conservation (Meyer et al. 2020; Watters et al. 2020) and is discussed further in Appendix A. This dissertation research demonstrates that there is still much to be learned about Antarctic zooplankton and the WAP pelagic ecosystem more generally. The results also present evidence for phenological and trophic flexibility that may promote resilience for zooplankton populations amidst environmental change. The only way to understand future changes is to continue long-term research programs. As marine ecologists Jane Lubchenco and Steve Gaines wrote in 2019, “The ocean is not too big to fail, nor is it too big to fix. It is too big to ignore.”

References

Archibald KM, Siegel DA, Doney SC (2019) Modeling the Impact of Zooplankton Diel Vertical Migration on the Carbon Export Flux of the Biological Pump. Global Biogeochemical Cycles 33:181–199.

Atkinson A, Hill SL, Reiss CS, Pakhomov EA, Beaugrand G, Tarling GA, Yang G, Steinberg DK, Schmidt K, Edwards M, Rombolá E, Perry FA (2022) Stepping stones towards Antarctica: Switch to southern spawning grounds explains an abrupt range shift in krill. Global Change Biology 28:1359–1375.

Beaugrand G, Kirby RR (2018) How Do Marine Pelagic Species Respond to Climate Change? Theories and Observations. Annual Review of Marine Science 10:169–197.

Benoit-Bird KJ, Patrick Welch T, Waluk CM, Barth JA, Wangen I, McGill P, Okuda C, Hollinger GA, Sato M, McCammon S (2018) Equipping an underwater glider with a new echosounder to explore ocean ecosystems. Limnology and Oceanography: Methods 16:734–749.

Bestley S, Ropert-Coudert Y, Bengtson Nash S, Brooks CM, Cotté C, Dewar M, Friedlaender AS, Jackson JA, Labrousse S, Lowther AD, McMahon CR, Phillips RA, Pistorius P, Puskic PS, Reis AO de A, Reisinger RR, Santos M, Tarszisz E, Tixier P, Trathan PN, Wege M, Wienecke B (2020) Marine Ecosystem Assessment for the Southern Ocean: Birds and Marine Mammals in a Changing Climate. Frontiers in Ecology and Evolution 8:566936.

Brierley AS, Saunders RA, Bone DG, Murphy EJ, Enderlein P, Conti SG, Demer DA (2006) Use of moored acoustic instruments to measure short-term variability in abundance of Antarctic krill. Limnology and Oceanography: Methods 4:18–29.

Cavan EL, Laurenceau-Cornec EC, Bressac M, Boyd PW (2019) Exploring the ecology of the mesopelagic biological pump. Progress in Oceanography 176:102125.

Cavanagh RD, Melbourne-Thomas J, Grant SM, Barnes DKA, Hughes KA, Halfter S, Meredith MP, Murphy EJ, Trebilco R, Hill SL (2021) Future Risk for Southern Ocean Ecosystem Services Under Climate Change. Frontiers in Marine Science 7:615214.

Constable AJ, Costa DP, Schofield O, Newman L, Urban ER, Fulton EA, Melbourne-Thomas J, Ballerini T, Boyd PW, Brandt A, de la Mare WK, Edwards M, Eléaume M, Emmerson L, Fennel K, Fielding S, Griffiths H, Gutt J, Hindell MA, Hofmann EE, Jennings S, La HS, McCurdy A, Mitchell BG, Moltmann T, Muelbert M, Murphy E, Press AJ, Raymond B, Reid K, Reiss C, Rice J, Salter I, Smith DC, Song S, Southwell C, Swadling KM, Van de Putte A, Willis Z (2016) Developing priority variables ("ecosystem Essential Ocean Variables" — eEOVs) for observing dynamics and change in Southern Ocean ecosystems. Journal of Marine Systems 161:26–41.

Ducklow HW, Stukel MR, Eveleth R, Doney SC, Jickells T, Schofield O, Baker AR, Brindle J, Chance R, Cassar N (2018) Spring–summer net community production, new production, particle export and related water column biogeochemical processes in the marginal sea ice zone of the Western Antarctic Peninsula 2012–2014. Philosophical Transactions of the Royal Society A 376:20170177.

Fossum TO, Fragoso GM, Davies EJ, Ullgren JE, Mendes R, Johnsen G, Ellingsen I, Eidsvik J, Ludvigsen M, Rajan K (2019) Toward adaptive robotic sampling of phytoplankton in the coastal ocean. Science Robotics 4:eaav3041.

Gleiber MR, Steinberg DK, Ducklow HW (2012) Time series of vertical flux of zooplankton

fecal pellets on the continental shelf of the western Antarctic Peninsula. Marine Ecology Progress Series 471:23–36.

Grorud-Colvert K, Sullivan-Stack J, Roberts C, Constant V, Horta e Costa B, Pike EP, Kingston N, Laffoley D, Sala E, Claudet J, Friedlander AM, Gill DA, Lester SE, Day JC, Gonçalves EJ, Ahmadia GN, Rand M, Villagomez A, Ban NC, Gurney GG, Spalding AK, Bennett NJ, Briggs J, Morgan LE, Moffitt R, Deguignet M, Pikitch EK, Darling ES, Jessen S, Hameed SO, Di Carlo G, Guidetti P, Harris JM, Torre J, Kizilkaya Z, Agardy T, Cury P, Shah NJ, Sack K, Cao L, Fernandez M, Lubchenco J (2021) The MPA Guide: A framework to achieve global goals for the ocean. Science 373:eabf0861.

Gruber N, Boyd PW, Frölicher TL, Vogt M (2021) Biogeochemical extremes and compound events in the ocean. Nature 600:395–407.

Henley SF, Cavan EL, Fawcett SE, Kerr R, Monteiro T, Sherrell RM, Bowie AR, Boyd PW, Barnes DKA, Schloss IR, Marshall T, Flynn R, Smith S (2020) Changing Biogeochemistry of the Southern Ocean and Its Ecosystem Implications. Frontiers in Marine Science 7:581.

Hewes CD, Holm-Hansen O, Sakshaug E (1985) Alternate Carbon Pathways at Lower Trophic Levels in the Antarctic Food Web. In: *Antarctic Nutrient Cycles and Food Webs*. Siegfried WR, Condy PR, Laws RM (eds) Springer, Berlin, Heidelberg, p 277–283

Hill SL, Phillips T, Atkinson A (2013) Potential Climate Change Effects on the Habitat of Antarctic Krill in the Weddell Quadrant of the Southern Ocean. PLOS ONE 8:e72246.

Johnston NM, Murphy EJ, Atkinson AA, Constable AJ, Cotté CS, Cox M, Daly K, Driscoll R, Flores H, Halfter S, Henschke N, Hill SL, Höfer J, Hunt BP, Kawaguchi S, Lindsay DJ, Loeb V, Manno C, Meyer B, Pakhomov E, Pinkerton MH, Reiss C, Richerson K, Smith

W, Steinberg DK, Swadling KM, Tarling GA, Thorpe SE, Veytia D, Ward P, Weldrick CK, Yang G (in press) Status, change and futures of zooplankton in the Southern Ocean. Frontiers in Ecology and Evolution.

Kenitz KM, Visser AW, Mariani P, Andersen KH (2017) Seasonal succession in zooplankton feeding traits reveals trophic trait coupling. Limnology and Oceanography 62:1184–1197.

Kim HH, Luo Y-W, Ducklow HW, Schofield OM, Steinberg DK, Doney SC (2021) WAP-1D-VAR v1.0: development and evaluation of a one-dimensional variational data assimilation model for the marine ecosystem along the West Antarctic Peninsula. Geoscientific Model Development 14:4939–4975.

La HS, Park K, Wåhlin A, Arrigo KR, Kim DS, Yang EJ, Atkinson A, Fielding S, Im J, Kim T-W, Shin HC, Lee S, Ha HK (2019) Zooplankton and micronekton respond to climate fluctuations in the Amundsen Sea polynya, Antarctica. Scientific Reports 9:1–7.

Lombard F, Boss E, Waite AM, Vogt M, Uitz J, Stemmann L, Sosik HM, Schulz J, Romagnan J-B, Picheral M, Pearlman J, Ohman MD, Niehoff B, Möller KO, Miloslavich P, Lara-Lpez A, Kudela R, Lopes RM, Kiko R, Karp-Boss L, Jaffe JS, Iversen MH, Irisson J-O, Fennel K, Hauss H, Guidi L, Gorsky G, Giering SLC, Gaube P, Gallager S, Dubelaar G, Cowen RK, Carlotti F, Briseño-Avena C, Berline L, Benoit-Bird K, Bax N, Batten S, Ayata SD, Artigas LF, Appeltans W (2019) Globally Consistent Quantitative Observations of Planktonic Ecosystems. Frontiers in Marine Science 6:196.

Lubchenco J, Gaines SD (2019) A new narrative for the ocean. Science 364:911–911.

Maas AE, Gossner H, Smith MJ, Blanco-Bercial L (2021) Use of optical imaging datasets to

assess biogeochemical contributions of the mesozooplankton. Journal of Plankton Research 43:475–491.

Manno C, Fielding S, Stowasser G, Murphy EJ, Thorpe SE, Tarling GA (2020) Continuous moulting by Antarctic krill drives major pulses of carbon export in the north Scotia Sea, Southern Ocean. Nature Communications 11:6051.

Mariani P, Andersen KH, Visser AW, Barton AD, Kiørboe T (2013) Control of plankton seasonal succession by adaptive grazing. Limnology and Oceanography 58:173–184.

McCormack SA, Melbourne-Thomas J, Trebilco R, Blanchard JL, Raymond B, Constable A (2021) Decades of dietary data demonstrate regional food web structures in the Southern Ocean. Ecology and Evolution 11:227–241.

Meyer B, Atkinson A, Bernard KS, Brierley AS, Driscoll R, Hill SL, Marschoff E, Maschette D, Perry FA, Reiss CS, Rombolá E, Tarling GA, Thorpe SE, Trathan PN, Zhu G, Kawaguchi S (2020) Successful ecosystem-based management of Antarctic krill should address uncertainties in krill recruitment, behaviour and ecological adaptation. Communications Earth & Environment 1:1–12.

Morley SA, Abele D, Barnes DKA, Cárdenas CA, Cotté C, Gutt J, Henley SF, Höfer J, Hughes KA, Martin SM, Moffat C, Raphael M, Stammerjohn SE, Suckling CC, Tulloch VJD, Waller CL, Constable AJ (2020) Global Drivers on Southern Ocean Ecosystems: Changing Physical Environments and Anthropogenic Pressures in an Earth System. Frontiers in Marine Science 7:547188.

Murphy EJ, Johnston NM, Hofmann EE, Phillips RA, Jackson JA, Constable AJ, Henley SF, Melbourne-Thomas J, Trebilco R, Cavanagh RD, Tarling GA, Saunders RA, Barnes DKA, Costa DP, Corney SP, Fraser CI, Höfer J, Hughes KA, Sands CJ, Thorpe SE,

Trathan PN, Xavier JC (2021) Global Connectivity of Southern Ocean Ecosystems. Frontiers in Ecology and Evolution 9:624451.

Ohman MD, Davis RE, Sherman JT, Grindley KR, Whitmore BM, Nickels CF, Ellen JS (2019) Zooglider: An autonomous vehicle for optical and acoustic sensing of zooplankton. Limnology and Oceanography: Methods 17:69–86.

Pinkerton MH, Boyd PW, Deppeler S, Hayward A, Höfer J, Moreau S (2021) Evidence for the Impact of Climate Change on Primary Producers in the Southern Ocean. Frontiers in Ecology and Evolution 9:592027.

Price HJ, Boyd KR, Boyd CM (1988) Omnivorous feeding behavior of the Antarctic krill *Euphausia superba*. Marine Biology 97:67–77.

Reiss CS, Cossio AM, Walsh J, Cutter GR, Watters GM (2021) Glider-Based Estimates of Meso-Zooplankton Biomass Density: A Fisheries Case Study on Antarctic Krill (*Euphausia superba*) Around the Northern Antarctic Peninsula. Frontiers in Marine Science 8:256.

Rogers AD, Frinault BAV, Barnes DKA, Bindoff NL, Downie R, Ducklow HW, Friedlaender AS, Hart T, Hill SL, Hofmann EE, Linse K, McMahon CR, Murphy EJ, Pakhomov EA, Reygondeau G, Staniland IJ, Wolf-Gladrow DA, Wright RM (2020) Antarctic Futures: An Assessment of Climate-Driven Changes in Ecosystem Structure, Function, and Service Provisioning in the Southern Ocean. Annual Review of Marine Science 12:87–120.

Sailley SF, Ducklow HW, Moeller HV, Fraser WR, Schofield OM, Steinberg DK, Garzio LM, Doney SC (2013) Carbon fluxes and pelagic ecosystem dynamics near two western

Antarctic Peninsula Adélie penguin colonies: an inverse model approach. Marine Ecology Progress Series 492:253–272.

Savoca MS, Czapanskiy MF, Kahane-Rapport SR, Gough WT, Fahlbusch JA, Bierlich KC, Segre PS, Di Clemente J, Penry GS, Wiley DN, Calambokidis J, Nowacek DP, Johnston DW, Pyenson ND, Friedlaender AS, Hazen EL, Goldbogen JA (2021) Baleen whale prey consumption based on high-resolution foraging measurements. Nature 599:85–90.

Schmidt K, Atkinson A (2016) Feeding and Food Processing in Antarctic Krill (*Euphausia superba* Dana). In: *Biology and Ecology of Antarctic Krill*. Advances in Polar Ecology, Siegel V (ed) Springer International Publishing, Cham, p 175–224

Schultz C, Doney SC, Hauck J, Kavanaugh MT, Schofield O (2021) Modeling Phytoplankton Blooms and Inorganic Carbon Responses to Sea-Ice Variability in the West Antarctic Peninsula. Journal of Geophysical Research: Biogeosciences 126:e2020JG006227.

Stukel MR, Asher E, Couto N, Schofield O, Strebel S, Tortell P, Ducklow HW (2015) The imbalance of new and export production in the Western Antarctic Peninsula, a potentially "leaky" ecosystem. Global Biogeochemical Cycles 29:1400–1420.

Sylvester ZT, Brooks CM (2020) Protecting Antarctica through Co-production of actionable science: Lessons from the CCAMLR marine protected area process. Marine Policy 111:103720.

Thibodeau PS, Steinberg DK, McBride CE, Conroy JA, Keul N, Ducklow HW (2020) Long-term observations of pteropod phenology along the Western Antarctic Peninsula. Deep Sea Research Part I 166:103363.

Veytia D, Corney S, Meiners KM, Kawaguchi S, Murphy EJ, Bestley S (2020) Circumpolar projections of Antarctic krill growth potential. Nature Climate Change 10:568–575.

Walsh J, Reiss CS, Watters GM (2020) Flexibility in Antarctic krill Euphausia superba decouples diet and recruitment from overwinter sea-ice conditions in the northern Antarctic Peninsula. Marine Ecology Progress Series 642:1–19.

Watters GM, Hinke JT, Reiss CS (2020) Long-term observations from Antarctica demonstrate that mismatched scales of fisheries management and predator-prey interaction lead to erroneous conclusions about precaution. Scientific Reports 10:1–9.

APPENDIX A
Linking Antarctic krill larval supply and recruitment along the Antarctic Peninsula

Please cite this appendix as: Conroy JA, Reiss CS, Gleiber MR, Steinberg DK. 2020. Linking Antarctic krill larval supply and recruitment along the Antarctic Peninsula. *Integrative and Comparative Biology* 60:1386-1400. https://doi.org/10.1093/icb/icaa111

Abstract

Antarctic krill (*Euphausia superba*) larval production and overwinter survival drive recruitment variability, which in turn determines abundance trends. The Antarctic Peninsula has been described as a recruitment hot spot and as a potentially important source region for larval and juvenile krill dispersal. However, there has been no analysis to spatially resolve regional-scale krill population dynamics across life stages. We assessed spatiotemporal patterns in krill demography using two decades of austral summer data collected along the North and West Antarctic Peninsula since 1993. We identified persistent spatial segregation in the summer distribution of euphausiid larvae (*E. superba* plus other species), which were concentrated in oceanic waters along the continental slope, and *E. superba* recruits, which were concentrated in shelf and coastal waters. Mature female *E. superba* were more abundant over the continental shelf than the slope or coast. Euphausiid larval abundance was relatively localized and weakly correlated between the North and West Antarctic Peninsula, while *E. superba* recruitment was generally synchronized throughout the entire region. Euphausiid larval abundance along the West Antarctic Peninsula slope explained *E. superba* recruitment in shelf and coastal waters the next year. Given the localized nature of krill productivity, it is critical to evaluate the connectivity between upstream and downstream areas of the Antarctic Peninsula and beyond. Krill fishery catch distributions and population projections in the context of a changing climate should account for ontogenetic habitat partitioning, regional population connectivity, and highly variable recruitment.

1. Introduction

The Antarctic Peninsula (AP) is a key region for understanding population dynamics of the Antarctic krill (*Euphausia superba*), a dominant species in the Southern Ocean food web and in biogeochemical cycles (Trathan and Hill 2016; Cavan et al. 2019). A recent study indicates that Antarctic krill distribution in the Southwest Atlantic sector shifted southward from the Scotia Sea to the AP shelf from 1976 to 2016 (Atkinson et al. 2019). This range contraction coincided with regional warming and reduced seasonal sea ice coverage during the second half of the 20th century (Meredith and King 2005; Stammerjohn et al. 2008b; Henley et al. 2019). Further twenty-first century ocean warming, acidification, and sea ice decline will likely impair recruitment by reducing larval survival over winter (Flores et al. 2012; but see Melbourne-Thomas et al. 2016). Although previously distributed throughout the Southern Ocean, commercial krill fishing effort has focused on the North Antarctic Peninsula (NAP) in the last two decades (Nicol and Foster 2016). Understanding krill demographic patterns will improve population dynamic studies in the context of AP climate change and fishing pressure.

It is well-established that *E. superba* recruitment is episodic throughout the Southwest Atlantic sector. From 1991 to 2013, 4- to 6-year cycles in *E. superba* post-larval abundance were apparent along the West Antarctic Peninsula (WAP) (Ross et al. 2014; Steinberg et al. 2015), NAP (Reiss 2016; Kinzey et al., 2019), and at South Georgia (Fielding et al. 2014). Larval abundance is relatively less studied despite its key role in mechanistic hypotheses explaining *E. superba* recruitment patterns (Siegel and Loeb 1995; Saba et al. 2014). Larvae spawned during summer develop to late stages and then overwinter before recruiting to the post-larval population the following summer. While feeding larvae are most abundant in oceanic waters during summer, recruits are instead concentrated on the continental shelf (Siegel and Watkins 2016;

Perry et al. 2019). Therefore, linking larval supply with recruitment must account for spatial segregation between these life stages.

Uncertainties in regional-scale connectivity further complicate Antarctic krill population dynamics. Physical model simulations suggest larvae spawned at the WAP and NAP can both be retained locally or advected northeast towards the Scotia Sea (Fach and Klinck 2006; Thorpe et al. 2007; Piñones et al. 2013). A mechanistic population model reproduced observed Antarctic krill biomass cycles at the WAP, NAP, and South Georgia only after allowing for transport among study areas (Wiedenmann et al. 2009). Available data suggest recruitment was positively correlated across these sites between 1983 and 2011 (Siegel et al. 2003; Reiss 2016), but larval abundance time series have not been compared across the region.

In this study we analyzed spatiotemporal patterns in larval euphausiid abundance as well as *E. superba* recruit and mature female abundance along the AP since 1993. Austral summer net sampling surveys were conducted along the WAP by the Palmer Antarctica Long-Term Ecological Research (PAL LTER) program and at the NAP by the United States Antarctic Marine Living Resources (U.S. AMLR) program. While *E. superba* recruitment was generally synchronized across the NAP and WAP, larval euphausiid abundance correlations were weaker between the two areas. The WAP continental slope was identified as a key larval supply region supporting *E. superba* recruitment the following summer on the continental shelf. Population connectivity must be considered to understand how krill will respond to climate change and to effectively distribute fishing effort.

2. Materials and Methods

2.1. Sample collection

2.1.1. U.S. AMLR – NAP

The U.S. AMLR Program conducted shipboard oceanographic and biological surveys in the NAP ecosystem during austral summer from 1993-2011, sampling an area of more than 124,000 km^2. The oceanographic survey usually consisted of two repeat legs. Leg-1 was typically conducted in mid-January and Leg-2 started several weeks later in February. The survey area extends from the southern end of Bransfield Strait to the tip of the AP at Joinville Island, and offshore into the Antarctic Circumpolar Current (ACC) on the north side of the South Shetland and Elephant Islands (Fig. 1). The number and location of sampling stations varied as the grid expanded throughout the time series. In general, 40−60 stations either 20 or 40 km apart along predefined transects were sampled during each leg.

For this analysis, the U.S. AMLR sampling grid was divided into Slope, Shelf, and Coast sub-regions (Fig. 1). The NAP Slope sub-region included sampling stations offshore of the 750 m isobath along the continental shelf break, following the definition used by PAL LTER at the WAP (Martinson et al., 2008). The NAP shelf was defined as the area bounded to the northwest by the shelf break and to the southeast by the South Shetland Islands and another 750 m isobath along the edge of a submarine canyon. The NAP Coast sub-region included stations southeast of the South Shetland Islands and the canyon edge and was restricted to the east by the Antarctic Peninsula and the continental shelf break.

At each sampling station a tow was made using a 1.8 m Isaacs-Kidd Midwater Trawl (IKMT) equipped with a 505 μm mesh net. The net frame was also equipped with a General Oceanics flowmeter to determine the volume of water filtered during each tow. The IKMT was

fished obliquely to either 170 m depth or 20 m above the bottom at stations <190 m deep using an attached pressure-sonde to determine net depth.

Aboard ship, zooplankton were sorted to species and enumerated. *Euphausia superba* post-larvae were identified by sex and maturity stage following Makarov and Denys (1981) and measured to the nearest 0.1 mm using Standard Length 1 (SL1) (Mauchline 1980). The SL1 measurement is taken from the anterior tip of the rostrum to the posterior tip of the uropod. From 1995 to 2011, euphausiid larvae were identified to species, staged and enumerated for each tow. Total euphausiid larvae (*E. superba* plus other species) were used for the analysis in this study, because larvae collected in the WAP were not identified to species. Annual *E. superba* and *Thysanoessa macrura* (another abundant euphausiid) larval abundances were compared to total euphausiid larval abundance using the available species-specific data from the NAP.

2.1.2. PAL LTER – WAP

The historical PAL LTER study region extends 400 km along the WAP from Anvers Island to Marguerite Bay and from coastal to slope waters approximately 200 km offshore (Ducklow et al. 2012) (Fig. 1). Sampling grid lines are spaced 100 km apart, with grid stations every 20 km along each grid line (Waters and Smith 1992). Zooplankton were collected on PAL LTER annual research cruises during austral summer (approx. 01 January – 10 February) since 1993. From 1993-2008 tows were conducted at each PAL LTER grid station from the 600 to 200 lines, and since 2009 on an extended grid an additional 300 km further south with decreased sampling frequency (Steinberg et al. 2015). The sampling grid is divided into North, South, and Far South latitudinal sub-regions as well as Coast, Shelf, and Slope sub-regions (Steinberg et al.,

2015). For this study, only data from the consistently sampled North and South sub-regions (600 to 200 lines) are included (Fig. 1).

Zooplankton were collected with two gear types on PAL LTER research cruises. Post-larval *E. superba* were collected with double oblique net tows from 0-120 m using a 2x2 m square frame net with 700 µm mesh. Euphausiid larvae were collected with double oblique net tows from 0-300 m using a 1x1 m square frame net with 333 µm mesh. Net depth was determined real time with a depth sensor attached to the bottom of the conducting hydro wire. Both nets were equipped with a General Oceanics flowmeter to record the volume of water filtered.

Post-larval *E. superba* were enumerated onboard, and a subsample of at least 100 randomly selected individuals were measured using SL1. Juvenile *E. superba* recruits belonging to age class 1 were defined as post-larval individuals < 31 mm in length (Saba et al. 2014; Atkinson et al. 2019). This same recruit definition was used for the WAP and NAP. Post-larval *E. superba* individuals with a visibly red thelycum were classified as mature females.

Once onboard, the 333 µm mesh net samples were preserved in 4% buffered formaldehyde and stored for subsequent laboratory analysis. A subset of samples was analyzed for larval euphausiid abundance: one Coast, one Shelf, and one Slope station on each of the 600, 400, and 200 grid lines from 1993-2013. The stations sampled on each grid line varied year-to-year within a 40-km radius. Preserved samples were sieved into three size fractions (> 5 mm, 1-5 mm, and 0.33-1 mm). The entire > 5 mm size fraction was enumerated, and the two smaller size fractions were subsampled as follows: the 1-5 mm size fraction was split with a Folsom Plankton Splitter (1-1/64 sample enumerated), and the 0.33-1 mm size fraction was subsampled using a Stempel pipet (1-1/180 sample enumerated; Postel et al. 2000). Samples were analyzed

using an Olympus SZX10 dissecting microscope with dark/bright field illumination at 8-20x magnification. Larval euphausiids in this analysis include the calyptopis and furcilia stages. Euphausiid larvae collected at the WAP were not identified to species. Most samples analyzed were from daytime tows (hours of darkness are limited to < 4 h during our sampling period in January); there was no significant difference between the abundance of calyptopis or furcilia larvae collected in day (n = 185) compared to night tows (n = 18; Wilcoxon rank-sum $p > 0.05$).

2.2. Statistical analysis

WAP sampling locations were rounded to the nearest grid line and grid station. Abundance values were averaged when the same PAL LTER station was sampled multiple times in a given year. The following data processing steps were applied to NAP and WAP sampling sub-regions: When a life stage was absent at a sampling station, zeros were replaced with one-half the lowest non-zero abundance value in a given sub-region data set (O'Brien 2013). Sampling station abundance values were then $\log_{10}$-transformed prior to calculating annual mean abundance for the sub-region. Abundance anomalies were calculated by subtracting annual mean abundance from the climatological mean of the given time series (Mackas and Beaugrand 2010; O'Brien 2013; Thibodeau et al. in review). A difference of 1.0 in annual mean abundance or abundance anomaly indicates an order of magnitude difference. Although annual mean abundance cannot be compared across different gear types, temporal comparisons of abundance anomalies are appropriate. All statistical analysis was conducted with R version 3.5.1 (R Core Team 2018), and the significance level was set at 0.05 unless otherwise noted.

Spatial differences in annual mean abundance were examined among sub-regions within the NAP and WAP areas each. Linear mixed models (LMMs) were fitted using the nlme package

by maximizing the restricted log-likelihood (Pinheiro et al. 2018). Annual mean abundance was the response variable, sub-region was included as a fixed effect, and year was included as a random effect to account for repeated sampling. This analysis was also conducted separately using *E. superba* larvae data available for the NAP. Tukey's honest significant differences tested for pairwise differences among individual sub-region means using the multcomp package (Hothorn et al. 2008).

Temporal synchrony in euphausiid larvae and *E. superba* recruit abundance across the study region was tested by calculating pairwise Pearson's correlations for the NAP Slope, Shelf, and Coast sub-regions as well as the WAP Coast, Shelf, and Slope. The same analysis was performed using available *E. superba* larvae data for the NAP. The significance level was set at 0.003 for this analysis according to the Bonferroni adjustment for multiple comparisons. The function 'acf' was used to test for autocorrelation in individual time series at the 0.05 significance level. This temporal analysis and all others described below were performed with data in anomaly form.

The relationship between total euphausiid larvae abundance and species-specific larvae abundance was investigated in each of the NAP sub-regions. Total euphausiid larvae abundance was compared to *T. macrura* larval abundance and to *E. superba* larval abundance using linear regression.

An information-theoretic approach was used to identify potential larval source areas impacting *E. superba* recruitment. This analysis was restricted to years with complete data coverage (1995-2010 for euphausiid larvae and 1996-2011 for *E. superba* recruits). All six individual sampling sub-regions were included as candidate larval source areas. The combined Shelf and Coast sub-regions for both the NAP and WAP were the recruitment areas of interest

based on elevated *E. superba* recruit abundance in the LMM analysis described above. Separate linear regressions were fitted for each combination of larval source and recruitment area, with *E. superba* recruit abundance as the response variable and the previous year's euphausiid larvae abundance as the explanatory variable. Comparable linear regressions were also repeated for the NAP using available *E. superba* larvae data. The corrected Akaike Information Criterion (AICc) was used to assess support for individual linear regression models (Hurvich and Tsai 1989; Burnham et al. 2011) and calculated with the MuMIn package (Bartoń 2019). Models with ΔAICc < 2 were considered to have substantial statistical support. AICc weight approximates the probability that each candidate model is the best option given the set of models considered (Symonds and Moussalli 2011).

The functional relationship between larval euphausiid abundance and the following year's *E. superba* recruitment was assessed with thin plate regression splines. This analysis focused on larval abundance at the WAP Slope based on the above model selection procedure and our ecological interpretation of those results. Five additional years of larval abundance data were available from the WAP Slope for this analysis (1993-2013). *Euphausia superba* recruit abundance at the combined Shelf and Coast for both the NAP and WAP were the response variables in separate models. The previous year's larval euphausiid abundance at the WAP Slope was the only explanatory variable in each regression. Thin plate regression splines were fitted using restricted maximum likelihood with the gam function in the mgcv package (Wood, 2003). This non-linear technique alleviated problematic patterns in the residuals and reduced AICc compared to linear regression when using all available data. The basis dimension of the smoother term was set at 4 to avoid overfitting and confirmed to be adequate using the gam.check

function. Model assumptions were verified by plotting residuals against fitted values, sampling year, and the explanatory variable (Zuur and Ieno, 2016).

3. Results

3.1. Spatial distribution of life stages

Larval euphausiid abundance was highest along the continental slope in both the NAP and WAP study areas. Annual mean larval euphausiid abundance was significantly different among sub-regions (LMM; NAP $p = < 0.0001$; WAP $p < 0.0001$) and was higher on the Slope than on the Shelf and Coast in both the NAP and WAP (Fig. 2A-B) (Tukey's test; $p < 0.0001$). Mean *E. superba* larval abundance was also different among NAP sub-regions (Supplemental Fig. 1) (LMM; $p = 0.011$). With species-level data, *E. superba* larvae were significantly more abundant at the Slope than Shelf (Tukey's test; $p = 0.004$), while the Slope and Coast were not significantly different ($p = 0.10$). However, *E. superba* larvae were less abundant at the Coast on average, and two anomalous years drove the lack of a statistical difference (Supplemental Fig. 1).

In contrast to the larval distribution, *E. superba* recruit abundance was highest over the continental shelf in both the NAP and WAP study areas. Annual mean *E. superba* recruit abundance was significantly different among sub-regions (LMM; NAP $p < 0.0001$; WAP $p < 0.0001$), and within the NAP was higher on both the Shelf and Coast than on the Slope (Fig. 2C) (Tukey's test; $p < 0.00001$), and within the WAP progressively increased from Slope to Shelf to Coast (Fig. 2D) (Tukey's test; $p < 0.005$).

Mature female *E. superba* distribution was also consistent across the offshore sampling gradient in the NAP and WAP study areas. Annual mean *E. superba* mature female abundance

differed among sub-regions (LMM; NAP $p = 0.0002$; WAP $p = 0.0008$) and was highest on the Shelf in both the NAP and WAP (Fig. 2E-F) (Tukey's test; $p < 0.02$).

3.2. Regional coherence

Larval euphausiid abundance was positively, significantly correlated between neighboring sub-regions from 1995-2011, but these correlations did not hold throughout the entire AP study region. There was a relatively weak positive correlation in euphausiid larvae abundance between the full WAP study area and the full NAP study area (Fig. 3A). Pairwise comparisons of individual sub-regions revealed larval abundance was strongly correlated between the adjacent Coast and Shelf sub-regions as well as the Shelf and Slope within both the NAP and WAP study areas (Table 1). The same result was found using *E. superba* larvae data for the NAP (Supplemental Table 1). There were no similarly strong cross-correlations between NAP and WAP sub-regions. Larval euphausiid abundance did not exhibit positive autocorrelation ($p > 0.05$).

Unlike larval euphausiid abundance, *E. superba* recruitment cycles were coherent across the AP study region. There was a relatively strong positive correlation in *E. superba* recruit abundance between the full WAP and NAP study areas compared to the euphausiid larvae time series (Fig. 3B). Recruit abundance in the WAP Coast sub-region was only significantly correlated with the WAP Shelf, an apparent exception to the pattern of synchronized recruitment throughout the AP study region (Table 1). Two to three successive years of positive *E. superba* recruit abundance anomalies were typically followed by two to three successive years of negative anomalies (Fig. 3B). Significant, positive autocorrelation at 5 to 6 years was identified in recruit abundance time series from all NAP sub-regions and the WAP Coast ($p < 0.05$).

3.3. Euphausiid larvae composition

The annual abundance of larval *E. superba* and *T. macrura* were both significantly, positively related to total euphausiid larvae abundance in all three NAP sub-regions ($p < 0.02$) (Fig. 4). Total euphausiid abundance was more strongly related to *T. macrura* larvae abundance than *E. superba* larvae abundance at the NAP Slope and Shelf.

Calyptopis stage larvae were numerically dominant compared to furcilia in the WAP samples. Calyptopes comprised 68% of larvae on average (median = 82%) in individual samples.

3.4. Larvae-recruit relationships

The NAP and WAP Slope had substantial statistical support for impacting subsequent *E. superba* recruitment on the continental shelf in both the NAP and WAP (Table 2). According to AICc, the WAP Slope model was preferable to the NAP Slope model in both cases. The importance of remote larval supply to the NAP was further supported by the lack of statistical relationships between *E. superba* larvae abundance and subsequent recruitment in this area (Supplemental Fig. 2) (linear regression; $p > 0.31$). Larval abundance at the NAP Shelf was identified as the best model for recruitment at the combined WAP Shelf and Coast (Table 2), but it is unlikely that larvae follow this transport path given regional circulation patterns. There was not support for larval abundance at the NAP Coast, WAP Coast, or WAP Shelf driving subsequent krill recruitment (Table 2).

The functional relationships between larval abundance in the WAP Slope sub-region and subsequent *E. superba* recruitment on the continental shelf differed between the NAP and WAP. WAP Slope larval abundance was positively, linearly related with next year's *E. superba* recruit abundance at the combined NAP Coast and Shelf ($n = 18$; $p = 0.006$; deviance explained = 45%)

(Fig. 5A). The larvae-recruit relationship at the WAP Coast and Shelf suggested a threshold response (n = 21; p = 0.011; deviance explained = 44%) (Fig. 5B). When larval abundance at the WAP Slope was below average (ranging two orders of magnitude), *E. superba* recruit abundance anomaly the following year was also negative but relatively stable. Following years with a positive larval abundance anomaly, *E. superba* recruitment increased with larval abundance.

4. Discussion

4.1. Spatial distribution of life stages

Two decades of time-series data confirm the importance of oceanic slope waters for larval euphausiid supply along the AP. Combined calyptopis and furcilia-stage abundance was elevated in the NAP and WAP Slope sub-regions. A January 2011 survey along the AP found *E. superba* calyptopes and furcilia were most abundant at the WAP continental slope, with a secondary peak at the NAP Slope (Siegel et al. 2013). A spatial analysis compiling *E. superba* data collected across the Southwest Atlantic sector from 1976-2011 showed calyptopes and furcilia were concentrated in waters deeper than 1000 m (Perry et al. 2019). A typical explanation for the offshore, oceanic distribution of *E. superba* feeding stage larvae is that embryos must sink to depths of roughly 1000 m without reaching the seafloor to successfully hatch (Hofmann et al. 1992). However, it is possible embryos can still hatch after reaching the benthos and it is uncertain where collected larvae were spawned.

Unlike larvae, *E. superba* recruits were concentrated in AP coastal and shelf waters, indicating persistent habitat partitioning. At the NAP and WAP, elevated *E. superba* recruit abundance coincided with low larval abundance in Coast and Shelf sub-regions. Concentration of juvenile *E. superba* in shelf and coastal waters is common along the AP and is consistent

across the southwest Atlantic sector (Lascara et al. 1999; Siegel et al. 2013; Perry et al. 2019). Elevated summer phytoplankton biomass along the coastal AP (Reiss et al. 2017, their Fig. 4A; Brown et al. 2019) promotes faster krill growth rates (Atkinson et al. 2006; Shelton et al. 2013) and makes these areas favorable juvenile habitat. Additionally, ontogenetic habitat partitioning may reduce food competition between krill larvae and recruits under limiting conditions (Siegel 1988; Ryabov et al. 2017), although we note adult *E. superba* are not phytoplankton food limited during summer at the WAP (Bernard et al. 2012).

Antarctic krill mature females were consistently most abundant in Shelf sub-regions along the AP. This distribution is consistent with the highest densities of krill embryos being concentrated on continental shelves (further inshore than feeding larvae) (Perry et al. 2019). The spatial mis-match between mature females and larvae suggests large numbers of embryos spawned over the continental shelf may fail to develop into feeding larvae. High mortality rates are likely in shallow shelf waters where embryos reach the seafloor before hatching (Hofmann et al. 1992; Thorpe et al. 2019). However, not all mature females are active spawners (Quetin and Ross 2001), and we did not distinguish by size or ovarian development stage. Adult krill on the AP shelf during summer are typically smaller than those further offshore (Lascara et al. 1999; Siegel et al. 2013; Siegel and Watkins 2016), and larger females typically produce larger embryo batches, although spawning output varies among individuals and years (Quetin and Ross 2001; Tarling et al. 2007). Therefore, the spatial distribution of mature females does not necessarily indicate the spatial distribution of reproductive output.

4.2. Regional coherence

Asynchrony in larval euphausiid abundance across the AP supports the existence of multiple localized *E. superba* spawning areas. The locations of these spawning areas are consistent with regional circulation patterns (reviewed in Moffat and Meredith 2018). The WAP's inner shelf is an isolated spawning area, and larvae that successfully develop in this area are likely retained locally by ocean currents and a longer sea ice season (Stammerjohn et al. 2008a; Piñones et al. 2013, Meyer et al., 2017). Larval abundance in the NAP is decoupled from the WAP further south, likely because the northern tip of the AP is influenced by water flowing from the Weddell Sea (Thompson et al. 2009) (Fig. 6). Inflow from the Antarctic Coastal Current and a cyclonic gyre appear to generally isolate NAP Coast, although its degree of exchange with the WAP remains unclear (Sangrà et al. 2017; Moffat and Meredith 2018). Larval abundance at the NAP may be coupled with downstream areas in the ACC as larvae are transported out of our study region and into the Scotia Sea (Thorpe et al. 2004; Fach and Klinck 2006) (Fig. 6). Differences in seasonal spawn timing (Spiridonov 1995) may also contribute to the lack of strong correlations between NAP and WAP summer larval abundances.

Unlike larval abundance, Antarctic krill recruit abundance was generally synchronized along the AP, indicating recruitment is a regional-scale process. A notable exception was the WAP Coast where *E. superba* recruits were abundant. Comparison of annual krill recruitment indices from the WAP, NAP, and South Georgia showed positive correlations among sampling areas from 1983 to 2000 (non-continuous time series) (Siegel et al. 2003). Although some studies suggest recruitment cycles became decoupled between the WAP and NAP from 2000 to 2008 (Loeb et al. 2010; Ross et al. 2014), our analysis shows recruitment remained synchronized until at least 2011, in agreement with recent work (Reiss 2016). Climate-scale environmental controls

such as the El Niño Southern Oscillation (ENSO) and the Southern Annular Mode (SAM) that affect sea ice and primary production (Stammerjohn et al. 2008b; Loeb et al. 2009; Saba et al. 2014; Kim et al. 2016) likely synchronize krill recruitment throughout the region. ENSO and SAM indices are linked to krill recruitment success at the AP and throughout the southwest Atlantic sector (Loeb et al. 2009; Ross et al. 2014; Atkinson et al. 2019).

The Antarctic krill life span (~6 years) coincides roughly with the period of its synchronized population cycles. One hypothesis suggests this long lifespan is an adaptive trait to deal with the environmental variability mentioned above, and it follows that successful *E. superba* recruitment would occur more frequently if environmental conditions were continuously favorable (Fraser and Hofmann 2003; Saba et al. 2014). An alternate view suggests *E. superba*'s relatively long lifespan causes periodic recruitment via intraspecific competition cycles that are independent of environmental variability (Ryabov et al. 2017). Regardless of the underlying mechanism driving periodic krill recruitment, climate-scale environmental forcing and larval dispersal are certainly important for its synchronization at the 1000-km scale of our study (Ripa 2000; Koenig 2002; Ryabov et al. 2017).

4.3. Euphausiid larvae composition

The grouping of all euphausiid larvae together is a limitation of our study. However, as our data analysis and interpretation depend upon relative temporal and spatial patterns, and are largely based on order of magnitude abundance differences between sampling years and sub-regions, we posit use of aggregated larval abundance is adequate. Larval euphausiid samples collected in autumn and winter 2001 at the WAP were numerically dominated by *E. superba* (typically > 95%) (Ashjian et al. 2008). The positive relationships between *E. superba* larvae and

total euphausiid larvae abundance anomalies in all NAP sub-regions also support our use of aggregated euphausiid data to understand *E. superba* population dynamics. Contamination from *T. macrura* due to its high numerical abundance (Loeb and Santora 2015; Steinberg et al. 2015) is the most likely source of error. *Euphausia superba* larvae were present in 50%, and *T. macrura* larvae in 60%, of NAP samples from 1995 to 2009, but mean abundance was 37% greater for *E. superba* larvae compared to *T. macrura* (Loeb and Santora 2015). Larval *E. superba* and *T. macrura* abundance was positively correlated within and between years (Loeb and Santora 2015). The strong relationship between total euphausiid and *T. macrura* larvae abundance supports previous work showing both species are highly positively correlated with phytoplankton productivity (Steinberg et al. 2015).

The numerical dominance of calyptopes in the WAP larvae samples also supports their use in the study of *E. superba* population dynamics. Antarctic krill calyptopes were an order of magnitude more abundant than furcilia at the AP during January (Siegel et al. 2013) when *T. macrura* larvae are typically in furcilia stages (Makarov 1979; Nordhausen 1992).

4.4. Larvae-recruit relationships

The statistical link between larval abundance at the WAP continental slope and *E. superba* recruitment on the shelf suggests offshore larval production drives recruitment. Larvae are produced within our AP study area and further southwest in the Bellingshausen Sea (upstream in the ACC) (Fig. 6). Above average phytoplankton biomass in the Bellingshausen Sea was associated with high larval euphausiid abundance at the WAP shelf break in autumn and strong *E. superba* recruitment the following summer (Marrari et al. 2008). Phytoplankton biomass and primary productivity are strong predictors of subsequent *E. superba* recruitment and

post-larval abundance along the NAP (Loeb et al., 2009) and WAP (Saba et al., 2014; Steinberg et al. 2015). Importantly, early spawn timing also contributes to successful recruitment (Siegel and Loeb 1995). Additional time for larval development under high phytoplankton conditions likely increases overwinter survival (Ross and Quetin 1989).

The shelf is key habitat for later stage *E. superba* larvae despite lower numerical abundance compared to the slope. In autumn 2001 and 2002, *E. superba* larvae were more developmentally advanced and had improved body condition on the shelf where phytoplankton biomass is typically higher than offshore waters (Pakhomov et al. 2004; Daly et al. 2004). Therefore, the proportion of larvae that reach shelf waters may be more developed going into winter and thus have greater recruitment success (Ross and Quetin 1989; Daly et al. 2004). Shelf waters may include a mix of larvae spawned locally and offshore (Wiebe et al. 2011; Piñones et al. 2013), but our data show larval abundance is an order of magnitude lower on the shelf compared to the slope and suggest the importance of shoreward transport to drive subsequent recruitment.

Coupling between larval euphausiid abundance at the WAP slope and recruitment at the NAP suggests meridional links along the AP are direct and important (Fig. 6). These areas are connected by northeastward flow of the ACC, and larval transport onto the shelf is likely common at canyons (Orsi et al. 1995; Martinson et al. 2008; Martinson and McKee 2012; Piñones et al. 2013). From 1980 to 2004, *E. superba* larvae abundance at Elephant Island was positively correlated with the following summer's proportional recruitment (Loeb et al. 2009). In contrast, our analysis suggests local larval production was not driving periodic recruitment in the NAP from 1995-2011.

Regional warming has had divergent impacts on AP ecosystems. Phytoplankton biomass and diatom proportion decreased at the NAP but increased further south along the WAP from the 1980s to 2000s (Montes-Hugo et al. 2009), likely having localized impacts on larval production and survival. While the WAP has shifted from perennial sea ice coverage to seasonal sea ice coverage, the NAP is now ice-free for most of the year (Stammerjohn et al. 2008b; Montes-Hugo et al. 2009; Reiss et al. 2017). This latitudinal gradient in the ecosystem may have increased the importance of larvae from the WAP recruiting at the NAP during this period of rapid environmental change. One study found that *E. superba* abundance declined at the NAP while remaining stable or increasing along the WAP from the 1970s to 2010s (Atkinson et al. 2019). However, another study using the same database found no substantial decline in krill abundance (Cox et al., 2018), and an integrated model also showed variability but no directional trend in krill spawning biomass or recruit abundance at the NAP over the same time period (Kinzey et al. 2019). Recent winter surveys do suggest krill recruitment at the NAP is decoupled from local larval abundance (Walsh et al. 2020) and support the importance of remote larval supply.

Our results suggest krill recruitment fails following years of below average offshore larval abundance. Recruitment increases with larval abundance following above-average larvae years. Krill year-class failure is well-documented at the AP (Reiss et al. 2008; Ross et al. 2014), but the spawner-recruit relationship remains uncertain (Kinzey et al. 2019). Given that larval abundance, but not spawning biomass, has a clear one-year lagged relationship with recruitment, it appears individual spawning output and timing are key drivers of krill recruitment (Siegel and Loeb 1995; Saba et al. 2014). Our findings suggest total egg production or larval abundance estimates may provide valuable information about krill reproductive potential within the fishery management framework (Murawski et al. 2001; Kell et al. 2016).

4.5. Implications for fishery management and climate-driven change

Commercial krill catch at the NAP reached at least 94% of the 155,000 ton limit for this subarea of the Southwest Atlantic each year from 2013-2018 (CCAMLR 2018; Cavan et al. 2019). The Commission for the Conservation of Antarctic Marine Living Resources, which manages the krill fishery, has determined that the catch limit may only be increased further if the catch is spatially subdivided (see Hewitt et al. 2004 for example allocation strategies) to limit the potential that the fishery takes the entire interim catch limit of 620,000 tons from a single location. Strategies to distribute the catch spatially may result in increased fishing pressure in critical areas of recruitment or larval production and should be carefully considered. Other spatial management frameworks are also being considered for the AP region, and these include the delineation of a marine protected area (MPA) (Hindell et al. 2020). Implementing effective spatial management requires careful consideration of the target species' life history, distribution, and larval dispersal (Hilborn et al. 2004; Manel et al. 2019). Understanding whether upstream production of krill larvae in the WAP is responsible for recruitment and population dynamics in other areas is critical to understand in order to develop appropriate protected areas in a changing environment.

Our findings emphasize the importance of considering cross-shelf and alongshore krill population connectivity for MPAs or spatial management frameworks to achieve their conservation goals. In agreement with current krill life history models, recruitment in shelf and coastal waters along the AP is likely the product of larval production over the continental slope. The consistent relationship between krill larval abundance at the WAP and subsequent recruitment at the NAP suggests the ACC and other regional current flows play an important role in larval dispersal (Fig. 6). Clarifying the impact of larval production in the Bellingshausen and

Weddell Seas remains a challenge. Additionally, recruits from the AP likely source the krill population near South Georgia where local recruitment is unsuccessful (Fach and Klink 2006; Tarling et al. 2007; Thorpe et al. 2007; Reid et al. 2010). Importantly, spatial catch distribution and MPA design should anticipate the impacts of continued climate-driven ecosystem shifts (Montes-Hugo et al. 2009; Flores et al. 2012; Atkinson et al. 2019; Hindell et al. 2020).

A management approach that distinguishes between successful and failed krill recruitment years may help achieve precautionary harvest rates and support ecosystem-based management goals. If held constant, the same fishery catch at the NAP is more detrimental to penguin performance during years of failed krill recruitment compared to successful recruitment years (Watters et al. 2020). Larval abundance estimates and length-based recruit abundance estimates effectively capture synchronized regional population cycles. Predator diet sampling as well as autonomous platforms equipped with optical and acoustic sensors can provide valuable information if ship-based surveys are not feasible. Fishery-independent time series provide the backbone for understanding krill ecology and population dynamics in a changing Southern Ocean.

Acknowledgements

Thank you to the Captains, officers, crews, and Antarctic Support Contract personnel for their support on U.S. AMLR and PAL LTER research cruises. We are grateful to the U.S. AMLR and PAL LTER field teams who collected and processed samples at sea. Joe Cope compiled and supplied data for this analysis. Schuyler Nardelli assisted with mapping. Comments from George Watters and two anonymous reviewers improved this manuscript. We thank SCAR Krill Action Group and PAL LTER colleagues for valuable discussions. This work was supported by the

National Science Foundation Antarctic Organisms and Ecosystems Program (PLR-1440435). The Commission for the Conservation of Antarctic Marine Living Resources funded J.A.C.'s attendance of the 2019 Scientific Committee on Antarctic Research Krill Action Group meeting where the idea for this manuscript was conceived. This is Contribution No. 3919 from the Virginia Institute of Marine Science.

References

Ashjian CJ, Davis CS, Gallager SM, Wiebe PH, Lawson GL. 2008. Distribution of larval krill and zooplankton in association with hydrography in Marguerite Bay, Antarctic Peninsula, in austral fall and winter 2001 described using the Video Plankton Recorder. Deep-Sea Res Pt II 55:455–71.

Atkinson A, Hill SL, Pakhomov EA, Siegel V, Reiss CS, Loeb VJ, Steinberg DK, Schmidt K, Tarling GA, Gerrish L, Sailley SF. 2019. Krill (*Euphausia superba*) distribution contracts southward during rapid regional warming. Nat Clim Change 9:142-47.

Atkinson A, Shreeve RS, Hirst AG, Rothery P, Tarling GA, Pond DW, Korb RE, Murphy EJ, Watkins JL. 2006. Natural growth rates in Antarctic krill (*Euphausia superba*): II. Predictive models based on food, temperature, body length, sex, and maturity stage. Limnol Oceanogr 51:973–87.

Bartoń K. 2019. MuMIn: Multi-Model Inference.

Bernard KS, Steinberg DK, Schofield OME. 2012. Summertime grazing impact of the dominant macrozooplankton off the Western Antarctic Peninsula. Deep-Sea Res Pt I 62:111–22.

Brown MS, Munro DR, Feehan CJ, Sweeney C, Ducklow HW, Schofield OM. 2019. Enhanced oceanic CO_2 uptake along the rapidly changing West Antarctic Peninsula. Nat Clim Chang 9:678–83.

Burnham KP, Anderson DR, Huyvaert KP. 2011. AIC model selection and multimodel inference in behavioral ecology: some background, observations, and comparisons. Behav Ecol Sociobiol 65:23–35.

Cavan EL, Belcher A, Atkinson A, Hill SL, Kawaguchi S, McCormack S, Meyer B, Nicol S,

Ratnarajah L, Schmidt K, Steinberg DK, Tarling GA, Boyd PW. 2019. The importance of Antarctic krill in biogeochemical cycles. Nat Commun 10:4742.

CCAMLR. 2018. Krill fisheries. (https://www.ccamlr.org/en/fisheries/krill). Accessed 1 April 2020.

Cox MJ, Candy S, de la Mare WK, Nicol S, Kawaguchi S, Gales N. 2018. No evidence for a decline in the density of Antarctic krill *Euphausia superba* Dana, 1850, in the Southwest Atlantic sector between 1976 and 2016. J Crustacean Biol 38:656–61.

Daly KL. 2004. Overwintering growth and development of larval Euphausia superba: an interannual comparison under varying environmental conditions west of the Antarctic Peninsula. Deep-Sea Res Pt II Topical Studies in Oceanography, 51:2139–68.

Ducklow H, Clarke A, Dickhut R, Doney SC, Geisz H, Huang K, Martinson DG, Meredith MP, Moeller HV, Montes-Hugo M, Schofield O, Stammerjohn SE, Steinberg D, Fraser W. 2012. The Marine System of the Western Antarctic Peninsula. In: Rogers AD, Johnston NM, Murphy EJ, Clarke A, editors. Antarctic Ecosystems John Wiley & Sons, Ltd. p. 121–59.

Fach BA, Klinck JM. 2006. Transport of Antarctic krill (*Euphausia superba*) across the Scotia Sea. Part I: Circulation and particle tracking simulations. Deep-Sea Res Pt I 53:987–1010.

Fielding S, Watkins JL, Trathan PN, Enderlein P, Waluda CM, Stowasser G, Tarling GA, Murphy EJ. 2014. Interannual variability in Antarctic krill (*Euphausia superba*) density at South Georgia, Southern Ocean: 1997–2013. ICES J Mar Sci 71:2578–88.

Flores H, Atkinson A, Kawaguchi S, Krafft BA, Milinevsky G, Nicol S, Reiss C, Tarling GA, Werner R, Bravo Rebolledo E, Cirelli V, Cuzin-Roudy J, Fielding S, Groeneveld JJ,

Haraldsson M, Lombana A, Marschoff E, Meyer B, Pakhomov EA, Rombolá E, Schmidt K, Siegel V, Teschke M, Tonkes H, Toullec JY, Trathan PN, Tremblay N, Van de Putte AP, van Franeker JA, Werner T. 2012. Impact of climate change on Antarctic krill. Mar Ecol Prog Ser 458:1–19.

Fraser WR, Hofmann EE. 2003. A predator's perspective on causal links between climate change, physical forcing and ecosystem response. Mar Ecol Prog Ser 265:1–15.

Henley SF, Schofield OM, Hendry KR, Schloss IR, Steinberg DK, Moffat C, Peck LS, Costa DP, Bakker DCE, Hughes C, Rozema PD, Ducklow HW, Abele D, Stefels J, Van Leeuwe MA, Brussaard CPD, Buma AGJ, Kohut J, Sahade R, Friedlaender AS, Stammerjohn SE, Venables HJ, Meredith MP. 2019. Variability and change in the west Antarctic Peninsula marine system: Research priorities and opportunities. Prog Oceanogr 173:208–37.

Hewitt RP, Watters G, Trathan PN, Croxall JP, Goebel ME, Ramm D, Reid K, Trivelpiece WZ, Watkins JL. 2004. Options for allocating the precautionary catch limit of krill among small-scale management units in the Scotia Sea. CCAMLR Sci 11:81–97.

Hilborn R, Stokes K, Maguire J-J, Smith T, Botsford LW, Mangel M, Orensanz J, Parma A, Rice J, Bell J. 2004. When can marine reserves improve fisheries management? Ocean Coast Manage 47:197–205.

Hindell MA, Reisinger RR, Ropert-Coudert Y, Hückstädt LA, Trathan PN, Bornemann H, Charrassin J-B, Chown SL, Costa DP, Danis B, Lea M-A, Thompson D, Torres LG, Van de Putte AP, Alderman R, Andrews-Goff V, Arthur B, Ballard G, Bengtson J, Bester MN, Blix AS, Boehme L, Bost C-A, Boveng P, Cleeland J, Constantine R, Corney S, Crawford RJM, Dalla Rosa L, de Bruyn PJN, Delord K, Descamps S, Double M,

Emmerson L, Fedak M, Friedlaender A, Gales N, Goebel ME, Goetz KT, Guinet C, Goldsworthy SD, Harcourt R, Hinke JT, Jerosch K, Kato A, Kerry KR, Kirkwood R, Kooyman GL, Kovacs KM, Lawton K, Lowther AD, Lydersen C, Lyver PO, Makhado AB, Márquez MEI, McDonald BI, McMahon CR, Muelbert M, Nachtsheim D, Nicholls KW, Nordøy ES, Olmastroni S, Phillips RA, Pistorius P, Plötz J, Pütz K, Ratcliffe N, Ryan PG, Santos M, Southwell C, Staniland I, Takahashi A, Tarroux A, Trivelpiece W, Wakefield E, Weimerskirch H, Wienecke B, Xavier JC, Wotherspoon S, Jonsen ID, Raymond B. 2020. Tracking of marine predators to protect Southern Ocean ecosystems. Nature 580: 87–92.

Hofmann EE, Capella JE, Ross RM, Quetin LB. 1992. Models of the early life history of *Euphausia superba*—Part I. Time and temperature dependence during the descent-ascent cycle. Deep Sea Research 39:1177–1200.

Hothorn T, Bretz F, Westfall P. 2008. Simultaneous Inference in General Parametric Models. Biometrical J 50:346–63.

Hurvich CM, Tsai C-L. 1989. Regression and time series model selection in small samples. Biometrika 76:297–307.

Kell LT, Nash RDM, Dickey-Collas M, Mosqueira I, Szuwalski C. 2016. Is spawning stock biomass a robust proxy for reproductive potential? Fish Fish 17:596–616.

Kim H, Doney SC, Iannuzzi RA, Meredith MP, Martinson DG, Ducklow HW. 2016. Climate forcing for dynamics of dissolved inorganic nutrients at Palmer Station, Antarctica: An interdecadal (1993-2013) analysis. J Geophys Res-Biogeo 121:2369–89.

Kinzey D, Watters GM, Reiss CS. 2019. Estimating recruitment variability and productivity in Antarctic krill. Fish Res 217:98–107.

Koenig WD. 2002. Global patterns of environmental synchrony and the Moran effect. Ecography 25:283–88.

Lascara CM, Hofmann EE, Ross RM, Quetin LB. 1999. Seasonal variability in the distribution of Antarctic krill, *Euphausia superba*, west of the Antarctic Peninsula. Deep-Sea Res Pt I 46:951–84.

Loeb V, Hofmann EE, Klinck JM, Holm-Hansen O. 2010. Hydrographic control of the marine ecosystem in the South Shetland-Elephant Island and Bransfield Strait region. Deep-Sea Res Pt II 57:519–542.

Loeb VJ, Hofmann EE, Klinck JM, Holm-Hansen O, White WB. 2009. ENSO and variability of the Antarctic Peninsula pelagic marine ecosystem. Antarct Sci 21:135–148.

Loeb VJ, Santora JA. 2015. Climate variability and spatiotemporal dynamics of five Southern Ocean krill species. Prog Oceanogr 134:93–122.

Mackas DL, Beaugrand G. 2010. Comparisons of zooplankton time series. J Marine Syst 79:286-304.

Makarov RR. 1979. Larval Distribution and Reproductive Ecology of *Thysanoessa macrura* (Crustacea: Euphausiacea) in the Scotia Sea. Mar Biol 52:377-386.

Makarov RR, Denys CJ. 1981. Stages of sexual maturity of *Euphausia superba* Dana. In: BIOMASS Handbook Cambridge: SCAR. p. 1–13.

Manel S, Loiseau N, Andrello M, Fietz K, Goñi R, Forcada A, Lenfant P, Kininmonth S, Marcos C, Marques V, Mallol S, Pérez-Ruzafa A, Breusing C, Puebla O, Mouillot D. 2019. Long-Distance Benefits of Marine Reserves: Myth or Reality? Trends Ecol Evol 34:342-354.

Marrari M, Daly KL, Hu C. 2008. Spatial and temporal variability of SeaWiFS chlorophyll *a*

distributions west of the Antarctic Peninsula: Implications for krill production. Deep-Sea Res Pt II 55:377–92.

Martinson DG, McKee DC. 2012. Transport of warm Upper Circumpolar Deep Water onto the western Antarctic Peninsula continental shelf. Ocean Sci 8:433–42.

Martinson DG, Stammerjohn SE, Iannuzzi RA, Smith RC, Vernet M. 2008. Western Antarctic Peninsula physical oceanography and spatio–temporal variability. Deep-Sea Res Pt II 55:1964–87.

Melbourne-Thomas J, Corney SP, Trebilco R, Meiners KM, Stevens RP, Kawaguchi S, Sumner MD, Constable AJ. 2016. Under ice habitats for Antarctic krill larvae: Could less mean more under climate warming? Geophys Res Lett 43:10322-10327.

Meredith MP, King JC. 2005. Rapid climate change in the ocean west of the Antarctic Peninsula during the second half of the 20th century. Geophys Res Lett 32:L19604.

Meyer B, Freier U, Grimm V, Groeneveld J, Hunt BPV, Kerwath S, King R, Klaas C, Pakhomov E, Meiners KM, Melbourne-Thomas J, Murphy EJ, Thorpe SE, Stammerjohn S, Wolf-Gladrow D, Auerswald L, Götz A, Halbach L, Jarman S, Kawaguchi S, Krumpen T, Nehrke G, Ricker R, Sumner M, Teschke M, Trebilco R, Yilmaz NI. 2017. The winter pack-ice zone provides a sheltered but food-poor habitat for larval Antarctic krill. Nat Ecol Evol 1:1853-1861.

Moffat C, Meredith M. 2018. Shelf–ocean exchange and hydrography west of the Antarctic Peninsula: a review. Phil Trans R Soc A 376:20170164.

Montes-Hugo M, Doney SC, Ducklow HW, Fraser W, Martinson D, Stammerjohn SE, Schofield O. 2009. Recent changes in phytoplankton communities associated with rapid regional climate change along the western Antarctic Peninsula. Science 323:1470–1473.

Murawski SA, Rago PJ, Trippel EA. 2001. Impacts of demographic variation in spawning characteristics on reference points for fishery management. ICES J Mar Sci 58:1002-1014.

Nicol S, Foster J. 2016. The Fishery for Antarctic Krill: Its Current Status and Management Regime. In: Siegel V, editor. Biology and Ecology of Antarctic Krill. Advances in Polar Ecology Cham: Springer International Publishing. p. 387–421.

Nordhausen W. 1992. Distribution and growth of larval and adult *Thysanoessa macrura* (Euphausiacea) in the Bransfield Strait Region, Antarctica. Mar Ecol Prog Ser 83:185-196.

O'Brien TD. 2013. Time-series data analysis and visualization. In: O'Brien TD, Wiebe PH, Falkenhaug T, editors. ICES Zooplankton Status Report 2010/2011. International Council for the Exploration of the Sea. p. 6-19.

Orsi AH, Whitworth T, Nowlin WD. 1995. On the meridional extent and fronts of the Antarctic Circumpolar Current. Deep-Sea Res Pt I 42:641–73.

Pakhomov EA, Atkinson A, Meyer B, Oettl B, Bathmann U. 2004. Daily rations and growth of larval krill *Euphausia superba* in the Eastern Bellingshausen Sea during austral autumn. Deep-Sea Res Pt II 51:2185–98.

Perry FA, Atkinson A, Sailley SF, Tarling GA, Hill SL, Lucas CH, Mayor DJ. 2019. Habitat partitioning in Antarctic krill: Spawning hotspots and nursery areas. PLoS One 14:e0219325.

Pinheiro J, Bates D, DebRoy S, Sarkar D, R Core Team. 2018. Nlme: Linear and Nonlinear Mixed Effects Models.

Piñones A, Hofmann EE, Daly KL, Dinniman MS, Klinck JM. 2013. Modeling the remote and

local connectivity of Antarctic krill populations along the western Antarctic Peninsula. Mar Ecol Prog Ser 481:69–92.

Postel L, Fock H, Hagen W. 2000. Biomass and abundance. In: Harris R, Wiebe P, Lenz J, Skjoldal HR, Huntley M. ICES Zooplankton Methodology Manual Elsevier. p. 83–192.

Quetin LB, Ross RM. 2001. Environmental Variability and Its Impact on the Reproductive Cycle of Antarctic Krill. Amer Zool 41:74-89.

R Core Team. 2018. R: A language and environment for statistical computing Vienna, Austria: R Foundation for Statistical Computing.

Reid K, Watkins JL, Murphy EJ, Trathan PN, Fielding S, Enderlein P. 2010. Krill population dynamics at South Georgia: implications for ecosystem-based fisheries management. Mar Ecol Prog Ser 399:243–52.

Reiss CS. 2016. Age, Growth, Mortality, and Recruitment of Antarctic Krill, *Euphausia superba*. In: Siegel V, editor. Biology and Ecology of Antarctic Krill. Advances in Polar Ecology Cham: Springer International Publishing. p. 101–44.

Reiss CS, Cossio A, Santora JA, Dietrich KS, Murray A, Mitchell BG, Walsh J, Weiss EL, Gimpel C, Jones CD, Watters GM. 2017. Overwinter habitat selection by Antarctic krill under varying sea-ice conditions: implications for top predators and fishery management. Mar Ecol Prog Ser 568:1–16.

Reiss CS, Cossio AM, Loeb V, Demer DA. 2008. Variations in the biomass of Antarctic krill (*Euphausia superba*) around the South Shetland Islands, 1996–2006. ICES J Mar Sci 65:497–508.

Ripa J. 2000. Analysing the Moran effect and dispersal: their significance and interaction in

synchronous population dynamics. Oikos 89:175–87.

Ross RM, Quetin LB. 1989. Energetic cost to develop to the first feeding stage of *Euphausia superba* Dana and the effect of delays in food availability. J Exp Mar Biol Ecol 133:103-127.

Ross RM, Quetin LB, Newberger T, Shaw CT, Jones JL, Oakes SA, Moore KJ. 2014. Trends, cycles, interannual variability for three pelagic species west of the Antarctic Peninsula 1993-2008. Mar Ecol Prog Ser 515:11–32.

Ryabov AB, de Roos AM, Meyer B, Kawaguchi S, Blasius B. 2017. Competition-induced starvation drives large-scale population cycles in Antarctic krill. Nat Ecol Evol 1:0177.

Saba GK, Fraser WR, Saba VS, Iannuzzi RA, Coleman KE, Doney SC, Ducklow HW, Martinson DG, Miles TN, Patterson-Fraser DL, Stammerjohn SE, Steinberg DK, Schofield OM. 2014. Winter and spring controls on the summer food web of the coastal West Antarctic Peninsula. Nat Commun 5:4318.

Sangrà P, Stegner A, Hernández-Arencibia M, Marrero-Díaz Á, Salinas C, Aguiar-González B, Henríquez-Pastene C, Mouriño-Carballido B. 2017. The Bransfield Gravity Current. Deep-Sea Res Pt I 119:1–15.

Shelton AO, Kinzey D, Reiss C, Munch S, Watters G, Mangel M. 2013. Among-year variation in growth of Antarctic krill *Euphausia superba* based on length-frequency data. Mar Ecol Prog Ser 481:53–67.

Siegel V. 1988. A Concept of Seasonal Variation of Krill (*Euphausia superba*) Distribution and Abundance West of the Antarctic Peninsula. In: Sahrhage D, editor. Antarctic Ocean and Resources Variability Berlin, Heidelberg: Springer. p. 219–30.

Siegel V, Loeb V. 1995. Recruitment of Antarctic krill *Euphausia superba* and possible causes

for its variability. Mar Ecol Prog Ser 123:45-56.

Siegel V, Reiss CS, Dietrich KS, Haraldsson M, Rohardt G. 2013. Distribution and abundance of Antarctic krill (*Euphausia superba*) along the Antarctic Peninsula. Deep-Sea Res Pt I 77:63–74.

Siegel V, Ross RM, Quetin LB. 2003. Krill (*Euphausia superba*) recruitment indices from the western Antarctic Peninsula: are they representative of larger regions? Polar Biol 26:672–79.

Siegel V, Watkins JL. 2016. Distribution, Biomass and Demography of Antarctic Krill, *Euphausia superba*. In: Siegel V, editor. Biology and Ecology of Antarctic Krill. Advances in Polar Ecology Cham: Springer International Publishing. p. 21–100.

Spiridonov VA. 1995. Spatial and temporal variability in reproductive timing of Antarctic krill (*Euphausia superba* Dana). Polar Biol 15:161-174.

Stammerjohn SE, Martinson DG, Smith RC, Iannuzzi RA. 2008a. Sea ice in the western Antarctic Peninsula region: Spatio-temporal variability from ecological and climate change perspectives. Deep-Sea Res Pt II 55:2041-2058.

Stammerjohn SE, Martinson DG, Smith RC, Yuan X, Rind D. 2008b. Trends in Antarctic annual sea ice retreat and advance and their relation to El Niño–Southern Oscillation and Southern Annular Mode variability. J Geophys Res 113:C03S90.

Steinberg DK, Ruck KE, Gleiber MR, Garzio LM, Cope JS, Bernard KS, Stammerjohn SE, Schofield OME, Quetin LB, Ross RM. 2015. Long-term (1993–2013) changes in macrozooplankton off the Western Antarctic Peninsula. Deep-Sea Res Pt I 101:54–70.

Symonds MRE, Moussalli A. 2011. A brief guide to model selection, multimodel inference and

model averaging in behavioural ecology using Akaike's information criterion. Behav Ecol Sociobiol 65:13-21.

Tarling GA, Cuzin-Roudy J, Thorpe SE, Shreeve RS, Ward P, Murphy EJ. 2007. Recruitment of Antarctic krill *Euphausia superba* in the South Georgia region: adult fecundity and the fate of larvae. Mar Ecol Prog Ser 331:161–79.

Thibodeau PS, Steinberg DK, McBride CE, Conroy JA, Keul N, Ducklow HW. in review. Long-term observations of pteropod phenology along the Western Antarctic Peninsula. Deep-Sea Res Pt I.

Thompson AF, Heywood KJ, Thorpe SE, Renner AH, Trasviña A. 2009. Surface circulation at the tip of the Antarctic Peninsula from drifters. J Phys Oceanogr 39:3–26.

Thorpe SE, Heywood KJ, Stevens DP, Brandon MA. 2004. Tracking passive drifters in a high resolution ocean model: implications for interannual variability of larval krill transport to South Georgia. Deep-Sea Res Pt I 51:909–20.

Thorpe SE, Murphy EJ, Watkins JL. 2007. Circumpolar connections between Antarctic krill (*Euphausia superba* Dana) populations: Investigating the roles of ocean and sea ice transport. Deep-Sea Res Pt I 54:792–810.

Thorpe SE, Tarling GA, Murphy EJ. 2019. Circumpolar patterns in Antarctic krill larval recruitment: an environmentally driven model. Mar Ecol Prog Ser 613:77–96.

Trathan PN, Hill SL. 2016. The Importance of Krill Predation in the Southern Ocean. In: Siegel V, editor. Biology and Ecology of Antarctic Krill. Advances in Polar Ecology Cham: Springer International Publishing. p. 321–50.

Walsh J, Reiss CS, Watters GW. 2020. Flexibility in Antarctic krill *Euphausia superba*

decouples diet and recruitment from overwinter sea-ice conditions in the northern Antarctic Peninsula. Mar Ecol Prog Ser 642:1-19.

Waters KJ, Smith RC. 1992. Palmer LTER: A sampling grid for the Palmer LTER program. Antarct J US 27:236–239.

Watters GM, Hinke JT, Reiss CS. 2020. Long-term observations from Antarctica demonstrate that mismatched scales of fisheries management and predator-prey interaction lead to erroneous conclusions about precaution. Sci Rep 10:2314.

Wiebe PH, Ashjian CJ, Lawson GL, Piñones A, Copley NJ. 2011. Horizontal and vertical distribution of euphausiid species on the Western Antarctic Peninsula U.S. GLOBEC Southern Ocean study site. Deep-Sea Res Pt II 58:1630–51.

Wiedenmann J, Cresswell KA, Mangel M. 2009. Connecting recruitment of Antarctic krill and sea ice. Limnol Oceanogr 54:799–811.

Wood SN. 2003. Thin-plate regression splines. Journal R Stat Soc B 65:95–114. Zuur AF, Ieno EN. 2016. A protocol for conducting and presenting results of regression-type analyses. Methods Ecol Evol 7:636–45.

Table 1. Pearson's correlation coefficients across study sub-regions for annual euphausiid larvae abundance from 1995-2011 (n = 17 years) (above the diagonal) and annual *Euphausia superba* recruit abundance from 1993-2011 (n = 19 years) (below the diagonal). Values in italics indicate $p < 0.003$.

	WAP Coast	**WAP Shelf**	**WAP Slope**	**NAP Coast**	**NAP Shelf**	**NAP Slope**
WAP Coast	-	*0.68*	0.61	0.15	0.38	0.31
WAP Shelf	*0.68*	-	*0.81*	0.08	0.39	0.50
WAP Slope	0.26	*0.75*	-	0.20	0.40	0.56
NAP Coast	0.47	*0.76*	*0.66*	-	*0.69*	0.57
NAP Shelf	0.50	*0.84*	*0.79*	*0.89*	-	*0.88*
NAP Slope	0.38	*0.65*	0.54	*0.83*	*0.86*	-

Table 2. Summary of model selection statistics from linear regression models assessing the relationship between euphausiid larvae abundance (1995-2010) and *Euphausia superba* recruit abundance (1996-2011) in the following year (n = 16 years). AICc: corrected Akaike Information Criterion; ΔAICc: difference from lowest AICc; AICc weight – relative model support or probability. Italics indicate models with ΔAICc < 2.

	NAP Coast & Shelf *Euphausia superba* recruits			**WAP Coast & Shelf *Euphausia superba* recruits**		
Explanatory variable (1-yr lag)	**AICc**	**ΔAICc**	**AICc weight**	**AICc**	**ΔAICc**	**AICc weight**
NAP Slope euphausiid larvae	*25.9*	*1.39*	*0.28*	*36.1*	*1.37*	*0.19*
WAP Slope euphausiid larvae	*24.5*	*0.00*	*0.56*	*35.5*	*0.78*	*0.26*
NAP Shelf euphausiid larvae	28.1	3.56	0.09	*34.7*	*0.00*	*0.38*
WAP Shelf euphausiid larvae	30.0	5.50	0.04	38.2	3.52	0.07
NAP Coast euphausiid larvae	32.2	7.74	0.01	37.6	2.87	0.09
WAP Coast euphausiid larvae	31.5	6.97	0.02	40.4	5.73	0.02

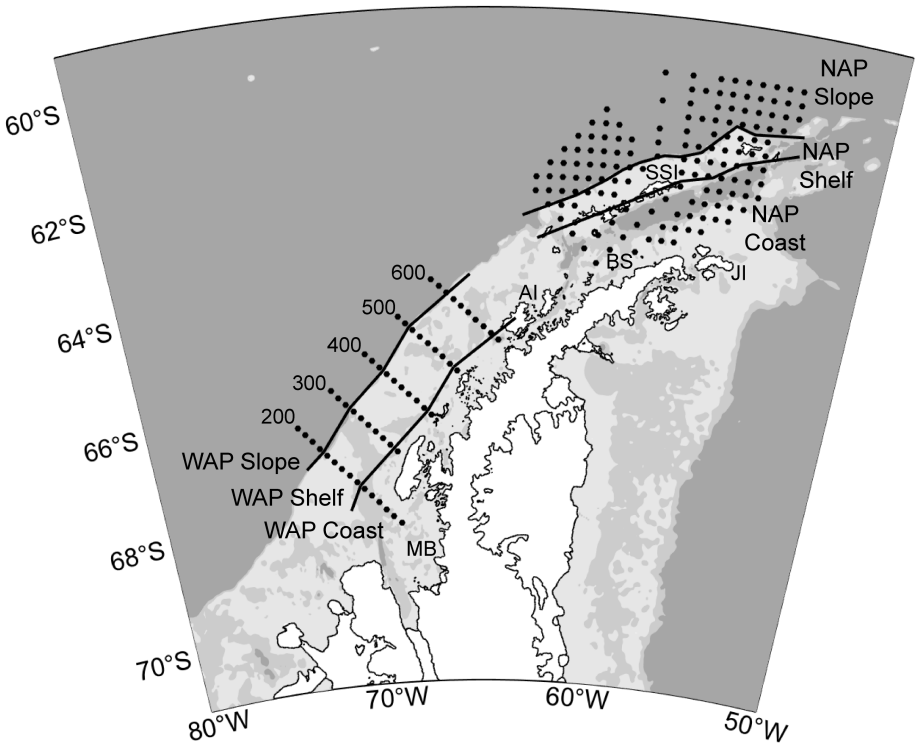

Figure 1. Map of the study area indicating U.S. AMLR sampling sub-regions in the North Antarctic Peninsula (NAP) and PAL LTER sampling sub-regions in the West Antarctic Peninsula (WAP). Bathymetric shading indicates 0-500, 500-1000, and > 1000 m depth intervals. Black dots indicate sampling stations, the occupation of which varied through time. SSI: South Shetland Islands, JI: Joinville Island, BS: Bransfield Strait, AI: Anvers Island, MB: Marguerite Bay, 600-200: PAL LTER sampling grid lines.

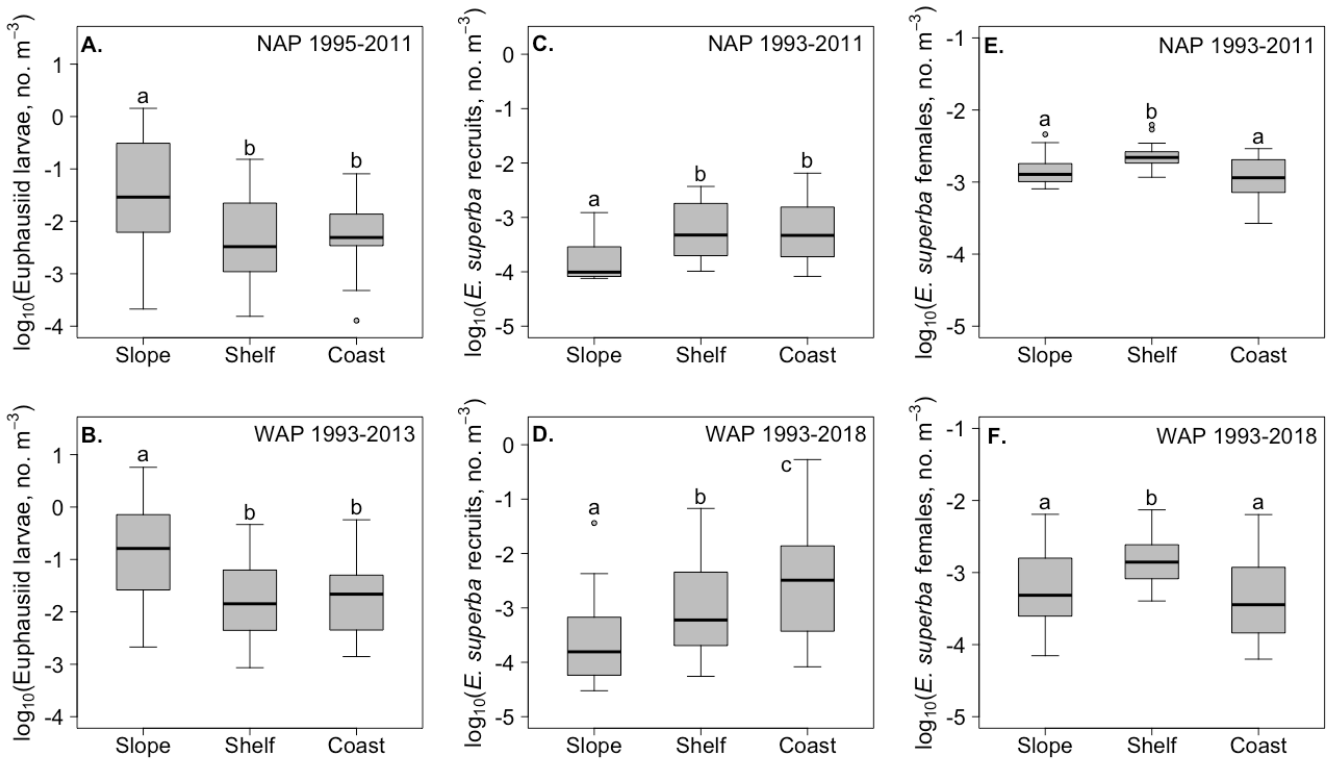

Figure 2. Spatial abundance comparisons. Annual mean $\log_{10}$-adjusted abundance for (A-B) euphausiid larvae, (C-D) *Euphausia superba* recruits, and (E-F) *E. superba* mature females at the North Antarctic Peninsula (NAP) Slope, Shelf, and Coast sub-regions (A, C, E) and West Antarctic Peninsula (WAP) Slope, Shelf, and Coast sub-regions (B, D, F). Thick black line indicates the median, gray box indicates the interquartile range, and whiskers indicate the range excluding outlier values indicated as points. Different lowercase letters indicate statistically different group means. Note different scales although abundance is not directly comparable across plots due to different sampling methods. Sample size n = 17-26 years.

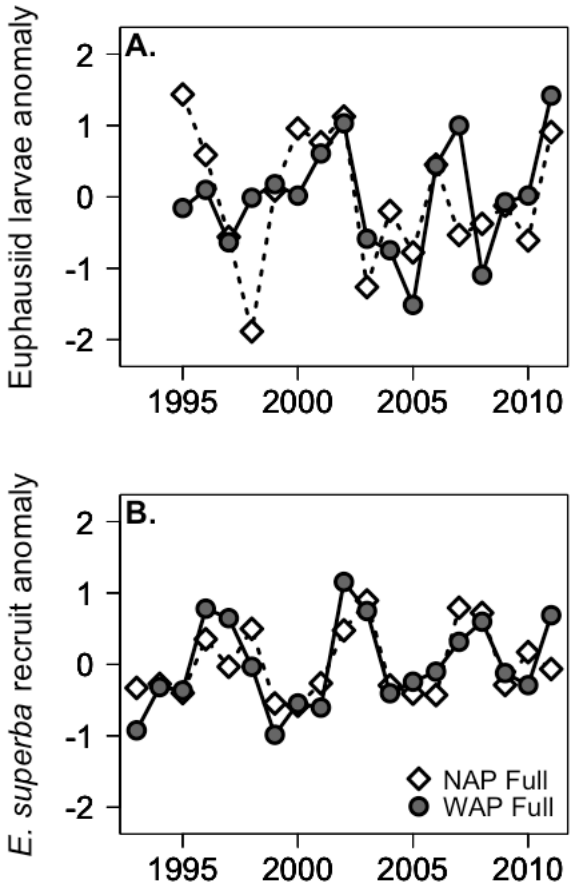

Figure 3. Annual abundance anomaly time series. (A) Euphausiid larvae abundance anomalies in the full NAP sampling area (dashed line, white diamonds) and the full WAP sampling area from 1995 to 2011 (solid line, gray circles) (n = 17; p = 0.05; Pearson's r = 0.47). (B) *Euphausia superba* recruit abundance anomalies for the same study areas from 1993 to 2011 (n = 19; p = 0.0004; Pearson's r = 0.72).

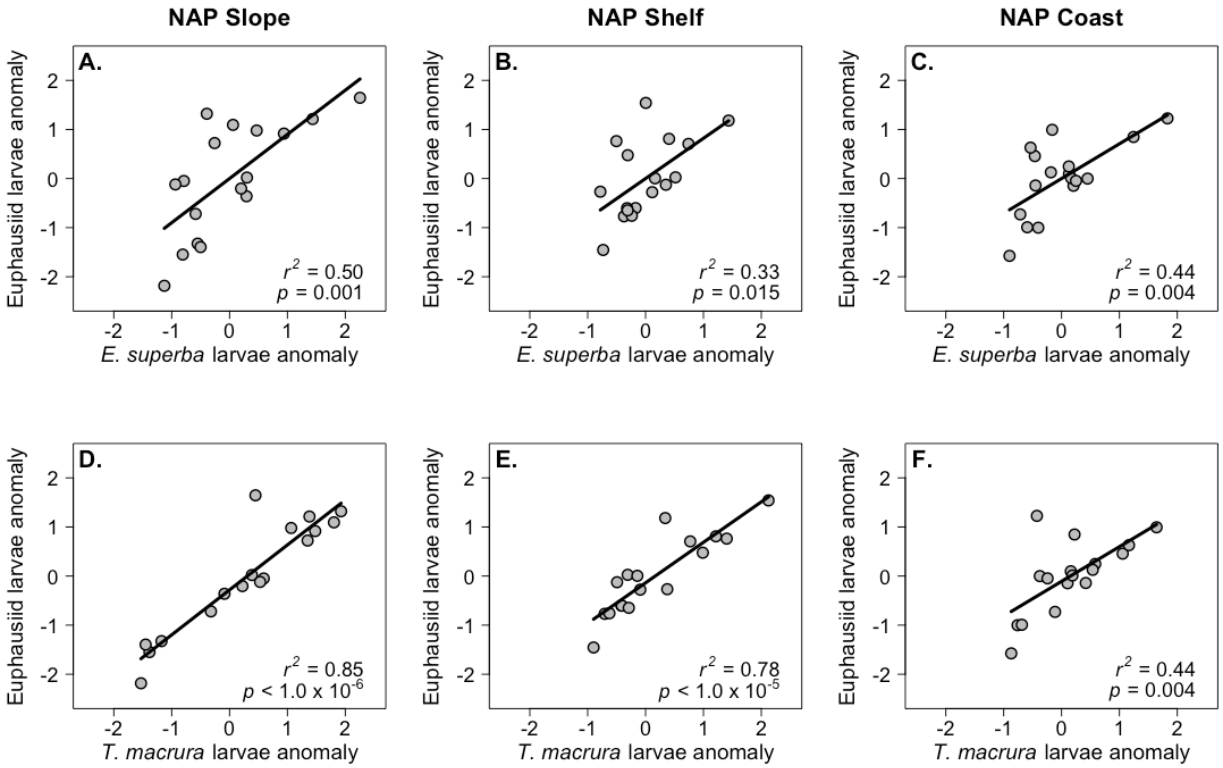

Figure 4. *Euphausia superba* larvae abundance anomaly (A-C) and *Thysanoessa macrura* larvae abundance anomaly (D-F) versus total euphausiid larvae abundance anomaly in the NAP Slope (A, D), Shelf (B, E), and Coast (C, F) sub-regions from 1995 to 2011 (n = 17 years). Black line indicates linear regression fit.

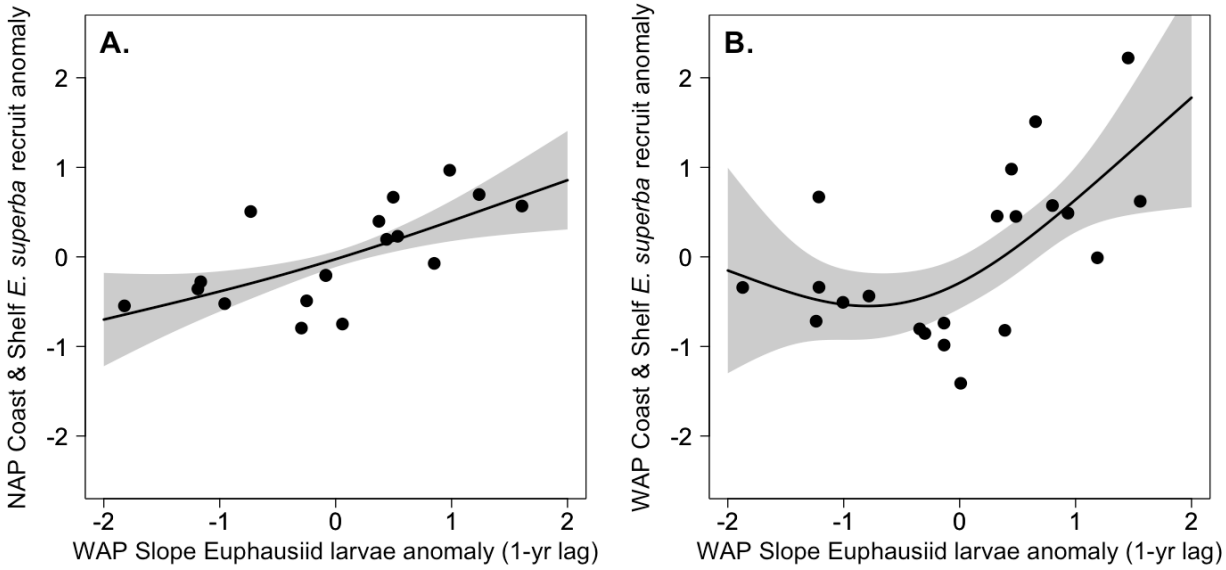

Figure 5. WAP Slope euphausiid larvae abundance anomaly versus the following year's *Euphausia superba* recruit abundance anomaly in the (A) combined NAP Coast and Shelf sub-regions from 1994 to 2011 (n = 18 years), and (B) combined WAP Coast and Shelf sub-regions from 1994 to 2014 (n = 21 years). Black line indicates the mean regression spline fit, and gray shading indicates the 95% confidence interval.

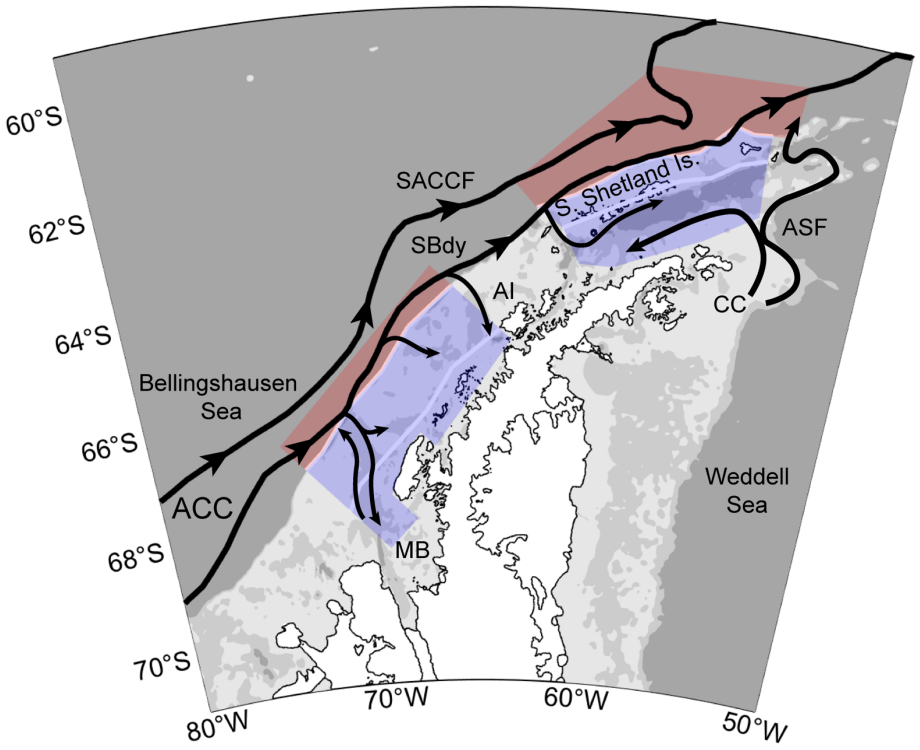

Figure 6. Conceptual diagram illustrating how regional ocean circulation relates to areas of relatively high krill larval abundance (red sub-regions) and recruit abundance (blue sub-regions) along the Antarctic Peninsula. The Antarctic Circumpolar Current (ACC) flows from the West Antarctic Peninsula to the North Antarctic Peninsula. Cross-shelf transport connects oceanic waters of the ACC to the Antarctic Peninsula shelf. Although not sampled in this study, the Bellingshausen and Weddell Seas likely influence krill population dynamics at the Antarctic Peninsula. Similarly, krill reproduction and recruitment at the Antarctic Peninsula likely impact abundance to the northeast in the Scotia Sea (not shown). See Fig. 1 for sampling sub-regions shown in this diagram. Ocean current locations and illustrations are from Orsi et al. 1995, and Moffatt and Meredith 2018. SACCF: Southern ACC Front, SBdy: Southern ACC Boundary, ASF: Antarctic Slope Front, CC: Antarctic Coastal Current, AI: Anvers Island, MB: Marguerite Bay.

Supplemental Table 1. Pearson's correlation coefficients across the North Antarctic Peninsula (NAP) sub-regions for annual *Euphausia superba* larvae abundance anomalies from 1995-2011 (n = 17 years).

	Pearson's *r*	***p***
NAP Slope vs. NAP Shelf	0.87	0.000003
NAP Slope vs. NAP Coast	0.58	0.014
NAP Shelf vs. NAP Coast	0.76	0.0003

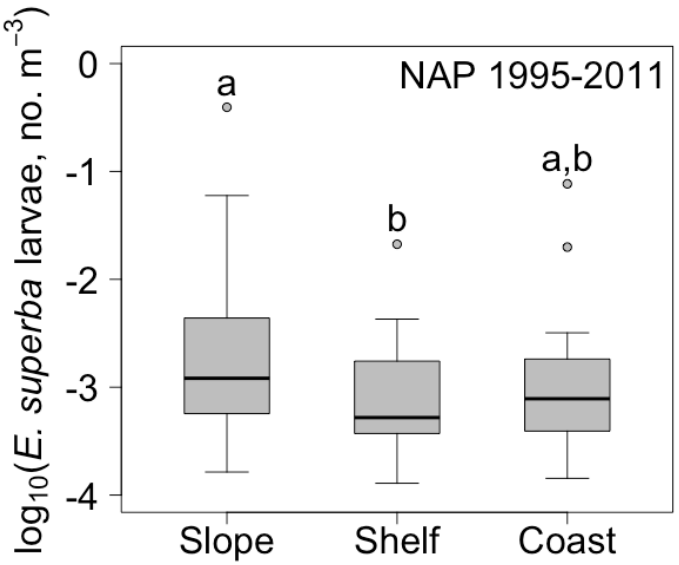

Supplemental Figure 1. Annual mean $\log_{10}$-adjusted abundance for *Euphausia superba* larvae at the North Antarctic Peninsula (NAP) Slope, Shelf, and Coast sub-regions. Thick black line indicates the median, gray box indicates the interquartile range, and whiskers indicate the range excluding outlier values indicated as points. Different lowercase letters indicate statistically different group means. Sample size n = 17 years.

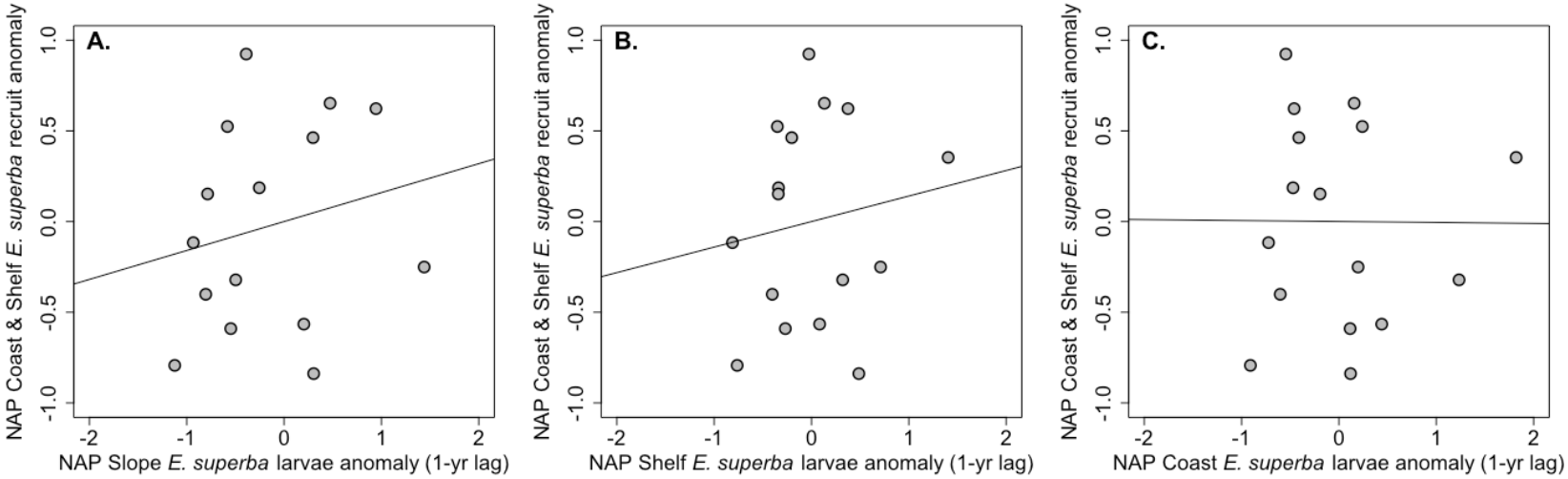

Supplemental Figure 2. *Euphausia superba* larvae abundance anomaly at the North Antarctic Peninsula (NAP) (A) Slope, (B) Shelf, and (C) Coast sub-regions versus the following year's *E. superba* recruit abundance anomaly in the combined NAP Coast and Shelf. Larvae data is from 1995 to 2010 and recruit data is from 1996 to 2011 (n = 16 years). Black line is the mean linear regression fit.

VITA

John (“Jack”) Conroy was born in Washington, DC and attended Bishop O’Connell High School. He was a visiting student at the University of Washington, Friday Harbor Laboratories in 2015 and graduated from William & Mary with a B.S. in biology in 2016. Jack matriculated at the Virginia Institute of Marine Science in 2016 and conducted research in Antarctica during five field seasons from 2015-2020. He is currently a Sea Grant Knauss Fellow placed with NOAA Ocean Exploration.